NORTHWESTERN UNIVERSITY

Highly Modular Protein Polymers for Multivalent Display, Liquid Crystalline Bacillary Polymers and Hydrogels for *in Situ* Tissue Engineering

A DISSERTATION

SUBMITTED TO THE GRADUATE SCHOOL IN PARTIAL FULFILLMENT OF THE REQUIREMENTS

for the degree

DOCTOR OF PHILOSOPHY

Field of Chemical Engineering

By

Nicolynn Elaine Davis

EVANSTON, ILLINOIS

December 2008

ABSTRACT

Highly Modular Protein Polymers for Multivalent Display, Liquid Crystalline Bacillary Polymers and Hydrogels for *in Situ* Tissue Engineering

Nicolynn Elaine Davis

The *de novo* design of bio-inspired materials with precisely controlled properties is challenging, but has potential applications in nano-biotechnology. Applications range from nanometer scaled assemblies to three-dimensional scaffolds for tissue engineering. Genetic engineering of protein-based polymers offers distinct advantages over traditionally synthesized polymers, *de novo* proteins can be produced with tremendous control over protein structure and properties. This enables the design of macromolecular materials with controlled structure while maintaining features of natural proteins. Molecular biology techniques were applied to create protein families that can be used as building blocks for the self-assembly of liquid crystalline materials, as multivalent scaffolds, and as tissue engineering hydrogels for regenerative medicine.

In the first section, a biosynthetic strategy was developed to prepare a new class of self-assembled macromolecules - dendronized protein polymers (DPPs) – that have well-defined cylindrical shapes with controlled molecular dimensions. The DPPs consisted of an alpha-helical polypeptide core that determined the molecular length (L) surrounded by grafted wedge-shaped dendrons that controlled the diameter (D). The DPPs self-assemble to form highly ordered liquid crystalline (LC) phases, where the type of LC ordering is controlled by DPP aspect ratio (L/D)

and concentration. This biophysical study of entropically-driven colloidal self-assembly shows the utility of combining biological and chemical synthetic tools towards preparation of new macromolecular blocks for nanoscale engineering.

In section two, a class of modular high-molecular weight protein polymers were constructed that can be derivatized with bioactive domains to create a multivalent scaffold. In addition, the inherent monodispersity of the protein polymer building blocks allowed for accurate determination of the bioactive domain valencies. Furthermore, these protein polymers were enzymatically crosslinked into hydrogels with controlled viscoelastic properties and bioactivity. Rheological studies indicated an *in situ* liquid-to-gel transition within minutes and the bulk material properties were affected by crosslink density and number, and gel composition. By combining these strategies, this new class of gelling materials can be tailored to have a range of bulk properties and can be easily decorated with bioactive domains for *in situ* tissue engineering.

To Martin and Julie

ACKNOWLEDGMENTS

I will always be grateful to those who have offered guidance, support, encouragement, humor, and love during my time in graduate school; without you this dissertation would not have been possible. To Annelise: thank you for allowing me to join your lab in the middle of my graduate experience, without you, I am not sure where I would be. You provided encouragement, energy, and enthusiasm, making my experience truly enjoyable. To Ilya: you motivated me to be a better scientist and stronger person; without you, I wouldn't know my full capacity. I would also like to thank all the graduate students in the Barron laboratory, especially: Lindsay, Sheng, Liese, Nate B., Ann, Russ, Ryan, and Wei. I really appreciate all your assistance and expert advice. I would like to especially acknowledge James for his assistance with my thesis. I also want to thank Hermann for providing his *in vivo* expertise. I feel tremendously lucky to have worked with such a terrific group of outstanding people. Thanks to my committee members: Professors Messersmith, Burghardt, and Ameer, for the input and guidance. Mom, Sandee and Craig: thank you so much for the constant love and support, not just in grad school but throughout my life. Lastly, I would like to thank my husband for his love and patience; through your humor I am constantly reminded to not take life too seriously.

TABLE OF CONTENTS

List of Figures

List of Tables

Chapter 1

Thesis Overview and Specific Aims

1.1 Motivation and Objective

Nature creates complex organizations and structures with diverse properties, based on relatively simple protein components. Despite years of research that elucidates these biological components, only recently have there been significant efforts focused on protein-based materials from an engineering perspective. One emerging method for the production of complex materials is by genetically engineering bacteria to express recombinant protein polymers. This technique allows for mimicking both natural proteins as well as synthetic polymers. Nature creates materials with unique organization and function not easily copied in synthetic polymers. For example, the amino acid sequence of silk fibers imparts both toughness and strength, where the chemical and mechanical properties have not been effectively mimicked in synthetic materials. These specific attributes, along with many others from natural proteins are attractive for biomaterial engineers, where the synthesis of protein analogs would be a step in elucidating the chemical compositions and conformations that translate to specific functions and structures in materials.

The emergence of synthetic polymers created by polymerization techniques has opened a new realm of creating customized materials due to the design flexibility. The composition and

structure of synthetic polymers can be tailored to the specific application needs, and therefore have been extensively studied in various biomaterial-based applications. However, chemically created materials have a distribution of molecular length, stereochemistry, and in some cases sequence, thus creating a non-uniform material.

As an alternative to chemical polymerization, genetic engineering and subsequent recombinant protein expression can be utilized to create homogeneous protein polymers from a designed DNA template. In contrast to chemical polymerization, recombinant protein expression allows for stereoregularity, monodispersity and controlled structure on the microscopic and macroscopic level. For example, these biosynthetic polymers can have controlled physical properties developed on the basis of structure, hydrophobicity and charge. The homogeneity in biologically produced molecules can lead to novel self-assembling systems with order on the length-scale of 1-100 nm commensurate with the size of the molecules. Furthermore, recombinant proteins have design flexibility similar to that of synthetic molecules, yet they can contain properties unique to natural proteins.

The general process for making biosynthetic polymers begins with designing a DNA gene, which encodes for a specific amino acid sequence (Figure 1.1). The DNA is chemically synthesized and then inserted into a cloning vector by a series of slicing and ligating reactions. The gene is placed into an expression vector which can be taken up by an acceptor cell in a host microorganism such as *E. coli*. The protein encoded by the DNA template, is transcribed into mRNA using the host system's natural machinery. The mRNA serves as a template for the host ribosomes to construct the synthetic protein. The target protein can then be easily removed from the natural cellular proteins. Genetic engineering and recombinant protein expression are

advantageous because the microorganisms can synthesize high molecular weight materials in relatively large quantities.

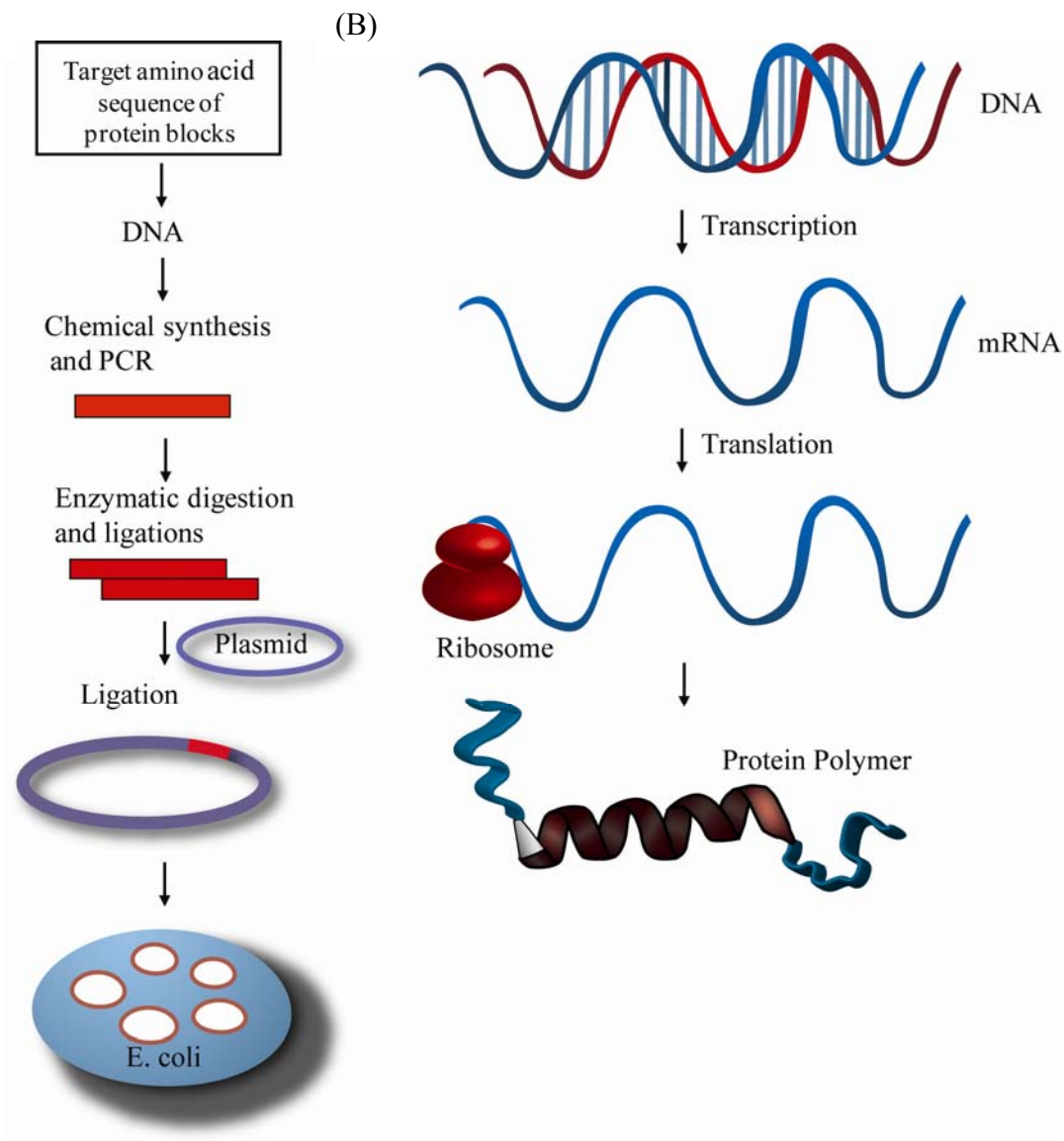

Figure 1.1: Schematic of the synthesis of recombinant biopolymers. (A) DNA cloning and insertion into the bacterial host, (B) Cellular protein biosynthesis

The goal of the research presented herein is to employ the utility and versatility displayed in natural proteins to expand the potential applications for protein-based materials. Chapter 2 gives a brief overview of the emerging field of protein synthesis and applications of recombinant protein polymers in the field of biotechnology. Chapter 2 is organized based on protein secondary structure, which is often essential to protein function.

In this thesis two unique applications of genetically engineered recombinant protein polymers which are essential to the design and function of the synthesized materials are presented. The first section, covering Chapters 3 and 4, extends the observation that monodisperse genetically engineered α-helical proteins can behave as rigid-rod like molecules that can self-assemble into liquid crystalline phases. In Chapter 3, we elaborate on the research first investigated by Tirrell *et. al.*, who showed the existence of a lamellar phase in monodisperse poly(γ-benzyl α,L-glutamate).[6] This work was furthered by: (1) improving the synthetic procedure to increase yield 40-fold and (2) determining the effects on LC phase formation as a function of the protein length and protein concentration. The biosynthesis required the development of a novel DNA cloning scheme to handle the highly repetitive amino acid sequence. In addition, an innovative protein expression and purification method was created to obtain gram quantities of purified proteins. Although phase transitions were observed, this method had a limited ability to study shape anisotropy effects on liquid crystalline properties.

In Chapter 4, a combined biosynthetic method is presented to prepare molecules with defined length (L) and diameter (D) that can self-assemble into nanostructures having long-range order controlled by the exact molecular dimensions. Previous researchers have attached dendrimers, highly-branched, wedge-shaped macromolecules, to flexible polymer chains; these

molecules had rigid shapes, but a distribution of lengths and a limited ability to form LC phases. Inspired by these studies and observing that proteins can be made with exact molecular weights by genetic engineering, we have developed a combined strategy to produce dendronized protein polymers (DPPs). The DPPs are built from a monodisperse protein polymer generated through recombinant protein expression. Dendrons with several generations and degrees of branching were added to the protein polymer backbone to vary molecular diameter and to determine their effects on molecular shape and backbone conformation. Furthermore, we were able to expand the number of anisotropic shapes and study the effects on phase formation. This research represented the first experimentally determined phase diagram for monodisperse cylindrical molecules. The ability to construct monodisperse macromolecules and precisely determine their intermolecular self-assembly has potentially important implications for material development for the fields of nanotechnology and biomaterials.

The second section of this thesis, discussed in Chapters 5-7, focuses on the development of a novel class of high-molecular weight, water-soluble protein polymers that lack secondary structure. These proteins are designed to have evenly-spaced modifiable amino acids to act as substrates for (1) chemical and enzymatic derivitazation to create a biofunctional scaffold and (2) for enzymatic crosslinking into hydrogels for tissue engineering applications. The design and characterization of cationic protein polymers for multivalent display is presented in Chapter 5. The versatility of grafting bioactive moieties enables the ability to create an array of materials with multiple pendant groups for biological applications. The precision of recombinant protein polymer scaffolds allows for exact determination of valency, which is nearly impossible in

chemically synthesized polymers. This highly modular class of *de novo* protein polymers is a promising candidate as a building block for multivalent display and tissue engineering hydrogels.

Chapter 6 focuses on the enzymatic crosslinking of two classes of disordered protein polymers to form hydrogels with viscoelastic properties. These hydrogels have the potential for a more uniform and controlled mesh size as a result of the protein polymer monodispersity. The mechanical properties of the hydrogel can also be customized due to the control over crosslinking density and the substrate spacing on the protein polymer backbone. This bottom-up approach facilitates customizable grafting of bioactive peptides on the hydrogel that can be chosen for the cell-signaling requirements of particular tissue applications. Herein we describe a unique platform for customizable enzymatic protein polymer-based hydrogels that can be used for diverse tissue engineering applications.

The final chapter in this section, Chapter 7, illustrates the use of protein block co-polymers to create truly modular building blocks at the genetic level by the introduction of self-assembly. In this work, proteins that associate into controlled secondary structures were added to disordered protein blocks. The protein association and overall secondary structure was directed by the composition and number of blocks in the protein block-copolymer. In addition, the protein block-copolymers were incorporated into enzymatically crosslinked hydrogel networks. The changes in material properties were assessed by solution rheometry.

The final chapter, Chapter 8, highlights the conclusions and limitations of the *de novo* protein polymers presented in this thesis. Additional experiments are suggested to elaborate and fully characterize the properties of these materials to create hydrogels with specific features for the biomaterial application. Finally, the potential modifications and applications of these

materials are discussed to elucidate the utility of sequence-controlled biomaterials and to drive recombinant protein polymer biomaterials out of its relative infancy into real-world applications.

Chapter 2

Designer Proteins for Biomaterials

2.1 Overview

Genetic engineering of recombinant proteins has been motivated by the search to find materials with exquisite control over structure and function. Recombinant protein polymers have been designed for potential applications ranging from fibers and coatings, to drug delivery and hydrogels for tissue engineering. The term "protein polymer" has been coined to describe a high molecular weight recombinant protein that is designed to have a highly repetitive amino acid sequence. The design of protein polymers has been primarily based on the repeating amino acid sequences found in natural proteins such as silk, collagen, and elastin.[7-15] However, the realm of protein polymers has advanced to create novel combinations of amino acid sequences to expand the range of protein-based materials beyond natural protein mimetics, producing materials with novel functionality. For example, *de novo* sequences that encode secondary structure have been utilized to create coiled-coil[16, 17] and elastin-like[18] block copolymer hydrogels, β-sheet layered structures,[19] and α-helical protein polymers for chemical modification[6, 20, 21]. Moreover, random coil, or unstructured, sequences have been developed as drag tags for capillary electrophoresis.[5] Furthermore, the incorporation of non-natural amino acids, pioneered by D. Tirrell, has expanded the range of functionality for *de novo* sequences.[22, 23] This chapter is dedicated to the discussion

of recombinant protein polymers and their applications based on secondary structure. This thesis focuses on *de novo* protein polymers that are random coil (Chapter 5, 6) and have a helical secondary structure (Chapter 3, 4, 7). For this reason the incorporation of non-natural amino acids will not be discussed (for further information on this topic, please see references[24, 25]).

2.2 Evolution and Synthesis of Protein Polymers

The creation of repetitive protein polymers requires the development of a stable DNA template. Doel *et al.* reported the first attempt to create a synthetic repetitive gene, but was limited to 900 base pairs.[26] By 1983, the laboratory of J. Cappello had demonstrated that biological expression could be used to produce a highly repetitive synthetic gene consisting of only a three amino acid monomer.[27] Furthermore, experiments with repetitive amino acid sequences acting as the analogs of structural proteins were shown to reproduce the defined properties of their natural counterparts.[27] Today, genetic engineering has progressed to the point where any segment of DNA can be introduced to a microorganism by commercially available plasmids.

As briefly mentioned in Chapter 1, protein polymers with precise composition can be effectively created using a microorganism host, where the scale of production is only limited to the size of the production vessel.[27] The production process first involves the generation of a gene by genetic engineering, followed by protein expression and purification. Gene construction starts with the design of a protein "monomer," composed of a sequence of amino acids that is to be repeated (Figure 2.1).

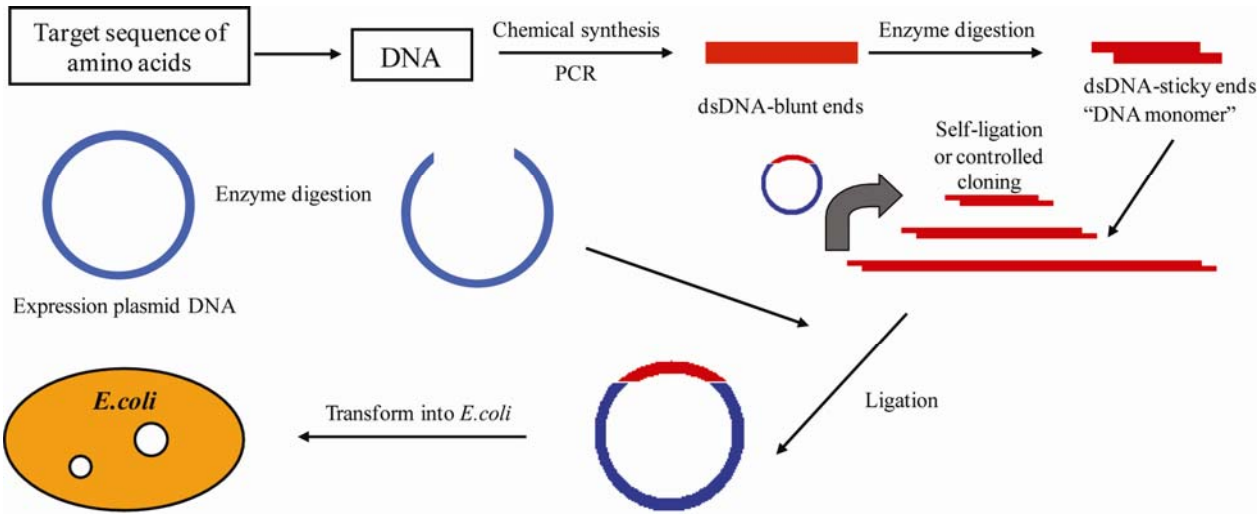

Figure 2.1: Scheme of gene creation using recombinant DNA technology.

The amino acid sequence is then converted into the correct DNA codons based on the preferences of the microorganism. The DNA monomer is created by chemical oligonucleotide synthesis, but is limited to ~ 150 base pairs. The monomer gene is then amplified by PCR or thermally annealed to increase concentration for cloning into a plasmid. The gene monomer can be used to clone multimers (multiple repeats of the gene) or block-gene sequences using natural enzymes for digestion and ligation reactions. The final gene is placed into an expression plasmid and introduced into a microorganism for protein synthesis. The microorganism host uses inherent methods for gene transcription and translation to synthesize the protein (see Chapter 1, Figure 1.1). Protein expression is tightly controlled by additional genes encoded in the expression plasmid, where expression is triggered by a chemical addition. Protein polymers are purified

from the cellular proteins by simple chromatographic methods. Although virtually any gene can be introduced to a microorganism host, this does not guarantee the ability to express the corresponding protein in high yields.

2.3 Protein Polymer Mimics of Natural Sequences

The majority of protein polymers have been created as mimics of natural protein sequences to replicate their function and properties. The two main classes of protein mimics have sequences derived from elastin and silk proteins, both with well defined three-dimensional structures.

2.3.1 Elastin-Like Proteins (ELPs)

The predominant recombinant protein mimics are based on natural elasin; these elastin-like protein polymers have been investigated for a broad range of applications as biomaterials. ELPs are gaining attention, in part due to their ease of purification and ability to self-assemble with a tunable range of material properties.

Natural elastin is an extracellular matrix protein with the repeating sequence of (Glycine-Valine-Glycine-Valine-Proline or GVGVP). Recombinant ELPs, extensively studied by Urry *et al.*, are of the general sequence VPGXG where X is a "guest residue" and can be any amino acid except proline.[28] Elastins and recombinant analogs exhibit a reversible phase transition based on temperature. Below the critical solution temperature (T_c), elastins are soluble in aqueous medium. At a temperature above T_c, elastin proteins undergo a phase transition and form aggregate structures with β-turns. The transition mechanism is proposed to involve hydration of the hydrophobic residues at temperatures below T_c; above T_c, the water becomes less-ordered

and the elastins aggregate by hydrophobic interactions.[28] The T_c can be controlled by elastin concentration,[29] length of the protein,[30] and amino acid composition[14].

Elastin analogs have gained recognition as important proteins for the creation of biomaterials, in part because of their inherent phase transition at a set T_c, and due to the fact that ELPs induce little immune response[31]. These proteins have been investigated for drug release, due to their good drug loading capabilities,[32] and unique thermal properties that have been exploited for targeting tumors *in vivo*.[30, 33] Moreover, several laboratories have investigated the use of elastin analogs as hydrogels for tissue engineering. The D. Tirrell laboratory used elastin-based hydrogels to study cell adhesion,[29, 34] and for applications including corneal onlyas[35] and stem cell niches[36]. Similarly, the Chilkoti laboratory at Duke University has used recombinant ELPs for drug delivery,[37] switchable-permeability membranes,[38] protein purification[39] and tissue repair[40].

Although ELPs can have a range of functionality, in general, the amino acid selection is still limited to the repetitive elastin consensus sequence. The confined amino acid sequence provides little ability to include bioactive domains, where the incorporation of additional amino acids will affect protein solution behavior and change T_c. Furthermore, ELPs self-assemble into hydrogels with limited mechanical strength, and often require additional crosslinking techniques to enhance material properties. However, researches have explored the inclusion of small sequences containing bioactive domains to incorporate functionality with a trade-off by the decreased strength of the elastin self-assembly. Due to these limitations and lack of modularity, elastin-based biomaterials are not ideal for many biomedical applications.

2.3.2 Silk-Like Proteins (SLPs)

Natural silk, a fibrous protein produced in specialized glands of silkworms, spiders, and other organisms, has exceptional properties and strength unmatched by synthetic materials. Consequently, artificial silk-like proteins have been explored to capture the material properties of natural silk. The properties of silk generally depend on the host organism and intended function; in general, the primary amino acid sequences in SLPs include repeats of alanine and glycine residues. Silks form a number of secondary structures; the most common is an anti-parallel β-pleated sheet, where the poly(alanine) regions are hypothesized to participate in the β-sheet formation.[41, 42] Recombinant silk analogs have been generally based on three different amino acid sequences (Table 2.1).[43]

Table 2.1: Natural Silk Amino Acid Sequences

Source	Sequence
B. mori	GAGAGSGAAG[SGAGAG]$_8$Y]
N. clavipes-1	GGAGQGGYGGLGSQGAGRGGLGGQGGAG
N. clavipes-2	GPGGYGGPGQQGPGGYAPGQQPSGPGS

Recombinant SLPs have been used for fiber spinning,[44] cast into films for wound dressings and employed as scaffolds for enzyme immobilization[45, 46]. The nanofiber assembly of these proteins created robust materials with high elastic moduli suitable for several material applications.[47] Furthermore, SLP-based hydrogels have been modified for cell interaction by chemical modification with cell adhesive binding domains and growth factors.[48, 49] Silk-like

amino acid sequences have also been used as fusion proteins for applications of drug delivery and cancer research,[50-53] as quantum dot-bioconjugates,[54] and as sensors[55, 56].

Although silk analogs have been successfully produced by genetic engineering, their inherent insolubility due to β-sheet formation, has affected yields and limited the ability for characterization for biomedical applications.[43] SLPs have been designed to have enhanced solubility by the incorporation of (GAGXGS) where X is valine or tyrosine; this mimics a sequence from *B. mori* that acts to enhance the solubility of natural silks in aqueous solutions[57] however, inclusion of this block only moderately enhances stability in solution. For these reasons, the instability and poor solubility have limited the applications of SLP-based materials.

2.4 *De novo* Protein Polymers and Block Copolymers

Artificial protein polymers are not limited to simple mimics of natural protein sequences. The design of *de novo* protein polymer sequences facilitates the inclusion of natural and non-natural functionality that can result in materials that have unique chemical and biological activities and a range of physical properties. The recombinant protein polymers produced to date have focused mainly on natural sequence mimics; consequently, few research laboratories have investigated *de novo* based biomaterials. This is due, in part, to the difficulty of predicting *de novo* protein production efficiency and functionality. Nonetheless, the following sections illustrate some examples of novel recombinant proteins and their applications.

2.4.1 Random Coil Protein Polymers

The first random coil *de novo* protein polymer was created by K. McGrath *et al*. with the sequence $(AG)_3$(PEG); the sequence was designed to have an unstructured conformation in aqueous solution.[58] Variations on this protein polymer were later used by K. Kiick to create galactose-bearing glycopolypeptides.[59] These protein polymers contained carboxylic acid functional groups, introduced by the glutamic acid residue, for covalent modification with saccharides. In addition, the $(AG)_3$PEG protein polymer sequence has been used as a non-functional region in block-copolymers; this sequence was hypothesized to act as a flexible domain to increase protein block-copolymer solubility.[16]

Recombinant random coil proteins have also been investigated in hybrid hydrogels to present bioactive domains. Hubbell *et al.* introduced random coil protein polymers with cell adhesion and enzyme cleavage sites as crosslinkers of synthetic polymers.[60-62] This research illustrated the utility of combining protein polymers with traditional polymers to create modular materials.

Finally, random coil protein polymers have been investigated by the Barron laboratory as drag-tags for free solution electrophoresis of DNA. For this application, a key criterion is that the drag-tag must be absolutely monodisperse, excluding the use of synthetic polymers. The recombinant proteins produced in the Barron laboratory are shown in Table 2.3.

Table 2.2: Random Coil Protein Polymer Drag-Tags

Amino Acid Sequence [4, 5]	**Comments**
Gly-Ser-Gly-Gln-Gly-Glu-Ser	Well expressed, water soluble
Gly-Ala-Gly-Gln-Gly-Glu-Ala	Well expressed, water soluble
Gly-Val-Gly-Gln-Gly-Glu-Val	Poorly expressed, difficult purification
Gly-Leu-Gly-Gln-Gly-Glu-Leu	Poorly expressed, difficult purification
Gly-Ala-Gly-Gln-Gly-Asn-Ala	Difficult purification; poor solubility
Gly-Ala-Gly-Ser-Gly-Ser-Ala	Poorly expressed
Gly-Ala-Gly-Thr-Gly-Ser-Ala	Well expressed, water soluble
Gly-Lys-Gly-Ser-Ala-Gln-Ala	Well expressed, water soluble

As presented in Table 2.3, the ability to predict the degree of expression and solubility of designed *de novo* protein polymer can be challenging, where a single amino acid replacement in the monomer can alter the host organism's response and the final protein behavior in solution.

2.4.2 α-Helical Protein Polymers

Recombinant helical proteins have been synthesized to mimic architectural features of alanine-rich proteins. Poly(alanine) sequences have served as a model for the folding of α-helical proteins due to alanine's high propensity to form a helix. The Kiick laboratory has created a family of helical *de novo* protein polymers based on the sequence (AAAAQ); variants included alternate glutamine spacing and glutamic acids residues to introduce reactive groups.[21, 63, 64] The conformational behavior and association of the helical protein polymers were investigated in biologically relevant conditions.[63] Furthermore, subsequent studies used variants as backbones for galactose-functionalization to act as high-affinity inhibitors of the cholera toxin.[64]

Helical protein polymers have also been investigated by Koltover *et al.* In this work, proteins with the sequence (A_3E) were used to form highly ordered complexes of the anionic protein polymers and cationic lipids.[65] The protein polymers had stable α-helical conformations with charge density matched to that of cationic lipid membranes, forming ordered complexes consisting of membrane stacks with anionic protein polymer layers absorbed on the surfaces of the cationic membrane bilayers. This research demonstrated the potential protein polymer directed electrostatic assembly of nanostructured materials. Similarly, the self-assembly of helical poly(glutamic acid) proteins have been investigated for the formation of LCs.[6, 66]

In general, helical stability is a function of amino acid sequence and temperature; the incorporation of poor helix-forming amino acids to introduce functionality, often results in a trade-off with material robustness and structure.

2.4.3 β-Sheet forming Protein Polymers

Recombinant proteins designed to form β-sheet secondary structures have recently been utilized for biomedical applications due to their self-assembling properties. *De novo* proteins that contain alternating polar and non-polar amino acids form β-sheets in either an anti-parallel or parallel pattern. The conformational properties, stability, and solubility are inherently dependent on amino acid sequence. One example is based on the repeat of AEAEAKAK (polyEAK), which forms β-sheet structures at low concentrations.[67] PolyEAK aggregates into amyloid-like fibers that have nanometer scale diameters (10-20 nm). In addition, alanine-glycine repeating units (AG) have been shown to form extended β-strands.[19, 68-72] For example, Tirrell *et al.* created polypeptides with the sequence $(AG)_xEG$ (x=3-6) that formed fibrils by β-sheet assembly.[72]

The limited research on recombinant β-sheet protein polymers may in part be due to the difficulty of synthesis which arises from their tendency to aggregate in solution. As protein polymer length increases, aggregation is amplified and the structures can be highly stable and resistant to denaturation, making purification difficult. Moreover, β-sheet aggregation can be difficult to control.

2.4.4 Coiled-Coil Protein Polymers

Coiled-coil self-assembly can be created by helical proteins that associate with each other through hydrophobic and electrostatic interactions. Coiled-coils are left-handed super-helical bundles composed of multiple right-handed helical proteins. The amino acid choice and placement in the α-helices allows for the design of coiled-coils with different association number as well as parallel and anti-parallel arrangements due to the electrostatic interactions.[73, 74] Coiled-coil recombinant protein polymers have been used to create hydrogels[16] and docking devices[75]. These recombinant proteins spontaneously self-assemble into well-defined supramolecular structures under the appropriate conditions. In addition, the specificity and stability can be altered by changing the hydrophobic core residues. The instability of the coiled-coil complex results in unfolding of the proteins, which can be advantageous for triggered superstructure collapse.

The first recombinant coiled-coil protein block copolymer, developed by Petka and Tirrell, was based on the residue pattern in the Jun oncogene protein which forms a weakly stabilized homodimer.[16, 76] These triblock proteins were [coiled-coil]-[random coil]-[coiled-coil] structures that showed reversible gelation behavior from the aggregation of the recombinant block-copolymers. Similarly, work in the Kopecek laboratory has shown that aggregation number,[77]

association state,[78] and aggregate stability[79] can have a range of values based on the primary sequence of the protein. Recombinant coiled-coils have been introduced into hybrid hydrogels with synthetic polymers for the display of receptor-binding epitopes.[73] In addition coiled-coils based on sequences from natural proteins have been used as crosslinkers of synthetic polymers, creating a temperature-sensitive hydrogel.[80] The temperature sensitivity was a result of changes in the primary structure of the coiled-coil domains.

Recombinant coiled-coil protein-based materials have been limited in application due to the instability of the coiled-coil superstructure. Coiled-coil recombinant proteins form networks above a set concentration; however, the networks dissolve when placed in excess buffer. For this reason, coiled-coil-based hydrogels require additional covalent bond formation for stabilization.[81] Furthermore, simple changes in amino acid sequence can appreciably affect recombinant protein polymer behavior and is difficult to predict *a priori*.

2.4.5 Protein Block-Copolymers

SLPs have been combined with ELPs to generate protein block-copolymers (SELPs) that can have different characteristics based on copolymer composition and sequence.[82] Incorporation of ELP blocks with SLPs generally increases the solubility and flexibility of the copolymers. Furthermore, molecular weight and amino acid sequence of the copolymers can be used to control the responsiveness of the protein to external stimuli, either forming a gel, or having reversible aggregation. SELPs have been investigated as injectable materials that self-assemble into hydrogels,[83] and the properties of these block-copolymers can be changed by altering the number of ELP or SELF blocks. For example, increasing the number of SLP blocks in the

copolymer can amplify the rate of gelation.[84] SELP-based hydrogels have been used for controlled release of bioactive agents has been investigated, where the release rate is controlled by molecular weight, composition of the proteins, and solution conditions.[82-84]

Silk and elastin-based and coiled-coil protein block-copolymers are the predominate copolymers studied to date, despite the fact that additional combinations of proteins sequences may produce novel materials with unpredicted functionality. The limited number of applied block protein copolymers may be due to difficulties with purification when each domain has very different hydrophobicity and charge. For example, a copolymer composed of a random coil sequence ($(AG)_3PEG_x$ where x = 8, 12, 16) and a highly hydrophobic α-helical sequence ($(GEG(LA)_5W(LA)_5Q_2$) was unable to be purified due to the very different solubilities of the corresponding blocks.[85]

2.5 Conclusions and Thesis Contributions

As illustrated by the examples presented, protein engineering offers unique contributions to biomaterial applications, where macromolecular architecture and function can be controlled at the nanoscale. Recombinant protein polymers combine biologically active domains of natural proteins with the flexibility of synthetic polymers. Nevertheless, the field of recombinant protein polymer-based materials is still in its infancy.

Research described in the following chapters expands the range of protein polymer-based materials. Two classes of *de novo* protein polymers as building blocks for producing novel materials were created. Chapters 3 and 4 exploit the stability and non-aggregating tendencies of α-helical proteins to create self-assembling materials. This research elucidates the entropic forces

between rigid helical protein polymers. Chapters 5-7 utilize random coil protein polymers as building blocks for biological applications. The *de novo* protein sequences generated overcome the difficulty of traditional recombinant protein polymers, where the inclusion of new bioactive or structural domains requires re-engineering of the entire gene. The research described in this thesis shows that recombinant protein polymer-based materials are a powerful tool to create new functional materials.

Chapter 3

Liquid Crystalline Properties of Benzylated Rod-Like Protein Polymers

3.1 Introduction

The ability to direct self-assembly of ordered molecular patterns is an important method toward development of new materials with structure and properties controlled at the nanoscale. Self-organization of monodisperse rod-shaped molecules and nanoparticles is an example of self-assembly that has been observed, for example, in concentrated solutions of virus particles and polymers with rigid backbones.[86] This self-assembly is driven by excluded volume interactions between the particles, and the resulting ordering should be directly controlled by the particle sizes and shapes. The phase diagrams of particle self-assembly have been extensively investigated using computer simulations.[2, 87] However, few studies have experimentally verified and exploited this phenomenon due to the lack of available methods for the synthesis of nanoscale rod-shaped particles with controlled diameter and length. While several pioneering studies demonstrated synthesis of polymers with rigid elongated backbones,[88] the resulting macromolecules had a distribution of lengths and, in some cases, concentration-dependent

conformations.[89] And while there exist natural virus particles with monodisperse rod shapes, it is difficult to engineer their dimensions or to adjust their inter-particle interactions.

The aims of this chapter are (i) to develop and optimize a method for synthesizing monodisperse cylindrical macromolecules with controlled nanoscale sizes and (ii) to experimentally investigate order and phase transitions in solutions of these novel molecules.

3.1.1 Macromolecular Self-Assembly

Spontaneous assembly and organization, is a common phenomenon in biological systems. Self-assembly can be driven by electrostatic interactions, hydrogen bonding, hydrophobic interactions, and dimensional interactions that, overall, reduce free energy of the self-assembling system. Dimensional interactions depend on the relative size, position, and accessibility of functional groups that can create energetically favorable associations between particles or macromolecules. Taking inspiration from natural systems, researchers are using self-assembly as a synthetic approach to generate complex structures from synthetically accessible building blocks. Strategies utilizing self-assembly have been created to make systems that range from the nano-scale, as in the case of nanoparticles[90, 91] to the millimeter-scale.[92, 93] These self-assembled materials have been pursued for a wide range of applications such as magnetic materials, nanoscale electronic devices, non-linear optical components, and biomaterials.[94-98]

3.1.2 Overview: Liquid Crystalline Materials

Liquid crystals (LCs) are a type of self-assembling system distinguished by having properties intermediate between those of a fully ordered crystalline solid and a disorganized

liquid. A requirement for a material to form LC phases, is that the building block must exhibit geometric anisotropy that promotes long range alignment.[99] Synthetic LCs have widespread commercial use in displays, and polymers in textile fibers.[100] This chapter presents the investigation of lyotropic rigid-rod like proteins that form LC phases depending on protein polymer concentration and particle aspect ratio.

LC phases can be classified into three distinct types based on positional and orientational arrangement: nematic, smectic, and hexagonal columnar. A nematic LC has an overall orientational order, where the molecules are oriented along an average direction (called the director). In the nematic phase there is no positional order among the molecules in relation to each other (Figure 3.1.1B). A smectic LC has both orientational and positional order; where the molecules form a layered structure with a random distribution of molecules within the layers (Figure 3.1.1C) The hexagonal columnar LC phase contains molecules that are positioned on a hexagonal lattice, where the distance from a molecule to its nearest neighbor is identical in all directions (Figure 3.1.1D). A hexagonal columnar phase typically has no additional lamellar ordering of the molecules – adding lamellar order moves the hexagonally ordered system into a class of so-called soft (disordered) solid.

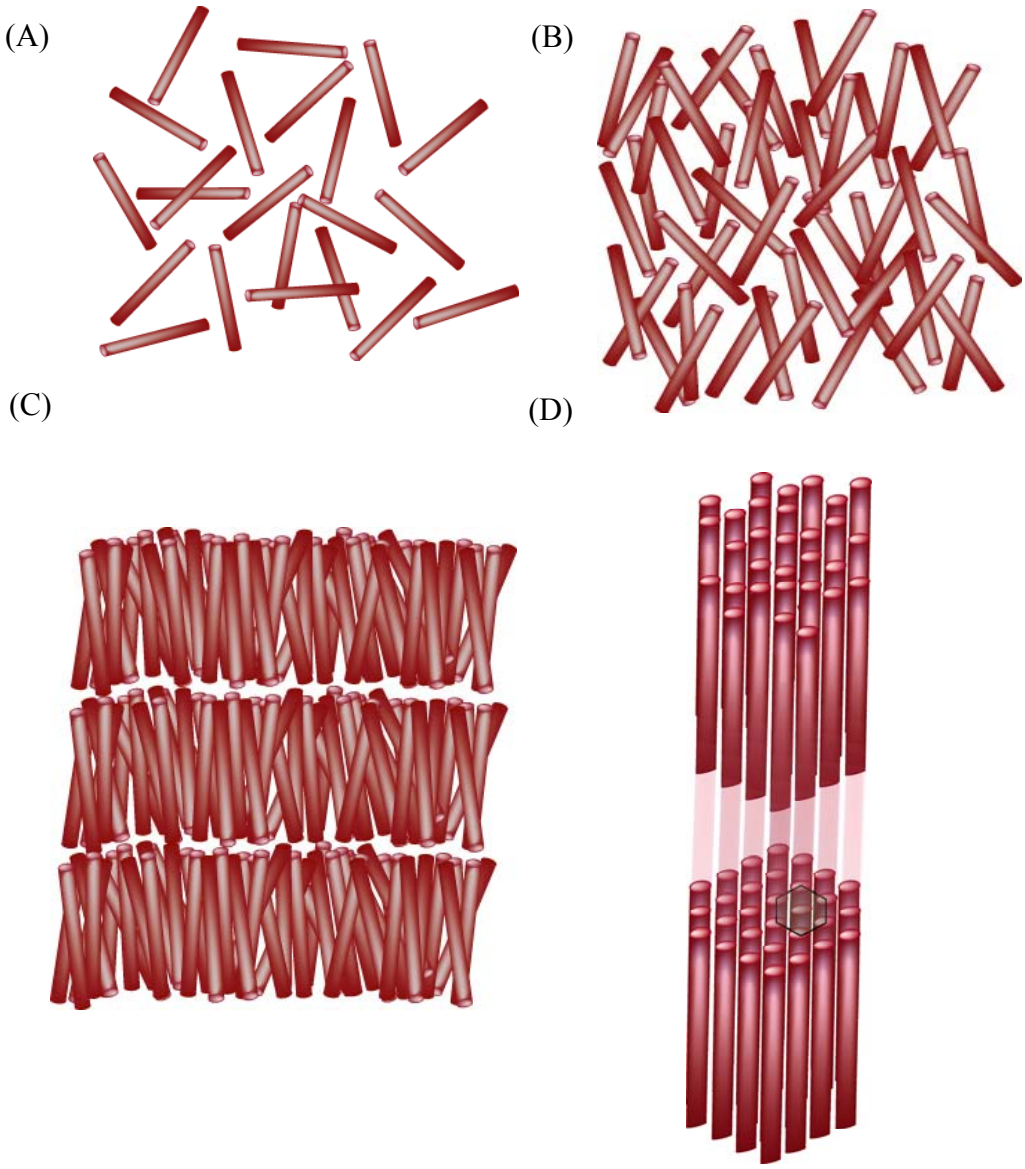

Figure 3.1.1: Schematic of the structural phases that can occur in solutions of rod-shaped molecules (A) liquid phase, (B) nematic liquid crystal, (C) smectic liquid crystal, (D) hexagonal liquid crystal with cross-sectional view.

To date there is little evidence for smectic phase occurrence in samples of chemical synthesized polymers due to their polydispersity. Monodisperse polymers and colloids, on the other hand,

are predicted to form stable smectic phases. For example, tobacco mosaic virus (TMV), a monodisperse rod-like particle forms smectic phases in concentrated aqueous solutions.[101]

3.1.3 Theoretic Predictions of LC Self-Assembly

The Gibbs phase rule[102] states that a two-component system cannot undergo an abrupt transition from isotropic (liquid) and fully LC state in response to changes in solute concentration. Rather, the system passes through a biphasic regime, where the volume fraction of LC phase increases over a finite concentration range. This biphasic region is where repulsive or excluded volume interactions dictate orientation and positional order. Theory based on first principles (mean-field theories of Flory)[87] predict a minimum length-to width ratio at which rods can self-assemble in LC phases, suggesting that LC phase formation is strongly controlled by concentration and aspect ratio.

The first model of LC ordering was developed in 1949 by L. Onsager. This model was created predominately to describe the ordering in TMV solutions.[103] The model describes rigid rod molecules of length L and diameter D, which only interact via hard-core repulsive forces. The Onsanger model assumed that there were no attractive interactions and LC phase formation was due to minimizing the free energy of the system, resulting in a maximum of entropy. The model showed that the transition from disordered to ordered phases was driven by an overall increase in entropy, implying that the stable LC ordered phase has higher entropy then the disordered phase. Furthermore, the model asserted that the number of accessible states in the stable ordered phase is larger than in the disordered phase at the same density, hence the formation of LC phases.

LC phase formation can also be explained by the lattice model as pioneered by P. Flory. The lattice theory stated that the steric repulsion between the particles are principally responsible for lyotropic LC systems.[87] The macromolecules were represented as "hard" bodies of a discrete size and shape with only repulsive interactions that occur if one molecule overlaps another since only one molecule at a time can occupy a given physical space. Furthermore, for the case of rigid rods, the aspect ratio of the macromolecules governs the concentration at which separation between the LCs occurs (Figure 3.1.2).

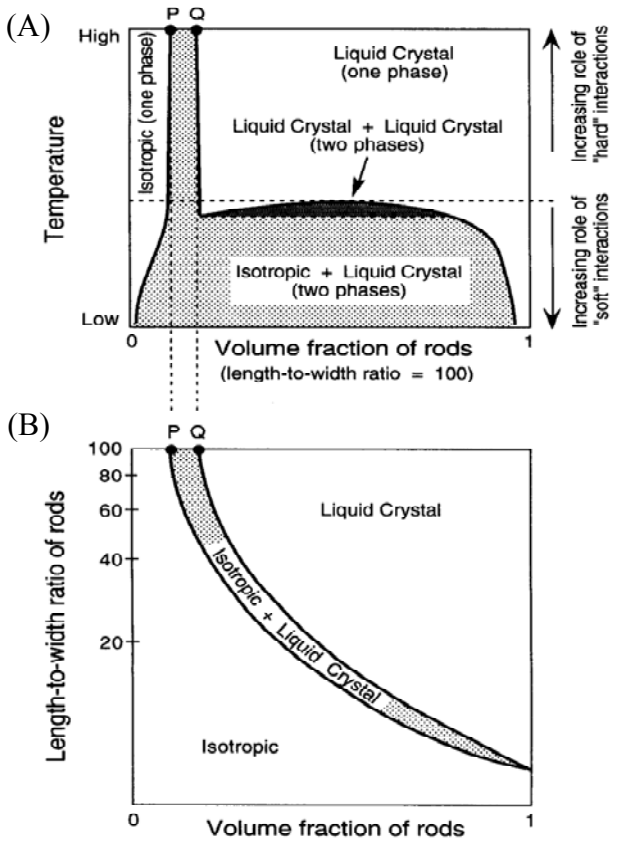

Figure 3.1.2: Phase diagram based on Flory theory. (A) Phase diagram for mesogens with an aspect ratio of 100. The narrow chimney of the biphasic region indicates conditions under which mesogen orientational order is dictated by hard-core interactions. (B) Limiting concentration range spanned by the biphasic chimney is a function of rod aspect ratio. (Figure from McGrath, 1997.)

A theoretical phase diagram was constructed using the lattice theory for polymer solutions by applying the model to a system composed of non-interacting, impenetrable rod-like solute particles. Using hard-core repulsive interactions as well as attractive forces, Flory concluded that a minimum aspect ratio of L/D=5.44 is required for co-existence of a LC and isotropic phase.[104] The Flory theory has been experimentally validated for polydisperse poly(γ-benzyl, α,L-glutamate) (PBLG); for example, Nakajima *et. al*. verified the Flory theory for the phase equilibria in the ternary systems PBLG-DMF-methanol and PBLG-DMF-water.[105]

A phase diagram for monodisperse hard rigid rod molecules as a function of shape anisotropy (aspect ratio, *L/D)* was calculated utilizing Monte Carlo simulations for particles with repulsive and hard-core interactions (Figure 3.1.3).[2]

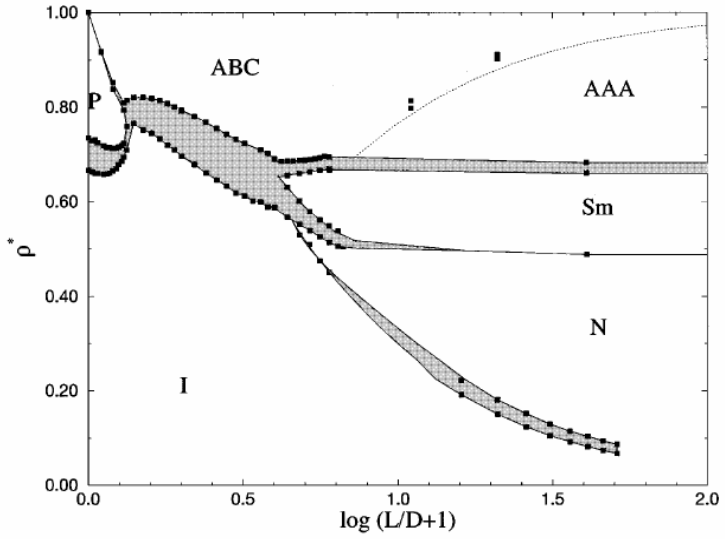

Figure 3.1.3: Phase diagram of predicted LC phases based on concentration as a function of aspect ratio for hard parallel rigid rods with L/D between 0 and 60. The shaded areas correspond to two-phase regions. For L/D > 3.7 the nematic (N) and smectic (Sm) phases are shown.[2] Note: AAA and ABC are different crystalline phases.

The simulation predicted formation of a smectic phase for *L/D* >3.7 and a triple point of coexistence between isotropic-nematic-smectic at an *L/D* = 3.7. This has not been experimentally validated due to the lack of availability of monodisperse rigid-rods.

3.1.4 Choice of a *De Novo* Protein Building Block

The polydispersity in synthesized polymers favors the hexagonal columnar ordering at the expense of the smectic ordering[106] and dilute LC solutions are generally limited to the nematic phase. Only monodisperse molecules are likely to form lamellar LC phases. Recently, it has been shown that genetically engineered molecules with stable α-helical structures can behave as anisotropic rod-like LC-forming molecules.[6] Inspired by research illustrating that polydisperse create poly(γ-benzyl-L-glutamate) (PBLG) can form liquid crystalline solutions[107] and ordered monolayer films,[108] Tirrell *et. al.* biologically synthesized monodisperse poly(α,L-glutamic acid) (PLGA), that when chemically benzylated to PBLG, display smectic ordering in solution.[6, 66]

Motivated by the work of Tirrell *el al.,* we have chosen PLGA as a starting material to fully investigate the LC phase diagram as a function of aspect ratio and concentration. First, the biosynthetic strategy was modified to overcome limitations in protein yields of the protein polymer. In addition, small amino acid domains were added to the N-terminus of PLGA to introduce potentially attractive forces for LC formation. It was hypothesized that mini-diblock polymers would have enhanced orientational and positional ordering, leading to a lower concentration to form smectic LC phases.

3.2 Experimental Materials and Methods

3.2.1 Genetic Engineering of Poly-Glutamic Acid

Short synthetic oligonucleotides were designed that were flanked by the restriction site *Bbs*I to encode the Glu_n monomers; monomer amino acids sequences were $EDE_{17}DE_2$ and $EDE_{35}DE_2$ (E = glutamic acid, D = aspartic acid) denoted $E_{20}D_2$ and $E_{38}D_2$, respectively (Figure 3.4.1). The oligonucleotides were purchased from Integrated DNA Technologies (IDT) (Coralville, IA) and used to created multimer genes using techniques of plasmid cloning in *E. coli* hosts.

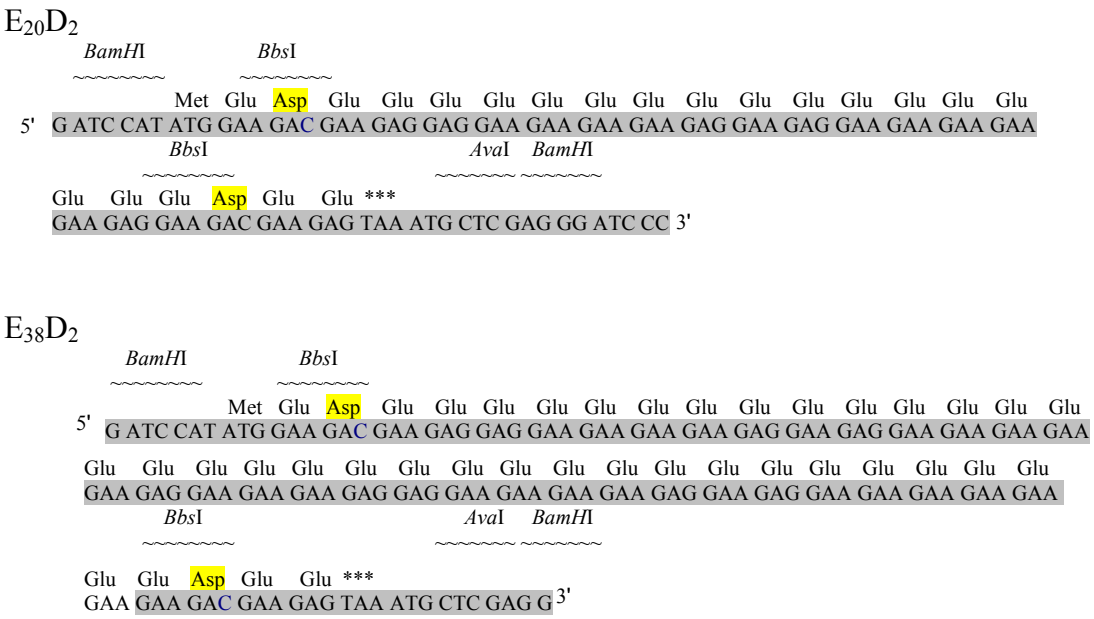

Figure 3.2.1: DNA oligonucleotides encoding $E_{20}D_2$ and $E_{38}D_2$ (E = glutamic acid, D = aspartic acid). The enzymatic restriction sites used in the gene construction are shown above. Note the generation of an D residue from the use of the *Bbs*I restriction site.

The forward and reverse oligonucleotides were purified separately by an 8% acrylamide denaturing gel, extracted and ethanol precipitated before annealing to form double-stranded monomers. The annealed $E_{38}D_2$ DNA monomers were purified by agarose gel electrophoresis. The DNA monomers had unpaired cohesive ends for T4 ligation into the *BamH*I digested pUC18 plasmid (Novagen, Madison, WI). Aliquots of the ligation mixture were used to transform competent cells of the *E. coli* strain NovaBlue (NB). Insertion of $E_{38}D_2$ was verified by a *Bam*HI digestion and gel electrophoresis analysis. $E_{20}D_2$ was prepared in a similar fashion. For subsequent cloning, one *Bbs*I restriction site was removed from $E_{38}D_2$ by a site-directed mutagenesis using a kit purchased from Stratagene (La Jolla, CA). Mutagenesis was performed according to manufacturer's recommendations and with primers (IDT, Coralville, IA) designed to change one of the D codons at the *Bbs*I site from GAC to GAG (into an E). After mutagenesis the gene was designated pUC18-$E_{39}D_1$ (cloning scheme illustrated in Figure 3.1.2).

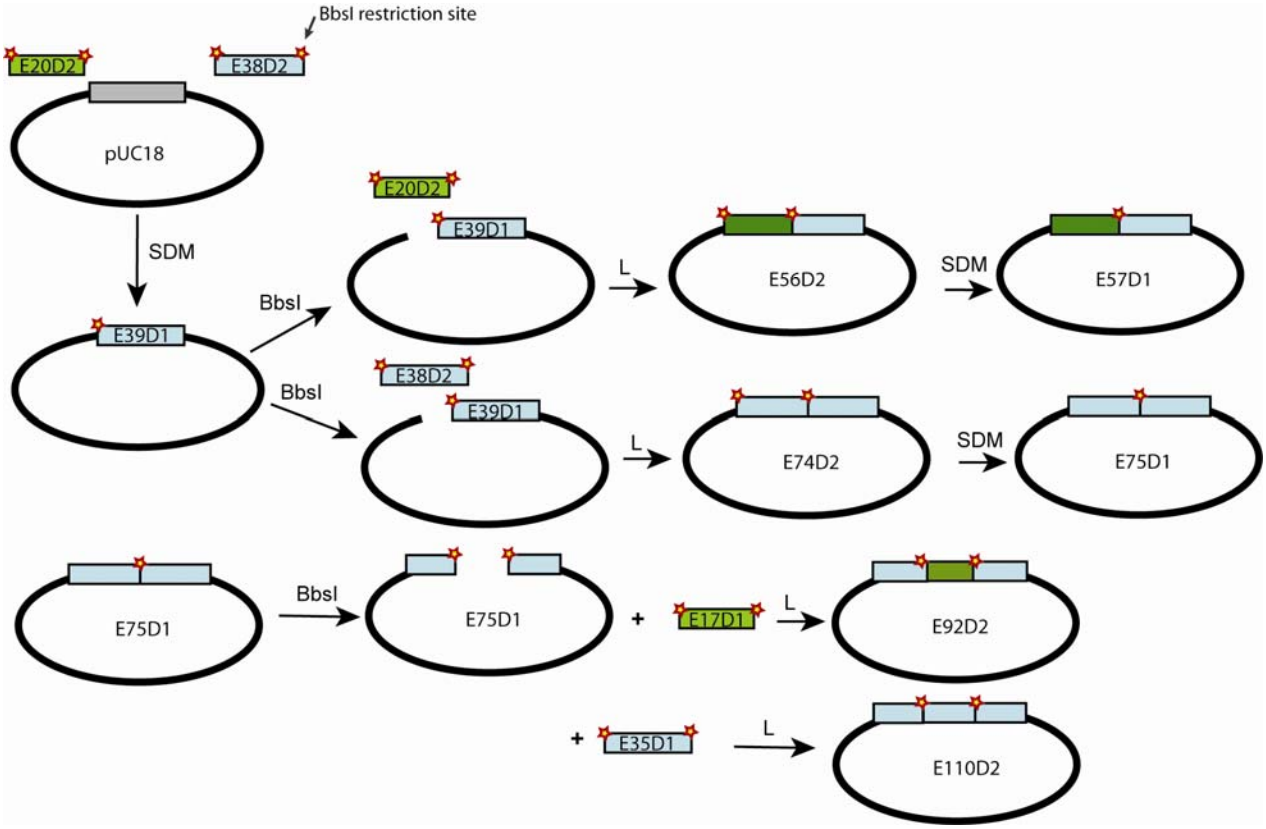

Figure 3.2.2 Cloning scheme to create different molecular lengths of E_nD_m. Star symbols denotes *Bbs*I restriction site. Cloning steps are abbreviated, where SDM is site-directed mutagenesis to remove a *Bbs*I restriction site (changing the D to an E), *Bbs*I represents an enzymatic digestion by the restriction enzyme, and L is a DNA ligation reaction by T4 ligase.

Success of mutagenesis was verified by *Bbs*I digestion and DNA sequencing. The pUC18-$E_{39}D_1$ was harvested from *E. Coli* NB cells and digested with *Bbs*I for multimer cloning. $E_{56}D_2$ was constructed by ligating *Bbs*I digested $E_{20}D_2$ into pUC18-$E_{39}D_1$ at the one remaining *Bbs*I restriction site. Similarly, $E_{74}D_2$ was produced by ligating digested $E_{38}D_2$ into pUC18-$E_{39}D_1$. For further cloning, one of the exterior Asp residues in both $E_{56}D_2$ and $E_{74}D_2$ were removed by site-directed mutagenesis and replaced by the glutamic acid codon GAG, thus eliminating the

*Bbs*I restriction sites; these genes were denoted $E_{57}D_1$ and $E_{75}D_1$, respectively, and used to generate longer sequences $E_{90}D_4$ and $E_{108}D_4$. $E_{90}D_4$ was cloned by ligating *Bbs*I digested $E_{20}D_2$ into $E_{75}D_1$ and $E_{108}D_4$ was created by ligating *Bbs*I digested $E_{39}D_1$ into $E_{75}D_1$. All ligations were performed using T4 ligase and insertion of the target genes into the pUC18 plasmid was verified by *BamH*I restriction digests of the rescued plasmids followed by gel electrophoresis.

The multimer genes were cloned into the expression vector pQE-15 (Qiagen, Inc. Valencia, CA) at the *Bgl*II site resulting in a fusion protein with dihydrofolate reductase (DHFR) and an N-terminal 6 x His tag (RGSHHHHHH). After transformation into *E. coli* M15 (Novagen, Gibbstown, NJ), the presence and orientation of insert was verified by an *Ava*I digestion and gel electrophoresis. DNA extracted from colonies containing the correct orientation and sequence was isolated and transformed into the *E. coli* expression strain BLR (DE3) (Novagen).

3.2.2 Cloning of Mini-Diblock Proteins

The mini-diblock segments, containing additional N-terminal amino acids, were first cloned into pUC18 using the restriction sites *Hind*III and *Eco*RI. For subsequent cloning, $E_{38}D_2$ was extracted from pUC18-$E_{38}D_2$ and digested overnight with *BbsI*. The $E_{38}D_2$ DNA was purified by a 2% agarose and then dimerized with T4 ligase for 2 hours at 16°C. A dimer of $E_{38}D_2$ (now $E_{74}D_2$), was extracted from a 2% agarose gel and then inserted into pUC18-miniblock at the *Bbs*I site. Correctly sequenced DNA was then BamHI digested and then ligated into the expression vector pQE15.

3.2.3 Protein Expression

Genetically engineered PLGA proteins were expressed as a fusion protein with histidine and dihydrofolate reductase (DHFR) tags at the N-terminal, (His-DHFR-E_nD_m) utilizing the expression system pQE-15 (Qiagen, Inc.). Protein expression was controlled by the T5 promoter system and carried out in a large scale fermentator. Briefly, a single colony of *E. coli* strain BLR (DE3) containing pQE15-E_nD_m was used to inoculate a 5 ml culture of 2 x YT media containing 200 μg/ml ampicillin and 250 μg/ml kanamycin. The starter culture was grown for 8 h at 37°C. Approximately 4 ml of starter culture was used to inoculate a 500 ml 2 x YT overnight culture, grown at 37°C with orbital shaking at 220 rpm. The cells were harvested by centrifugation at 3,000 rpm and resuspended in 500 ml of Super Broth medium. The suspension was added to a 12 L culture of Super Broth containing 200 μg/ml ampicillin, 25 μg/ml kanamycin, and 0.1 μg/ml antifoam in a Bioflow IV fermentation system under controlled conditions of dissolved oxygen 20% and a pH 7.3. The culture was induced with 0.1 mM β-isopropyl thiogalactoside at an OD_{600nm} of 2.0.

After 8 hours, cells were harvested by centrifugation. The wet cell mass was resuspended in ddH_2O at a concentration of 0.5 g/ml, three successive freeze thaw cycles were performed at -80°C and 37 °C to initiate breakup of the cell membranes. DNase (10 g/μl), RNAse (10 g/μl), $MgCl_2$ (5 mM) and phenylmethylsulfonyl (1 mM) were added to the cell lysate and the solution was incubated at 37°C overnight with agitation. The solution was centrifuged (40 min, 35,000 g, 4 °C) to separate soluble and insoluble fractions. The insoluble fraction was resuspended in denaturing buffer (100 mM NaH_2PO_4, 10 mM Tris·Cl, 8 M urea pH 8.0). Purification of the fusion protein was performed using Ni-NTA affinity chromatography (Chelating Sepharose FF,

GE Healthcare, Piscataway, New Jersey) under denaturing conditions. The fusion protein eluted in 250 mM imidazole buffer.

Following salt removal, proteins were separated from the (6 x His)-DHFR by cleaving with cyanogen bromide at the methionine residue. The Cleavage reaction was performed at a protein concentration of 2 mg/ml in Gn·HCl (guanidinium hydrochloride), 0.1 M HCl, 50 mM CNBr for 72 h. Cyanogen bromide was removed by rotary evaporation followed by dialysis (Spectrapor MWCO3000 membrane) against deionized water. After dialysis, the proteins were dissolved in 25 mM Tris buffer (pH 8.0); the soluble fraction was purified by anion-exchange chromatography (HiLoad 16/10 Q Sepharose HP column, GE Healthcare) using 1 M NaCl gradient elution and isolated by dialysis and lyophilization. Typical yields were 50 mg of purified protein per liter of expression culture and the amount of expressed protein was inversely proportional to the length of the protein construct. Protein purity was assessed by amino acid analysis and MALDI-TOF mass spectrometry (Table 3.1.1). Purified proteins were designated Glu_x where x is the total number of amino acids.

Table 3.1.1: Glu_x Proteins Expressed

Polypeptide cores	AA sequence	Number of residues	Measured and Calculated Molecular Weight (Da)	Amino Acid Composition (Approximate # of reisudes)
Glu_{40}	$EDE_{35}DE_2$	40	5860.3 (5852.1)	NA
Glu_{58}	$E_{37}DE_{20}$	58	7493.1 (7493.7)	NA
Glu_{76}	$E_{37}DE_{38}$	76	9812.5 (9812.2)	E:D: 74.6 : 1.1
Glu_{94}	$E_{37}DE_{17}DE_{38}$	94	12125.2 (12122.0)	E:D: 90 : 2.2
Glu_{112}	$E_{37}DE_{35}DE_{38}$	112	16502.3 (16436.0)	E:D: 106.3 : 2.4

3.2.4 Benzylation of Purified PLGA Proteins

Phenyldiazomethane was synthesized by first dissolving benzaldehyde tosylhyradzone (2.7 mM) in benzene with heating to 40°C. Next, a 14% (w/w) aq. NaOH solution containing 0.03 mM of benzyltriethylammonium chloride was added to the mixture and refluxed with stirring at 80°C for 5 hours in the dark. The benzene phase containing the phenyldiazomethane was separated, washed with water and dried over Na_2SO_4.

Benzylated protein, denoted Glu_x-D_0 (chemically identical to PBLG) was created by acidifying the protein Glu_x (0.6 mM) in a dioxane HCL solution with a pH of 1.1, (Figure 3.2.4).

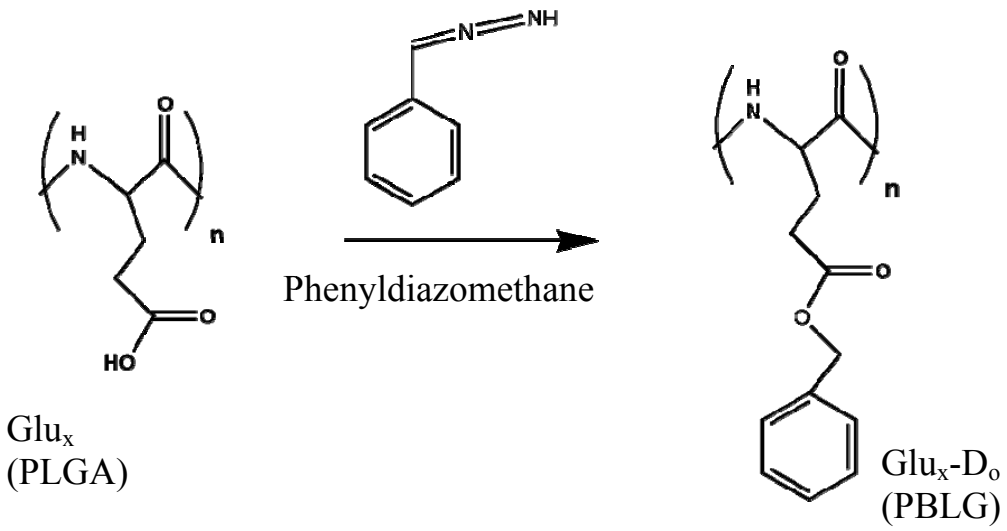

Figure 3.2.3: Monodisperse Glu_x-D_0 was formed by reacting phenyldiazomethane with genetically engineered Glu_x.

With the carboxylic acid completely acidified, the dioxane was removed by rotary evaporation and the Glu_x was washed extensively with water. This was then lyophilized and dissolved in DMSO. Phenyldiazomethane solution was added and the mixture stirred for 2 days at room temperature. The remaining DMSO was removed by vacuum distillation at 60°C and the residual solids were dissolved in methylene chloride and precipitated by addition to cold TBME (tert-butyl methyl ether) followed by final precipitation in cold pentane.

3.2.5 Protein Molecular Characterization

Secondary structure of purified Glu_x-D_0 protein polymers was determined by circular dichroism (CD), wide-angle X-ray scattering (WAXS), and ^{13}C NMR. CD spectra were recorded on a Jasco-715 spectrometer with 0.2 nm scan step and 5nm bandwidth. CD

experiments were conducted at 25 °C, using a 1 mm path-length cuvette with solutions of 5 μM Glu_x in dioxane. WAXS was performed on pulled polypeptide fibers at Northwestern University, Evanston, Illinois, USA.

Solution ^{1}H-NMR was used to confirmed backbone confirmation. NMR spectra were recorded using a Varian INOVA 500 FT-NMR spectrometer (499.6 MHz for ^{1}H NMR, 125.6 MHz for ^{13}C NMR). ^{1}H or ^{13}C NMR chemical shifts are reported downfield from Me_4Si and were determined by reference to the residual ^{1}H or ^{13}C solvent peaks, with CHd_2Cl peak being the one of choice for solvent mixtures. Approximately, 5 mg of protein was dissolved in 1 ml of $CDCl_3$ with 1% w/w trifluoroacetic acid (CF_3COOD). Unless indicated, peaks in NMR spectra are singlets.

3.2.6 X-ray Diffraction of Glu_x-D_0 LCs

Liquid crystalline solutions were prepared by dissolving solid Glu_x-D_0 (x = 58, 76, 94) in m-cresol at various concentrations and used for X-ray diffraction experiments. Approximately 30 mg of the proteins were dissolved in the appropriate amount of m-cresol. All measurements of solvent and sample were weighed in triplicate using a high-precision microbalance. Samples were mixed by repeated centrifugation upright and inverted and annealed at 70°C for seven days. Additionally, dried thin films of Glu_x-D_0 (x = 58, 76, 94) were prepared by slowly concentrating the polymer in solutions of 3% TFA / 97% $CHCl_3$. These were then placed on a Teflon plate and annealed at room temperature for several days with solvent transfer of $CHCl_3$ and varying amounts of TFA (1-3%). The solvent was evaporated over another several days and the film was removed from the Teflon and used for polarized optical microscopy and X-ray diffraction experiments.

For the X-ray experiments, samples were transferred into sample holders that consisted of two 20-μm-thick mica windows separated by a 1 mm teflon spacer. Synchotron X-ray diffraction experiments were conducted at the 5-IDD beam line of the DuPont-Northwestern-Dow Collaborative Access Team (DND-CAT) Synchrotron Research Center at the Advanced Photon Source (Argonne National Laboratory, Chicago, IL). Undulator X-ray beam was monochromatized to 13.5 keV with Si double-bounce monochromator and defined to a 0.15-mm^2 size using a set of four slits. X-ray diffraction patterns were recorded on an MAR-CCD detector with 162 mm diameter and 78.75 μm^2 pixels and analyzed using FIT-2D software (ESRF). Sample to detector distance ranged from 0.5 to 3m. Typical scans consisted of three averaged 10-second exposure frames. No sample degradation due to radiation damage was observed over 10 minutes of repetitive exposures. Ring diffraction patterns were indicative of powder samples (lacking alignment) and were integrated to give 2D intensity plots to determine intermolecular spacing of the LC phases.

3.2.7 Polarized Optical Microscopy of LCs

Polarized optical microscopy was conducted with Glu_x-D_0 (x = 58, 76, 94) in m-cresol solution at a range of weight percentages. Briefly, samples were applied to a glass cover slide and were immediately viewed using a Nikon Optiphot-200 microscope with a 20 x objective. Images were captured using a cooled color CCD camera.

3.3 Results and Discussion

3.3.1 Synthesis and Purification of Glu_x Proteins

The biosynthetic strategy to create the DNA genes was optimized to limit the non-glutamic acid residues encoded in the gene. The restriction enzyme *Bbs*I, which cleaves at the recognition sequence GAAGAC, was utilized so that the GAA encoded glutamic acid (E) and the GAC corresponded to aspartic acid (D). Gene multimerization resulted in D codons near each gene termini and one to two residues in the gene interior. The terminal D codons were removed by site-directed mutagenesis, where one DNA base pair was modified to change the codon to E. This effectively limited the potential for acidic degradation at the D residues in the corresponding protein during benzylation and subsequent handling steps.[109]

Previously, bacterial expression of Glu_x generally resulted in low yields of pure polypeptides. Tirrell *et. al.* reported yields on the order of 4-10 mg/L and expression levels inversely proportional to polypeptide length.[110] The low level of Glu_x production in *E. coli* bacteria is caused by poor translation at the ribosomal level.[111] *E. coli* ribosomes initiate translation on mRNA by binding to the Shine-Dalgarno (SD) sequence upstream of the initiation codon. The minimum consensus SD sequence is GAGG or GGAG, but can consist of up to 9 nucleotides (UAAGGAGGU).[112-114] As shown in Figure 3.2.1, the *E. coli* DNA codons for glutamic acid are either GAG or GAA. As a consequence, the codon sequence for Glu_x is rich in purines and contains regions similar to the SD consensus sequence. During translation, ribosome units become complexed with the Glu_x RNA within the gene and was hypothesized to slow down translation,[111] ultimately resulting in low protein yield.

For this reason, Glu_x was expressed as a fusion protein with DHFR, which effectively increases stabilization of the recombinant protein. In addition, the *E. Coli* cell strain BLR(DE3) was used for protein expression, where the BLR plasmid assists in stabilizing DNA encoding highly repetitive sequences. The BLR(DE3) cell line resulted in slower cell growth as compared to other common production strains. Protein production was enhanced by large scale expression in a 15 L fermentor with pH and dissolved oxygen control to ensure proper growing conditions. Furthermore, the concentration of IPTG used to induce expression, was decreased 10-fold (from a typical level of 1 μM) to 0.1 μM, and administered at an optical density of two, followed by protein expression for eight hours. Ultimately, this resulted in a decreased number of cells expressing protein for a longer period of time. Finally, the expressed proteins were removed from the fusion tags by cyanogen bromide cleavage in a non-conventional buffer (0.1M HCl, 6M GuHCl). The replacement of buffer, from the traditional 70% formic acid, allowed for a longer cleavage reaction and prevented the damage and formylation of proteins that can occur by formic acid.[115] Collectively, the alterations in biosynthetic strategy from previously reported methods[66] resulted in a 40-fold increase in protein yield (typical yield was ~ 50 mg/L). These increased quantities of purified PLGA were essential to explore a larger portion of the PBLG concentration –dependent phase diagram space.

3.3.2 Glu_x-D_0 Protein Molecular Characterization

Secondary structure (fold) of benzylated proteins was determined by CD spectroscopy. In general, organic solvents that dissolve Glu_x-D_0 (e.g. methylene chloride) strongly absorb in the far-UV spectral region (below 240 nm) characteristic of the CD signals of polypeptide

backbones. Samples for CD were prepared in dioxane because it was reasonably transparent down to 220 nm while still able to dissolve Glu_x-D_0 to a concentration sufficient to collect reliable CD spectra. A representative CD spectrum of Glu_{76}-D_0 has negative maxima at ~ 223 and 210 (Figure 3.3.1B). The basic shape of Glu_{76}-D_0 closely resembles that of a typical α-helix as shown in Figure 3.3.1A.

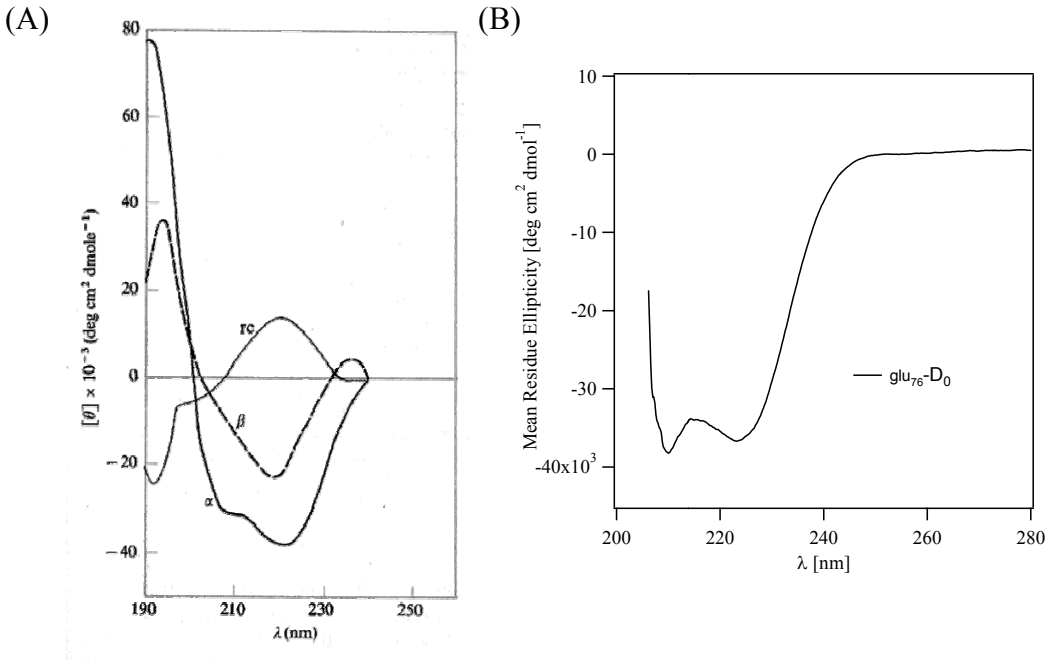

Figure 3.3.1: (A) CD spectra for α-helix, β-sheet, and random coil conformations, produced from the spectra of proteins of known three-dimensional structure. (B) CD spectra for Glu_{76}-D_0 at a concentration of 5 μM in dioxane.

WAXS scans of polydisperse Glu-D_0 exhibit scattering, where, the labeled layer line from diffraction in different horizontal planes, yields a helix pitch of 5.41Å (Figure 3.3.2). A tilted fiber produced a reflection at 1.5Å along the meridian, corresponding to spacing between amino acids along the polypeptide chain. The ratio of 5.41 to 1.5 results in 3.6 residues per turn, as expected for a well-defined polypeptide α-helix.

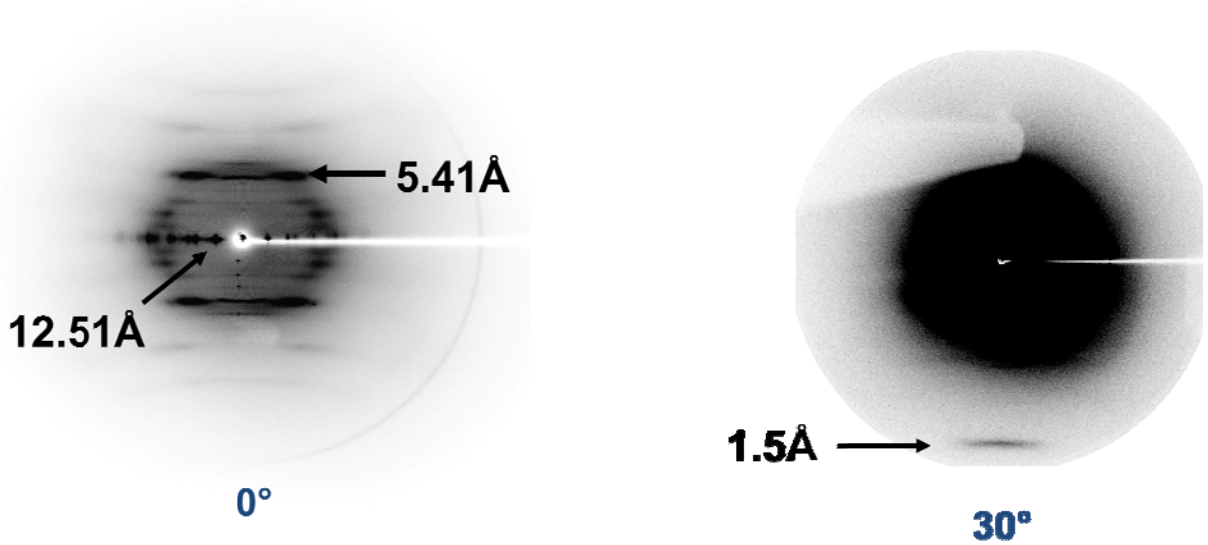

Figure 3.3.2: Wide-angle X-ray diffraction of a polydisperse Glu-D_0 fiber at 0˚ tilt. Fibers pulled from a 50% Glu-D_0 solution in dioxane. The helical pitch is given by the 5.41Å layer line. The axial rise per residue of 1.5Å is given by X-ray diffraction when the fiber is tilted 30˚. The ratio of 5.41 to 1.5 results in 3.6 residues per turn which is expected for a right-handed α-helix.

The scattering from polydisperse Glu-D_0 is similar to scatter from a known 3.6 residues per turn right-handed α-helix,[116] thus confirming that polydisperse Glu-D_0 is α-helical. We hypothesized that the WAXS scatter of polydisperse Glu-D_0 would be similar to the monodisperse protein polymers investigated in this study.

Finally, secondary structure of the monodisperse Glu_x-D_0 was confirmed by solution ^{1}H-NMR spectroscopy. NMR spectra will vary depending on protein conformation and can be detected by comparing an α-helical versus a random coil protein. As helicity of the peptide backbone is decreased by addition of trifluoro acetic acid (TFA) the spectra peaks become sharp due to increasing the fluidity of the disordered polypeptide chains. Moreover, as the α-helix is denatured, NMR α-carbon peaks shift upfield.[117] As TFA concentration was increased, the NMR spectra of Glu_{76}-D_0 displayed the characteristic peak shifts corresponding to protein unfolding (Figure 3.3.3).

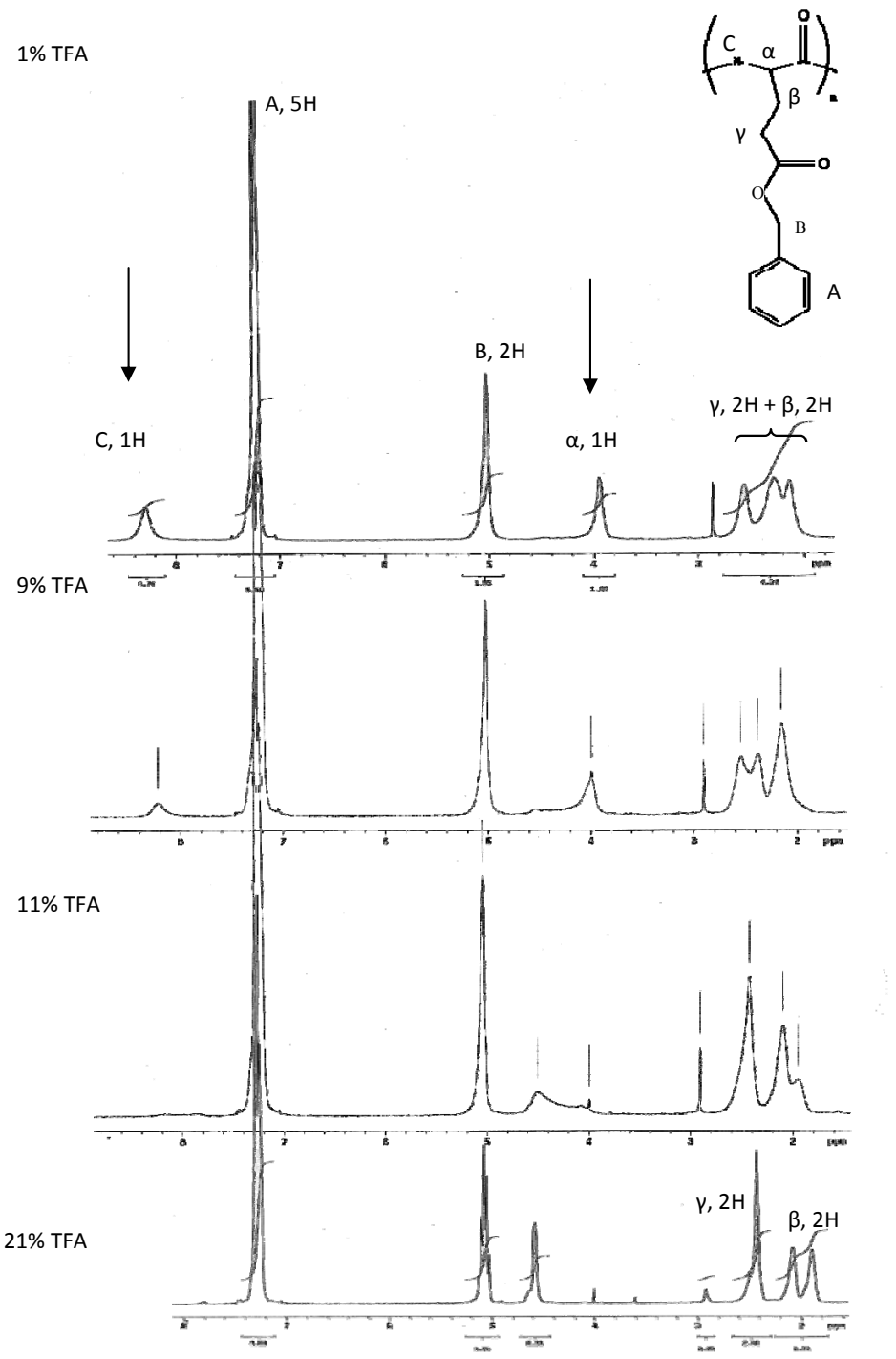

Figure 3.3.3: Glu_{76}-D_0 1H-NMR spectra with varied TFA concentration. Inset shows Glu_{76}-D_0 structure with labeled bonds

All NMR spectra show four distinctive sets of peaks corresponding to protons of outer phenyl rings, aryl protons of inner generations, benzyl protons, and amino acid backbone. The shift of the α-carbon hydrogen clearly moves from 3.9 to ~ 4.55ppm; in addition the amine proton peak disappears as a result of transition to the random coil conformation. Taken together, CD, NMR and WAXS strongly suggest that benzylated protein polymers are α-helical in solution and cast films.

3.3.3 LC Phases Characterized by X-ray Diffraction

X-ray diffraction was used to characterize long-range intermolecular order in the liquid crystalline materials. X-ray analysis maps the position of the molecules within the sample and determines the liquid crystalline phase. Intensity peaks are due to constructive interference that arises from periodicity in structure. Low-angle scattering was used to measure q_L which gave a repeat spacing equal to molecular length in the smectic LC phases. High-angle diffraction was used to measure q_T which indicated the spacing between molecules (Figure 3.3.4).

(A)

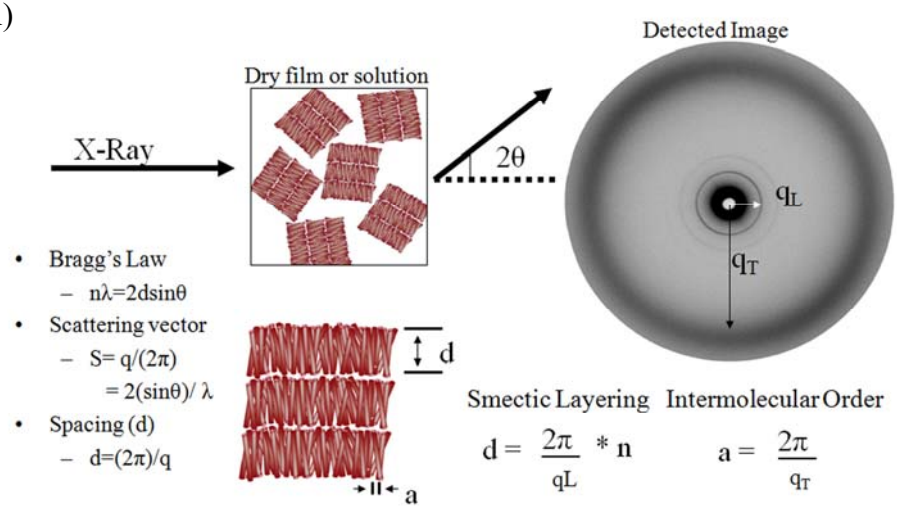

(B)

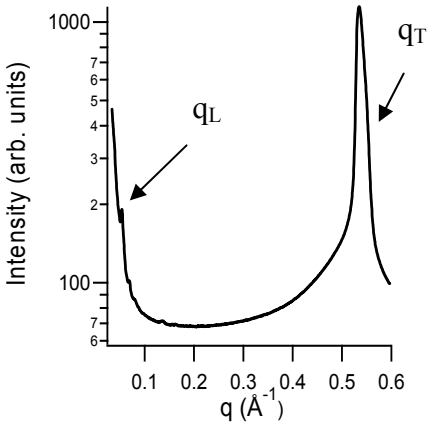

Figure 3.3.4: (A) Schematic of X-ray diffraction technique to characterize intermolecular order. Layer thickness and intermolecular spacing are given by the equations listed, where q_L is related to layer thickness d and n an integer arising from Bragg's law, q_T is related to intermolecular spacing a. Note: the concentric scattering circle indicates a powdered (non-aligned) sample. (B) Example intensity versus q spacing plot, created by intensity integration from the detected image.

The films of Glu_x-D_0 display different liquid crystalline phases as a function of TFA concentration used in sample casting. TFA was included in solvent casting because evidence suggests that Glu_x-D_0 has a strong tendency to aggregate in solutions at high concentration and TFA has been reported to inhibit aggregation while maintaining the protein rod-like behavior.[118] In the absence of TFA, wide angle X-ray diffraction patterns of Glu_{58}-D_0 and Glu_{76}-D_0 displayed a coexistence of nematic and hexagonal columnar phases, as indicated by the sharp peak, arising from hexagonal intermolecular order, and the broad shoulder from variation in intermolecular order in the nematic phase (Figure 3.3.5). The Glu_{94}-D_0 protein, however, exclusively developed hexagonal columnar phase as indicated by the shape peak at ~ 0.48 $\dot{A}^{-1}$. As the concentration of

TFA increased to 1.5%, all proteins were organized in the smectic phases (as indicated by the peaks at small q values). Increasing TFA to 3% when casting samples of Glu_{76}-D_0, appeared to decrease smectic order, indicated by the minimization of diffraction peaks. This affect is likely due to helical disruption by TFA as shown in Figure 3.3.3.

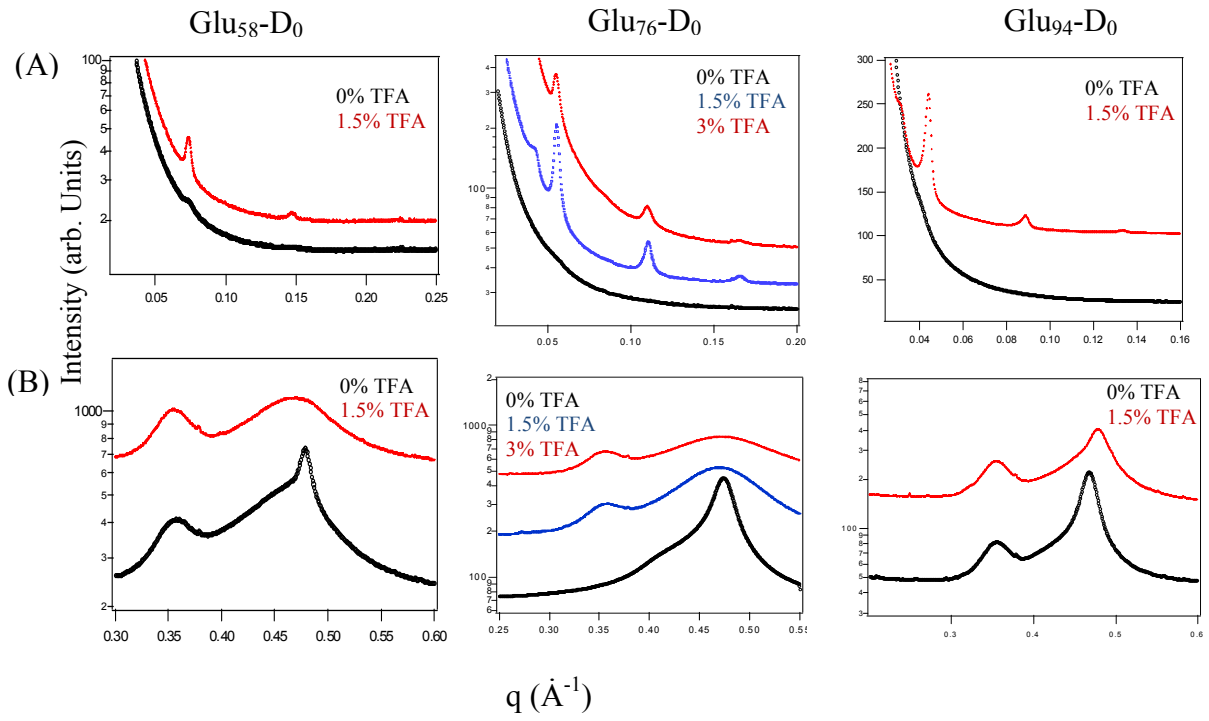

Figure 3.3.5: X-ray diffraction of thin films of Glu_x-D_0 cast from $CHCl_3$ with 0-3% TFA. (A) Small angle diffraction peaks indicate smectic LC phase. (B) Wide angle diffraction indicates intermolecular order to characterize hexagonal and smectic LC phases. Note samples contain an artifact peak at q=0.36Å^{-1} due to sample mounts.

Interestingly, the films displayed smectic phase for all protein lengths analyzed, contrary to the results observed previously by Tirrell et al. Thier study showed smectic-like odering in Glu_{76}-D_0 and Glu_{94}-D_0 in thin films cast from 3% TFA, however, Glu_{58}-D_0 did not show evidence of LC

behavior.[66] Despite the observations by Tirrell, the X-ray diffraction data illustrated in Figure 3.3.5 suggests that Glu_{58}-D_0 forms both smectic and hexagonal/nematic LC phases.

Furthermore, thin film X-ray diffraction was used to determine molecular length *L*. It was hypothesized that in the absence of solvent, dry films allow for the approximation of molecular length L, where L ≈ d. The X-ray diffraction smectic order peaks of thin films cast from 1.5% TFA of Glu_{58}-D_0, Glu_{76}-D_0, and Glu_{94}-D_0 were used to determine protein length (Figure 3.3.6).

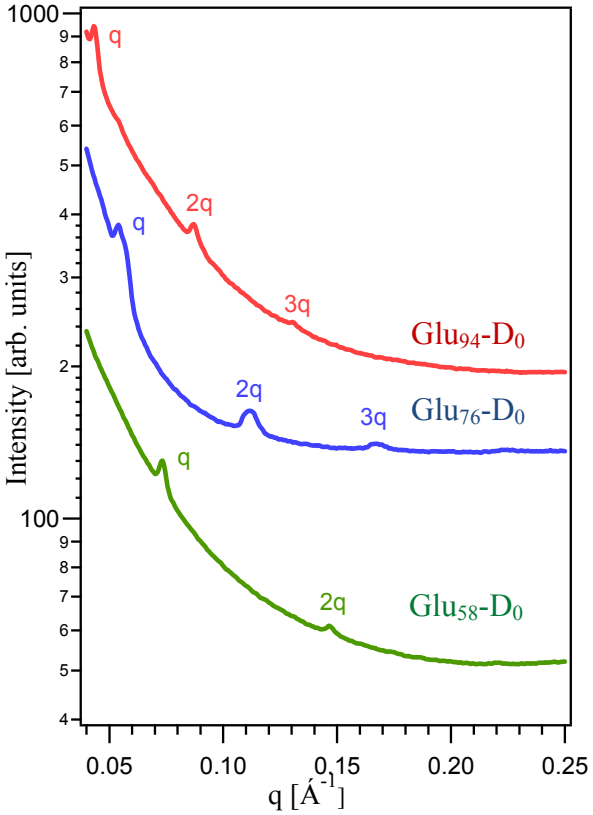

Figure 3.3.6: Low-angle X-ray diffraction scattering of Glu_x-D_0 films cast from 1.5% TFA/ $CHCl_3$ solution. Smectic phase diffraction peaks are observed with a spacing of 86Å for Glu_{58}-D_0, 114 Å for Glu_{76}-D_0, and 144 Å for Glu_{94}-D_0, determined from q values.

The q_L determined the observed molecular length using the equation $d = 2\pi / q$. The observed molecular length corresponded closely to the predicted length based on number of residues multiplied by 1.5 Å for an α-helical protein; Glu_{58}-D_0 observed at 86 Å (calculated 87 Å), Glu_{76}-D_0 observed at 114 Å (calculated 114 Å), and Glu_{94}-D_0 observed at 144 Å (calculated 141 Å).

Liquid crystalline phase behavior was investigated at varying concentrations of Glu_x-D_0 in m-cresol solution. As illustrated for Glu_{94}-D_0 LC phases of nematic, smectic and hexagonal are inferred from the X-ray scattering peaks (Figure 3.3.7).

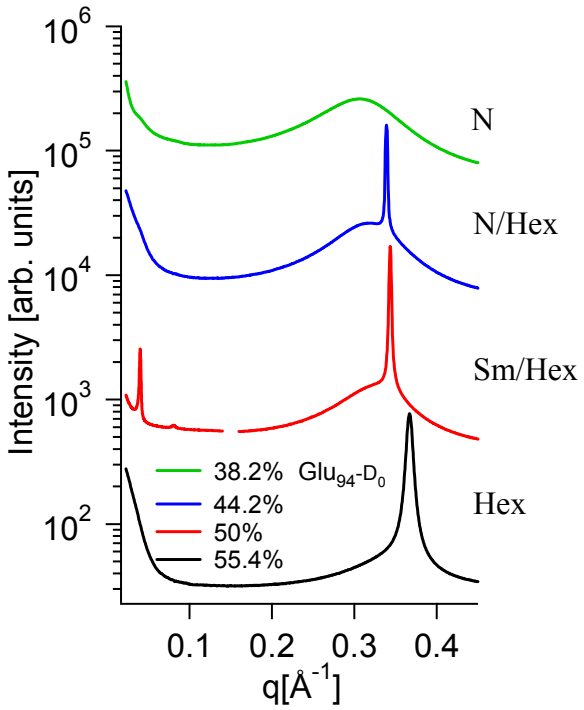

Figure 3.3.7: X-ray diffraction patterns of Glu_{94}-D_0 in m-cresol. LC phases are a function of protein concentration. LC phases are labeled where N denotes the nematic phase, Sm the smectic phase, and Hex the hexagonal columnar phase.

The nematic LC phase threshold for Glu_{94}-D_0 was near 40 wt% protein as indicated by the broad peak at ~ 0.3 $\dot{A}^{-1}$. As protein concentration was increased to 44.2 wt%, the LC phase transitioned to a coexistence between the hexagonal phase, indicated by the sharp peak due to regular close packing of molecules, and the nematic phase, where a broad distribution of intermolecular spacing and less closely spaced molecules, resulted in a broad scatter peak shifted toward smaller q. The SAXS diffraction peaks indicated the existence of the smectic LC phase at 50 wt% polymer (at small q). The narrow WAXS peak (at large q) of protein at 55.4 wt% implies the molecules are ordered in the hexagonal LC phase. The WAXS diffraction peaks shift to higher q values as protein concentration was increased; this indicates closer packing and less solvent between molecules.

Similarly, the LC phase formation for Glu_{58}-D_0 was dependent on protein concentration. The SAXS diffraction pattern, in concentrated samples of Glu_{58}-D_0 (73% protein), indicated smectic phase formation, based on the diffraction peak at 0.08$\dot{A}^{-1}$ (Figure 3.3.8A) and the broad peak at 0.43 $\dot{A}^{-1}$ (Figure 3.3.8B).

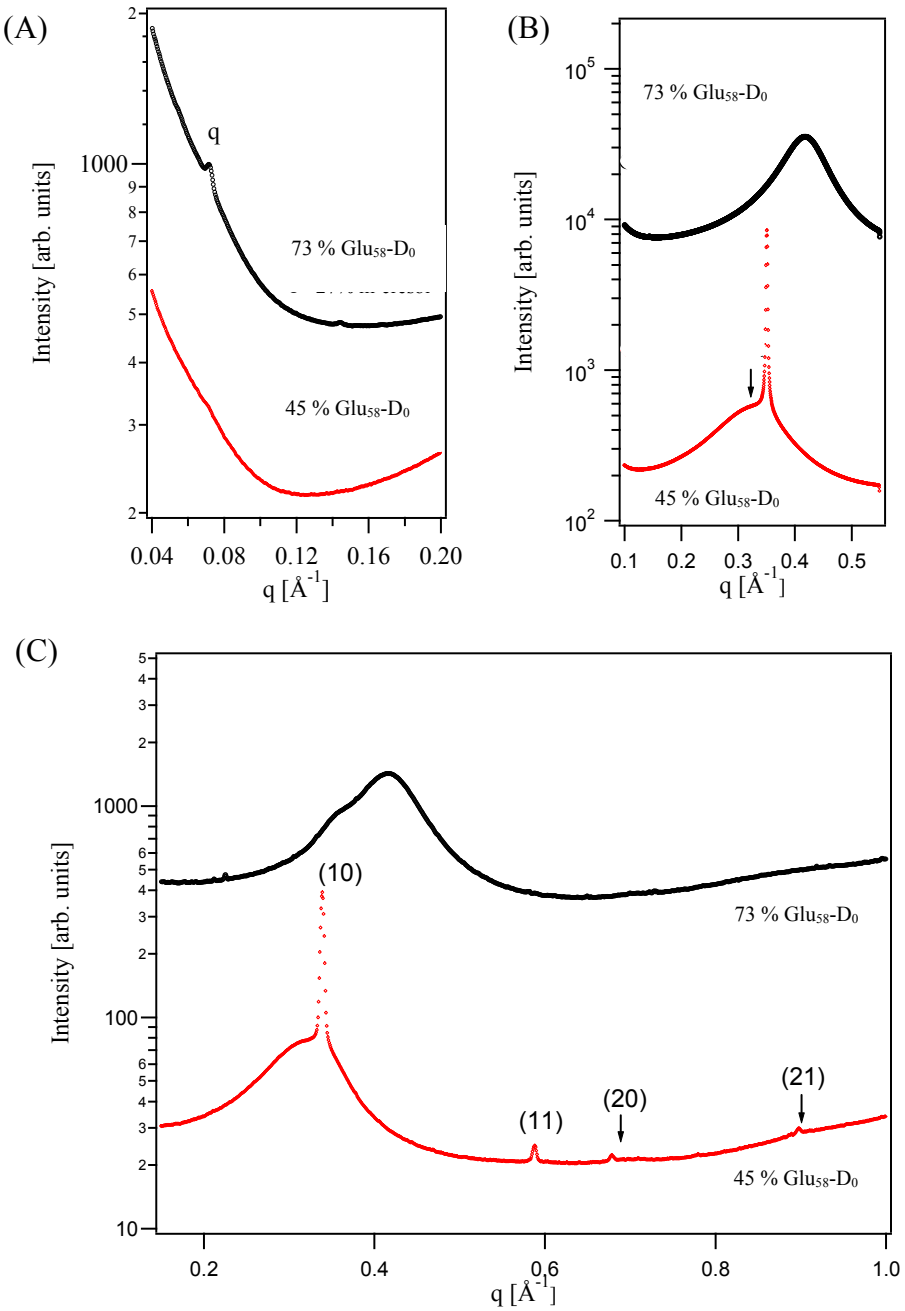

Figure 3.3.8: X-ray diffraction for solutions of Glu_{58}-D_0 as a function of m-cresol concentration. (A) Small angle scattering of Glu_{58}-D_0. Smectic liquid crystalline phase is evident in 73% protein. (B) Spectra mid angle indicates the absence of hexagonal phase (broad peak) in the 73% protein sample. The 45% protein sample displays both nematic phase (as shown by the arrow) and hexagonal phase (as indicated by sharp peak). (C) Wide angle scattering of Glu_{58}-D_0. The 45% protein sample displays nematic and hexagonal phase as indicated by sharp peak and labeled harmonics.

Glu_{58}-D_0 had diffraction peaks solely at 0.3 $Å^{-1}$ and 0.35 $Å^{-1}$, indicative of a coexistence between hexagonal and nematic LC phases. Furthermore, the WAXS diffraction plots display harmonics of hexagonal packing for Glu_{58}-D_0 at 45 wt%, suggesting long range hexagonal packing. This is consistent with previous research that demonstrated coexistence of nematic and hexagonal phase in polydisperse Glu-D_0 at 40%wt concentration in m-cresol.[119] Similarly, Glu_{76}-D_0 displayed different types of LC phases based on particle concentration. These observations confirm Glu_x-D_0 protein polymers are lytrophic, having concentration dependent LC formation and length of the protein affects phase transition thresholds.

3.3.4 Glu_x-D_0 LC Phases Confirmed by POM

Polarized optical microscopy allowed for the identification of LC phases based on optical texture generated from defects in molecular alignment and topology. In an isotropic (liquid) sample, the light is extinquished by the 90° crossed polarizers. LC samples, however, are birefringent and give rise to optical anisotropy, which results in an optical texture that gives information relating to the arrangement of the molecules within the phase.

The nematic phase typically has abrupt changes in director creating defects throughout the sample; these defects generate a Schlieren brush where optical extinction is caused by molecular alignment with the polarizers (Figure 3.3.9A and B). A focal-conic fan texture is observed with molecules ordered in the smectic phase due to energetically favorable packing of the layered structures, resulting in a system of curved equally spaced layers. In smectic phase, optical

discontinuities from structural arrangement of molecules within the phase appear as dark lines (Figure 3.3.9B).

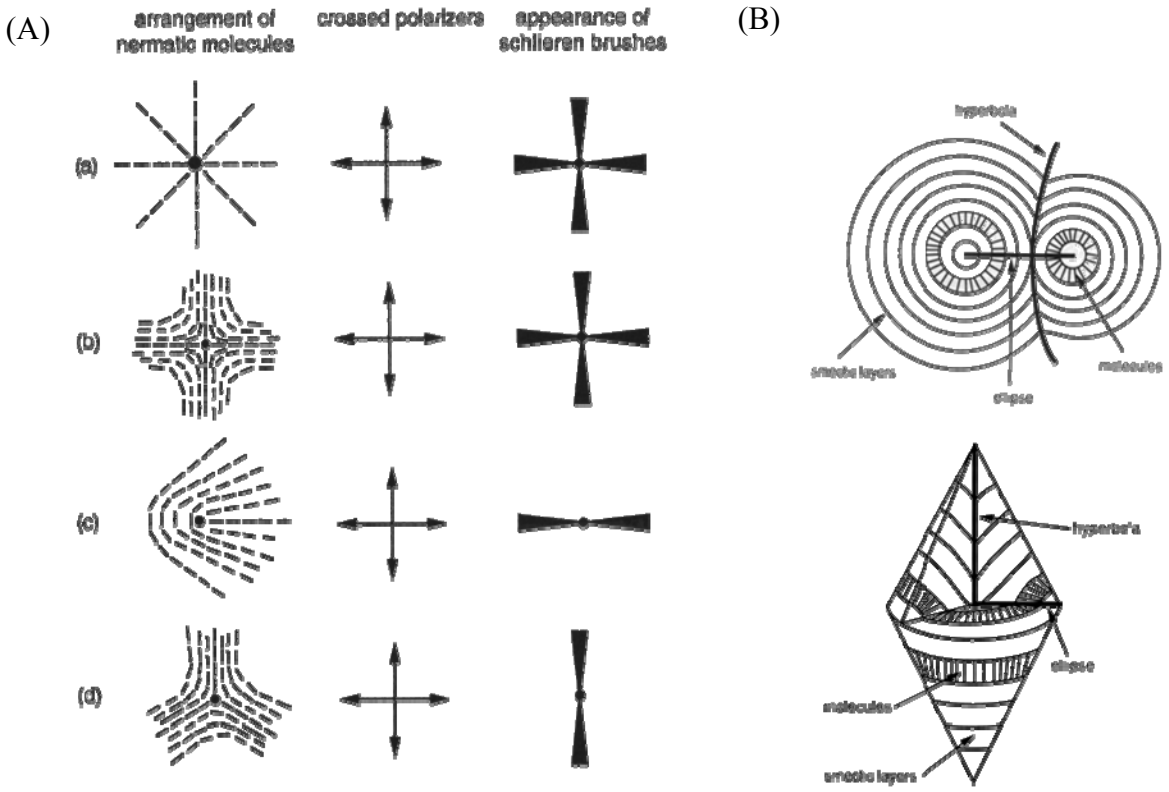

Figure 3.3.9: LC phase influence on POM textures.[1] (A) Nematic phase results in appearance of schlieren brushes where the director is aligned with the crossed polarizers. (B) Smectic phase results in the appearance in focal-conic fan textures due to layer packing.

Previous investigations have shown the change in optical texture as Glu_x-D_0 concentration increased; initially the solution separated into two phases, where more concentrated phase was birefringent and appeared as spherical liquid droplets.[66] In the current study, the POM images of Glu_{58}-D_0 at 30 wt% suggested a nematic LC phase based on the characteristic schlieren texture

observed (Figure 3.3.10 A). At an elevated concentration of 73 wt%, the POM images displayed the fan-like texture characteristic of the smectic LC phase (Figure 3.3.10 B).

(A) 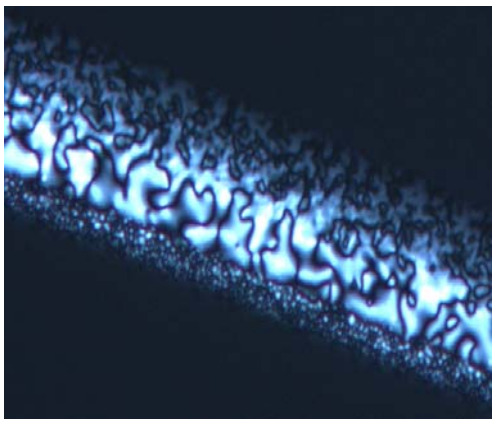 (B) 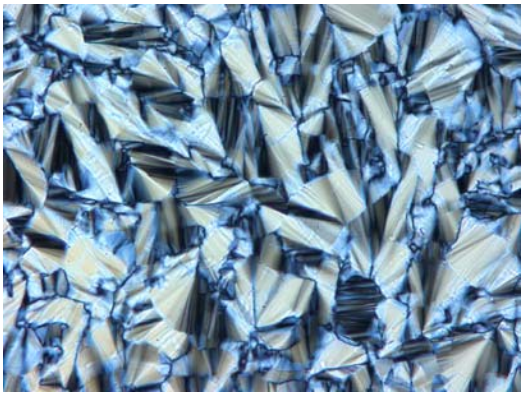

Figure 3.3.10: POM images of Glu_{58}-D_0 at (A) 30% protein, displaying the characteristic texture of nematic phase. The large black regions are due to sample preparation. (B) 73% protein shows the characteristic fan-like texture of the smectic phase.

3.3.5 Lyotropic Glu_x-D_0 LC Phase Diagram

The X-ray diffraction and POM results were used to generate a phase diagram based on aspect ratio and protein concentration. The aspect ratio was determined from the molecular length *L* calculated from Figure 3.3.6 and the diameter D calculated from X-ray diffraction peaks of the hexagonal phase in dry films (Figure 3.3.5). The range of aspect ratios of molecules used in the current experiments are shown in Table 3.2.

Table 3.3.2 Protein Aspect Ratios Based on Molecular

	Glu_{38}-D_0	Glu_{58}-D_0	Glu_{76}-D_0	Glu_{94}-D_0	Glu_{112}-D_0
Number of residues	38	58	76	94	112
Molecular Length	57Å	86Å	114Å	141Å	168 Å
Molecular Diameter	12.5Å	12.5Å	12.5Å	12.5Å	12.5Å
Aspect Ratio (L/D)	**4.6**	**6.9**	**9.1**	**11.3**	**13.4**

The LC phases as determined by X-ray diffraction and POM imaging were plotted as a function of protein concentration and aspect ratio (Figure 3.3.11).

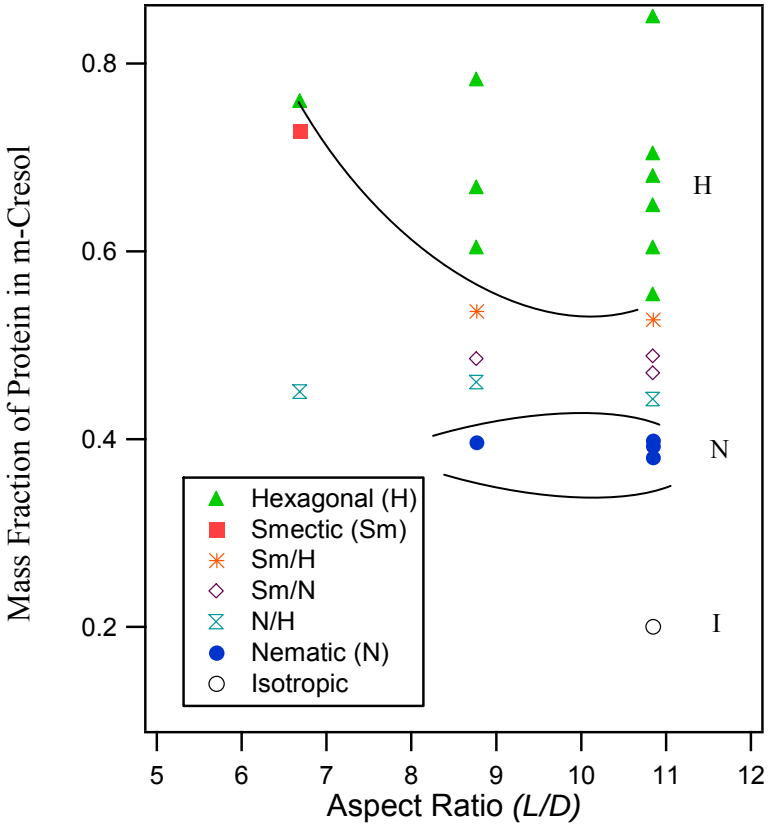

Figure 3.3.11: Phase diagram of Glu_x-D_0 in solutions of m-cresol. LC phase formation is a function of aspect ratio and mass fraction.

The phase diagram shows the approximate concentration and aspect ratio threshold to form LC phases. The smectic LC phase was observed at a low aspect ratio of 7.0 and a concentration of 74 wt% protein. In addition, a large region of coexisting phases was observed between all the LC phases. The phase diagram suggested that at higher aspect ratios the hexagonal phase had a lower threshold concentration.

The phase diagram differs from the data presented by Tirrell *et al.*; previously, POM images of Glu_{58}-D_0 did not indicate the formation LC phases at concentrations as high as 40 wt% protein in CH_3Cl.[66] The results presented in Figure 3.3.10 and Figure 3.3.11 indicated a nematic phase at a lower concentration of 30 wt% for Glu_{58}-D_0. Higher length proteins, Glu_{76}-D_0 and Glu_{94}-D_0 displayed exhibited nematic, smectic, and hexagonal LC phases both in the previous and the current investigation. Although, initial LC phase formation of benzylated protein polymers has been investigated, the lack of available materials limited the assessment of effects over a range of concentration. The ability to increase protein polymer yield allowed for the investigation of the full phase diagram. For this reason, the phase diagram identifies the necessary concentration and aspect ratio for the boundary points between the LC phases

Theoretic predictions based on Flory's rod-ordering theory suggest the minimum aspect ratio for the formation of a nematic LC phase is 6.42.[87] We, however, only observed a purely nematic phase at an aspect ratio of > 8. This may be due the deviations of this experimental system from an ideal "hard-rod" case, primarily due to attractive interactions between Glu_x-D_0 macromolecules. Incomplete shielding of the hydrophilic protein backbone by the benzyl side-chains could lead to effective attractive interactions (aggregation) between protein polymer

molecules. Moreover, the overall dipole moment of the polypeptide α-helix may also introduce additional dipole-dipole attractive interactions.

3.3.6 Mini-Diblock Proteins

Two mini-diblock proteins were created to investigate the effect of hydrogen-bonding and hydrophobic interactions on LC phase formation. The mini-diblocks were expressed with the addition of 2 or 3 amino acids to the N-terminus of the protein chain; it was hypothesized that the addition of a small number of residues would not disrupt LC phase formation. A mini-diblock composed of three L (leucine) residues preceding Glu_x-D_0 was created to study attraction forces due to hydrophobicity. The L resides are hydrophobic amino acids and have a high propensity to form α-helices which we hypothesized would not appreciably change the overall hydrophobicity, secondary structure or solubility of the proteins. We hypothesized that the un-benzylated L residues may aid in end-to-end association of the Glu_x-D_0 helices and encourage formation of the smectic phase. The second mini-diblock contained two Q (glutamine) residues preceding Glu_x-D_0. The Q residues were expected to maintain the α-helical secondary structure, and have a high propensity to form hydrogen bonds. It was hypothesized that the short Q block would encourage smectic LC phase formation at a lower concentration of molecules.

Both mini-diblocks appeared to enhance the formation of smectic phase, however the L block copolymer displayed a more ordered smectic phase, indicated by the larger SAXS peak at ~ 0.04 $\dot{A}^{-1}$ and the observance of the second bragg peak (n = 2) at ~ 0.1 $\dot{A}^{-1}$ (Figure 3.3.12).

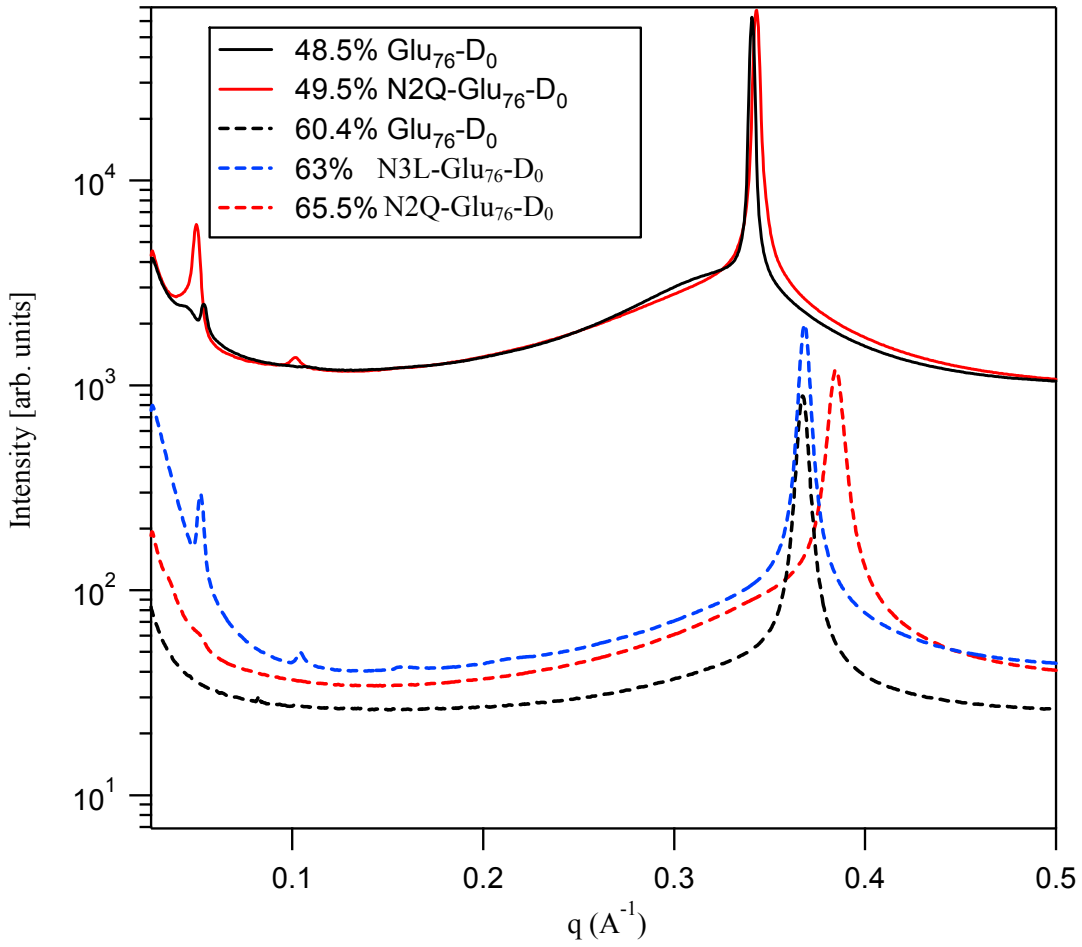

Figure 3.3.12: X-ray diffraction scattering of Glu_{76}-D_0, N3Leu- Glu_{76}-D_0, and N2Q-Glu_{76}-D_0.

At a concentration of ~ 60% protein, Glu_{76}-D_0 and N2Q-Glu_{76}-D_0 displayed hexagonal LC phase, whereas N3Leu-Glu_{76}-D_0 had low-angle diffraction peaks indicating smectic phase formation. This suggested that the hydrophobicity of the leucine residues may encourage aggregation and ultimately smectic phase formation. At a slightly higher concentration of protein (~ 49.5 wt% versus 48.5 wt% for Glu_{76}-D_0), the mini-diblock protein N2Q-Glu_{76}-D_0 had more pronounced low-angle peaks suggesting an enhancement of smectic layering. The hydrogen-

bonding effects of the glutamine mini-block only appeared to be applicable at relatively high protein concentrations. This could suggest the forces of hydrogen-bonding occur over shorter distances, which would be the case in a more closely packed (concentrated) sample. Conversely, hydrophobic aggregation may have longer range attraction effects. The mini-diblock proteins did not display increased lamellar spacing indicating a very strong *N*-terminal to *N*-terminal complexation (dimerization), where layer spacing would equal 2 times molecular length.

3.4 Conclusions and Future Directions

In summary, a biosynthetic strategy was created to increase yields of the Glu_x-D_0 proteins. This allowed for ample material to construct an experimental phase diagram of LC phase formation as a function of protein aspect ratio and concentration. The Glu_x-D_0 proteins were shown to have lyotropic liquid crystalline phases by high-resolution synchrotron X-ray diffraction and polarized optical microcopy. As concentration increased, LC phases transitioned from isotropic to nematic, to a coexistence region (between smectic, hexagonal, and nematic phases) and finally hexagonal columnar LC phase. We observed, for the first time, a smectic phase in Glu_{58}-D_0 samples, previously not observed. Solution-cast films of Glu_x-D_0 formed smectic LC phases where the layer spacing was approximately the same as expected molecular length. The addition of mini-diblocks that introduce some attractive force appeared to enhance smectic phase formation. These protein polymers may promote a fundamental understanding of the physics of rigid-rod-like protein self-assembly into LC phases. The precisely controlled

molecular dimensions of these proteins, due to the biosynthetic strategy, afford the formation of LC phases not accessible by polydisperse molecules.

Chapter 4

Liquid Crystalline Properties of Dendronized Protein Polymers

4.1 Introduction

As discussed in Chapter 3, self-assembly of ordered molecular patterns is a powerful route toward new materials. Success of this synthetic strategy, however, depends on the availability of well-defined molecular building blocks with nanoscale dimensions. In Chapter 3 we investigated LC phase formation as a function of concentration and molecule aspect ratio. The biosynthetic strategy presented, however, was limited in that only the molecular length *L* was able to be controlled, where the length was determined by the number of amino acids in the helical protein core. In this chapter we explore the use of dendrons to control molecular diameter *D* and investigate the LC properties as a function of concentration and shape anisotropy.

4.1.1 Dendronized Polymers

Dendrimers, highly branched macromolecules consisting of dendritic wedges (dendrons) attached to a small core are one type of a nanoscale building block.[120] Current uses of

dendronized molecules include catalysis,[121] drug delivery devices,[122, 123] biomedical magnetic resonance imaging,[124] and as biomaterial scaffolds.[125] Although most dendrimers have spherical architectures, recently the preparation of dendrimers with rod-like, cylindrical shapes has been described. Percec[126, 127] and Schluter[128, 129] have shown that the polymerization of dendronized monomers can give rise to dendritic polymers with elongated shapes, while Tomalia demonstrated that rod-shaped dendrimers can be prepared by step-wise growth of dendritic side-chains from a polymeric initiator backbone[130]. In these materials the focal points of the dendrons were connected to the pendant functional groups along the polymer backbone.

The combination of dendrimers and polymers (Figure 4.1.1A) has led to the development of hybrid architectures that are interesting for a multitude of applications.[3]

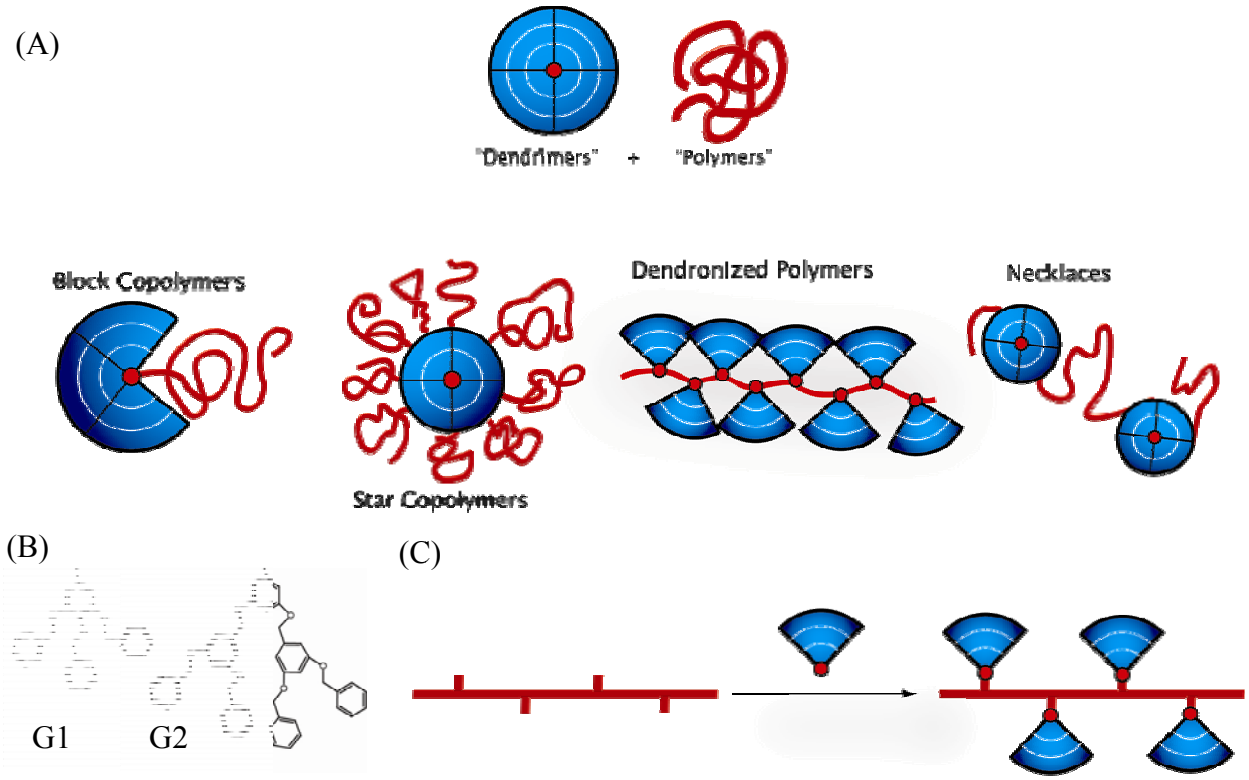

Figure 4.1.1: (A) Schematic illustration of the architectures derived from polymers and dendrimers (B) Frechet type dendrons, G1 and G2 denote generation one and two respectively. (C) Schematic illustration of Frechet type dendron grafting technique. Adapted schematics.[3]

The most common dendritic structures are dendronized polymers, created by a synthetic approach pioneered by R. Frechet (Figure 4.1.1B).[131] Typically, Frechet type dendrons are attached by the graft-to-route strategy, where the fully synthesized dendron is then grafted onto the polymer (Figure 4.1.1C).

Dendrimers prepared by these pioneering strategies possess well-defined diameters (*D*) and rigid shapes, but have a statistical distribution of lengths (*L*). Regardless, drendrimers have been shown to self-assembly into different structures, where the conformational behavior of dendronized polymers is influenced by steric repulsive force, and an attractive force due to π-π stacking of the dendritic side chains.[3]

In order to control molecular diameter of the protein polymers, we have chosen to combine dendrons with the approaches presented in Chapter 3. The monodisperse, α-helical polypeptide backbone Glu_x defines the length and overall rod shape of the target cylindrical macromolecule. Synthetic dendrons are then grafted to the reactive amino acid side-chains along the peptide backbone, covering it with a dendritic shell whose thickness is controlled by the generation and chemical structure of the dendrons (Figure 4.1.2). Theoretically, the wedge-shaped dendrons should pack nicely along the rod-like macromolecule backbone, we hypothesized that this would enhance the α-helix and rigid-rod stability. The resulting dendronized protein polymer (DPP) has length *L* and diameter *D* defined by the biological and chemical synthetic components, respectively.

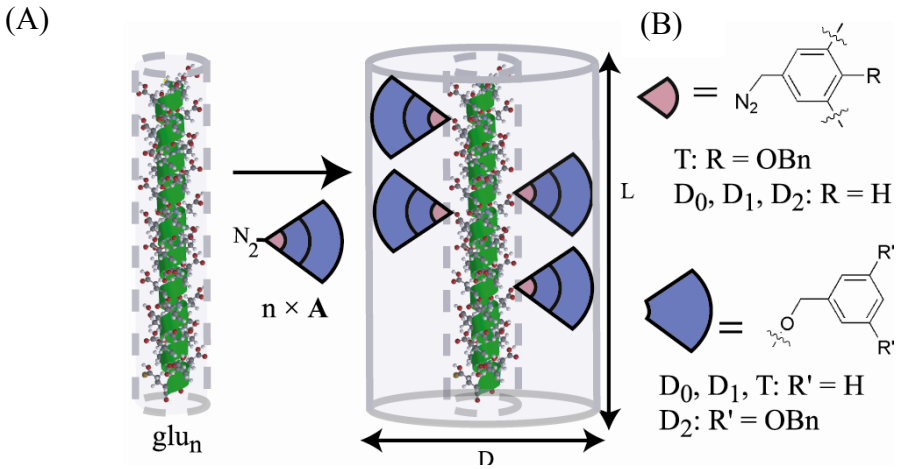

Figure 4.1.2: (A) Schematic of the biosynthesis of the DPPs. (B) Molecular scheme of dendritic wedges that are grafted onto the PLGA backbone.

The well packed dendrons around the polypeptide core would cause stiffening of the polymeric backbone due to steric repulsion between the pendant dendrons. In densely functionalized versions, the macromolecule would behave as a molecular cylinder with defined dimensions controlled by the dendron generation.[132] The defined rigid-rod molecules are predicted to form liquid crystalline phases based on concentration and shape, controlled by dendron generation and protein length.

4.2 Experimental Section

4.2.1 Dendronization of the PLGA Macromolecules

Cloning, expression, and purification of the Glu$_x$ proteins, where x = 38, 58, 76, 94, 112, is described in Chapter 3. The synthesis of benzylated (zero-order) Glu$_x$-D$_0$ was discussed in Chapter 3. The additional dendritic side chains were prepared using the convergent approach

developed by Frechet.[133] Dendrons were synthesized and purified by M. Zhuravel (details in Appendix B). Briefly, poly(benzyl ether) dendrons with an aldehyde function at the focal point were converted to tosylhydrazones, which resulted in the corresponding diazo-fuctionalized dendrons upon treatment with an aqueous base. Reaction of excess dendron with the carboxylic acid side chains of the Glu_x cores in DMSO efficiently positioned the wedge-shaped benzyl ether dendrons around the rod-like helical peptide core to complete the DPP cylinder. The large molecular weight difference between monodisperse DPPs (25-81 kDa, depending on peptide length and dendron type) and non-reacted dendron byproducts (0.1-1 kDa) combined with good solubility of the Glu_x-D_1, D_2 macromolecules, allowed us to purify DPPs in a single step using size-exclusion chromatography. Purified DPPs were isolated as white solids, and were completely soluble in the same common organic solvents as monomeric dendrons (chloroform, methylene chloride, dioxane), indicating complete sequestration of the polar peptide cores within the dendritic jackets. Dendrons of either primary or secondary generation with two (D) and three (T) peripheral benzyls were created with size increasing in the order of $D_0 < D_1 < T < D_2$. The resulting DPPs were analyzed using low-resolution MALDI-TOF spectrometry, recorded by Dr. David Headstrand (CMU research corporation) on a Bruker Autoflex spectrometer, with a dithranol/Ag(CF_3COO) matrix.

H^1 NMR spectroscopy characterization of DPP samples was done by dissolving the appropriate DPP (5mg) in $CDCl_3$ (1 ml containing 1% protein w/w). The addition of trifluoroacetic acid was required to dissolve Glu_x-D_0 exclusively, so for consistency 1% w/w CF_3COOD was added to all the $CDCl_3$ solutions of DPPs. NMR was done by Dr. Ilya Koltover on a Varian INOVA 500 FT-NMR spectrometer. All NMR spectra show four distinctive sets of

peaks: outer phenyl rings, aryl protons of inner generations, benzyl protons, and amino acid backbone. The integration results are consistent with a complete dendronization of the polypeptide cores, with the exception of Glu_{94}-D_1 (90% degree of dendronization).

4.2.2 Molecular Modeling of the DPPs

Molecular models of the DPPs were constructed using the Materials Studio software package (Accelrys). Peptide backbones were assembled from the corresponding amino acid residues using the conventional 18/5 α-helix dihedral angles. The dendritic side-chains were attached to the carboxylic acids of the helical peptides, and the entire molecule conformation was subjected to energy minimization with fixed conformation of the peptide backbone.

4.2.3 Characterization of DPP Conformations

FTIR and Circular dichroism (CD) spectroscopy were used to examine the conformations of the resulting DPPs. FTIR experiments were conducted with DPP solutions in organic solvent drop-cast on KBr disks. Transmission-mode Fourier-Transform Infrared (FTIR) spectra were recorded at 4 cm^{-1} resolution on the Nicolet Nexus-870 spectrometer. CD experiments were conducted using a 1mm path-length cuvette with solutions of DPPs at 5 μM in dioxane. Circular dichroism (CD) spectra were recorded on Jasco-715 spectrometer with 0.2 nm scan step and 5 nm bandwidth.

4.2.4 Characterization of the DPP LC Order

Liquid crystalline solutions were prepared by dissolving solid DPPs in m-cresol in a range of concentrations. Approximately 30 mg of the DPPs were dissolved in the corresponding amount of m-cresol. DPP samples in m-cresol and dried thin films were prepared as described in Chapter 3. Sample molecular dimensions were determined by film and solution sample X-ray diffraction patterns.

X-diffraction conducted at the 5-IDD beam line of the DuPont-Northwestern-Dow Collaborative Access Team (DND-CAT) Synchrotron Research Center at the Advanced Photon Source (Argonne National Laboratory, Chicago, IL) was used to characterize long-range intermolecular order in the liquid crystalline materials (as described in Chapter 3). Ring diffraction patterns were indicative of powder samples (lacking alignment) and integrated to give 2D intensity plots to determine molecular spacing.

Polarized optical microscopy was conducted with DPPs in m-cresol solution at a range of concentrations. Samples were applied to a glass cover slide and immediately viewed using a Nikon Optiphot-200 microscope with crossed polarizers.

4.3 Results and Discussion

4.3.1 Dendron Synthesis and Conjugation

The Glu_x proteins were conjugated with hydrophobic dendrons to stabilize the α-helical conformation of the protein core by forcing intramolecular hydrogen bonding between the aromatic branches. The Glu_x proteins were conjugated with hydrophobic dendrons ranging from

zero order (D_0), first-order with either two (D_1) or three peripheral benzyls (T), to second order dendrons (D_2) (Figure 4.3.1).

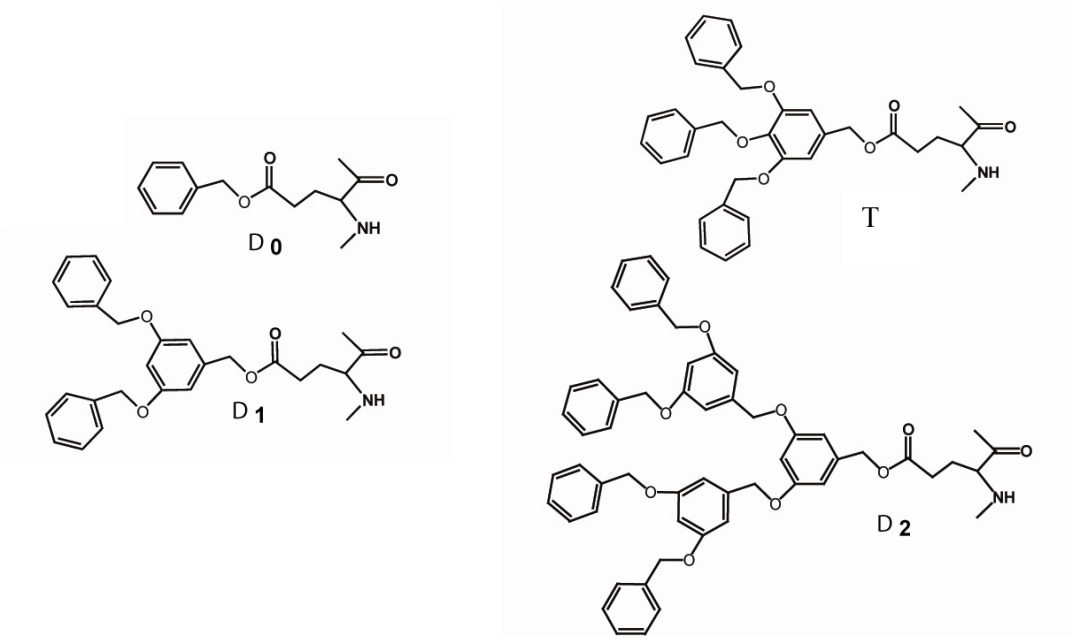

Figure 4.3.1: Schematic of dendron wedges that were synthesized by Dr. M. Zhuravel. Zero-order dendron was denoted D_0, first generation wedges are denoted D_1 and T, second generation dendron is denoted D_2.

Zero-order dendrons were added to acidified Glu_x by a reaction with phenyldiazomethane (as discussed in Chapter 3). For first and second-order dendrons, Frechet-type poly(benzyl ether) dendrons with an aldehyde function focal point were converted to tosylhydrazones and the treatment with base created the final diazo-fuctionalized dendron. The dendron diazo group was reacted with the acidified carboxyl group on the Glu_x proteins (Figure 4.3.2).

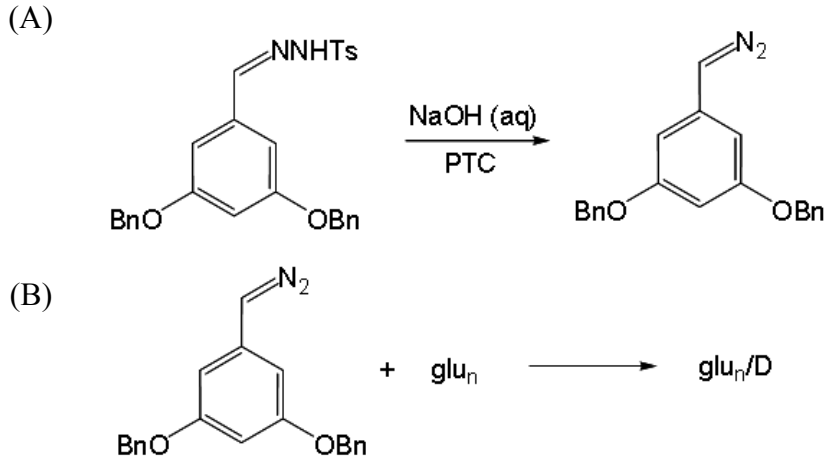

Figure 4.3.2: Synthesis of DPPs. Dendrons are activated to the diazo group (A) which reacts with acidified carboxyl groups on Glu_x (B).

Frechet type dendrons were chosen due to their ease of synthesis, non-polar side chains, and controlled topology. The added steric bulk, introduced into the macromolecules by the dendrons enhanced backbone shielding from the solvent, leading to more stable and soluble compounds. As determined by NMR and MALDI-TOF, dendronization was greater than 94%. Glu_{38}-D_1 (calc. 17106) observed 17251, Glu_{58}-D_1 (calc. 25030) observed 25422, Glu_{76}-D_1 (calc. 32793) observed 32913, Glu_{76}-D_2 (calc. 65054) observed 66455, Glu_{76}-T (calc. 40858) observed 38753, Glu_{94}-D_1 (calc. 40549) observed 40844, Glu_{94}-T (calc. 50524) observed 45907, Glu_{112}-D_1 (calc. 48317) observed 48619. Gel permeation chromatography showed a PDI of close to 1.

4.3.2 Molecular Characterization of DPPs

FTIR and CD spectroscopies were used to examine the conformations of the DPPs. Circular dichroism was used to verify secondary structure of the DPPs and to determine length.

The DPPs displayed characteristic spectra with a minimum at 223 – 225 nm suggesting an α-helical backbone conformation (Figure 4.3.3A). The per residue molar ellipticity decreased with increasing degree of dendronization, suggesting that the bulky side chains decreased the overall helicity. However, this observation could also be explained by the increased number of dendrons having UV absorbance and distorting the CD signal. FTIR scans of DPPs with Glu_{76} cores exhibited amide I and amide II bands at ~ 1654 and ~1550 cm^1, respectively, characteristic of an α-helical secondary structure of DPP polypeptide backbones (Figure 4.3.3B). The positions of the amide bands with polymers of the four dendritic side-chains were essentially identical. Combined with the fact that polydisperse analogues of Glu_x-D_0 polymer are known to have the classical 18/5 α-helix conformation,[134] the CD and FTIR data strongly suggests that all prepared DPPs have helical backbones.

Taken together the FTIR and CD data, and the molecular dimensions of the molecules deduced from the X-ray diffraction data (see below) suggested α-helical conformations of the DPP backbones. The exact backbone dimensions, however, varied slightly with increasing dendron side-chain size and shape. For example, the Glu_{76}-T DPP FTIR spectra had a slight shift in amide bands and a different shape in the CD spectrum, suggesting that the T dendrons caused a distortion of the DPP backbone conformation due to side-chain packing.

(A)

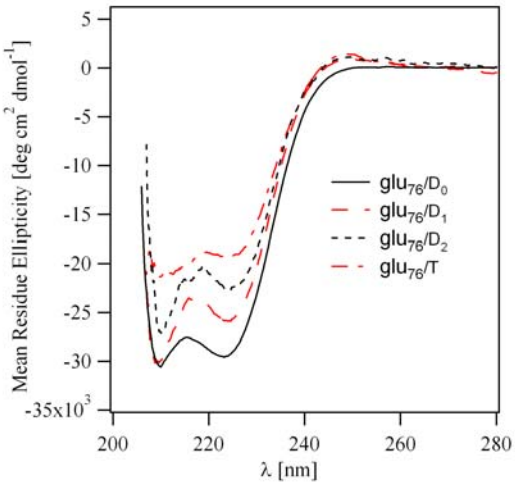

(B)

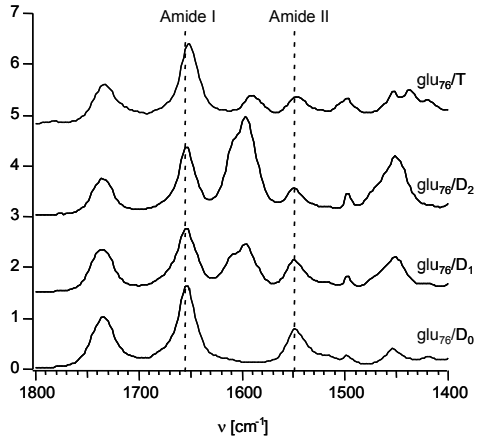

(C)

	Amide I, cm^{-1}	Amide II, cm^{-1}
glu$_{76}$/D$_0$	1653	1549
glu$_{76}$/D	1654	1550
glu$_{76}$/D$_2$	1654	1550
glu$_{76}$/T	1652	1548
Typical for α-helix	1652-1655	1545-1550

Amide I – C=O stretch
Amide II – N-H deformation, C-N stretch

Figure 4.3.3: (A) CD spectra of Glu$_{76}$-D$_x$ DPPs and (B) FTIR spectra and table showing the amide I and amide II bands, both characteristic α-helical conformation.

The CD and FTIR spectra suggest an α-helical backbone conformation, from this the protein molecular length is estimated by L = 1.5Å/residue x number of residues.

4.3.3 Liquid Crystalline Properties of DPPs

The self-assembly of the DPPs was investigated in *m*-cresol. Concentrated DPP/*m*-cresol solutions exhibited optical anisotropy (birefringence) that increased with the DPP concentrations, indicating formation of ordered LC structures. Small-angle x-ray diffraction (SAXD) patterns of DPP/*m*-cresol solutions, sealed between mica windows and oriented by gentle shearing, showed two orthogonal sets of sharp diffraction peaks (Figure 4.3.4A). The data corresponds to a partially oriented sample obtained from shearing. The angular width of the diffraction arcs are a function of sample preparation rather than a true indication of the orientational order in the sample. In unsheared samples the diffraction pattern consists of uniform rings. Reflections with ratios of 1:√3:√4 along the xy-plane indicated hexagonal packing of DPP cylinders with well-defined spacing between the cylinder axis (*a)*. Along the z-axis, reflections with ratios 1:2:3:4 revealed a layered structure with periodicity of layer size (*d*), where $d >> a$. The diffraction pattern was consistent with the structure shown in Figure 4.3.4B: cylindrical DPPs formed periodically stacked layers with thickness equal to *L*, and hexagonal packing of molecules within each layer; solvent occupied the space between the molecules in each layer ($a > D$) and between the layers ($d > L$).

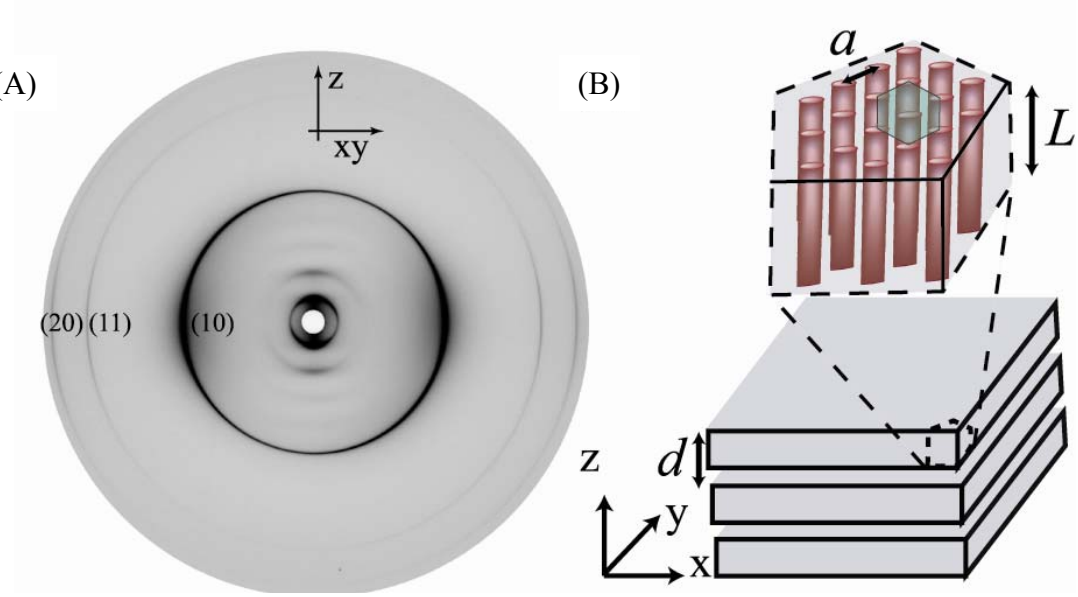

Figure 4.3.4: (A) SAXD pattern of Glu_{76}-D_1 dissolved in m-cresol at 60 wt % DPP. The pattern shows lamellar diffraction peaks along the z-axis and hexagonal reflections along the xy-plane. The hexagonal reflections along the xy-plane are labeled. (B) Schematic illustration of the self-assembled structure of the DPP in solution that corresponds to the pattern in (A). Layer length *d* is determined from the interior diffraction rings and the intermolecular spacing, *a*, is given by the xy diffraction.

The observed long-range ordered self-assembly of the DPP materials is likely driven by excluded volume interactions between the rigid DPP cylinders, as suggested from theoretical models[2]. The volume available for each cylindrical molecule in a concentrated suspension was maximized when the DPP molecules separated into well-defined layers with efficient hexagonal packed order in the layer[135] (as illustrated in Figure 4.3.4B).

4.3.4 Molecular Geometry of DPPs Determined by SAXD

The LC phases of the DPPs were determined as a function of the monodisperse DPP molecular dimensions. The diameters of the DPPs corresponding to the different types of

dendron side-chains were experimentally determined by dry films diffraction patterns. SAXD scans showed the expected increase of cylinder diameters *D* with increasing size of the dendron side-chains (Figure 4.3.5A). Remarkably, the measured *D* values agreed very well with dimensional estimates that were based on simple geometrical computer models of helical peptide backbones surrounded by dendritic side-chains (Figure 4.3.5B).

(A)

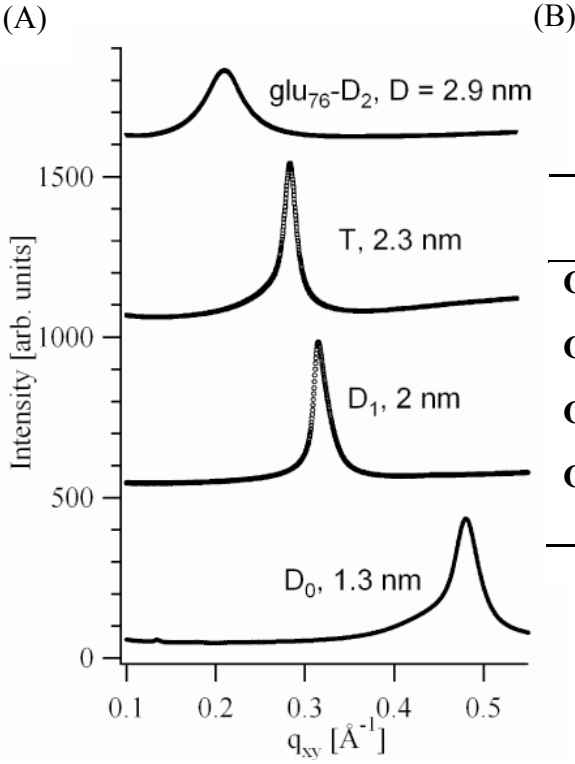

(B)

	Observed *D* (nm)	**Calculated *D* (nm)**
Glu_{76}-D_0	1.3	12.9
Glu_{76}-D_1	2.0	2.0
Glu_{76}-T	2.3	2.4
Glu_{76}-D_2	2.9	2.9

Figure 4.3.5: (A) SAXD scattering of DPPs in solutions of m-cresol. Scatter spacing was used to determine molecular diameter using the equation D = (2*π) / q.

The expected molecular length of the DPPs was calculated based on the spacing of residues for an α-helical, where *L* = the number of residues (N) x 1.5 Å per residue. SAXD intensity plots

of DPPs in the smectic LC phase allowed for the experimental determination of molecular length (Figure 4.3.6A).

(A)

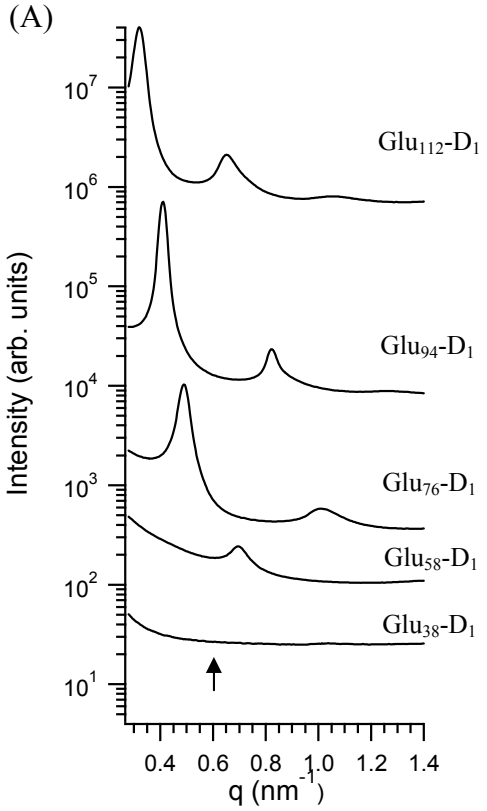

(B)

	Observed *L* (nm)	**Calculated *L* (nm)**
Glu_{38}-D_1	6.0	5.7
Glu_{58}-D_1	9.1	8.7
Glu_{76}-D_1	12.8	11.4
Glu_{94}-D_1	15.4	14.1
Glu_{112}-D_1	17.1	16.8

Figure 4.3.6: (A) SAXD data of Glu_x-D_1 samples at a constant 60 wt % protein concentration showing lamellar stacking peaks. q-spacing values were used to determine molecular length *L*, since $L \approx d$. (B) comparison of observed molecular length vs. calculated *L* based on DPP models.

The periodicity of smectic layers increases with DPP length (Figure 4.3.6A). Note that the layering periodicity *d* along the z-axis is the sum of the smectic layer thickness (equal to the length *L* of the molecules) and the width of the solvent layer between the molecular layers. Thus, *d* varies as a function of the solvent concentration in the samples. The layer thickness was estimated from SAXD scattering and the known concentration of solvent in each sample; the

thickness of DPP layers was calculated to be 5.7, 8.7, 11.4, 14.1 and 16.8 nm, essentially identical to the expected length *L* of the DPP molecules (Figure 4.3.6B).

4.3.5 DPP LC Phases Transitions

The liquid crystalline properties of DPPs in a single solution was confirmed by POM. For consistency with Glu_x-D_0 POM images, all DPPs were dissolved in m-cresol. POM images of DPPs in solution showed the characteristic patterns for LC phases (Figure 4.3.7).

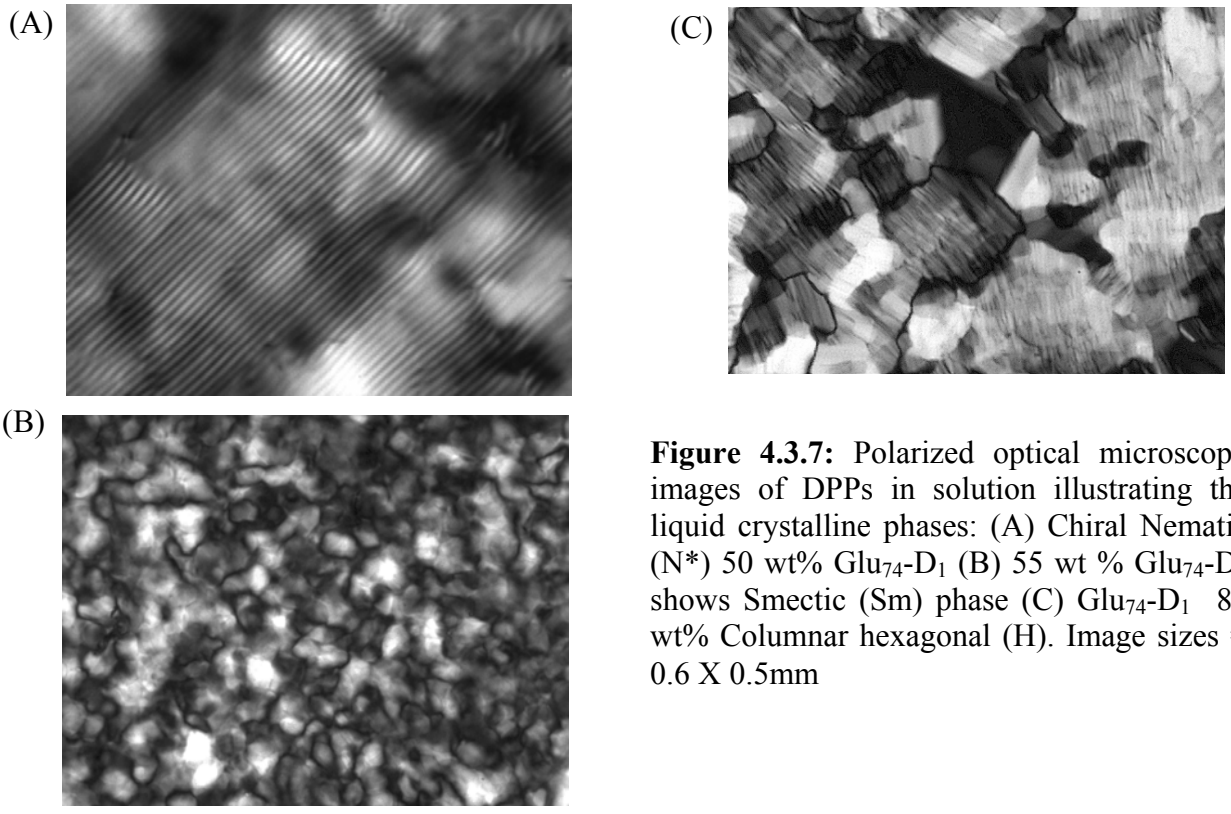

Figure 4.3.7: Polarized optical microscopy images of DPPs in solution illustrating the liquid crystalline phases: (A) Chiral Nematic (N*) 50 wt% Glu_{74}-D_1 (B) 55 wt % Glu_{74}-D_1 shows Smectic (Sm) phase (C) Glu_{74}-D_1 80 wt% Columnar hexagonal (H). Image sizes = 0.6 X 0.5mm

The POM images displayed changes in optical texture based on concentration of Glu_{74}-D_1 in solution. This observation is further supported by imaging DPP samples that were allowed to dry under the polarized optical microscope; images exhibit changes in optical texture as samples become more concentrated do to sample evaporation (Figure 4.3.8).

(A)

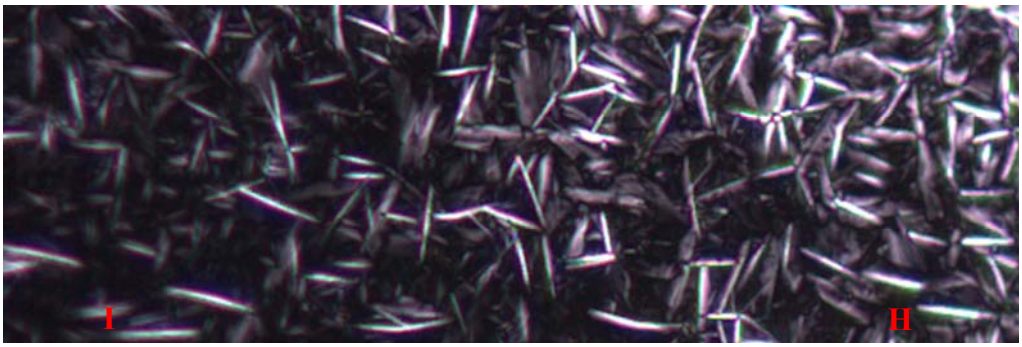

(B)

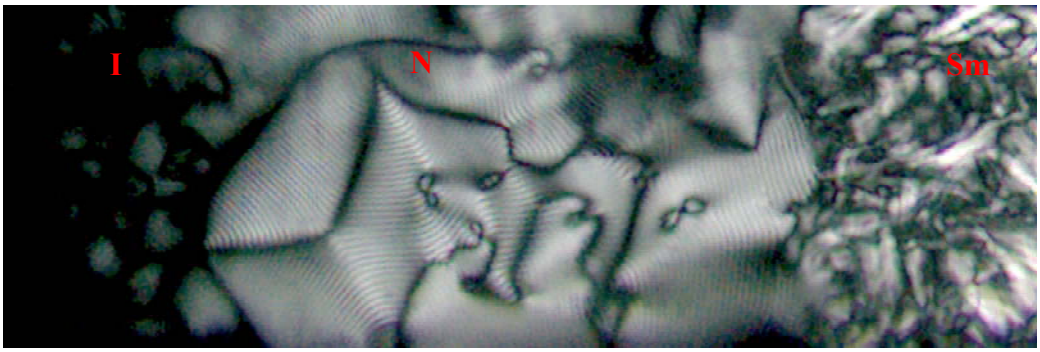

Figure 4.3.8: POM images of samples in m-cresol drying from left to right under the microscope; (A) Glu_{58}-D_2 (B) Glu_{112}-D_1. Where possible, LC phases are denoted on the images.

The DPP Glu_{58}-D_2 had a needle-like optical texture during solvent evaporation, where as Glu_{112}-D_1 had clear transition between isotropic, nematic and smectic texture. The POM images while drying confirm that concentration of DPPs influence LC phase formation.

X-ray diffraction images of DPPs provided a more precise indication of LC phases based on intermolecular spacing. SAXS scans of DPPs in solution revealed, as a function of the concentration, transitions from isotropic to nematic, to smectic and finally hexagonal columnar liquid crystal phases. A typical transition is illustrated in Figure 4.3.9A for Glu_{94}-D_1. At approximately 45% DPP, the nematic phase was observed, indicated by the broad peak at $q \approx 2.3$ nm^{-1}. As concentration increased to 58% DPP, SAXS diffraction rings were observed ($q_{n=1} \approx 0.4$ nm^{-1}, $q_{n=2} \approx 0.8$ nm^{-1}) indicating a smectic phase. The most concentrated sample (84% DPP), exclusively had low-angle scattering, suggesting hexagonal packing. The transitions of higher order DPPs markably differs from that of zero-order DPPs shown previously in Chapter 3. For example, Glu_{94}-D_0 transitions from a state of nematic-hexagonal coexistence at 46 wt%, then to a smectic phase at 50 wt%, and hexagonal phase at a 55 wt% concentration (Figure 4.3.9B).

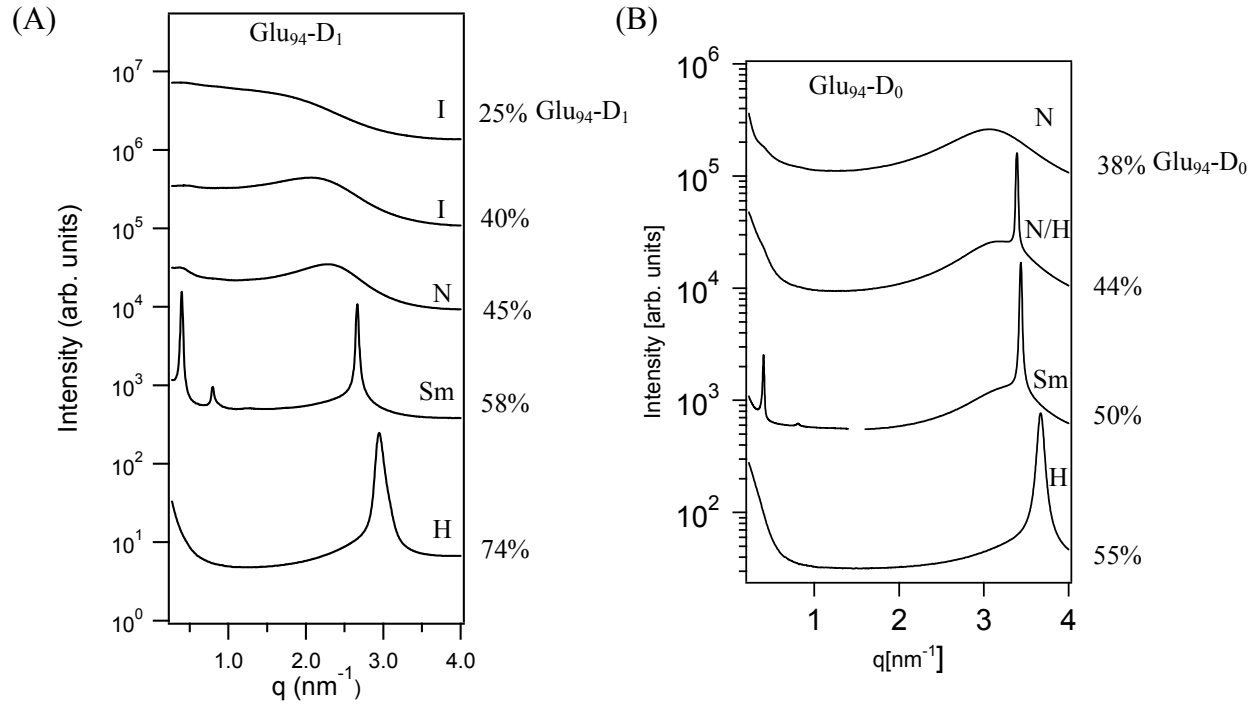

Figure 4.3.9: Diffraction peaks of (A) Glu_{94}-D_1 and (B) Glu_{94}-D_1 as a function of concentration given in wt %. LC phases are labeled for clarity.

The Glu_{94}-D_0 transitioned to the hexagonal phase at a much lower concentration than Glu_{94}-D_1, confirming the previous results, that phase transitions are a function of degree of dendronization. As dendronization increased, the corresponding DPP diameter increased; which then changed the aspect ratio. As observed in Chapter 3, phase transitions are a function of concentration and aspect ratio; this trend was also exhibited by Glu_{76}-y (y = D_1, D_2, T) (Figure 4.3.10).

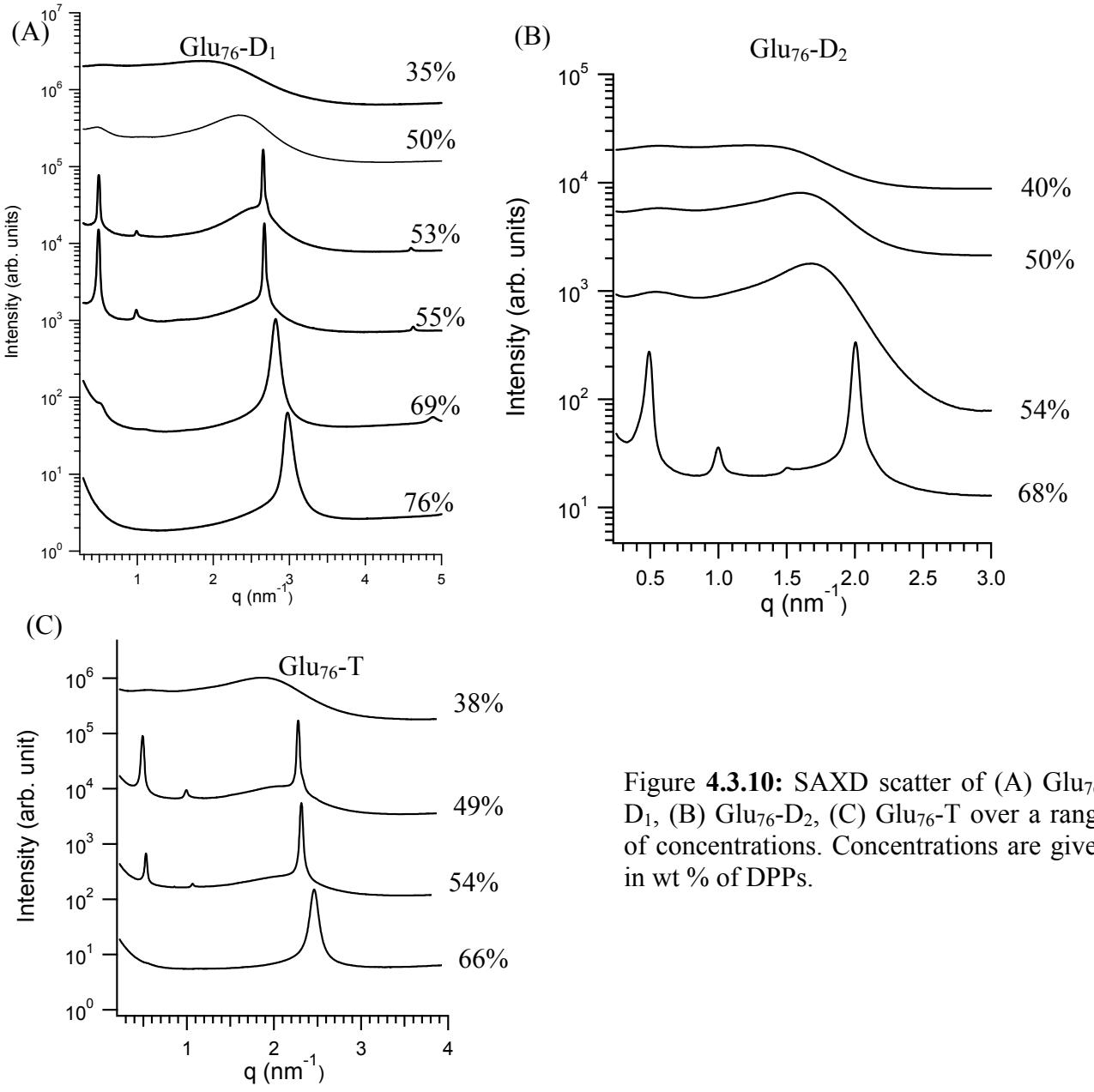

Figure **4.3.10:** SAXD scatter of (A) Glu_{76}-D_1, (B) Glu_{76}-D_2, (C) Glu_{76}-T over a range of concentrations. Concentrations are given in wt % of DPPs.

Figure 4.3.10 shows that Glu_{76}-D_1 and Glu_{76}-T both have lamellar (smectic) order at a concentration of 54 wt%. Conversely, at a similar concentration, Glu_{76}-D_2 had no lamellar order and formed the nematic phase. At a higher concentration of 68 wt%, both Glu_{76}-D_1 and Glu_{76}-D_t had hexagonal order, where at nearly the same concentration Glu_{76}-D_2 displayed lamellar order. This suggested that the transition between to hexagonal columnar phase for Glu_{76}-D_2 occurred at a higher concentration that Glu_{76}-D_1 and Glu_{76}-T, most likely because of differences in DPP shape. Surprisingly, however, Glu_{76}-T formed a lamellar phase at lower DPP concentration than Glu_{76}-D_1, suggesting that perhaps shape is not the only factor to determine transition points, as explained in the next section.

4.3.6 DPP LC Phase Diagram

Based on the observations made in section 4.3.5, we investigated the LC phases formed over a large range of aspect ratios and concentrations. As mentioned previously, the molecular length and diameter was varied by increasing the number of residues in the Glu_x core and increasing the degree of dendronization, respectively. The final DPPs ranged in aspect ratio from (2.85 to 11.28) (Table 4.3.1).

Table 4.3.1: Calculated aspect ratios as a function of molecular length and degree of dendronization.

	D_0	D_1	T	D_2
Glu_{38}	X	2.85	X	X
Glu_{58}	6.96	4.35	3.70	3.11
Glu_{76}	9.12	5.70	4.85	4.07
Glu_{94}	11.28	7.05	6.00	5.04
Glu_{112}	X	8.40	7.15	6.00

X-ray diffraction data was used to determine the LC phases formed from a broad range of DPP aspect ratios and concentrations in m-cresol, and POM images were used to verify the results based on optical texture. Figure 4.3.11 shows the phase diagram for DPPs with Glu_x-y (where y = D_1, T, D_2).

As aspect ratio increased, the concentration required to form a lamellar phase decreased (also observed in Figure 4.3.10). At aspect ratios below 4.0, there was no formation of the nematic phase. Furthermore, no clear lamellar (smectic) phase was observed with molecules that had the smallest aspect ratio of 2.85; on the contrary these DPPs exhibited a coexistence between multiple LC phases.

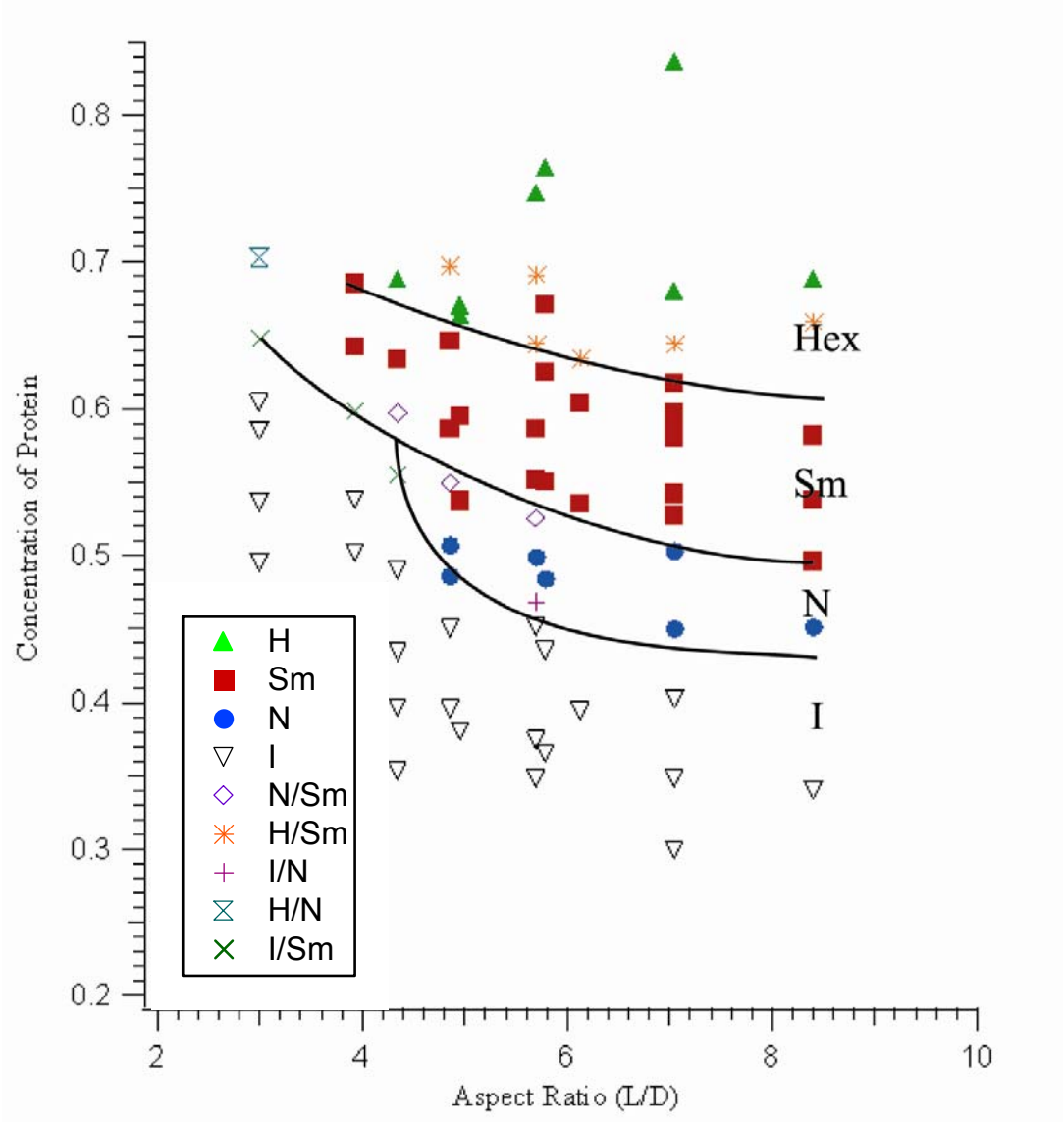

Figure 4.3.11: Phase diagram of DPPs in m-cresol. DPPs of first and second generation are shown.

In the case of higher order DPPs the smectic phase was observed at a much lower aspect ratio than the predicted L/D>7 based on Flory theory simulations for monodisperse molecules.[87] The current investigation expands the boundary for lamellar phase formation.

The phase diagram proposed by Bolhuis and Frenkel,[2] more closely corresponds to Figure 4.3.11. The experimental phase diagram of the higher-order DPPs was the first system to validate the predicted smectic phase formation for rigid rods. Bolhuis and Frenkel predicted a smectic phase formation for molecules with L/D > 3.7 (Figure 4.3.12).[2] The experimental phase diagram in Figure 4.3.11 suggests a limit of L/D = 4 for the existence of nematic phase, which is close to the predicted limit. Similar to the simulation presented in Figure 4.3.12, the DPP molecules with L/D < 4 transitioned from isotropic directly to smectic phase, however, for L/D>4 there was an intermediate nematic phase. In addition, the triple point at L/D ≈ 4 was observed by DPPs in solution.

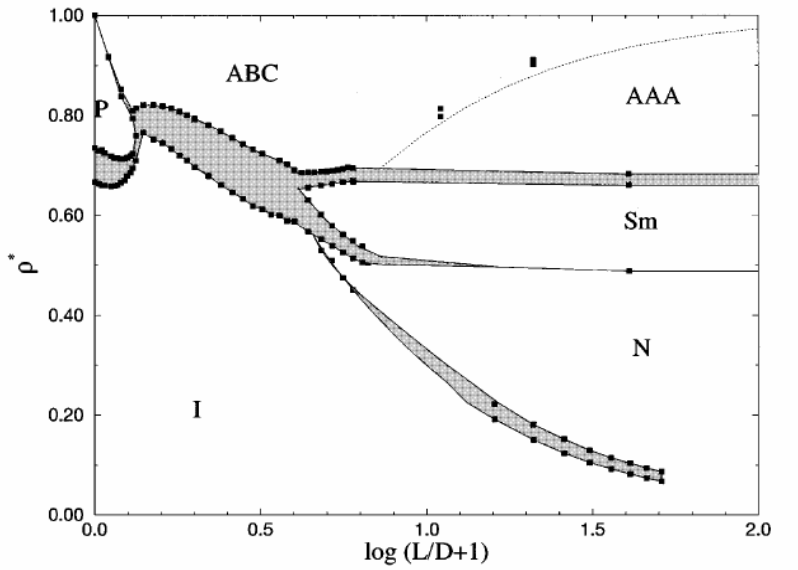

Figure 4.3.12: Phase diagram of hard parallel rigid rods with L/D between 0 and 60. The shaded areas correspond to two-phase regions. For *L/D* > 4.0 the nematic (N) and *L/D* > 3.7 smectic (Sm) phases are shown.[2]

The Glu_x-D_0 proteins described in Chapter 3 displayed a slightly different phase diagram (Figure 3.3.11). For zero-order DPPs, the nematic phase was observed at a much higher aspect ratio of ≈ L/D>8. In addition, the appearance of smectic phase was often observed with a

coexistence of other phases. This suggested that the larger dendritic wedges maximized the steric stabilization of the DPP shape, leading to a more ideal rigid-rod. This is consistent with simple geometric models, which suggested that the single benzyl groups (D_0) are too small to completely shield the polar peptide backbone from solvent, while higher generation dendrons fully cover the backbone (Figure 4.3.13).

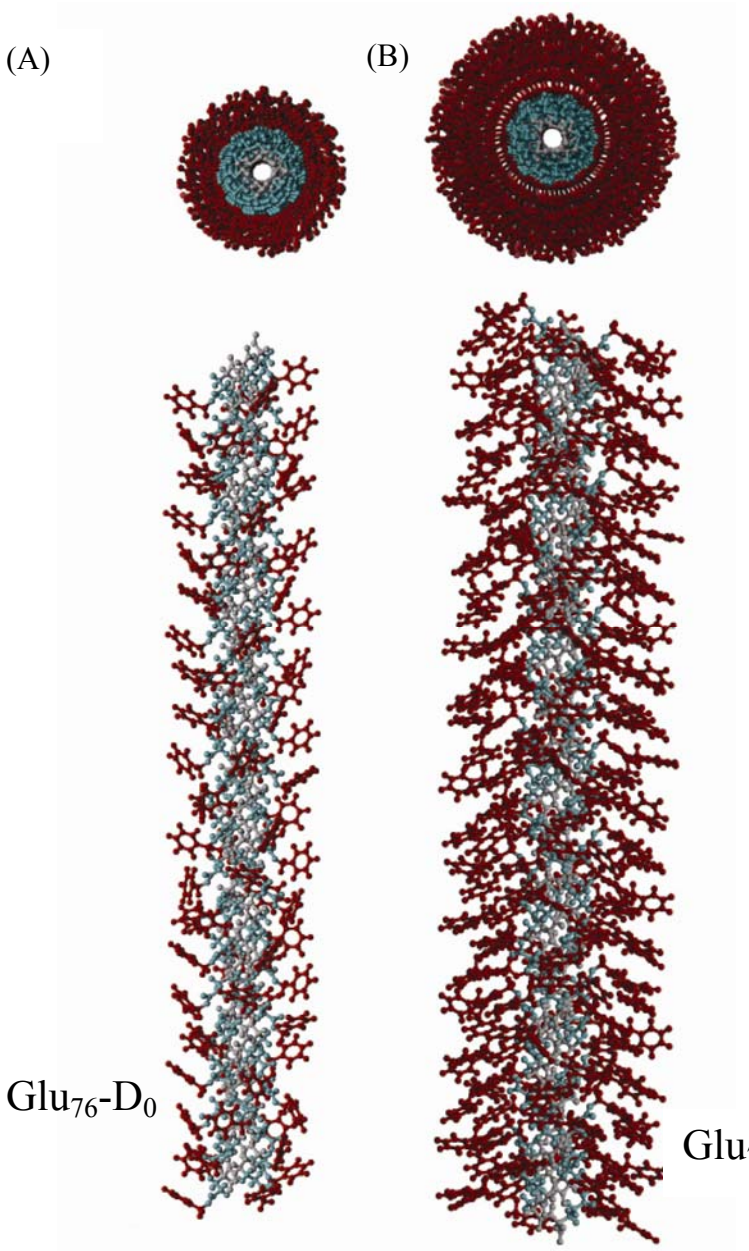

Figure 4.3.13: Molecular models of (A) Glu_{76}-D_0 and (B) Glu_{76}-D_1. The models were subjected to energy minimization with fixed conformation of the peptide backbone.

We hypothesized that the main driving force for self-assembly was due to excluded volume interactions. The molecular models may indicate that solvent interaction with the D_0 proteins can account for the differences in phase diagrams; where incomplete backbone shielding could introduce additional attractive forces driving self-assembly. The similarities between the experimental phase diagram for higher-order DPPs (Figure 4.3.11) and the phase diagram calculated by Bolhuis and Frenkel (Figure 4.3.12), suggest that excluded volume is the predominate factor driving self-assembly. Furthermore, no evidence of dipole-dipole attractive forces was observed that would result in end-to-end layering, creating a smectic phase with $d \approx 2L$.

4.4 Conclusion and Future Directions

We created a biosynthetic technique to vary molecular diameter by the addition of dendritic wedges to the α-helical proteins. The dendronized proteins displayed increased macromolecular solubility and liquid crystal phase stability in solution. Theoretical models for hard spherocylinders, pioneered by D. Frenkel, suggest a phase diagram of liquid crystalline phases as a function of shape anisotropy (L/D, for cylinders of length L and diameter D).[2] The ability to change molecular diameter, combined with control of length (discussed in Chapter 3) allowed for the study of LC phases based on additional aspect ratios. This study not only represents the first experimentally determined phase diagram for monodisperse cylindrical molecules, but also is the first experimental observation of liquid crystal phases in rigid-rod molecules at the nanoscale.

This research presents the first comprehensive phase diagram at the nanoscale, of self-assembled protein-based materials, and elaborates on both the possibilities and limitations of dendronized protein polymers (DPPs) for nanomaterials. The modular nature of this synthetic strategy can be used to expand the range of accessible DPP interactions and shapes through the variation of peptide sequences, dendron functionality, and dendron architectures. In addition this system can be used to determine the relationship between molecular shape and excluded volume interactions of monodipserse molecules. The ability to construct these macromolecules and determine precisely their intermolecular self-assembly has important implication for material development for the fields of nanotechnology and biomaterials.

Chapter 5

Random Coil Protein Polymers for Multivalent Display

5.1 Introduction

Chapters 3 and 4 illustrated the use of monodisperse protein building blocks that self-assembled into liquid crystals when functionalized with dendrons. This section describes random coil multivalent display monodisperse protein polymers. These protein polymers enable variation in chemical structure, such as chain length, protein block-copolymers, and the three-dimensional branching architecture as well as the type, position, and density of functional groups at the macromolecular level. Due to their inherent monodispersity and modularity, protein polymers are ideal building blocks to create comb-like architectures for biological applications.

5.1.1 Multivalent Display in Biology

Multiple, simultaneous interactions, an effect known as multivalency, often occur in biology to enhance the affinity and specificity of binding of receptor ligand pairs.[21] Synthetic

biomaterials that can display multiple functionalities are of increasing interest to biotechnology for the study of biological interactions and drug delivery applications. In biology, many types of recognition events require multiple interactions between ligands and receptors, where avidity and specificity are both affected by the valency.[136-138] Increasing the number of bioactive agents on a single macromolecule often increases activity; for example, linear polymers with elements displayed in comb-like architectures have been shown to bind antibodies with increased antigenicity in comparison to the equivalent concentration of free epitopes.[139] In drug delivery, the attachment of small biologically active compounds to a macromolecular scaffold can alter drug pharmacological properties, thereby increasing solubility and retention.[140] These scaffolds can be functionalized with targeting moieties to enhance drug selectivity and receptor-mediated delivery,[141] such as dendrimers,[142-145] liposomes,[146] and polymers[137, 147-150].

Scaffolds created by synthetic approaches can obtain high pendant group valencies and have versatile conjugation chemistries, however, traditional chemical synthesis results in materials that are inherently polydisperse. The distribution of molecular weight complicate characterization of biological activity[151] and *in vivo* toxicity[152]. New polymer synthesis techniques, such as ring-opening metathesis polymerization (ROMP) or atom transfer radical polymerization (ATRP), have been investigated to create linear multivalent scaffolds with a narrower molecular weight distribution. These methods, however, lack stereochemical selection preference and cannot achieve true monodispersity.

5.1.2 Biopolymers for Multivalent Display

As a viable alternative to chemical synthesis, molecular biology and genetic engineering techniques can create homogeneous protein polymer scaffolds. The precision of artificial protein polymer scaffolds allows for exact determination of valency. The modular biosynthetic strategy which uses genetically engineered protein polymers as a backbone for chemical modification, has resulted in new multivalent materials. Recently, the Kiick research group created α-helical alanine-rich protein polymers that contained evenly spaced glutamic acid residues for conjugation of saccharides to the carboxyl groups. The α-helical secondary structure of the protein polymer, which has dependence on temperature and amino acid sequence, provided a rigid backbone for controlling the spacing of the pendant groups. The resulting galactose functionalized protein polymer had a 200-fold improvement in inhibition to cholera toxin than the galactose monomers.[59] The rigid helical structure had enhanced toxin inhibition than an unstructured analog.[21]

Inspired by research with genetically engineered proteins containing single amino acid incorporation for increased functionality, we present a class of modular random coil cationic protein polymers that contain evenly spaced reactive groups. Unlike proteins with enhanced secondary structure, a random coil protein polymer mimics the flexibility of synthetic polymers while maintaining homogeneous properties. The effects of flexibility on activity and recognition events could be better studied with a non-ordered, multivalent protein scaffold. As mentioned in Chapter 2, as of May 2008, the majority of research into protein polymers is focused on molecules composed of amino acid sequences inspired by silk, collagen, and elastin, which have

folded secondary structures. Therefore, very little research has been conducted on random coil protein polymers, with the exception of producing flexible spacer sequences.[16]

Herein, we describe the synthesis and characterization of protein polymers that vary in protein length and lysine spacing. These proteins have been found to be water soluble and retain a random coil conformation over a range of temperatures. Additionally, these proteins have low toxicity at concentrations relevant to drug delivery, in the low μM range. The proteins have a chemically active lysine located at controlled intervals, which contain a reactive primary amine. This free amine allows for chemical or enzymatic grafting of bioactive pendant groups. Chemical conjugation can be achieved by a wide range of amine-reactive chemistries, and has been used to covalently couple bioactive peptides, polymers, peptoids, and small organic molecules onto the cationic protein polymers.

In addition to providing a reactive group for chemical conjugation, the lysine in these protein polymers serves as a substrate for enzymatic conjugation by tissue trasnglutaminase. Transglutaminases catalyze the formation of bonds between glutamine and lysine residues under mild and biocompatible reaction conditions.[153] Transglutaminase enzymes have been used to covalently link bioactive peptides to fibrin matrices[154-156] and self-assembled fibrillar structures.[157] Inspired by this research, we have created a protein polymer multivalent scaffold by enzymatic conjugation with a bioactive peptide. This class of *de novo* protein polymers is a promising candidate as building blocks for multivalent display and tissue engineering hydrogels due to the ability for chemically and enzymatically grafting.

5.2 Experimental Section

Standard molecular biology techniques were used for gene synthesis, protein expression, and protein purification, unless otherwise noted. DNA amplification was completed by polymerase chain reactions (PCR) with Taq polymerase (Promega, Madison, WI) according to manufacturer's recommendations. All enzymes for cloning were supplied by New England Biolabs (Ipswich, MA).

5.2.1 DNA Gene Design and Synthesis

The DNA sequences encoding the monomers of the protein polymer amino acids were designed to incorporate the codon preferences for *E. coli*[158] and to prevent DNA and RNA secondary structure formation that may inhibit cloning and expression. DNA oligonucleotides (Integrated DNA Technologies, Coralville, IA) encoding the three different sequences of protein polymers (Figure 5.2.1) were amplified by PCR, purified by electrophoresis on a 2% agarose gel and excised with the QIAquick Gel Extraction Kit (Qiagen, Valencia, CA). After *Ear*I digestion and purification the monomers were self ligated by T4 ligase to form multimers. The multimers were ligated into the cloning vector pUC18 (Life Technologies, USA) and transformed into NovaBlue cells (Novagen Inc., Madison, WI).

(A)

(Gly Lys Gly Ser Gly Lys Gly Ala Gly Lys Gly Ser Gly Lys Gly Ala Gly
G CTA GCC ATA T**GC TCT TC**A GGT AAA GGT TCC GGT AAA GGC GCA GGT AAA GGT TCC GGT AAA GGC GCG GGT
↑

Lys Gly Ser Gly Lys Gly Ala Gly)
AAA GGT TCC GGT AAA GGC GCC GGT T**GA AGA G**GG ATC CAC TAG T
↑

(B**)**

(Gly Lys Gly Thr Gly Ala Gly Lys Gly Thr Gly Ala Gly Lys Gly Thr Gly Ala
G CTA GCC ATA T**GC TCT TC**A GGT AAA GGT ACC GGC GCG GGT AAA GGC ACG GGT GCA GGC AAA GGT ACT GGC GCG
↑

Gly Lys Gly Thr Gly Ala Gly)
GGT AAA GGT ACC GGC GCG GGT T**GA AGA G**GG ATC CAC TAG T
↑

(C)

(Gly Lys Ala Gly Thr Gly Ser Ala Gly Lys Ala Gly Thr Gly Ser Ala Gly
G CTA GCC ATA T**GC TCT TC**A GGT AAA GCC GGT ACC GGC TCC GCA GGC AAG GCG GGT ACG GGC TCT GCA GGT
↑

Lys Ala Gly Thr Gly Ser Ala Gly)
AAA GCT GGT ACT GGC TCC GCG GGT T**GA AGA G**GG ATC CAC TAG T
↑

Figure 5.2.1: DNA oligonucleotide sequences used to create repetitive genes, (A) K4 (B) K6 (C) K8. *Ear*I restriction sites are in bold, and ↑ denotes the cleavage site.

Concatemer genes were created by the controlled cloning method (Figure 5.2.2)[159] with the restriction enzyme *Ear*I as an isoschizomer of *Eam*1104 I. Briefly, the plasmid containing multimers was amplified by PCR primers to eliminate one of the flanking *Sap*I sites. This was split into two fractions; one was digested by *Ear*I and one with *Sap*I. The *Ear*I fraction was dephosphorylated with calf intestinal phosphatase and then ligated to the *Sap*I digested fraction. The 5' terminal phosphate group was replaced on the resulting concatemer using T4 polynucleotide kinase and then the concatemer was digested with *Ear*I. This gene was ligated into pUC18 and transformed into NovaBlue cloning cells. Single colonies were isolated by

miniprep (Qiagen) and gene insertion was verified by an *Ear*I digestion and visualized on a 2% agarose slab gel. This process was repeated to obtain concatemer genes of the desired lengths.

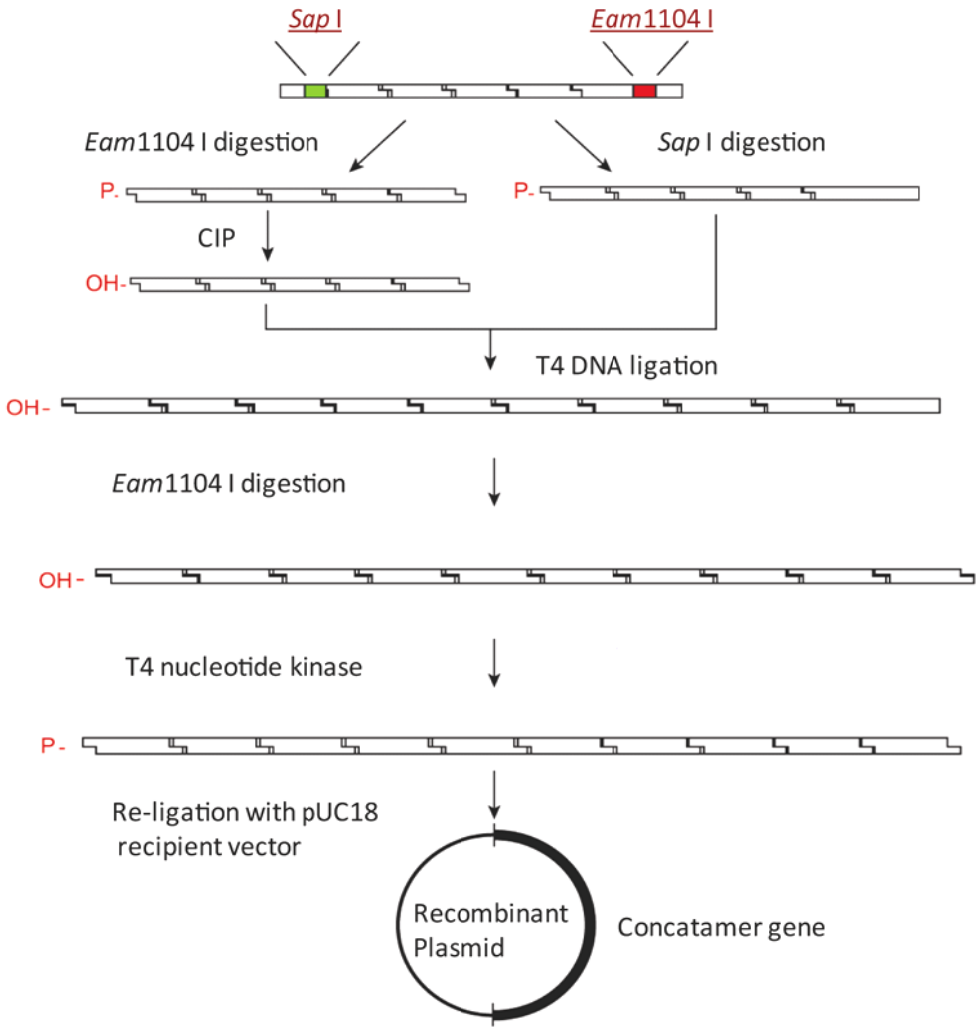

Figure 5.2.2: Controlled cloning scheme to make DNA concatamer genes.

The expression vector, pET-19b (Novagen Inc.) was modified to remove the internal *Sap* I site using QuickChange Site-Directed Mutagenesis (Stratagene, La Jolla, CA) to change a single base in the restriction site. The mutated vector was then amplified by PCR with primers

containing *Ear*I recognition sites as well as a stop codon. The amplified linear plasmid was digested with *Ear*I to create complementary termini for the concatemer genes. These concatemer genes were ligated into the plasmid with T4 DNA ligase and transformed into NovaBlue cells. Correct insertion was verified by electrophoresis of double digested genes with *Bam*HI and *Nde*I restriction enzymes and through DNA sequencing (SeqWright, Houston, TX). Ligation into the expression vector resulted in the gene of interest expressed as a fusion protein with an *N*-terminal histidine tag (tag amino acid sequence: GH_{10}SSGHIDDDDKHM).

5.2.2 Protein Expression and Purification

Plasmids containing the desired genes were transformed into *E. coli* expression strain BLR(DE3) cells (Novagen Inc.). A 5 ml starter culture in LB Broth (Fisher Scientific, Waltham, MA) was grown from a single colony for 8 hours. This was used to inoculate an overnight 100 ml LB broth culture, both supplemented with 200 μg/ml ampicillin (Sigma, St. Louis, MO) and 12.5 μg/ml tetracycline (Fisher Scientific). One liter cultures of Difco Terrific Broth (Fisher Scientific) supplemented with 200 μg/ml ampicillin and 12.5 μg/ml tetracycline, were inoculated with 15-20 ml from the overnight culture. All bacterial cultures were grown at 37°C with orbital shaking. The culture was induced with 0.5 mM isopropyl thiogalactoside (IPTG) (US Biologicals, Swampscott, MA) when the OD_{600} was between 0.6 to 0.8. The cells were harvested after 4 hours by centrifugation and the cell pellet was resuspended in 6M guanidine hydrochloride, 20 mM sodium phosphate, 500 mM NaCl, pH 7.8 buffer. The cells were lysed by three successive freeze (-80°C) thaw (37°C) cycles followed by sonication. Cellular debris was removed by centrifugation for 40 minutes at 8000 rpm 4°C. The protein was purified with

Chelating Sepharose Fast Flow nickel charged resin (GE Healthcare, Piscataway, NJ) under denaturing conditions with imidazole 250 mM competitive elution. The fractions containing purified protein, as determined by sodium dodecyl sulfate polyacrylamide gel electrophoresis (SDS-PAGE), were dialyzed against deionized water and then lyophilized.

5.2.3 General Characterization

Protein molecular weight was determined by matrix assisted laser desorption ionization time of flight mass spectrometry (MALDI-TOF MS) (Perseptive Biosystems Voyager Pro DE) using sinapinic acid matrix at Northwestern University's Analytical Services Laboratory. Samples were dissolved in 50% acetonitrile solution containing 0.1% trifluoroacetic acid. Amino acid analysis was conducted by the Yale Keck Facility (Yale University, New Haven, CT).

5.2.4 Turbidity

The phase behavior of protein polymers in solution was characterized as a function of temperature on a Varian Cary 500 UV-Vis-NIR spectrophotometer (Palo Alto, CA) with peltier temperature control. Proteins were dissolved at 1 mg/ml in ddH_2O and placed in a 1 cm path length quartz cuvette. Temperature was ramped at 1°C/min from 5°C to 80°C and then back down to 5°C. The spectrophotometer recorded the optical density at 500 nm and automatically subtracted the blank optical density.

5.2.5 Circular Dichroism

Circular dichroism (CD) spectroscopy was conducted with a J-715 Jasco Inc. (Easton, MD) spectrometer with peltier temperature control. Samples were placed in a quartz cuvette, with a path length of 1mm. Scans ranging from 280 to 185 nm were collected with a bandwidth of 1.0 nm, resolution of 0.2 nm, and a scan speed of 100 nm/min. An average of forty scans was reported for each condition. Samples were prepared from stock solution of approximately 2 mg/ml in ddH_2O. Protein dilutions were made between 1-10 μM for CD measurements. Stock solution and all dilutions were weighed in triplicate using a high precision microbalance. Blank background scans were collected for every condition and manually subtracted from the sample scans. The results are given as mean residue molar ellipticity [Θ] in deg cm^2 $dmol^{-1}$ res^{-1} calculated by [Θ] = CD * 100,000 / (L * C * N) where CD is the observed ellipticity in μdeg, L is the path length in cm, C protein concentration in μM and N is the number of amino acid residues in the protein.

5.2.6 Cell Culture and Viability

NIH3T3 fibroblasts (ATCC, Manassas, VA) were cultured at 37 °C and 5% CO_2 in DMEM (Gibco) supplemented with 1 % sodium pyruvate, 1% penicillin-streptomycin, 1.5 g/L $NaHCO_3$, and 10% fetal bovine serum (Gibco). Cells were grown to approximately 75% confluence and removed with 0.05% Trypsin-EDTA in Hanks' Balanced Salt Solution with phenol red (Fisher Scientific). For cell viability experiments, cells were seeded at a density of 15,000 cells per well in 96-well plates (100 μl total volume) and cultured overnight. Cells were then washed with 100

µl of Hanks' Balanced Salt Solution without phenol red (HBSS) (Fisher Scientific). Protein polymers in concentrations ranging from 100 µM to 5 mM were dissolved in HBSS and added to the wells containing cells. After 4 hours of incubation, the media was removed and the cells were washed with 100 µl HBSS. Cells were detached with 50 µl of 0.05% trypsin-EDTA (Invitrogen, Carlsbad, CA) solution. Approximately, 150 µl of Guava reagent was added per sample. Samples were added to a Guava EasyCyte Mini system (Guava Technologies, Hayward, CA) and cell viability was determined by the Guava ViaCount™ assay according to manufacturers' recommendations. At minimum, each experimental condition was repeated in triplicate. Samples incubated without protein polymer served as positive treated controls.

5.2.7 Protease Degradation

Protein polymers in solution were incubated at 37°C with either trypsin or plasmin. For trypsin digestion, 400 µl of protein polymer at 1 mg/ml was added to 100 µl of trypsin solution (495 units/ml of trypsin) in 50 mM Tris-HCl pH 7.1. For plasmin digestion, 400 µl of protein polymer at 1.6 mg/ml was added to 100 µl of plasmin solution (0.5 units/ml) in 20 mM Tris 150 mM NaCl pH 7.6. Samples were collected at set time points and proteases were inactivated by incubation with 1% (w/v) SDS at 100 °C. Proteolytic degradation over time was monitored by a 12% SDS-PAGE gel.

5.2.8 Peptide and Peptoid-Peptide Hybrid Synthesis

Peptide synthesis reagents were supplied by Aldrich (Milwaukee, WI) and Applied Biosystems (Foster City, CA). Resin and Fmoc-protected amino acids were purchased from NovaBiochem (San Diego, CA). The peptide, (**1**) Ac-EGSGRGDSP-NH_2 was synthesized on Rink amide resin using FastMoc™ (Applied Biosystems) chemistry on an ABI 433A automated peptide synthesizer (Applied Biosystems). The second peptide, (**2**) Ac-GQQQLGSEGRGDSP-NH_2 was synthesized at the Northwestern Institute for Bionanotechnology in Medicine center. The peptoid-peptide hybrid, (**3**) Ac-$(FKG)_2$-$(NMeg)_4$-E-NH_2, was also synthesized on the ABI 433A on Rink amide resin using a submonomer protocol.[160] The peptides and peptoid-peptide hybrid were cleaved from resin with a mixture of 2.5% triisopropylsilane 2.5% H_2O, and 95% trifluoroacetic acid (TFA) for 1.5 hours at room temperature. The peptides and peptoid-peptide hybrid were purified on a Varian preparative RP-HPLC system using a Peeke C18 preparative column, 20 mm x 250 mm (Palo Alto, CA) using a linear gradient of 0%-35% acetonitrile/water over 70 minutes for peptides, and 10-50% acetonitrile over 60 minutes for the peptoid-peptide hybrid, at 20 ml/min, both eluents contained 0.1% TFA. The peptides and peptoid-peptide hybrid molecular weights and purities were confirmed using MALDI-TOF spectroscopy and electrospray ionization spectrometry at Northwestern University's Analytical Services Laboratory.

5.2.9 Chemical Conjugation

The Ac-EGSGRGDSP-NH_2 peptide (**1**) and the peptoid-peptide hybrid Ac-$(FKG)_2$-$(NMEG)_4$-E-NH_2 (**3**) were grafted onto the protein polymer using 1-ethyl-3-carbodiimide hydrochloride (EDC, Pierce, Rockford, IL) and N-hydroxysulfosuccinimide (Sulfo-NHS, Pierce). The protein polymer was dissolved at 1 mg/ml in aqueous 0.1 M 4-morpholineethanesulfonic acid (MES), 0.5 M NaCl pH 6.0. A 2.5 molar excess of peptide **1** or peptoid-peptide hybrid (**3)** was added to the solution; reagent was added so the final concentration resulted in 50 mM EDC and 65 mM Sulfo-NHS. The reactions proceeded for 24 h before dialysis and analysis by MALDI-TOF spectroscopy. The number of molecules conjugated to the protein polymer was determined by the shift in molecular weight divided by the molecular weight of the pendant molecules.

An amine reactive poly(ethylene glycol) (PEG), NHS-m-dPEG™ (MW 333) was purchased from Quanta BioDesign Ltd.(Powell, OH). A solution was prepared of 97.56 mg NHS-m-dPEG™ diluted in 5 ml ddH_2O. A second solution of protein polymer was dissolved at 10 mg/ml in 0.1 M Sodium Phosphate, 0.15 M NaCl pH 7.2. The NHS-m-dPEG™ solution was added to 1 ml of protein polymer and reacted at room temperature for 1 hr. The degree of PEGylation was determined by MALDI-TOF spectroscopy. The number of conjugated PEGs was determined by the change in molecular weight.

The fluorophore, Alexa-fluor 488 5-TFP (Invitrogen), was conjugated onto the protein polymer as a example small molecular weight organic compound. Protein polymer was dissolved at 1.16 mg/ml in 0.1 M sodium bicarbonate, pH 9.0 and AlexaFluor 488 5-TFP was dissolved at 1 mg/µl in DMF. Approximately 50 µl of the AlexaFluor solution was added to 5 ml of protein

polymer solution. The reaction was incubated at room temperature with continuous stirring for 1 hr. Unreacted fluorophore and salt were removed by a centrisep spin column from Princeton Separations (Adelphia, NJ). The number of conjugated fluorophores was determined by MALDI-TOF spectroscopy.

The MALDI-TOF data was used to determine polydispersity of the multivalent scaffolds by:

$$M_n = \sum(N_i M_i) / \sum N_i \qquad \text{Eq. 1}$$

$$M_w = \sum(N_i M_i^2) / \sum(N_i M_i) \qquad \text{Eq. 2}$$

$$D = M_w / M_n \qquad \text{Eq. 3}$$

M_n = number average molecular weight, M_w = weight average molecular weight, N_i = signal intensity at point i, M_i = mass at point i, D = polydispersity.

5.2.10 Enzymatic Conjugation

Peptide **(2)** Ac-GQQQLGSEGRGDSP-NH_2 was conjugated to the protein polymer by tissue transglutaminase (tTG). Protein polymer was dissolved at 12 mg/ml in 200 mM 3-(N-Morpholino)propanesulfonic acid (MOPS), 20 mM $CaCl_2$, pH 7.7 buffer and peptide (**2**) was dissolved at 50 mg/ml in 2 mM (Ethylenedinitrilo)tetraeacetic acid (EDTA) pH 7.3 buffer. Approximately, 3.9 units of tTG were dissolved in 50 µl of 2 mM EDTA, 20 mM DL-Dithiothreitol (DTT), pH 7.7 buffer. Enzymatic grafting of peptide (**2**) was completed with 200 µl of protein polymer solution, 93 µl peptide (**2**) solution and 30 µl of tTG solution. The reaction was incubated at 37°C for 1 hour. MALDI-TOF spectroscopy was used to determine the number of peptides conjugated.

5.2.11 Gelation

Protein polymers were crosslinked at 10 wt% in 20 mM sodium phosphate 0.15 M NaCl by the addition of amine reactive crosslinkers. Bis(sulfosuccinimidyl) suberate (BS^3) was added to the protein polymer solution at approximately 80 mM. In a second gelation experiment, β-[Tris(hydroxymethyl)phosphino] propionic acid (THPP) was added to the protein polymer solution at a final concentration of 50 mM. For incorporation of the fluorophore, 1% of the total solution volume was composed of protein polymer-AlexaFluor conjugate, the remaining fraction was ungrafted protein; both were dissolved in MOPS buffer. Solutions were mixed vigorously and incubated at 37°C for 1 hour. Gelation was tested by sample inversion. Image of the fluorescent gel was captured on a Kodak Image Station (Rochester, New York) with UV transillumination, a 465nm excitation filter, 535nm emission filter with 5 second exposures.

5.3 Results

5.3.1 Rationale and Design of Protein Sequence

A new class of flexible, random-coil protein polymers was designed to display chemically reactive functional groups with a various distributions based on the controlled spacing of reactive functional groups. To accomplish this, we created a *de novo* repetitive protein sequence designed to be soluble in aqueous media at the appropriate concentrations for the intended applications. A critical parameter in the *de novo* protein design is the choice of amino acid sequence, since sequence can determine the overall protein solubility and structure. These parameters, however, can be challenging to predict and there can be unintended secondary and tertiary affects that

influence the final protein solubility at physiological conditions.[61] In addition, amino acid hydrophobicity and spacing may lead to protein aggregation.

The choice of amino acid sequence employed in our proteins polymers was based on previous research with random coil proteins. Previously, we reported on well-expressed, random coil, water soluble protein polymers with the sequences GAGQGSA[5], GAGQGEA[5], and GKGSAQA[159]. Additional combinations of the amino acids (Gly, Ala, Gln, Ser, Thr, Lys, Glu, Val) were also investigated. These genes either did not express well, or formed insoluble products (see Chapter 2). In the current investigation, the amino acid sequence was altered for better functionality, solubility, and stability. Glutamine residues were removed because they can undergo deamidation after exposure to acidic conditions.[161] In addition, glutamine is a hydrogen bond forming amino acid and may consequently aid in aggregation at elevated concentrations. The polar amino acids (threonine and serine) were added to promote water solubility. Evenly spaced lysine residues were included to introduce functional primary amine groups, as an alternative to carboxylate chemistry from the incorporation of a glutamic acid residue. Previous researchers have included sparsely spaced lysines in ELP proteins for chemical crosslinking and stabilization.[162] Based on their results and previous research with random coil lysine containing proteins,[159] lysine frequency was chosen at every 4, 6, and 8 amino acids.

5.3.2 Gene Construction

Three synthetic oligonucleotides which encode repeats of K4, K6, and K8 (GKGASGKGA, GKGTGA, and GKAGTGSA respectively) (Figure 5.2.1) were designed and PCR-amplified. The genes flanked by *Ear*I restriction sites were cleaved to create monomers.

The monomers were isolated and ligated together to produce multimers for controlled cloning. Controlled cloning allowed for the production of large concatemer genes without an amino acid sequence requirement. This technique enabled controlled creation of higher-order multimers (concatemers) by the reconcatemerization of pre-multimerized genes. In addition, this method prevented multimer intramolecular cyclization, which occurs during the self-ligation reaction and prevents gene insertion into the recipient vector.[159] Genes encoding 30 repeats of K4, 40 repeats of K6, and 30, 60, and 120 repeats of K8 were created by these techniques (Figure 5.3.1A).

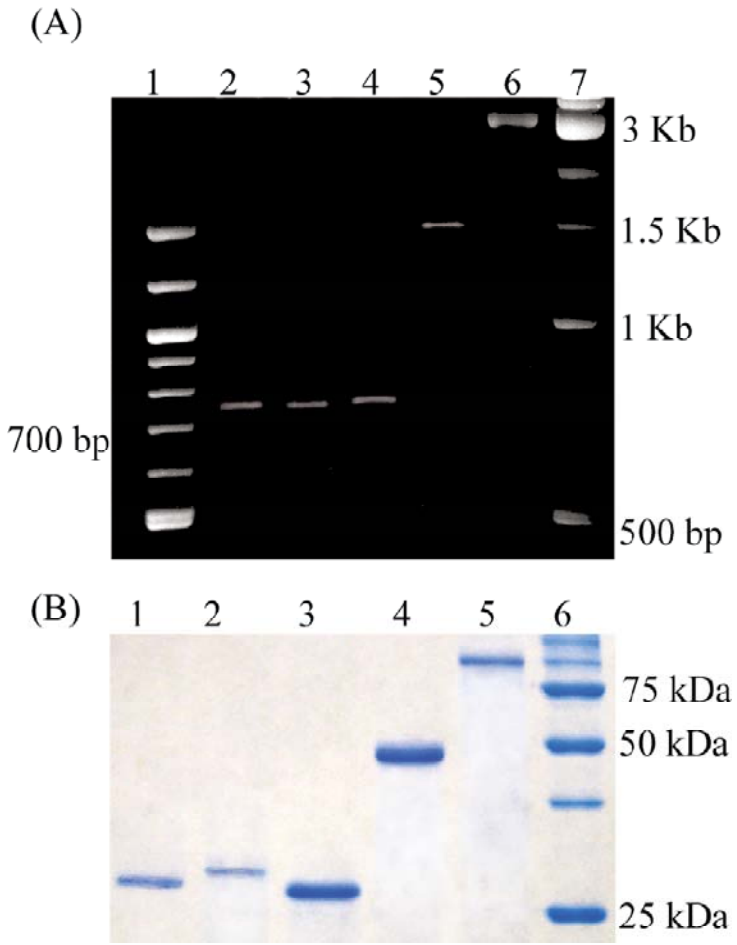

Figure 5.3.1: (A) 2% agarose gel of DNA genes digested out of the pET19 plasmid with *Nde*I and *BamH*I. Lane 1: 100bp marker, lane 2: $K6_{40}$, lane 3: $K4_{30}$, lane 4: $K8_{30}$, lane 5: $K8_{60}$, lane 6: $K8_{120}$ lane 7: 1kbp marker (B) 12% SDS-PAGE gel of purified protein polymers. Lane 1: $K6_{40}$, lane 2: $K4_{30}$, lane 3: $K8_{30}$, lane 4: $K8_{60}$, lane 5: $K8_{120}$ lane 6: protein standard.

5.3.3 Protein Expression and Purification

The proteins were successfully expressed in *E. coli* cells with the pET19 expression vector, despite previous concern that expressing proteins with high concentration of cationic residues could cause increased toxicity to the bacterial host.[163] During expression, toxicity was not observed with any of the recombinant proteins (Appendix B). The target proteins were easily purified utilizing nickel affinity chromatography (Figure 5.3.1B). Although the SDS-PAGE shows the proteins migrating at higher than expected molecular weights, this is not uncommon for engineered proteins, and was most likely due to charge and solvent effects.[164] Protein polymer expected mass was confirmed by MALDI-TOF MS analysis (Table 5.3.1) and amino acid results (data not shown). The yields ranged from 40 to 75 mgs of purified protein per liter of bacteria culture (Table 5.3.1).

Table 5.3.1: Protein polymer yield and MALDI-TOF

	Yield (mg/L)[a]	Expected Mass (Da)	Observed Mass (Da)
$K4_{30}$	54	22,110	22,086
$K6_{40}$	42	21,702	21,786
$K8_{30}$	75	21,732	21,789
$K8_{60}$	65	40,622	40,671
$K8_{120}$	52	78,402	79,020

[a]Yield given in mg of purified protein per liter of cell culture

5.3.4 Protein Characterization

The phase behavior of protein polymers in an aqueous solution was investigated by temperature-dependent turbidimetry. The cationic protein polymers were designed based on amino acid sequence to be water soluble over a large range of temperatures. Protein solubility was monitored by UV absorbance at 500 nm, as a function of temperature. Heating and cooling profiles for the protein polymers at a concentration of 1 mg/ml (12.7 to 46 μM), relevant to study ligand-receptor interactions and drug delivery, were essentially flat (Appendix C). However, the protein polymers showed a slight increase in absorbance at 80°C. The increase in absorbance did not appear to be reversible as indicated by the small hysteresis observed when cooling. The protein polymer length affected the initial solution absorbance, where longer proteins with the same amino acid sequence had a higher initial value, suggesting a decrease in protein polymer solubility determined by length. Protein amino acid sequence, in this set of constructs, had minimal influence on phase behavior. The three constructs, differing in lysine spacing, had essentially the same initial absorbance. However, $K8_{30}$ had a non-reversible shift in turbidity at elevated temperatures. At low concentrations, the higher concentration of charged groups in the K4 and K6 constructs likely assisted in solubility.

Circular dichroism (CD) was used to characterize secondary structure of the protein polymers in aqueous solution as a function of amino acid sequence, protein polymer length, and temperature. The CD spectra exhibited a minimum signal at 195 nm and a maximum at 212 nm, indicating that the proteins adopt a random coil conformation (Figure 5.3.2). As hypothesized the proteins do not adopt a folded secondary structure (β-sheet or α-helical structure), which can lead to protein aggregation and decreased solubility. Interestingly, for all the proteins, the per

residue molar ellipticity decreased as temperature increased, suggesting more flexibility and a distrubition of rotations of the peptide bond. Similarly, as protein polymer length increased, the spectra maintained the characteristic random coil conformation and the molar ellipticity per residue increased, suggesting a more disordered state and variation in rotation of the peptide bond with longer molecules (Figure 5.3.2B). Protein polymer lysine spacing and amino acid sequence did not appreciably affect conformation (Figure 5.3.2C). However, the amino acid sequence appeared to have influenced the per residue molar ellipticity. As spacing of the lysines increased there was a decrease in molar ellipticity, suggesting more restraint of the rotation of the peptide bond. This restraint may be caused by charge repulsion of the closely spaced cationic residues.

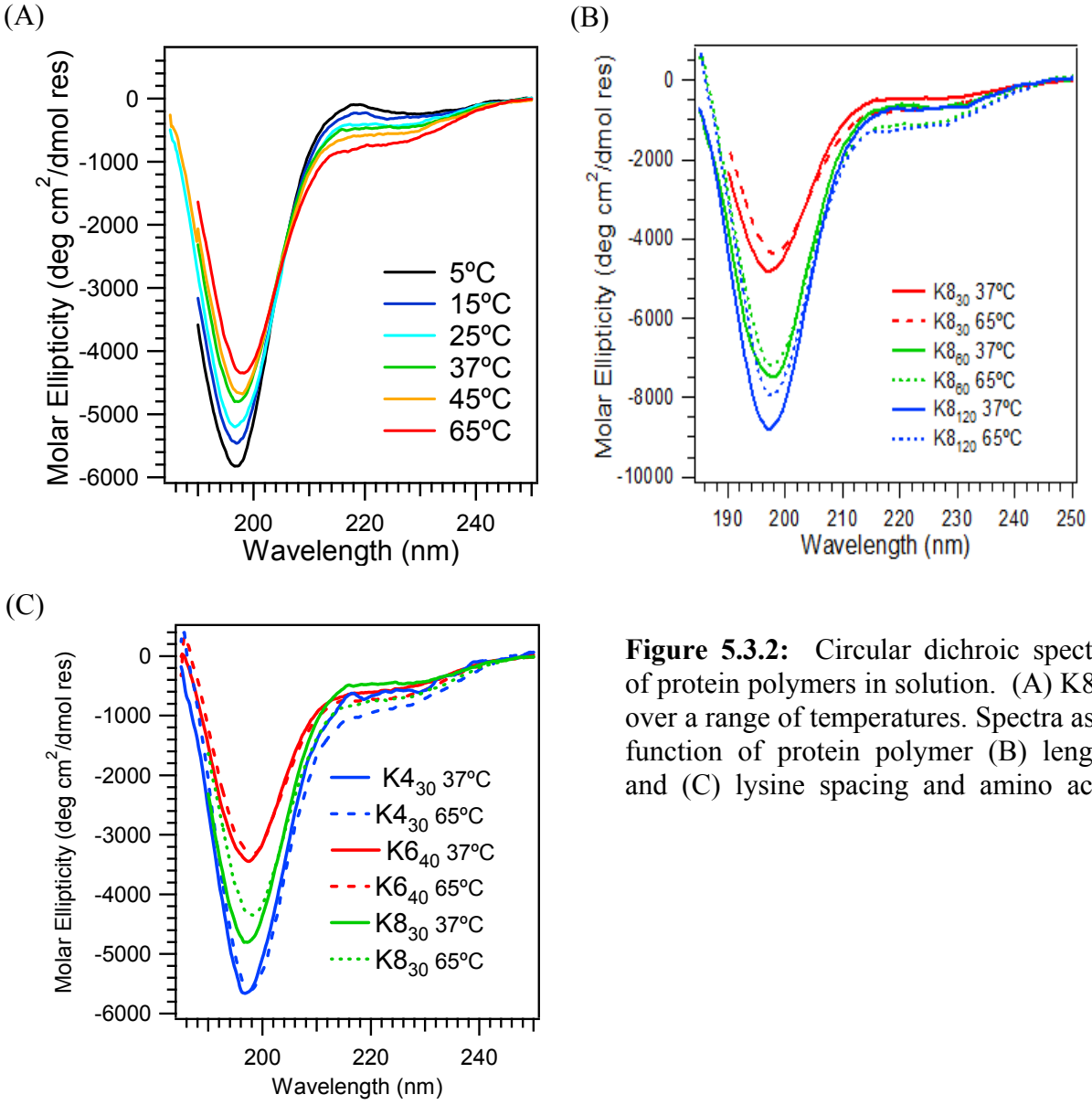

Figure 5.3.2: Circular dichroic spectra of protein polymers in solution. (A) $K8_{30}$ over a range of temperatures. Spectra as a function of protein polymer (B) length and (C) lysine spacing and amino acid

5.3.5 Biocompatibility of Cationic Protein Polymers

For further studies, protein polymers with lysine spaced every 8 amino acids (K8 proteins) were chosen as the model system because we anticipated less toxicity for biological applications due to the reduced number of lysine groups. The K8 protein polymers in solution at

concentrations between 10 μM to 5 mM were incubated with NIH 3T3 mouse fibroblasts and cell viability was examined after 4 hours. The percent of viable cells was determined from a Guava ViaCount™ Assay which determines cell viability based on permeability of DNA-binding dyes and can distinguish viable, apoptotic, and dead cells. Cells incubated with $K8_{30}$ at a concentration as high as 5 mM had low toxicity, with 98.8% viable cells (Figure 5.3.3). Proteins $K8_{60}$ and $K8_{120}$ were unable to be tested at 5mM concentration due to increased solution turbidity, which resulted in low cell counts with the Guava ViaCount™ system. Proteins with the same amino acid sequence, displayed some toxicity at elevated concentrations with increased protein length. The increased toxicity was possibly due to the concentration of cationic lysine groups, as poly(lysine) is known to be toxic to a wide range of mammalian cells.[165, 166] The $K8_{30}$ construct with 31 lysines per molecule exhibited the least toxicity; $K8_{60}$ with 61 lysines per molecule, had some toxicity starting at 1 mM concentration; and $K8_{120}$, containing the most lysines at 121 per molecule had toxic onset at a concentration of 50μM. Although the percentage of lysines remained constant with an increase in protein molecular weight, the total number of cationic residues clearly affect cell viability.

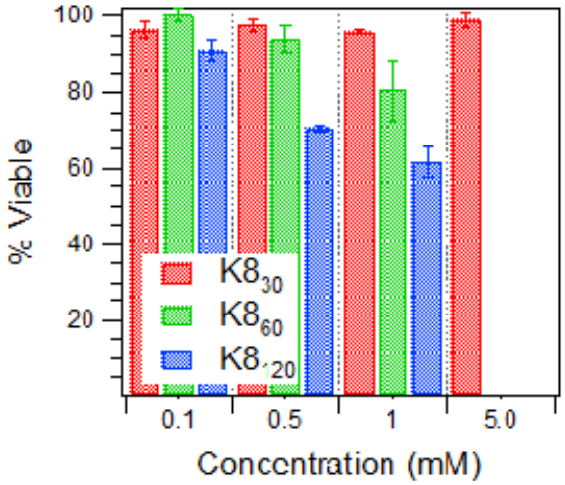

Figure 5.3.3: Relative cell viability after incubation with protein polymers. Viability determined by the Guava ViaCount™ Assay after 4 h incubation.

5.3.6 Protein Polymers as Protease Substrates

The protein polymers were determined to be degradable by two lysine targeted proteases. Trypsin, a pancreatic endoprotease and member of the serine protease family, hydrolyzes peptide bonds on the carboxyl side of lysine and arginine residues. The protein polymer $K8_{30}$ was fully digested by trypsin in under 30 minutes as indicated by a Coomassie-stained SDS-PAGE gel of the protein construct and its degradation products (Figure 5.3.4A). The second protease, plasmin, is a lysine targeted protease that cleaves the carboxyl side of lysine residues and arginine residues with a higher specificity than trypsin. *In vivo*, plasmin converts fibrin into solublized products for clearance. The lysine-based protein polymers were highly susceptible to plasmin cleavage; after 24 h incubation, virtually no full length $K8_{30}$ remained (Figure 5.3.4B). The multiple degradation sites in the protein allow for rapid degradation and potential polymer clearance *in vivo*. This would facilitate the release of the pendant molecules conjugated to the protein backbone.

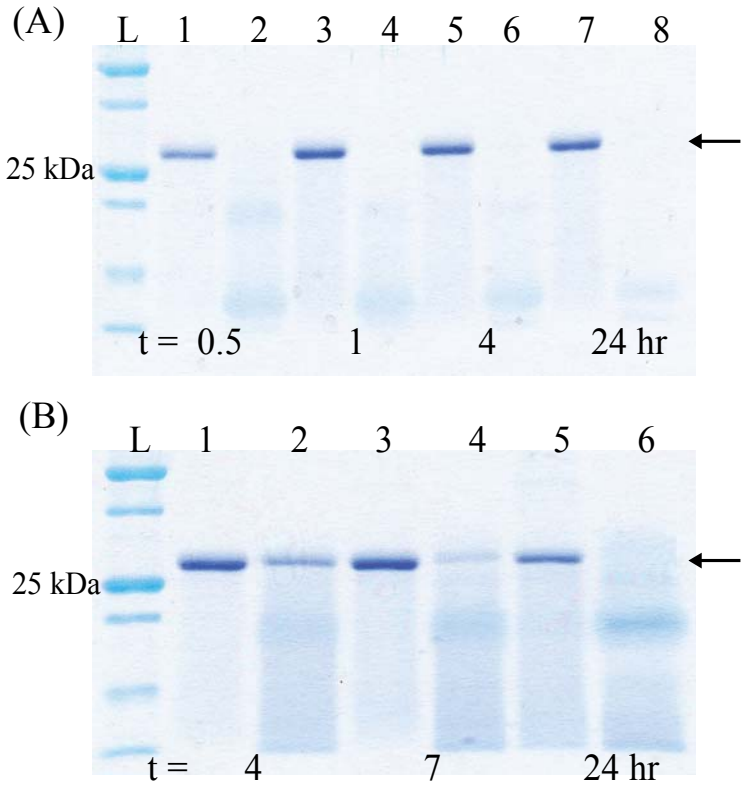

Figure 5.3.4: Protease degradation of K830 in solution with (A) trypsin and (B) plasmin. Control samples, incubated without proteases are displayed in odd lane numbers for each time point. Full length protein is indicated by the arrows. The protein $K4_{30}$ was also investigated for protease degradation, however there were complications with enzyme activity, for this reason, results are not presented.

5.3.7 Chemical Conjugation

The cationic protein polymers were designed to have reactive lysine that are susceptible to a variety of linking chemistries; the primary amines from the lysines can react with chemical groups such as N-hydroxysuccinimide ester (NHS) and with imidoester reactions. In this example, coupling was completed using 1-ethyl-3-(3-dimethylaminopropyl)carbodiimide hydrochloride (EDC), which links primary amines with carboxyl groups (Scheme 5.3.1).

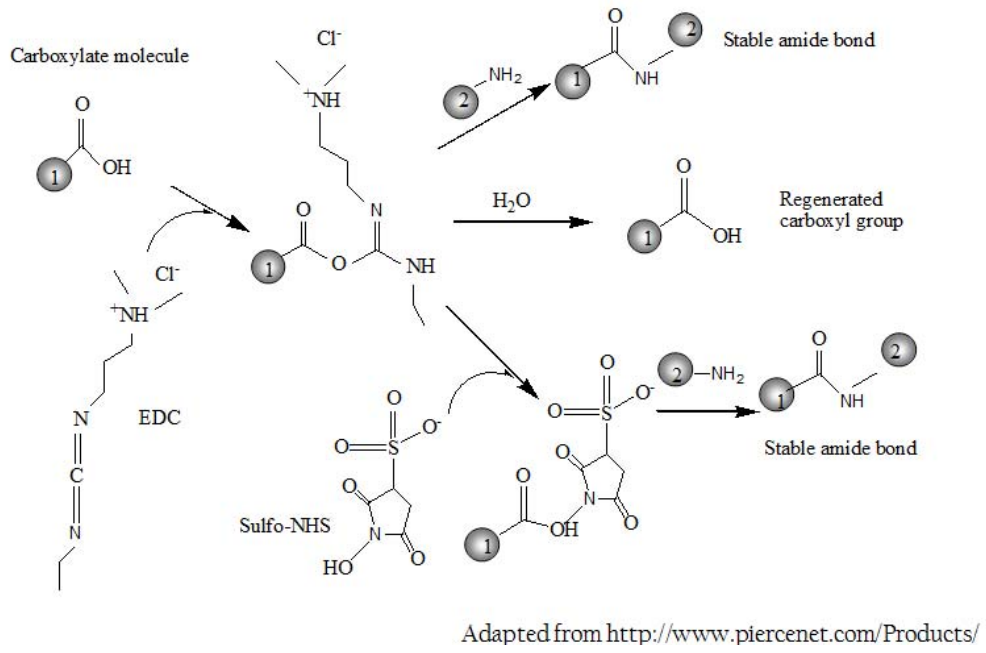

Scheme 5.3.1: Schematic of the chemical conjugation using EDC and Sulfo-NHS

The water-soluble EDC was used to form active ester functional groups with carboxyl groups on the pendant molecules using N-hydroxysulfosuccinimide (sulfo-NHS). A stable amide linkage was created in the presence of the protein polymer amine group, which attacks the carbonyl group of the ester and eliminates the NHS group. EDC conjugation in the presence of sulfo-NHS was efficient and increased the yield of conjugation versus EDC alone by mitigating the competitive reaction with water.[167]

Protein polymers were conjugated with a short bioactive peptide or peptoid-peptide hybrid using the EDC/Sulfo-NHS coupling method. The peptide Ac-EGSGRGDSP-NH_2, was employed

as a prototypical bioactive ligand for conjugation to the protein polymer backbone. This peptide contained the GRGDSP sequence, which is derived from the cell attachment site of fibronectin and recognized by a number of integrin receptors.[168] The peptide (**1**) was designed to have a water soluble glycine-serine spacer, after the glutamic acid residue, which afforded the carboxyl group for chemical conjugation. The bioactive peptide was coupled to $K8_{30}$; Figure 5.3.5A shows the incorporation of 8 RGD containing peptides (**1**) onto the 31 amine sites in $K8_{30}$ for 26% grafting. In the second example, a peptoid-peptide hybrid (**3**) was chemically crosslinked to the protein polymer. Peptoids, or poly-*N*-substituted glycines, have the amino acid side chains appended to the nitrogen rather than the α-carbon in the peptide backbone.[169, 170] Peptoids are extremely stable even to large temperature changes, proteases, and other denaturing conditions,[171, 172] and been shown to have non-fouling properties[173]. The peptoid-peptide hybrid potentially introduces non-fouling properties into the scaffold to possibly prevent protein and cell absorption. The peptoid-peptide hybrid (**3**), Ac-$(FKG)_2$-$(NMEG)_4$-E-NH_2 was synthesized on resin to include a free carboxyl group near the *C*'-terminus by the inclusion of a glutamic acid residue. The amine terminus contained an FKG repeat that could act as either an additional amine site for chemical grafting or as an enzymatic recognition site.[174] Through EDC/sulfo-NHS coupling, 6 peptoid-peptide hybrids (**3**) were conjugated onto $K8_{30}$, resulting in 20% coverage (Figure 5.3.5B). In principle, any peptide or peptoid-peptide hybrid could be coupled using this technique, introducing a range of functionality and modularity to the protein polymer scaffolds. Recently, using the same conjugation chemistry our lab has reported on the coupling of gadolinium chelators to these protein polymer scaffolds for use as MRI contrast agents.[175]

The protein polymers were also conjugated with PEG as a representative example synthetic polymer. PEG has been shown to be biocompatible and to increase the circulation time *in vivo* of drug carriers due to its slower clearance from the body,[176] a multivalent scaffold that is PEGylated may have some advantages in increasing scaffold solubility and retention, reducing aggregation and providing non-immunogenicity. PEG was incorporated onto $K8_{30}$ by the reaction of a low molecular weight, monodisperse functionalized NHS-PEG to the lysines in the protein polymer, forming stable amide bonds. We incorporated 12 PEGs onto $K8_{30}$ resulting in 39% grafting (Figure 5.3.5A).

A small molecular weight fluorophore was added to the protein polymer scaffold to allow *in vivo* and *in vitro* visualization. The Alexa Fluor 488 5-TFP has been used in applications such as photolithographic patterning of PEG based hydrogels[177] and labeling proteins for electrophoresis on microchips,[178] and was chosen as a prototypical small organic molecule for conjugation. The Alexa Fluor 488 5-TFP contained a tetrafluorophenyl ester for amine labeling. The fluorophore was successfully conjugated onto 4 sites on the $K8_{30}$ protein polymer, for 13% conjugation (Figure 5.3.5C). Since the fluorophore is very sensitive, the particularly low level of derivitization was desired as it leaves more lysine sites available for conjugation with other moieties or for aqueous solubility.

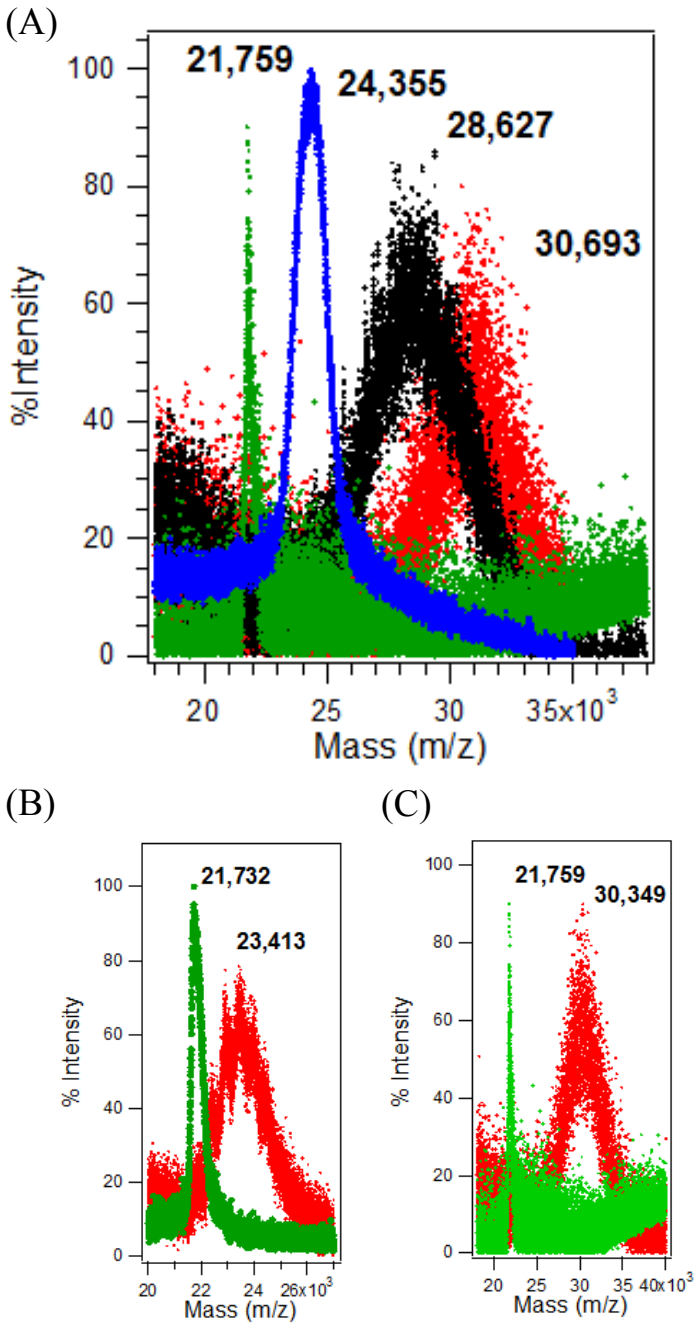

Figure 5.3.5: MALDI-TOF spectra of chemically conjugated protein polymer scaffolds. The protein $K8_{30}$ (green) was conjugated with (A) a RGD peptide (**1**) (black), PEG (blue), RGD and PEG (red), (B) peptoid-peptide hybrid (**3**) (C) Alexa Fluor 488. The unconjugated MALDI spectrum of $K8_{30}$ is shown in green in all graphs.

In these examples, the active ester conjugation techniques did not react to completion, allowing for multivalent coupling. Multivalent conjugation can be performed in a step-by-step or batch-wise coupling. For illustration, $K8_{30}$ was first conjugated with the bioactive RGD peptide (**1**) by the methods described above, and then in a second step was coupled with NHS-m-PEG. The resulting multivalent scaffold had 8 out of 31 sites occupied by the bioactive peptide (**1**) and 7 sites with PEG, resulting in 48% total coverage (Figure 5.3.5A). The remaining free amines in the scaffold aided in aqueous solubility.

As an alternative to chemical conjugation, enzymatic coupling by tissue transglutaminase (tTG) was investigated. Transglutaminases catalyze the formation of an isopeptide bond between the γ-carboxamide group on a glutamine residue and the ε-amino group on a lysine residue under biocompatible reaction conditions.[153] The covalent bonds created by tTG are highly protease resistant.[179] Successful enzymatic grafting was favored since the tTG sequence specificity is less stringent for amines than for glutamine residues.[180] The glutamine substrate on the short peptide sequence (**2**) was chosen based on research by Hu and Messersmith, where the sequence GQQQL was found to have high specificity towards tTG.[174] The protein polymers were tested as an acyl acceptor (lysine substrate) for tTG by coupling with these short peptides containing the acyl donor (glutamine substrate). Figure 5.3.6 shows tTG grafting of 15 monomers of peptides **2** onto the protein polymer $K8_{30}$ resulting in 48% coverage. Note; the glutamine substrate peptide (**2**) also contained the RGD cell adhesion sequence for presentation of an integrin-binding domain.

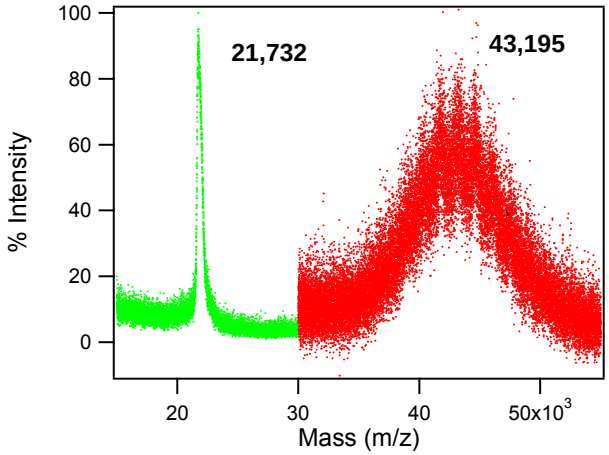

Figure 5.3.6: MALDI-TOF spectra of unconjugated (green) and conjugated (red) $K8_{30}$ protein polymers. The protein $K8_{30}$ was conjugated with peptide 2 by tTG.

One advantage of protein polymer scaffolds is their inherent monodispersity. Conjugation with non-natural proteins, however, does introduce some distribution of molecular weight. For this reason, the polydispersity index (PDI) was calculated for the conjugated protein constructs using equations (1-3). Table 5.3.2 shows the calculated PDI based on the MALDI-TOF MS spectra for each conjugate. In the case of polymers with low PDI (< 1.1), MALDI-TOF analysis gives a good estimate of molecular weight distribution.[181] The protein polymers conjugated the pendant molecules show a slight increase of PDI, however the conjugates are still extremely close to being monodisperse (PDI = 1.00). The very narrow range of molecular weight can be attributed to the monodisperse protein, which acted as the building block for the multivalent scaffold. The ability to conjugate a wide variety of materials to a scaffold and still maintain a nearly monodisperse product is advantageous for many biological applications.

Table 5.3.2: Estimated PDI for Protein Polymer Scaffolds Based on MALDI-TOF Spectra

	PDI
$K8_{30}$	1.000
$K8_{30}$-RGDpeptide	1.005
$K8_{30}$-PEG	1.001
$K8_{30}$-RGDpeptide-PEG	1.008
$K8_{30}$-peptoid-peptide conjugate	1.000
$K8_{30}$-Alexa Fluor 488	1.001
$K8_{30}$-Q-RGD	1.011

5.3.8 Gelation

The protein polymers were able to form self-sustaining hydrogels using amine-reactive crosslinkers, suggesting the possibility of creating multivalent gels. The first crosslinker investigated was bis(sulfosuccinimidyl) suberate (BS^3), a water-soluble homobifunctional NHS ester that reacts with primary amine groups at a pH 7-9 to form stable amide bonds. The unconjugated protein $K8_{30}$ was reacted with BS^3, and a hydrogel formed within 2 minutes (Figure 5.3.7A). The second chemical crosslinker tested was β-[Tris(hydroxymethyl)phosphino] propionic acid (THPP). THPP is a water-soluble trifunctional crosslinker that reacts with both primary and secondary amines to produce covalent linkages by a Mannich-type reaction. In addition, THPP has been shown to be a biocompatible chemical crosslinker to fibroblast cells,[182] suggesting that THPP crosslinking may be used for biocompatible *in situ* hydrogel formation.

The unconjugated protein $K8_{30}$ was dissolved in aqueous media and crosslinked with THPP; gelation was observed in under a 10 minutes (Figure 5.3.7B). The ability to chemically crosslink multivalent scaffolds with our protein polymers was recently shown with Gd chelators conjugated to $K8_{30}$. Gels crosslinked with glutaraldehyde showed increased contrast over controls.[175] In the present study, we incorporated $K8_{30}$-AF488 into the protein polymer hydrogel by chemical crosslinking with BS^3. As expected, the fluorophore activity was not affected by hydrogel incorporation and allowed for gel visualization (Figure 5.3.8). Both these examples demonstrate the feasibility to create multivalent hydrogels. Future studies will focus on adding bioactive domains to hydrogel surfaces to control cell behavior.

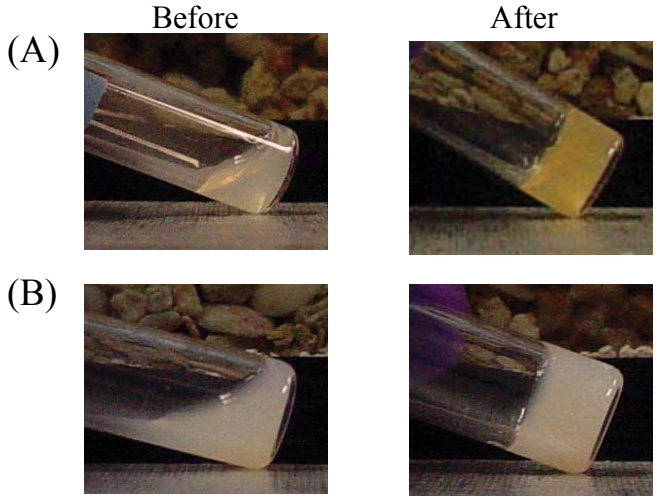

Figure 5.3.7: Photographs of $K8_{30}$ precursor solution before and after gelation with (A) THPP (B) BS^3 chemical crosslinking.

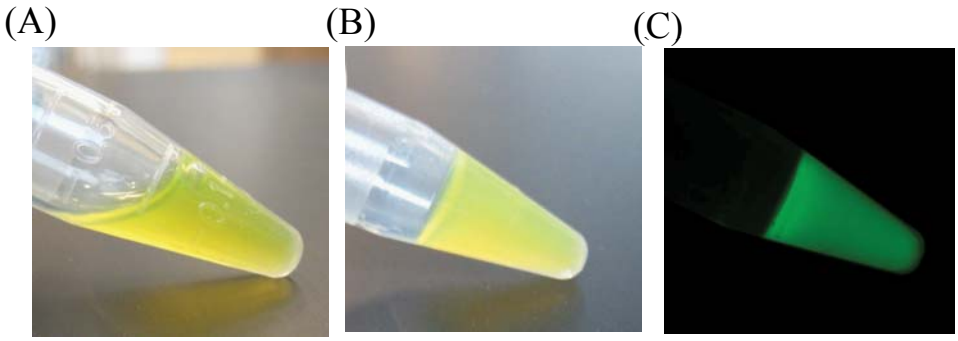

Figure 5.3.8: Photographs of $K8_{30}$-AF488 precursor solution (A) before and (B) after gelation with BS^3 chemical crosslinking. (C) Fluorescent image after gelation.

5.4 Conclusions

This chapter demonstrated the synthesis and characterization of a new class of cationic protein polymers with precisely defined molecular weight and reactive group spacing. We have used genetic engineering and recombinant protein expression to produce proteins that varying in length and molecular weight, creating proteins up to 79.2 kDa. The protein polymer length and amino acid sequence was shown to affect protein bulk properties in solution. As designed, the proteins were confirmed to be water soluble and random coil at physiological conditions. The protein polymers were biocompatible to mammalian cells at concentrations necessary form thearaputic delivery applications. Moreover, the $K8_{30}$ protein polymer was virtually non-toxic up to a concentration of 5 mM; however, as protein length increased the $K8_n$ n = 60 and 120 proteins displayed toxicity at concentrations above 0.1 mM. The cationic proteins showed some toxicity at elevated lysine concentrations which could be reduced by derivitization of the lysines through chemical or enzymatic grafting of non-toxic pendant groups. We have shown the ability

to chemically and enzymatically couple a range of molecules to the protein polymers. Chemically conjugation was utilized to covalently couple a short peptide containing a cell adhesion domain, and a peptoid-peptide hybrid to the protein polymer by the EDC/Sulfo-NHS reaction. In addition, amine reactive PEG and a small fluorophore were coupled to provide immune protection, and potential fluorescent material tracking respectively. Enzymatic grafting with tTG allowed the mild and biocompatible coupling of a second adhesion peptide. The ability to both chemically and enzymatically conjugate a range of pendant groups illustrates the versatility and modularity of the protein polymers as multivalent scaffolds. We also demonstrated the ability to create a polyvalent scaffold by the step-wise conjugation of a bioactive peptide and a non-immunogenic polymer onto the same protein polymer backbone, derivatizing 46% of the available lysines. Furthermore, these protein polymers had remaining free reactive sites that could undergo chemical crosslinking to form self-sustaining hydrogels using di- and tri-functional amine chemical crosslinkers. These results suggest the ability to create a multitude of materials with multiple pendant groups for biological applications. These materials are being investigated as multivalent display surfaces or gels for biomedical research.

Chapter 6

Properties of Protein Polymer-Based Enzymatically Crosslinked Hydrogels

6.1 Chapter Introduction

Previously, we described the development of a class of recombinant protein polymers that have potential application for multivalent display in solution or incorporated into hydrogels by chemical crosslinking. Furthermore, it was shown by enzymatic grafting of short peptides that the lysines in the protein polymers could serve as amine substrates for tissue transglutaminase (tTG). As a continuation, this chapter explores the use of tTG to engineer protein polymer-based hydrogels. The enzymatically crosslinked hydrogels are derived from mixtures of the lysine containing protein polymers and a new family of protein polymers that contain a tTG glutamine substrate. In the presence of enzyme, these proteins rapidly form self-sustaining hydrogels. This approach was used to develop a modular protein polymer-based hydrogel that would be ideal for *in situ* gelation and have a range of material properties depending on formulation. The resulting hydrogels were investigated initially as platforms for islet cell encapsulation for the treatment of type I diabetes.

6.1.1 Tissue Engineering with *In Situ* Hydrogels

Biomaterials are a central feature in tissue engineering for regenerative medicine. For cell-based therapies, the biomaterials are designed to provide the appropriate signals to promote tissue development and ultimately restore normal tissue function *in vivo*. To achieve this goal, the biomaterials must provide a three-dimensional support and interact with cells to control cellular function and guide the multicellular processes of tissue formation and regeneration.[183] Hydrogels currently used in research are formed from natural or synthetic materials. Natural materials often have biological functionality and are nontoxic, but sources can be limited, properties vary from batch-to-batch, there is a confined ability to control material structure and properties, and there can be complexities associated with pathogen transmission and immunogenicity.[183] Synthetic polymers have been applied as biomaterials for tissue engineering because they address these shortcomings while providing more design flexibility and control over material properties. Polymers made from chemical synthesis, however, do not contain biological function, and may be toxic due to residual monomers and crosslinkers. Recombinant protein polymer-based materials, however, can combine the advantages of both natural and synthetic materials while avoiding some of the limitations.

In the last decade, research has shifted from pre-formed hydrogel implants to injectable materials that form a gel at the site of injection.[184] These materials can be introduced to the body by minimally invasive procedures, such as laparoscopy.[185] Non-invasive delivery is not appropriate for preformed scaffolds, where the surgery for implant has inherent safety risks and can result in damage of the surrounding tissue. These risks and the potential to increase the site of injury can be substantially eliminated by having an *in situ* gelling material. *In situ* material

precursors are delivered prior to solidification, where gelation is triggered *in vivo* by chemical or physical changes.[186] Materials that form at the site of injury can adapt to the shape of the defect site. In addition, these materials have the potential to deliver multiple therapeutic agents simultaneously in a non-invasive manner. Approaches to create *in situ* gelling materials are reviewed below.

6.1.2 Mechanism of *In Situ* Gelation

Many natural *in situ* gelling materials solidify in response to temperature, pH, or by self-assembly. Natural materials, derived from biological sources, often form and are stable under mild conditions of temperature and pH. For example, fibrin, a natural component of the body, gels at room temperature in the presence of thrombin; thrombin cleaves soluble fibrinogen into insoluble strands of fibrin which then self-assembles and is further crosslinked by a transgulatminase enzyme, factor XIII. Many natural materials, however, do not require the use of an enzyme for gel formation. For example, the polysaccharide, chitosan, found in the shells of crustaceans, gels in response to pH changes from acidic to neutral conditions,[187] and by solution ionic strength[188]. Alginate, another polysaccharide from brown algae, is a well-known injectable material due to its ability to rapidly gel by ionic crosslinks through the complexation with divalent cations. In addition, collagen-based materials have been engineered to have *in situ* gel formation. Collagen-materials can be designed to undergo a temperature-sensitive gelation when heated, allowing for delivery by injection. Similarly, elastin is a protein-based material that self-assembles at a set temperature (as discussed in Chapter 2).

These natural materials are advantageous because they are easy to use, readily available and relatively inexpensive. Furthermore, they support cellular growth, contain biological recognition, and are biocompatible. For example, fibrin has proteolytic sites that allow for cellular remodeling which result in a neither non-toxic degradation nor inflammatory reaction.[189] Despite these advantages, there are significant disadvantages associated with natural *in situ* gelling materials. Natural materials require careful measures to avoid an immunogenic response and may not be biocompatible depending on source (such as alginate and chitosan). Materials from exogenous animal sources have the potential to cause viral transmission. For these reasons complete purification is necessary, particularly in hyaluronate, which requires thorough purification to remove impurities and endotoxins.[190] In many cases, the self-assembly or association is relatively weak.[189] For example, the ionic complexation of alginate often dissolves unpredictably. In order to improve the mechanical strength of some natural scaffolds, additional crosslinking schemes have been investigated. To this end, the materials require modification before they can be gelled *in situ*. For example, hyaluronic acid requires the incorporation of polymerizable groups before *in situ* gelling.[191] Chemical crosslinking with agents such as glutaraldehyde, in the case of collagen, improves mechanical strength. However, the possibility for residual crosslinking agents remaining in the final gel can be problematic due to toxicity to surrounding cells. For this reason, chemical crosslinking is not appropriate to be used for *in situ* gelation. As an alternative, photopolymerization has been used to crosslink hyaluronate.[192] In these cases, the chemical nature and location of the crosslinking site can be unregulated, creating non-uniformity on the microscale.[193] Despite these additional crosslinking schemes, the degree and the range of mechanical strength for natural materials are still limited.

6.1.3 Synthetic *in situ* gelling materials

Hydrogels from synthetic materials have been developed to overcome some of the above mentioned problems, potentially providing a greater range of mechanical properties, having more control over tissue responses, tunable durability and degradation rate *in vivo*. Self-assembling systems like β-sheet forming peptides,[194] or peptide amphiphiles,[195, 196] can be formulated to have stimulus-sensitive gelation based on pH or ionic strength. Moreover, synthetic polymers have been modified for self-assembly, for example, block copolymers composed of poly(ethylene glycol) (PEG), polypropylene glycol (PPG), or polylactic acid (PLGA), have gelation based on block hydrophobicity. Poly(N-isopropylacrylamide) (Poly(PNIPAAm)), similar to elastin-based materials, can be developed such that a hydrogel forms *in situ* above a critical phase transition temperature.[197] Physical polymeric gels, however, traditionally have limited mechanical strength. For this reason, polymers, like PEG, PLLA, and polycaprolactone, have been modified for *in situ* photopolymerization.[60, 198-200] However, photocrosslinking has limited penetration ability, requires harmful catalysts, and is an exothermic process which may consequently damage nearby cells making it less favorable.

6.1.4 Enzymatic Crosslinking by Transglutaminase

Natural enzymatic crosslinking overcomes the disadvantages of other synthetic crosslinking schemes. Most importantly, it does not require toxic crosslinking components or a UV light source, but still forms strong covalent bonds. Tissue transglutaminase (tTG) is a

naturally occurring enzyme found throughout the body that forms covalent bonds with mild and biocompatible conditions. The enzyme catalyzes a calcium-dependent acyl transfer between the γ-carboxamide group of a glutamine residue and the ε-amino group of a lysine residue. Furthermore, mammalian tTG recognizes many endogenous and exogenous proteins[179] and primary amines on small polyamines such as spermidine and putrescine.[201] The biocompatibility of the enzyme ensures that there are no toxic byproducts and tTG substrate recognition can be moderately controlled by amino acid sequence, thus allowing specificity of the reaction. The ability for tTG to crosslink amines from proteins as well as small polyamines allows for the incorporation of natural and synthetic molecules, thus conferring flexibility. Since tTG bond formation is calcium-dependent, the reaction can be controlled by adding calcium to the medium.[153] Finally, the bonds formed by tTG are highly protease resistant, ensuring sustained crosslinking *in vivo*. For these reasons, the extracellular matrix crosslinker, tTG was selected for the *in situ* formation of hydrogels composed of the random coil protein polymers.

Griffith *et al*. first investigated transglutaminase for the formation of a hydrogel network of functionalized PEG.[202] Motivated by this investigation, Barron and Messersmith *et al*. crosslinked a 4-armed PEG in which each arm terminated with a recognition peptide sequence for factor XIIIa, a member of the transglutaminase family.[203] Through this enzymatic crosslinking, the 4-armed PEG formed robust, elastic solids with a dense morphology. More recently, the crosslinking chemistry of factor XIIIa was replicated for coupling cell adhesion ligands and growth factors to multi-arm PEG and for simultaneous hydrogel formation.[204, 205] Likewise, enzymatic gelation by transglutaminase has been applied to genetically engineered ELP hydrogels to create an injectable *in situ* crosslinking scaffold and resulted in an increase in

the dynamic shear stiffness of the resulting material.[206] Inspired by this research, we investigated hydrogel formation by tTG with random coil protein polymers. The protein polymers were designed with more densely spaced reactive sites in comparison to the ELPs to improve mechanical properties.

6.1.5 Design of Protein Polymers that serve as a TG substrate

Enzymatically crosslinked protein polymer hydrogels required the creation of proteins that could serve as lysine and glutamine substrates. As shown in Chapter 5, the lysine containing protein polymers were able to act as an amine sites when enzymatically crosslinking bioactive peptides onto the protein. Initially, we intended to chemically attach glutamine containing peptides onto the lysine-based protein polymers and then crosslink with unmodified lysine proteins. However, no gelation was observed possibly due to intramolecular crosslinking due to incomplete peptide coupling to the lysine sites. For this reason, a second family of protein polymers was created that contained the glutamine substrate, GQQQLG, which has been shown to have high reactivity to tTG.[174]

6.1.6 Preliminary Application: Islet Cell Encapsulation

The initial application of the enzymatically crosslinked protein polymer hydrogels was for islet cell encapsulation for the treatment of type I diabetes. Early onset type I diabetes is an autoimmune disease that results in the permanent destruction of insulin producing β-islet cells of the pancreas. Current, treatment options include insulin replacement therapy, by insulin

injection, whole pancreatic transplantation, or β-cell replacement. These treatments are limited-insulin replacement therapy is a lifetime commitment and pancreatic transplant requires life-long immunosuppression. Although islet cell transplantation requires immunosuppression, it is less invasive than major surgery and has shown some relief from continuous insulin supplements.[207] Despite these promising results, several key obstacles have to be overcome for successful islet replacement therapy, including minimization of the damage to islets during isolation, preventing islet death after implantation, and increasing long-term *in vivo* function of islets. The development of islet encapsulating materials is one approach to meet these goals; where the biomaterial can prevent cell death by promoting revascularization and increase islet function, by delivering growth factors and biologically active peptides, to ultimately reduce the number of required islets for disease reversal.

Initial biomaterial approaches for islet encapsulation were designed to provide immunoisolation of islets to suppress an inflammation response. In this work, islets were enclosed in a semi-permeable membrane that allows the passage of glucose, insulin and other nutrients to reach the islets, but prevents immune cells and antibodies from crossing the membrane. The immunoisolation approach, however, ultimately failed due to limited oxygen supply to the islets and incomplete immunoprotection, due to the passage of small pro-inflammatory factors into the biomaterial.[208] Recent approaches focus on the delivery of growth factors and peptides from a biomaterial to encourage revascularization and promote islet function.[209-211] For example, the Anseth laboratory has investiaged PEG-based multilayer, multifunctional hydrogels as islet encapsulation barriers that provide a localized biologically active islet microenvironment by covalently coupled peptides,[212] while presenting an inert,

immunoprotective exterior surface to the host environment, to minimize graft-host interactions.[212] Furthermore, apoptosis-inducing monoclonal antibodies have been attached to PEG-modified hydrogels to create a material surface that actively down-regulates the immune response.[213] Inspired by these approaches, we were motivated to apply protein polymers as a platform for a multi-functional hydrogel for islet encapsulation.

6.2 Experimental Section

6.2.1 Protein Polymer Synthesis

The lysine containing protein polymer amino acid sequences, and cloning and expression techniques are presented in Chapter 5. The BQ proteins were cloned using the controlled cloning[159] procedure described in Chapter 5. BQ DNA genes were composed of two blocks, block *a* contained the glutamine amino acid sequence for tTG and block *b* contained a highly water soluble amino acid sequence (Figure 6.2.1).

a-block

(Gly Gln Gln Gln Leu Gly Gly Ala Gly
G CTA GCC ATA T**GC TCT TC**A GGT CAG CAA CAG CTG GGT GGT GCC GGT

Thr Gly Ser Ala Gly Gln Gln Gln Leu Gly Gly Ala Gly Thr Gly
ACC GGC TCC GCA GGT CAG CAA CAG CTG GGT GGC GCG GGT ACG GGC

Ser Ala)
TCT GCA GGT T**GA AGA G**GG ATC CAC TAG T

b-block

(Gly Ala Gly Gln Gly Glu Ala Gly Ala
G CTA GCC ATA T**GC TCT TC**A GGT GCG GGC CAA GGA GAA GCA GGT GCT

Gly Gln Gly Glu Ala Gly Ala Gly Gln Gly Glu Ala)
GGA CAG GGC GAG GCA GGA GCT GGC CAA GGT GAA GCG GGT T**GA AGA**

GGG ATC CAC TAG T

Figure 6.2.1: Oligonucleotide sequences of block a and b to create the protein polymer BQ. DNA bases in blue denote *Eam*1104 I and *Sap*I recognition sites

DNA single-stranded oligonucleotides *a* and *b* were amplified separately by PCR then digested with the enzyme *Eam*1104 I and ligated into pUC18 cloning plasmid. The insert of *a* in the pUC18 plasmid was amplified by bacterial culture and extracted by plasmid miniprep, while insert of *b* was amplified by PCR with primers that eliminate one of the *Sap* I restriction sites adjacent to the DNA sequence of interest. Since *Eam*1104 I and *Sap* I have restriction sites that vary by one nucleotide, *Eam*1104 I can digest all *Sap* I sites, but not vice versa. Utilizing this

concept, both *a* and *b* were digested by *Sap* I to produce *a* with double cohesive ends and *b* with one cohesive end. By removing the phosphate group of *a* with calf intestinal phosphatase, only one possible ligation site existed, enabling a controlled reaction between the two nucleotide strands. A 5′ phosphate group was added and the gene was digested to create two cohesive ends for ligation into the pUC18 plasmid, resulting in a combined gene of *a* and *b*. Gene multimers were created as previously described. Protein expression with pQE15 and immobilized metal affinity chromatography purification techniques are the same as that used for the lysine containing proteins in Chapter 5. The purified glutamine containing proteins had the sequence $[(GQ_3LG_2AGTGSA)_2(GAGQGEA)_3]_n$ where n=1, 6, 12, and further denoted as BQ_n. MALDI-TOF analysis was used to analyze the molecular weight of the resulting proteins.

6.2.2 Hydrogel Formation

The general procedure for protein polymer hydrogel formation was as follows: *Solution 1:* the lysine containing protein $K8_x$ was resuspended in 200 mM MOPS, 20 mM $CaCl_2$, pH 7.65 at 10 wt% unless otherwise indicated; *Solution 2:* the glutamine containing protein BQ_n was resuspended in 2 mM EDTA pH 7.3 at 10 wt% unless otherwise indicated; *Solution 3*: 0.02 units/ μl of tTG from guinea pig liver (Sigma) was dissolved in 2 mM EDTA, 20mM DTT pH 7.7. For swelling, degradation, toxicity, and SEM experiments, the final gelation volume was composed of 37.5% *Solution 1*, 37.5% *Solution 2*, and 25% *Solution 3*. For rheological experiments Solution 3 was prepared so tTG was at the appropriate molar ratio depending on test conditions.

Rheological experiments were also performed with a hybrid hydrogel with a 4-armed PEG that had each arm terminating in the glutamine substrate for tTG[174] (graciously provided by

M. Jones and the Messersmith laboratory at Northwestern University). The hybrid hydrogels were composed of $K8_n$ (n = 30, 120) at 10 wt% in *Solution 1*; PEG-Q at 10 wt% in *Solution 2*; and the appropriate enzyme concentration to maintain molar ratio of enzyme units to lysine sites, in *Solution 3.* For all rheological experiments, prior to the addition of *solution 3*, the appropriate amounts of *solution 1 & 2* were vortexed together; *solution 3* was added in place and mixed with the protein precursor solution by pipette.

6.2.3 Swelling and Degradation

Hydrogels were cast into disks for swelling and degradation experiments. Approximately, 20 µl of both protein solutions (*Solution 1 &2*) were mixed by vortexing and then dropped onto a slide treated with SigmaCote (Sigma) that created a hydrophobic glass slide surface to prevent solution spreading. Enzyme solution was added and mixed (13.3 µl *Solution 3*) by pipetting solution up and down. Spacers of 2 mm thickness were used to cast gels of uniform thickness. A second hydrophobic glass slide was placed on top of the spacers and the top and bottom slide were clamped with clips. The precursor solution spread to form a disk of uniform thickness. Disks were approximately 2mm think with a diameter of ~ 5.4 mm. The solution was then allowed to gel in a humid environment for 45 minutes. After gelation, the hydrogel was gently removed from the slide and placed into an eppendorf tube with buffer for subsequent experiments.

Swelling experiments were conducted by incubating the gels in 1.5 ml of ddH_2O or PBS for up to 48 h. Swollen gels were removed from solution and the surface was blotted dry before weighing to determine wet mass, M_W. No observable change in wet mass was detected in PBS

vs. ddH_2O (data not shown), for this reason, swelling is reported in water. The gels were weighed after 6, 24, and 48 h; after 24 h, no change in mass was observed, thus all swelling data is reported after a 24 h incubation in water. Hydrogel dry weight, M_D, was determined by gel lyophilization and then weighing. All mass determinations were done on a high precision balance. Degree of swelling was calculated by $(M_W-M_D)/M_D$.

The recombinant protein polymer hydrogels were characterized in terms of their biochemical degradability by plasmin (Sigma). Hydrogels were prepared as disks described above. After gelation for 1 hr, hydrogels were allowed to swell in 20 mM Tris, 150 mM NaCl, pH 7.6 for 24 hours. Initial wet weight was determined and the hydrogel was lyophilized to determine initial dry weight, M_{D0}, before introduction of enzyme. The lyophilized hydrogels were allowed to swell in buffer for 24 h. Swelling buffer was removed and 1 ml of plasmin solution (0.3 units/ml 20 mM Tris, 150 mM NaCl pH 7.6) was added to the samples. At each time point, plasmin solution was replaced with ddH_2O and hydrogel wet mass was determined by weighing the gel (surfaces were blotted with a kimwipe to remove excess water). Two additional changes in water were done to remove residual salt and plasmin. Samples remained in water for 6 hours before being lyophilized. After lyophilization, sample dry weight was determined by measuring, M_D. Mass loss was determined by M_D-M_{D0}/ M_{D0}.

6.2.4 Cell Culture and Viability Assays

NIH3T3 fibroblasts (ATCC, Manassas, VA) were cultured at 37 °C and 5% CO_2 in DMEM (Gibco) supplemented with 1 % sodium pyruvate, 1% penicillin-streptomycin, 1.5 g/L $NaHCO_3$, and 10% fetal bovine serum (Gibco). Cells were grown to approximately 75% confluence and

removed with 0.05% Trypsin-EDTA in Hanks' Balanced Salt Solution with phenol red (Fisher Scientific). Fibroblasts encapsulated in the hydrogel were created as follows: the NIH3T3 cells were trypsined and resuspended in normal culture media and gently centrifuged at 2,000 rpm for 3 min, media was removed from the cell pellet and the cells were resuspended in 15 µl of *Solution* 1 and 15 µl of *Solution 2*. After gentle mixing by pipetting, the suspension was added to the well of a cell culture dish with a coverslip bottom. Approximately 10 µl of *Solution 3* with tTG was added and mixed by pipetting; gelation occurred within 10 min at 37°C. Cell culture media was added and cells were incubated for 24 h before the assay. The viability of encapsulated cells was determined using a LIVE/DEAD Viability/Cytotoxicity Kit (Molecular Probes, Invitrogen, Carlsbad, CA) which determines membrane integrity of the cells. Approximately, 20 µl of LIVE/DEAD reagent was added directly to the cell culture media and allowed to react in a dark environment for 1 h. Confocal microscopy was used to visualize the fluorescently stained cells.

Mouse islet cell isolation and viability staining was conducted by Hermann Kissler at the Northwestern Islet Transplantation Laboratory. Islets were isolated from ten 13-week old male C57BL/6 donor mice. Approximately 50 islets were encapsulated in a 50 µl total volume polymer hydrogel, composed of 18.75 µl $K8_n$ 10 wt%, 18.75 µl BQ_6 15 wt%, and 12.5 µl tTG (0.04 units/µl). The precursor solution was allowed to pre-gel for 3 min before the addition of islets. Encapsulated islets were cultured for 36 h before fluorescent staining. Islet viability was determined by fluorescein (FDA) and propidium iodide (PI) staining. In addition, islet mitochondrial membrane integrity was determined using tetramethylrhodamine (TMRE), which

fluorescently stains intact mitochondria red. Mictochondria that have undergone apoptosis are stained given by a non-specific interaction of YOPRO to DNA.

6.2.5 SEM

Hydrogel morphology was determined by variable pressure scanning electron microscopy (VP-SEM) and traditional scanning electron microscopy (SEM). Hydrogel samples were prepared on hydrophobic glass slides as described above, except that a cover slide was not used. A total volume 20 µl of solution was used to cast the gel. After gelation at 37°C for 45 min, hydrogels were placed in ddH_2O for 24 h to allow complete swelling. For traditional SEM, swollen gels were dehydrated at room temperature in ethanol solutions of increasing concentrations (10, 20, 40, 60, 80, 90, 100% ethanol). For each concentration, gels were incubated in solution two times for 10 min each. The samples were critical point dried, mounted, and sputter-coated with 9nm of Pb/Au. VP-SEM samples were kept in ddH_2O prior to imaging. All SEM imaging was done using a Hitachi S3400-N VP-SEM with an accelerating voltage of 10-20kV, working distance of 5 mm, SE or BSE detector, and pressure of 50 Pa in VP mode.

6.2.6 Viscoelastic Properties

Time for gelation on the microscale was determined by particle tracking microrheology. The particle tracking system was composed of a lab-build epifluorescent videomicroscope with a Nikon TE200 inverted microscope using a 0.5" CCD TM-6710-CL camera. Videos were collected at 10-120 frames/sec and analyzed using IDL software and tracking code.[4] Samples were composed of 1.5 wt% $K8_{30}$, 1.5 wt% BQ_6 and 8.5 units/ml of tTG were suspended in 15 µl

gelation buffer with neutral ~ 0.5 μm fluorescent tracer particles. The mean square displacement for the particles was calculated at each time interval prior and after enzyme addition.

Hydrogel bulk material properties were determined by oscillatory rheology. Rheological experiments were performed with a Paar Physica MCR300 Rheometer with peltier temperature control. A stainless steel cone and plate (25mm diameter, 2° angle) device was used with 250 μl final sample volume. Approximately 93.75 μl of the lysine containing protein and 93.75 μl of the glutamine containing protein were mixed by vortexing before pipetting onto the device. Enzyme, in the appropriate concentration to maintain the same molar ratio of units to lysine reactive sites, in a volume of 62.5 μl was then added directly to the solution on the rheometer platform. Sample mixing was achieved by carefully pipetting up and down to ensure no air bubble formation. A humid chamber was achieved by placing a layer of wet kimwipes around the platform then and placing a chamber cover on top. For frequency and strain sweep experiments, the cone and plate was lowered to the measuring height and held for 1 h with a temperature of 37°C using a thermostatted plate with pieltier temperature control. For time measurements, oscillatory test began directly after sample mixing. The measurements of the storage and loss modulus during frequency sweeps were taken in the oscillator mode at 1 % strain, and strain sweep experiments were performed with a strain ranging from 1% to 100% at an angular frequency of 10 s^{-1}.

6.2.7 Preliminary *In Vivo* Islet Encapsulation Assays

Preliminary hydrogel islet encapsulation was conducted in collaboration with Hermann Kissler in the Kaufman laboratory at the Northwestern Islet Transplantation Laboratory. Approximately, 250 islets were transplanted into the epididymal fat pad of age matched

CB57BL/6 recipient mice. Before transplant, mice underwent sreptozotocin-induced diabetes with 220 mg in 0.9% NaCl of sreptozotocin per kg of mice body mass. Positive control groups included 5 normal mice without the treatment with sreptozotocin. The negative control group consisted of 4 mice that were chemically induced to be diabetic and not further treated. Three groups of transplants were conducted; the first with control islets not encapsulated in a hydrogel (2 mice), one group with islets encapsulated in a hydrogel composed of 4 wt% $K8_{30}$ and 6 wt% BQ_6 and 10 units/ml of tTG (2 mice), and islets encapsulated in a hydrogel composed of 4 wt% $K8_{60}$ and 6 wt% BQ_6 and 10 units/ml tTG (2 mice).

The blood glucose levels and weight of all transplant and control groups were monitored bi-weekly. Intraperitoneal glucose tolerance tests were conducted in weeks 2, 4, 6 after transplant and at week 11 after epididymal fat pad removal. Fasting mice were injected with glucose in the intraperitoneal space and the blood glucose level as a function of time was monitored. After graft removal, histology was done with the epididymal fat pad paraffin embedded and stained by hematoxylin and eosin Y (H&E). Hematoxylin stains basophilic structures containing nucleic acids, with a blue-purple hue, and acidic eosin Y stains eosinophilic structures composed of intracellular or extracellular protein pink. Graft histology was investigated using insulin staining.

6.3 Results and Discussion

Previous results indicated that although $K8_n$ does not contain the preferred lysine substrate for tTG (FKG), it still serves as an amine group for enzymatic bond formation. A completely protein polymer-based hydrogel was created using the $K8_n$ proteins and a new family

of proteins, designated BQ. The BQ sequence [(**GQQQLG**GAGTGSA)$_2$(GAGQGEA)$_3$]$_n$G contained a block with a well behaving glutamine substrate for tTG and a second block containing a water soluble region. Although the water soluble block also contained a glutamine residue, it was hypothesized that it would have marginal tTG recognition due to the higher specificity of the glutamine substrate.[174]

6.3.1 Hydrogel Formation

The optimal gelation conditions of substrate and enzyme concentrations were determined by visual observation and sample inversion. Precursor solutions of protein polymer were slightly turbid due to limited protein polymer solubility. However, the proteins appeared uniformly suspended at the maximum concentration investigated, 10 wt% K and 15 wt% BQ in the precursor solution, respectively. Prior to enzyme addition, the substrate solution appeared to have slightly increased viscosity (as compared to buffer solutions). After enzyme addition and incubation at 37°C, a solid gel was formed and was stable at room temperature in aqueous buffer (Figure 6.3.1).

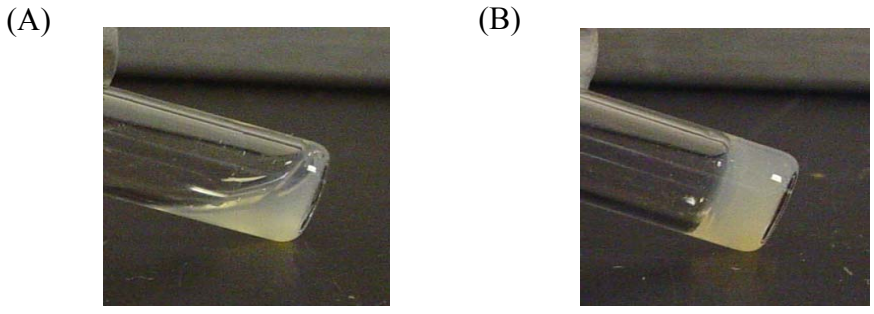

Figure 6.3.1: Photograph of the precursor solution (A) before and (B) after enzymatic gelation at 37°C for 30 minutes.

6.3.2 Hydrogel Morphology

SEM micrographs of critical point dried gels suggest a morphology dependence on hydrogel composition (Figure 6.3.2). Dehydrated hydrogels composed of $K8_{30}$ and BQ_6 have an irregular porous structure, with pores ranging from less than 1 μm up to 5 μm; the $K8_{60}$ and BQ_6 hydrogel appears as a woven network with an average pore size of ~ 2 μm. The largest molecular weight protein gel, $K8_{120}$ and BQ_{12} formed a dense structure composed of pores less than 1 μm. During sample preparation, hydrogel volume decreased as ethanol concentration increased, suggesting dehydration caused some collapse of the network. For this reason, variable pressure SEM was used to visualize unprocessed hydrated hydrogel networks. In variable pressure SEM, the sample is at higher than traditional SEM pressures due to the introduction of water vapor in the sample chamber; this permits direct imaging of insulating materials without the need for a conductive surface coating. Hydrated $K8_{30}/BQ_6$ shows a highly porous woven network with pore size ranging from 3 to 7 μm. The increase in pore size of hydrated samples confirms the network collapse that occurs from ethanol treatment and critical point drying.

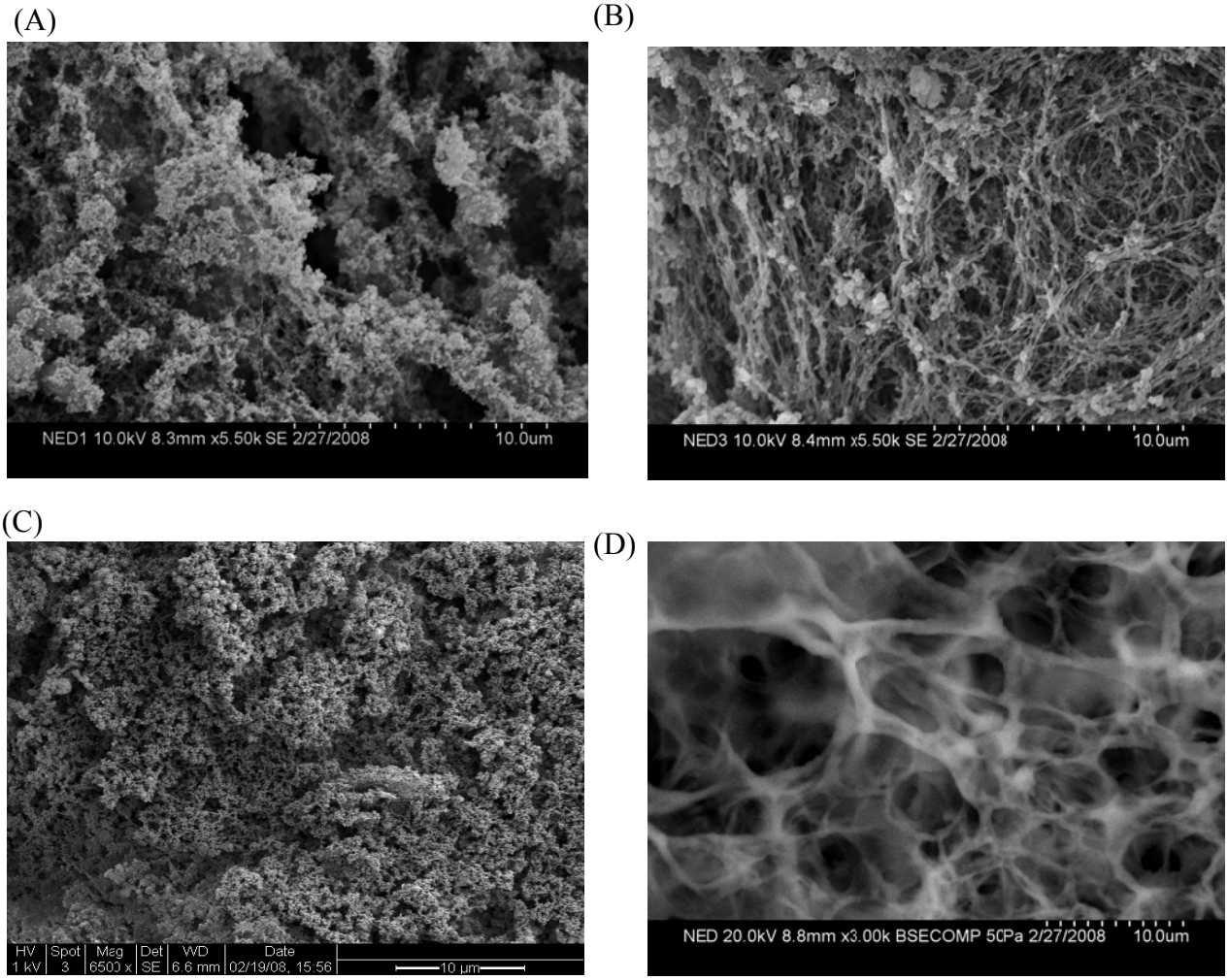

Figure 6.3.2: (A) SEM micrograph of hydrogel (4 wt% $K8_{30,}$ 4 wt% $BQ_{6,}$4 unit/ml of tTG), (B) SEM micrograph of hydrogel (4 wt% $K8_{60,}$ 4 wt% $BQ_{6,}$4 unit/ml of tTG), (C) SEM micrograph of hydrogel (4 wt% $K8_{120,}$ 4 wt% $BQ_{12,}$ 5.6 unit/ml of tTG) (D) VP-SEM image of hydrated hydrogel composed of 4 wt% $K8_{30,}$ 4 wt% $BQ_{6,}$ 4 unit/ml of tTG

Literature suggests that hydrogel pore size directly influences the strategy cells use to migrate through the material; when pore sizes are comparable to cell size (~10 μm for fibroblasts), cells utilize amoeboid migration. In tighter gel networks, cells use proteolytic strategies to first degrade or create holes in the surrounding matrix.[183] The observed pore sized of the protein polymer hydrogels suggest encapsulated migratory cells; where fibroblasts would

need to secrete proteases to allow movement throughout the gel. Non-migratory cells can be effectively embedded in the protein polymer hydrogels due to the small pore size.

6.3.3 Hydrogel Swelling and Protease Degradation

Equilibrium swelling studies suggest swelling ratio was a function of hydrogel precursor components. Protein polymer substrates with smaller molecular weights were observed to have increased swelling over larger protein polymers at similar substrate and enzyme ratio (Figure 6.3.3). The hydrogels formed with $K8_{30}$, however, had a statistically significant increase in swelling ratio when BQ substrate increased in molecular weight. On the contrary, the $K8_{60}$-BQ_{12} hydrogel had a significantly reduced swelling ratio than the $K8_{60}$ hydrogel with the BQ_6 precursor. The largest K protein, $K8_{120}$ had drastically decreased swelling, only ~ 3.5 times initial hydrogel mass, suggesting structural differences in the hydrogel due to crosslink density.

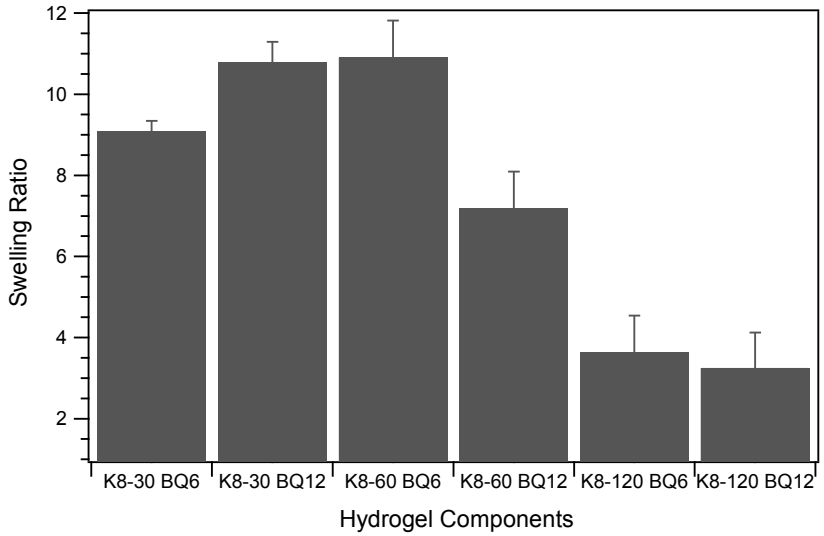

Figure 6.3.3: Swelling ratio as a function of hydrogel precursor components. Gel final composition was 4 wt% of each protein polymer and enzyme concentration was kept at the same molar ratio to the number of K crosslinking sites.

The difference in swelling ratio, based on hydrogel composition, also corresponds to the SEM data presented in Figure 6.3.3. Hydrogels composed of the highest molecular weight precursors had very small pore size, which ultimately resulted in a reduced swelling. On the contrary, the middle molecular weight precursors, $K8_{60}$ and BQ_6 had the highest swelling and a large woven pore size even in the case of the dehydrated SEM samples. Furthermore, the VP SEM of $K8_{30}$ and BQ_6 shows very high porosity which corresponds to the large swelling ratio.

The swelling and morphology of hydrogels will change as they undergo degradation in solution. The degradation of the protein polymer hydrogels was investigated by proteolytic remodeling by plasmin. The lysine containing proteins in solution were shown to be degraded by plasmin, which cleaves at lysine residues, within 24 h (see Chapter 5). Protein polymer hydrogels, however, had much slower degradation that was dependent on gel composition (Figure 6.3.4). All gel formulations showed a rapid initial mass loss of between 20 to 45 % in the first 24 h. After 4 days, the rate of degradation significantly decreased to less than 15% mass loss for up to two weeks.

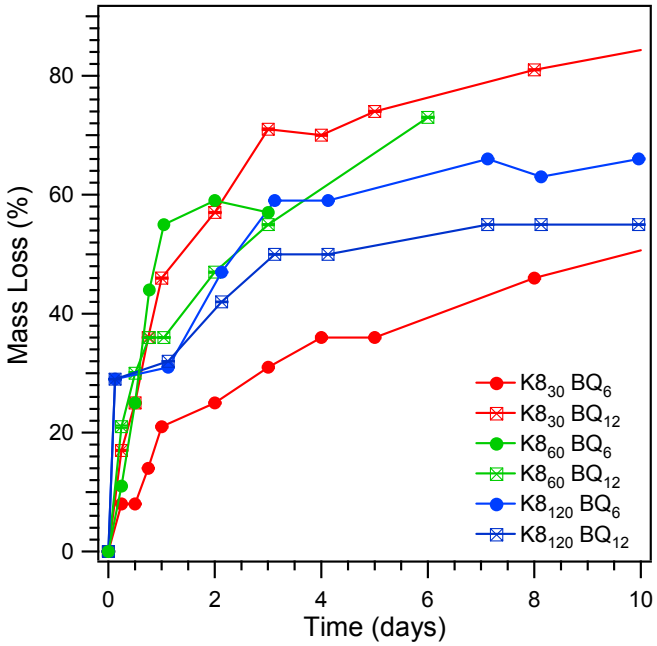

Figure 6.3.4: Hydrogel mass loss by plasmin proteolytic degradation.

The degradation of $K8_{60}$ samples was conducted over 1 week, due to difficulties with sample handling; as mass loss increased, the gel typically became weaker and often broke into pieces. The standard deviation in mass loss in Figure 6.3.4 was large due to decreases in sample integrity as degradation progressed. However, the $K8_{120}$-based samples were more manageable, possibly due to the increased crosslink density and lower swelling ratio. Figure 6.3.4 supports the hypothesis that protein hydrogel degradation would be significantly decreased from that of proteins in solution due to less available recognition sites consumed by enzymatic crosslinking. The ability for the protein polymer hydrogels to be remolded by secreted proteases, suggests that migratory cell would be able to move through the material by degrading the gel, as required base on hydrogel pore size.

The swelling behavior of the protein polymer hydrogels was monitored during proteolytic degradation. Previous research suggested that as the network degrades, the hydrogel has increased swelling due to the decrease in crosslinking density.[214] This was supported for hydrogels created from $K8_{120}$ proteins (Figure 6.3.5). Interestingly, gels created by $K8_{30}$ and $K8_{60}$ proteins had an unexplained initial decrease in swelling ratio during the first 12 h.

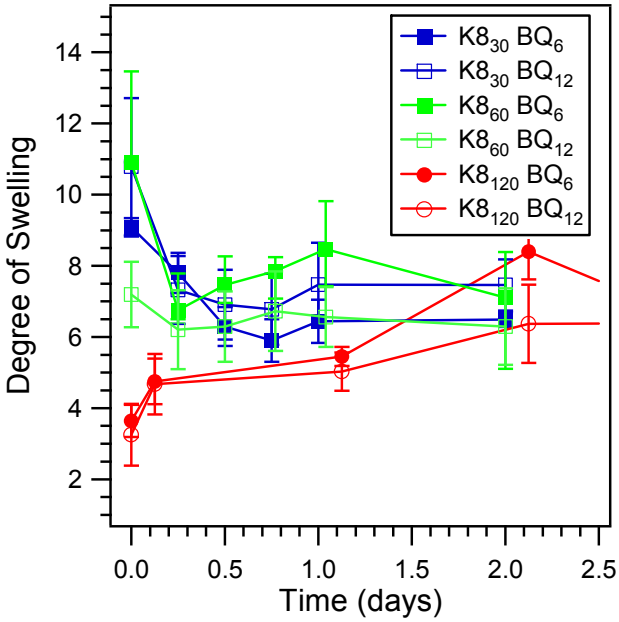

Figure 6.3.5: Hydrogel swelling during proteolytic degradation by plasmin.

6.3.4 Viscoelastic Properties of Crosslinked Hydrogels

Enzymatic time for gelation was assessed with passive particle tracking microrheology by tracing the Brownian motion of tracer particles in gelling solution. The generalized Stokes-Einstein relation for materials with viscoelastic properties provides a theoretical basis for passive microrheology,[215, 216] presented as follows:

$$\langle \Delta \tilde{r}^2(s) \rangle = \frac{dk_B T}{3\pi a s \tilde{G}(s)}$$

where $\langle \Delta \tilde{r}^2(s) \rangle$ is the Lapace transform of the tracer particles' mean-squared displacement (MSD), d is the dimensionality of the displacement vector (2 in videomicroscopy), s is the Laplace frequency, a is the radius of the particles, and $\tilde{G}$ is the Laplace representation of the complex modulus, which includes the storage (G') and the loss (G'') moduli.[217]

In viscous liquids, particles diffuse freely and the MSD versus lag time has a slope of 1 in a log-log plot.[215] The particle MSD in an elastic gel, however, is limited, resulting in a slope of zero. In protein polymer hydrogels, the tracer particles have a fixed initial MSD of ~ 0.04 μm^2; upon the addition of enzyme, the displacement rapidly decreases and approaches zero, indicating the formation of the hydrogel (Figure 6.3.6).

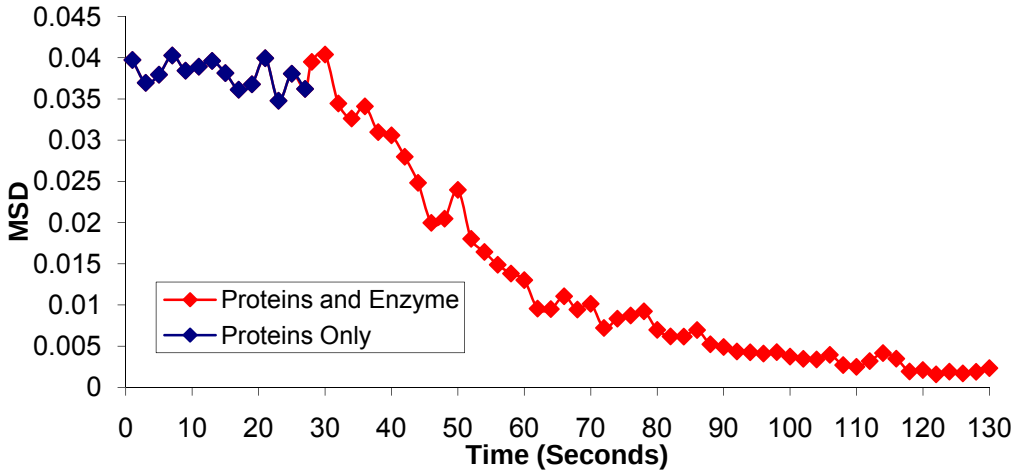

Figure 6.3.6: Mean-square-displacement as a function of lag time for tracer particles in a protein polymer solution 1.5 wt% $K8_{30,}$ 1.5 wt% BQ_6. Enzyme (8.5 units/ml) is added at 30 s.

At low concentration of protein polymer (3 wt% total), roughly 90% of gelation occurs within the first 30 s after enzyme addition. After, 1.5 min the MSD of the tracer particles approached zero and reached steady state (Figure 6.3.6). Experiments conducted with higher protein concentration rapidly gelled and did not allow sufficient time for data collection.

Moreover, rapid gelation was confirmed by bulk rheological experiments using oscillatory rheometry. Precursor solution was place on a thermostatted rheometer plate at 37°C; the cone was lowered immediately after enzyme addition. Within 30 s, the hydrogel composed of $K8_{30}$ and BQ_6 had a storage modulus (G′) higher than the loss modulus (G″), and the phase angle (δ) approached zero, indicating rapid gelation (Figure 6.3.7). Following this experiment, a frequency and strain sweep were completed to study the effects on storage modulus. Essentially, both sweeps were flat with respect to the storage modulus, indicating the hydrogel behaved as a robust elastic solid. However, the strain sweep exhibited a small decrease of storage modulus at strains above 10% strain, indicative of damage to the gel structure. Further rheological measurements were conducted within the linear viscoelastic region were the storage modulus was independent of the applied strain.

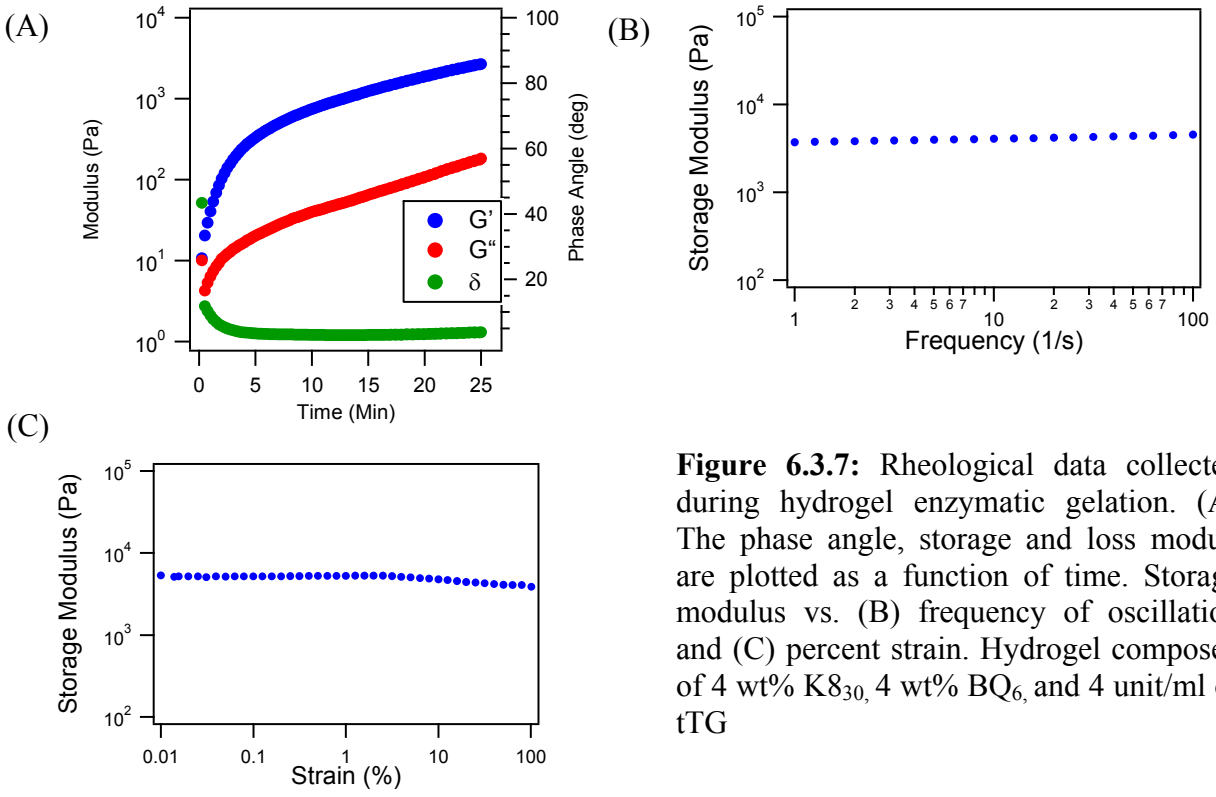

Figure 6.3.7: Rheological data collected during hydrogel enzymatic gelation. (A) The phase angle, storage and loss moduli are plotted as a function of time. Storage modulus vs. (B) frequency of oscillation and (C) percent strain. Hydrogel composed of 4 wt% $K8_{30,}$ 4 wt% $BQ_{6,}$ and 4 unit/ml of tTG

The storage modulus was investigated as a function of gel composition. The effect of crosslink density was studied by varying the reactive group spacing in the lysine-containing substrate. At similar molecular weight and molar ratios between lysine and glutamine substrates and enzyme concentration, the storage modulus increased with more closely spaced lysine groups. The total number of crosslinks should theoretically be the same since the molar ratio of enzyme to lysines was kept constant; however, an increase in crosslink density would increase the measure of hydrogel strength and stiffness (storage modulus). Furthermore, the storage modulus ranged from 4- 16 kPa based on the molecular weight of the protein precursors (Figure 6.3.9). This suggests that the magnitude of the viscoelastic behavior of the polymer network is

determined by the length of the flexible protein polymers. Longer protein polymers have longer relaxtion times and form highly crosslinked networks. This is confirmed by the SEM images of gels formed with $K8_{120}$ and BQ_{12} (Figure 6.3.2). The effect of high crosslinking density to achieve a greater storage modulus resulted in a limited ability of the network to expand in aqueous solution, as observed by the limited swelling of higher molecular weight gels (Figure 6.3.3).

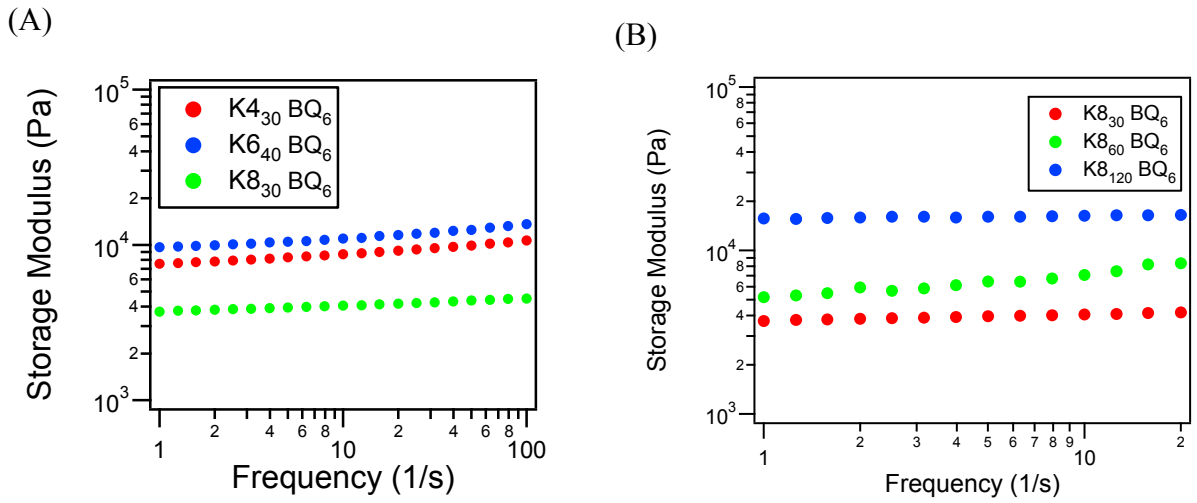

Figure 6.3.9: Plots of rheological after a 1 h gelation. Hydrogel storage modulus as a function of (A) lysine substrate spacing and (B) protein molecular weight/length of the lysine containing precursor enzymatically gelled with BQ_6.

The mostly flat curves in Figure 6.3.9 indicated that the networks are very stable when exposed to a wide range of perturbation frequencies. The samples exhibited a plateau in the lower frequency range, 1-10 1/s, suggesting a stable crosslinked network. Furthermore, the storage modulus generally showed a slight increase with frequency indicated that the hydrogels have good mechanical-damping ability over a wide frequency range.

The material properties of hybrid hydrogels were investigated to determine the effects of changing molecular weight of the crosslinking group and the number of crosslinking sites. Hybrid hydrogels, composed of the $K8_n$ protein polymer and a 4-armed PEG containing the qlutamine substrate on each end (Figure 6.3.10A), were evaluated in terms of their rheological properties. Hydrogels composed of enzymatically crosslinked PEG-Q to the protein polymers $K8_{30}$ and $K8_{120}$ displayed a lower storage modulus than purely protein polymer-based hydrogels for both compositions (Figure 6.3.10B).

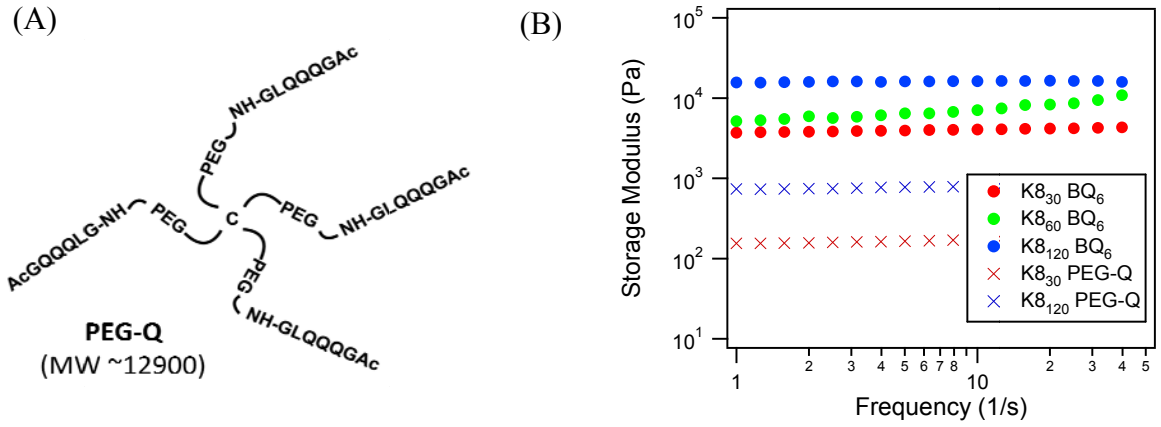

Figure 6.3.10: (A) Schematic of the PEG-Q substrate, (B) Plot of rheological data after 1 h gelation between PEG-Q and $K8_n$ protein polymers. For comparison protein polymer hydrogels are shown.

The PEG-Q/$K8_n$ hybrid hydrogel storage modulus was an order of magnitude less than that of the protein polymer hydrogels; which may be explained by the decreased number of Q substrates per PEG monomer and the decrease in crosslinker molecular weight. The PEG-Q crosslinker was essentially half the molecular weight of BQ_6. As suggested by the change in storage modulus with increases in $K8_n$ molecular weight (Figure 6.3.9B), the molecular weight of crosslinker has

a profound influence on overall material strength. The decreased number of available tTG glutamine substrates per crosslinker also contributes to the decrease in storage modulus. As indicated in figure 6.3.9A, decreasing the number of reactive sites decreases the storage modulus of the gel.

For comparison, previous PEG (molecular weight of ~ 18 kDa) based hydrogels crosslinked by factor XIII created by Barron *et al.* displayed a storage modulus of approximately 1.2 kPa., even though, the total bioconjugate concentration was almost 15 wt% in the final gel,[203] In this study protein polymer hydrogels composed of 8 wt% protein precursor, only slightly larger in size, 22-24 kDa versus 18 kDa, had a significantly greater storage modulus. Furthermore, surprisingly the protein polymer hydrogels have a greater storage modulus then many natural and synthetic materials (Table 6.3).

Table 6.3: Complex modulus of hydrogel materials*

	Concentration (mg/ml)	G* (kPa)
Crosslinked P(NIPAAm-co-Aac) 37°C	**50**	**0.09**
Matrigel	**NA**	**≈ 0.1**
Collagen	**37**	**0.15**
Crosslinked Hyaluronan	**15**	**0.30**
Alginate	**20**	**2.31**
Articular cartilage	**NA**	**440.00**
Chemically crosslinked ELP	**50**	**3.00**
tTG crosslinked ELP	**100**	**0.26**
tTG crosslinked unfolded Protein polymers	**60**	**≈ 4 -16**

* *adapted from McHale, M. K 2005*

Interestingly, the enzymatically crosslinked random coil protein polymers presented herein have a greater modulus compared to recombinant elastin-like proteins that are self-assembled and further crosslinked by tTG.

6.3.5 Encapsulated Cell Viability

Mouse 3T3 fibroblasts were encapsulated in enzymatically crosslinked hydrogels and cultured at 37°C for 24 h. A LIVE/DEAD Viability/Cytotoxicity Kit was used to determine the membrane integrity of the cells where viable cells fluoresce green through the reaction of calcein AM with intracellular esterase and non-viable cells fluoresce red due to the diffusion of ethidium homodimer into cells with damaged membranes and binds with the nucleic acids. Fluorescent confocal microscopy images of cells stained with the LIVE/DEAD reagent show cells tolerated encapsulation in the hydrogels (Figure 6.3.12).

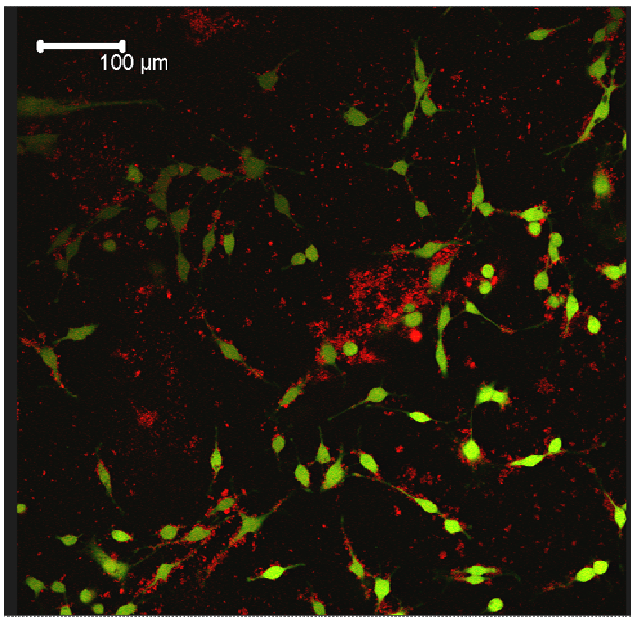

Figure 6.3.12: Confocal fluorescent microscopy of fibroblasts encapsulated in enzymatically crosslinked hydrogels.

It should be noted, that the red staining is from unexplained background interference of the ethidium interacting with the hydrogel material. As shown above, the encapsulated fibroblasts appear to be spreading as indicated by the elongated shapes. Furthermore, the cells appeared evenly distributed throughout the gel, indicating the encapsulation procedure and gelation time were adequate for additional studies.

Encapsulated mouse islet viability was assessed after a 36 h culture suspended in protein polymer hydrogels. Islets were stained with FDA/PI and TMRE/YOPRO (Figure 6.3.13), which determine apoptotic cells and mitochondria, respectively. Specifically, live cells with intact membranes are distinguished by their ability to exclude the PI dye which easily penetrates dead or damaged cells resulting in a red fluorescence. FDA assesses cellular esterase activity, where fluorescence is produced by esterase cleavage of a lipid-soluble probe, resulting in a fluorescent stain that is retained in the membrane of an intact cell (green). In addition, islet mitochondrial membrane integrity was determined using tetramethylrhodamine (TMRE), which fluorescently stains intact mitochondria red. Apoptosed mitochondria are stained given by a non-specific interaction of YOPRO to DNA.

Whole cell staining indicated islets encapsulated in the hydrogels were smaller, less than half the size of non-encapsulated control islets. Islets cultured in hydrogels composed of $K8_{30}/BQ_6$ and $K8_{60}/BQ_6$ had slightly less viability as determined by FDA/PI staining. Mitochondrial stains TMRE/YOPRO, showed some indication of islets in the hydrogel undergoing early apoptosis, as indicated by green staining (Figure 6.3.13D).

(A)

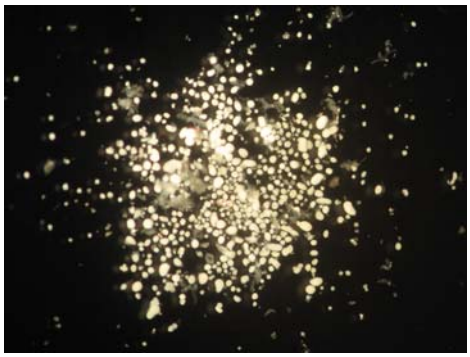

(B)

$K8_{30}/BQ_6$

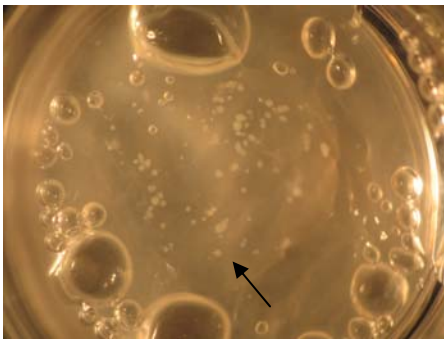

$K8_{30}/BQ_6$

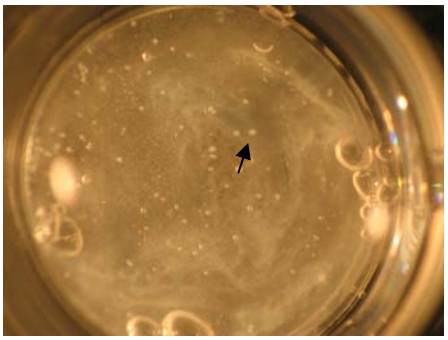

(C)

Control

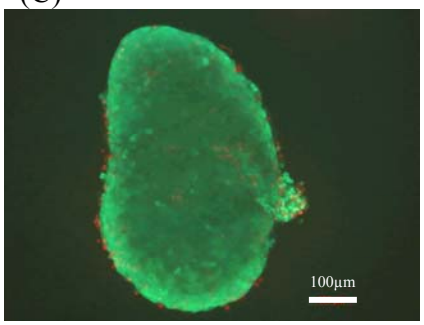

$K8_{30}/BQ_6$

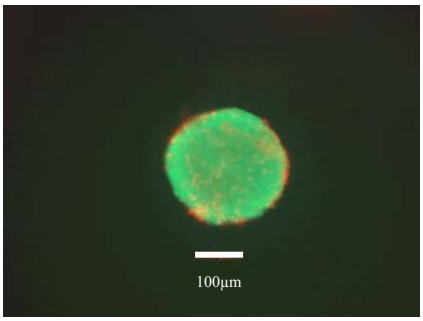

$K8_{60}/BQ_6$

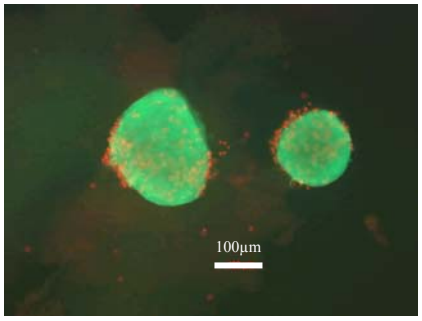

(D)

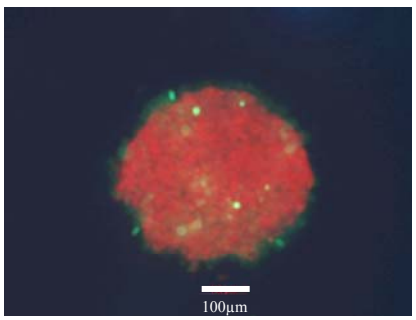

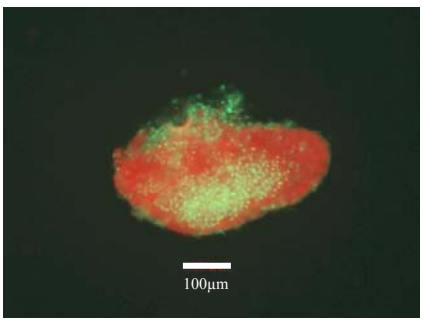

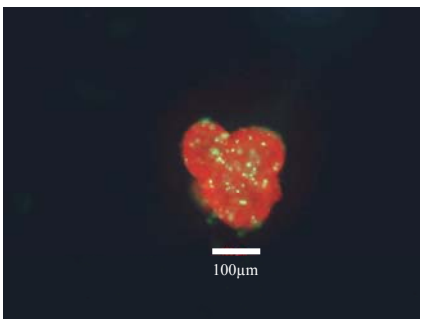

Figure 6.3.13: *In vitro* viability of islets encapsulated in protein polymer hydrogels after culture for 36 h. (A) Image of islets harvested for encapsulation, 50 islets per sample (B) Photograph of islets entrapped in the hydrogels (C) Islets stained with FDA/PI, green stain live cells, and red stain cells undergoing late apoptosis (D) Islets stained with TMRE/YOPRO, red indicates live mitochondria and green stains cells undergoing early apoptosis. Control indicates non-encapsulated islets.

It is important to note, the β-cells are located in the interior of the islets and the mitochondrial damage localized in the center of the islets may indicate damage to the insulin producing cells.

From fluorescent images, islet cells were approximated to be 100 to 200 μm, much larger than the average pore size of the protein polymer hydrogels (< 10 μm). As expected, this suggested that the protein polymer hydrogels may act as a promising material to contain the islets within a localized gel when transplanted *in vivo*.

6.3.6 Preliminary *In Vivo* Results

The preliminary *in vivo* efficacy of islet isografts encapsulated in protein polymer hydrogels was assessed in a small animal study (n = 2 mice per hydrogel). Islets were transplanted into the epididymal fat pad, a fatty tissue surrounding the testes, of age matched male mice that were diabetic due to chemical induction by streptozotocin. The epididymal fat pad is ideal site for islet transplantation due to its easy access and well vascularized nature. The intra-abdominal fat pad was spread out and approximately 50 μl of hydrogel was dropped onto a well-vascularized region.[218] Immediately afterwards, 250 islets were placed on top. As the protein polymer precursor solution gelled, the islets became entrapped in the hydrogel (Figure 6.3.14).

(A) (B)

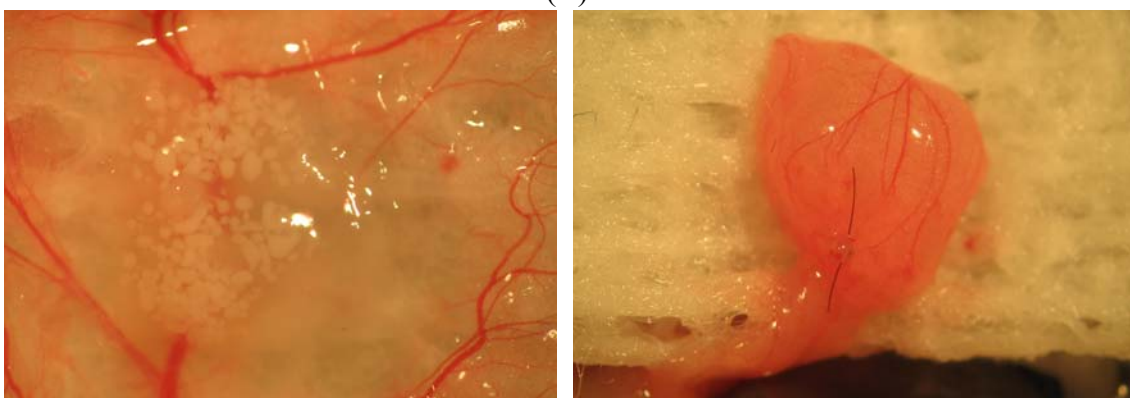

Figure 6.3.14: Photographs of 250 islets encapsulated in enzymatically crosslinked protein polymer hydrogel transplated into the epididymal fat pad of mice (A) Stretched epididymal fat pad showing islets and gel (B) epididymal fat pad after suture.

After replacement of the fat pad, the animal's blood glucose and weight were measured over the course of 11 weeks (Figure 6.3.15). Euglycemia was indicated with a blood glucose level below 200 mg/dl. All mice, excluding the normal controls, had a high and stable blood glucose level before transplant.

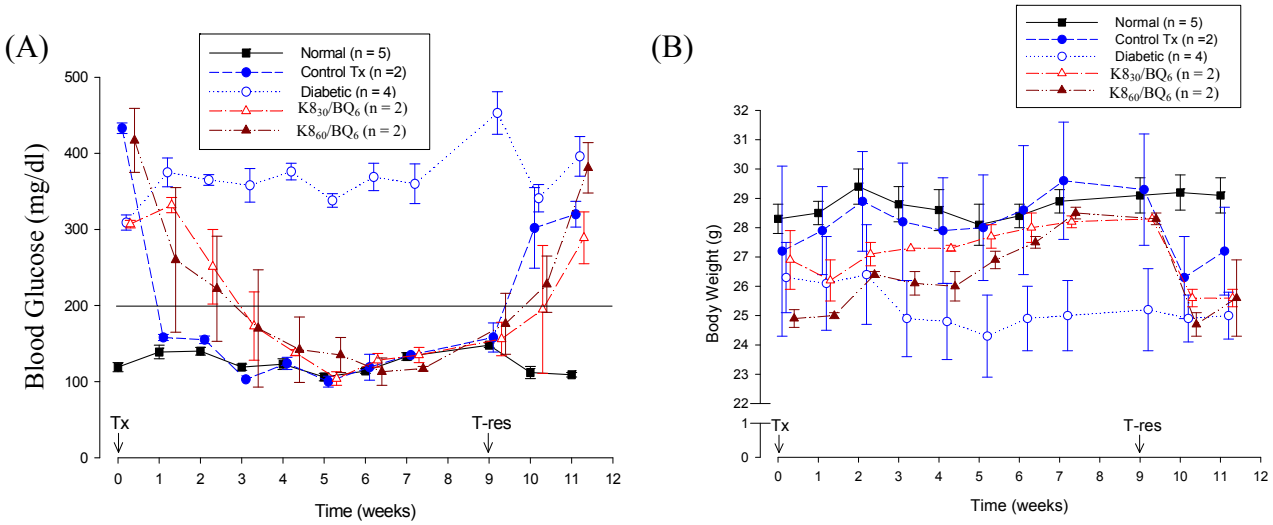

Figure 6.3.15: (A) Blood glucose level of mice over the course of the experiment. Euglycimia is indicated by a blood glucose level of above 200 mg/dl. (B) Body mass of mice throughout the experiment. Tx denotes transplant insertion into the epididymal fat pad. T-res denotes resection of the fat pad.

Mice with islets encapsulated in either formulation of the protein polymer hydrogel showed a longer lag time to reach euglycimia. Mice with non-encapsulated islets had normal blood glucose levels after one week post implant; mice with encapsulated islets in hydrogels, however, required approximately 3 weeks to reach euglycimia. It was hypothesized that the delay of onset of euglycimia in mice with hydrogels may be due to islet damage during encapsulation. This theory is supported by research in the Kaufman laboratory at Northwestern University that indicated the time to reach euglycimia increased as the number of implanted islets decreased.[218] All mice transplanted however, once reached euglycimia, maintained normal blood glucose levels until transplant removal. In addition, body mass of transplanted mice remained relatively constant until graft removal, whereas the diabetic mice lost weight during the experiment.

To further assess transplanted islet activity, the islet response to an intraperitoneal glucose injection was measured on fasting mice. Normal, well-functioning islets, should have a rapid response to increased glucose levels and return to basal blood glucose levels in minimal time, graphically, the area under the curve should be small. The islet time response for blood glucose control was monitored at 2, 4, and 6 weeks, and after transplant (Figure 6.3.16).

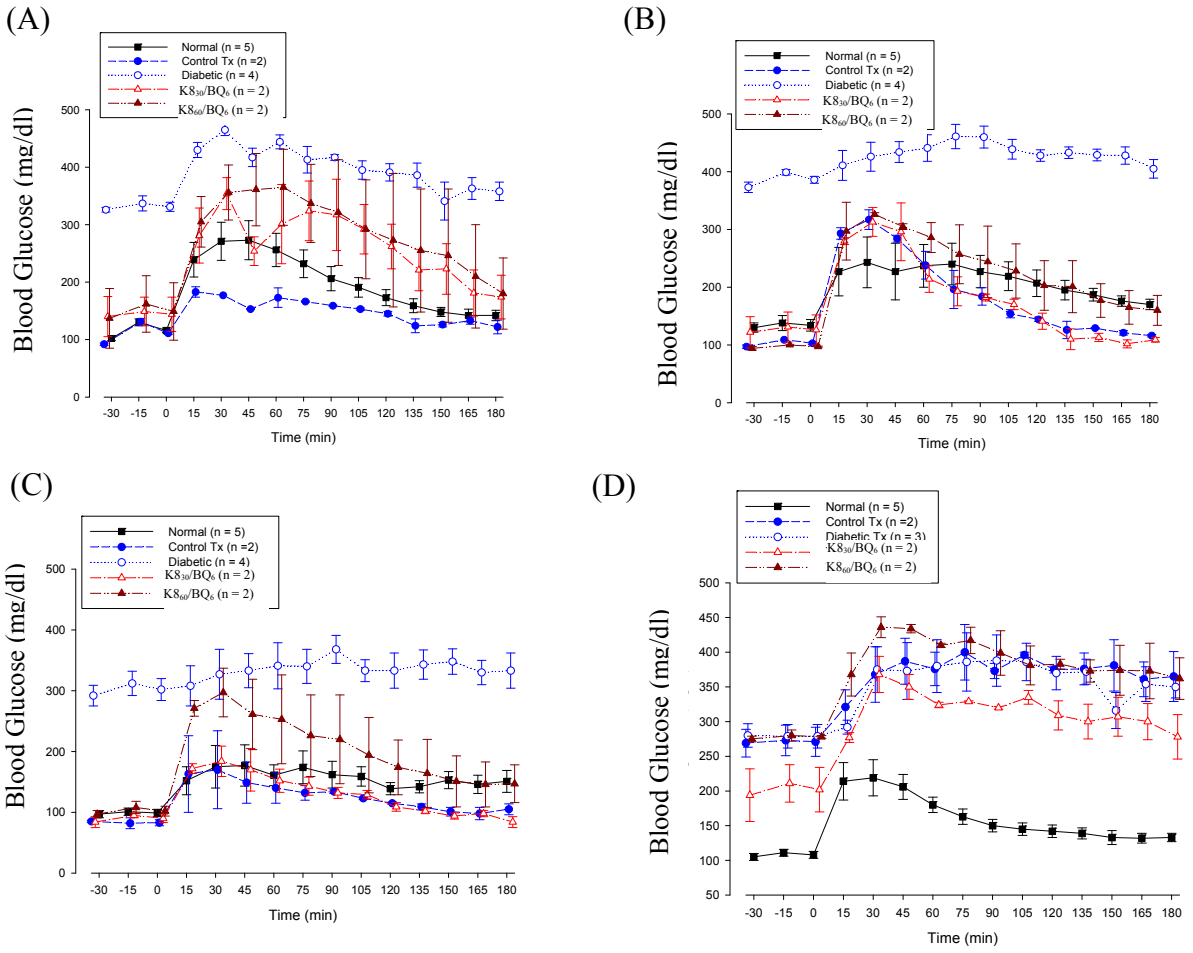

Figure 6.3.16: Intraparateneal glucose tolerance test at (A) 2 weeks, (B) 4 weeks, (C) 6 weeks after transplant, and (D) after transplant removal.

As expected, the diabetic control mice were unable to regulate blood glucose levels and did not return to the basal blood glucose level following intraperitoneal glucose injection. At 2 weeks post transplant, the healthy mice and islets only control groups had tightly controlled blood glucose levels with a response time of ~ 100 min to return to basal levels. Islets encapsulated in hydrogels had a slower response time and did not return to the basal blood glucose level, possibly supporting the hypothesis of islet damage during encapsulation. However, 4 and 6

weeks post transplant, islets encapsulated in the $K8_{30}$-BQ_6 responded similar to the islets only control group. Furthermore, islets encapsulated in the $K8_{60}$-BQ_6 hydrogel had a slower response time, but were still able to control blood glucose levels. At all time points, the $K8_{60}$-BQ_6 hydrogel had a slower regulation and a larger shift in blood glucose level following injection. The mechanism behind this response has not yet been elucidated, however a greater degree of crosslinking in $K8_{60}$-BQ_6 may increase islet apoptosis during encapsulation and transplant. As supported by research in the Messersmith group, the crosslinking reaction by transglutaminase, however, is unlikely to damage islets alone,[219] suggesting the tight network of the gel may be the primary cause of cell death. After transplant resection, all animals returned to the diabetic state and were unable to regulate blood glucose level following an insulin injection, confirming transplanted islets were responsible for maintaining eugylcemia.

Histology was performed on the fat pad after graft removal to assess the health of the islets. Islets implanted with hydrogels displayed a pronounced immune cell infiltration compared to islets alone (Figure 6.3.17).

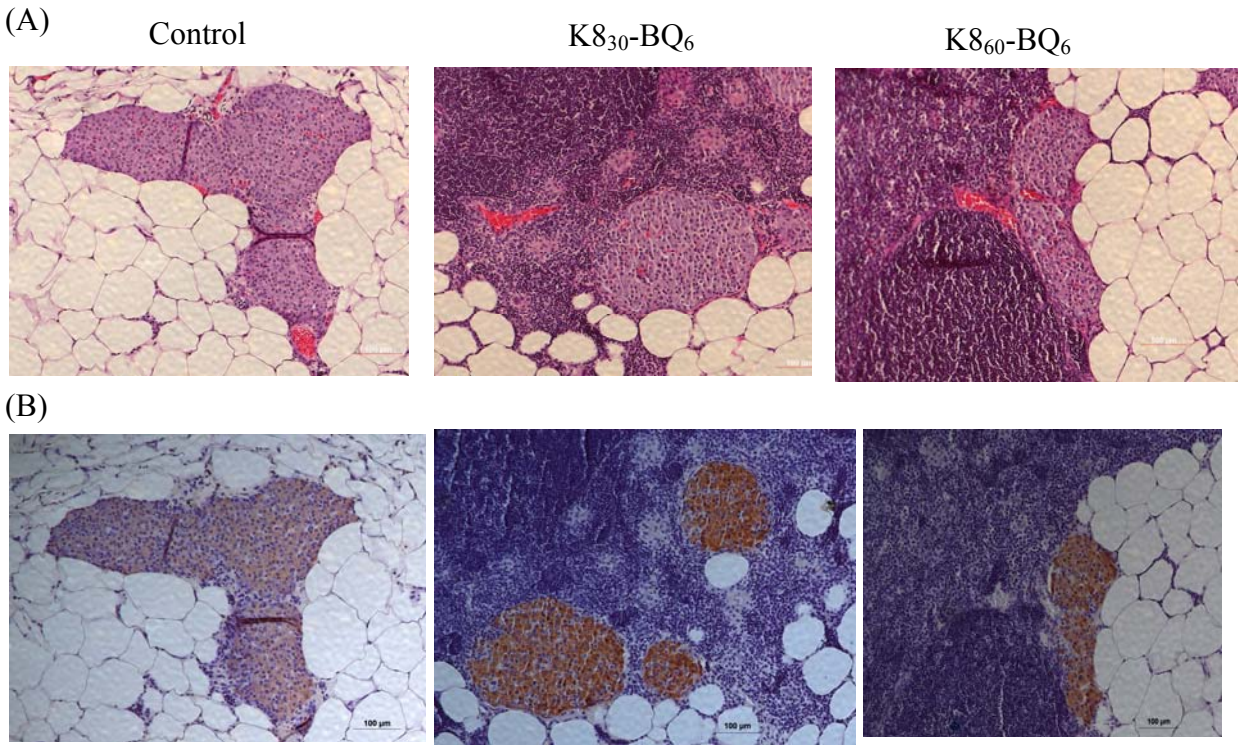

Figure 6.3.17: (A) Histology of epidiymal fat pad after resection by H&E stain. Adipose tissue is indicated by the large white cells. Islets have a globular morphology with many stained cell nuclei. Hydrogels are immunogenic as indicated by the deep purple stained immune cells. (B) Insulin staining after transplant resection. Brown indicates the presence of insulin.

Subsequent experiments by Lindsay Karfeld and Hermann Kissler, have suggested that these immune cells are composed of macrophages and T-cells. Furthermore, it is suspected that the immune response could be due to high levels of endotoxin which can accompany bacterially produced proteins; this is being further investigated by Liese Rothkopf in the Barron laboratory. Despite the large inflammatory response at the site of implantation, the islet cells encapsulated in the hydrogels maintained insulin secretion as indicated by Figure 6.3.17B.

6.4 Chapter Conclusions and Future Directions

The enzymatically crosslinked protein polymer hydrogels presented herein, display not only rapid gelation but also different material properties based on formulation. The degree of swelling and gel degradation rate were functions of molecular weight of the protein precursors. Furthermore, the viscoelastic properties ranged based on composition, with a 4-fold increase in storage modulus dependent on protein gel precursors. The ability to modulate material properties is advantageous for customization to specific applications. For example, Chen *et. al*, based on the knowledge that adherent cells are strongly influenced by the mechanical properties of biomaterials, studied cell response to mechanically patterned surfaces and showed increased migration and accumulation of cells on the stiffer regions. Moreover, stem cell differentiation is dependent on material stiffness.[220] These results suggest that material properties of the hydrogel microenvironment have significant implications for cell behavior.

The morphology within the hydrogel microenvironment is also important for controlling cell migration. Hydrogel morphology by VP-SEM indicated a porous network with pores ranging from 3 to 7 μm, implying that cells require protease secretion for migration within the material.

Future studies should include a complete analysis of viscoelastic properties using higher concentrations of enzyme and additional formulations of hydrogels. The ability to graft bioactive peptides on the protein polymer backbone (as discussed in Chapter 5) should be explored to incorporate bio-functionality to the hydrogel scaffolds to ultimately control cellular function. Some suggested *in vitro* applications include using protein polymer hydrogels for stem cell proliferation and differentiation, and to study selective cell migration.

The initial application explored was islet cell transplantation for the treatment of type I diabetes. Preliminary studies of encapsulated islets in the enzymatically crosslinked hydrogel suggested that the hydrogels had a permissive environment for islet function but not an ideal microenvironment. Moreover, these results suggested that a percentage of islets were damaged during hydrogel encapsulation; future research should include encapsulating islets in a lower crosslinked material. Due to the islet slow response time to reach euglycemia and the high immune response, it was concluded that the current formulation of protein polymer hydrogels is non-ideal. Future experiments should first address the immune response of the protein polymer hydrogels. The endotoxin level of the protein polymers should be assayed, since recombinantly expressed proteins can carry endotoxins, which evoke macrophage infiltration.[221] If endotoxin levels are sufficiently high, this could explain the inflammation. Regardless, there are published methods for endotoxin removal from recombinant proteins.[221] In addition, the immune response may be reduced by incorporating PEG into the hydrogel by either covalently attaching to the protein backbone (as illustrated in Chapter 5) or by creating hybrid hydrogels with PEG crosslinking.

Foremost, continued *in vivo* islet delivery studies must include an increased number of animals per condition to achieve statistically relevant data. Future islet encapsulation experiments may be enhanced by the delivery of growth factors, peptides, genes, and small molecular weight drugs directly from the hydrogel. Growth factors such as vascular endothelial growth factor (VEGF) can enhance vascularization in the implant and ultimately promote long-term cell viability.[210] Moreover, peptides such as exendin[222, 223] when delivered from a hydrogel may enhance islet growth and insulin secretion. Furthermore, islet activity can be enhanced by

gene delivery[224, 225] which could potentially be incorporated into the hydrogel. Finally, the delivery of small molecular weight drugs by microsphere encapsulation in the hydrogel should be explored to perhaps decrease the immune response, by the delivery of deoxyspergualin[226]. These improvements may make protein polymer hydrogels a promising candidate for islet cell encapsulation.

Chapter 7

Coiled-Coil, Protein Polymer-Based, Enzymatically Crosslinked Hydrogels

7.1 Introduction

Hydrogels formed by both self-assembly and enzymatic crosslinking may be promising for *in situ* applications, due to the rapid formation of biocompatible hydrogel with potential modular material properties. Inclusion of self-assembling domains within the hydrogels are hypothesized to allow further control and customization of hydrogel architecture, including pore size and spacing of covalent crosslinks, which will ultimately affect material properties and elasticity. Specifically, we have chosen to include self-assembling coiled-coil domains periodically in the protein polymer backbone.

7.1.1 Background and Motivation

In 1953, Keratin, an α-helical protein with long range packing was first observed to form multistranded cables.[227] Shortly thereafter, Crick proposed that very long chains of amino acids could form what was termed "coiled-coil" secondary structures.[228] The first amino acid sequence

that formed a coiled-coil was discovered from tropomyosin, where the stabilization of the super coiled helices resulted from a 3-4 hydrophobic amino acid repeat.[229, 230] From these observations the coiled-coil folding pattern was determined to consist of two or more right-handed α-helices winding together to form a super-helix (Figure 7.1.1). The amino acid sequence pattern has been described as a heptad repeat *(a, b, c, d, e, f, g)*, where the *a* and *d* residues are hydrophobic and the remaining residues are polar for aqueous solubility. The helices associate into a coiled-coil super helix by the association of the hydrophobic faces and is further stabilized by the electrostatic interactions of charged amino acids in the *e* and *g* positions.

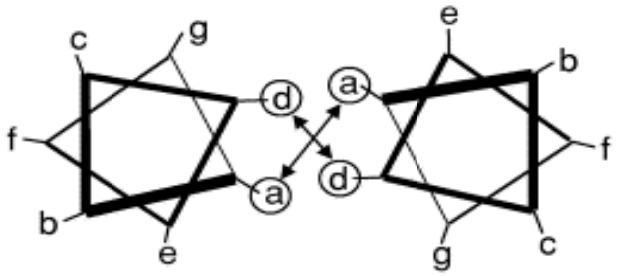

Figure 7.1.1: Helical wheel diagram for coiled-coil proteins. The hydrophobic *a* and *d* amino acids create a hydrophobic face which drives self-assembly. The charged *e* and *g* amino acids provide electrostatic stabilization of the super-helix.

Pioneering studies of recombinant coiled-coil proteins were based on the leucine zipper portion of the yeast transcription factor GCN4.[16] Petka and Tirrell created a tri-block protein (ABA), where the A block was based on the GCN4 amino acid sequence, and the B block was a random coil protein. These protein block-copolymers underwent reversible gelation in response to pH and temperature. More recently, Kopeček *et al.* created hybrid coiled-coil hydrogels using recombinant coiled-coil protein domains, consisting of the amino acid sequence $(VSSLEK)_n$,

covalently attached to hydrophilic polymers of PEG, N-(2-hydroxypropyl)-methacrylamide (HPMA), or *N*-(*N'*,*N'*-dicarboxymethylaminopropyl)ethacrylamide.[230] These novel hybrid hydrogels were assembled by the physical association of the coiled-coil protein domains. Furthermore, these hydrogels were reversible by dissociation of the coiled-coil domains at elevated temperatures and in denaturants. In addition, the block-copolymer-based hydrogels had controlled material properties, such as porosity and elasticity, based on the length of the coiled-coil domain.[231]

Motivated by the research of Kopeček and Petka, we designed protein block-copolymers including coiled-coil domains with both the random coil lysine $K8_n$ and glutamine BQ_n containing proteins. By using the proteins that contain tTG crosslinking substrates, the block-copolymer hydrogels can undergo physical formation and also enzymatic crosslinking. The temperature sensitivity of the coiled-coil association may allow for thermally triggered changes in the hydrogel porosity and mechanical properties. In addition, we hypothesize that under shear or stretching the coiled-coil domains may reversibly unwind, imparting additional elasticity to the hydrogels. The aim of this chapter was to create a multi-domain protein polymer that maintained solution behavior and functionality.

7.1.2 Coiled-Coil Protein Polymer Design

The amino acid sequence was based on research with short peptides from Kim and Lumb,[78] that contained a hydrophobic leucine face and either glutamic acids in the case of ACID or lysines in the case of BASE in the *e* and *g* position (Figure 7.1.2).

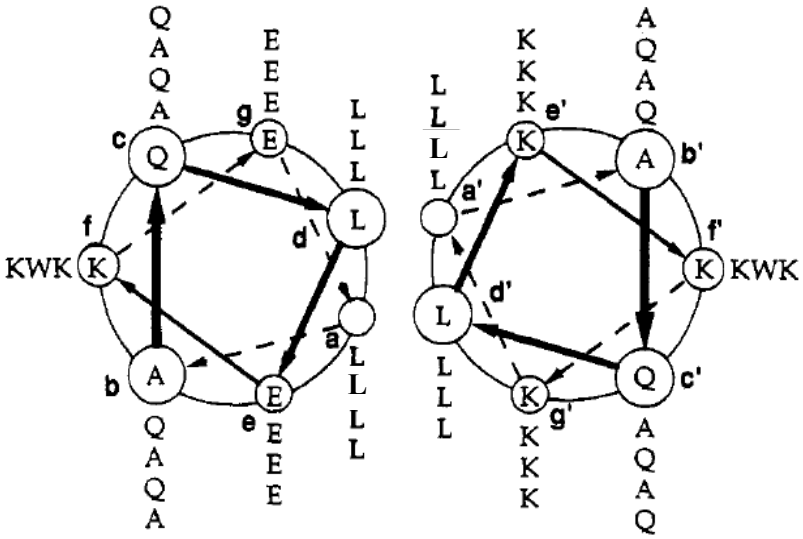

Figure 7.1.2: Helical wheel representation of ACID and BASE (illustration adapted from Lumb and Kim 1995).

These sequences were selected due to their unique association states as determined by sedimentation equilibrium; ACID at pH 7 in PBS fits a monomer-dimer-tetramer equilibrium, while at neutral pH, BASE is dimeric. Furthermore, both exhibited thermally induced unfolding transitions, BASE was determined to be more stable than ACID. A unique property of these sequences is that a new helical species is formed on mixing of ACID and BASE; sedimentation equilibrium indicated a heterotetramer association state with a maximum helicity when the stoichiometry of the two peptides was 1:1.

We hypothesized that the association states of ACID and BASE when included as a protein block-copolymer would affect hydrogel porosity, viscoelastic properties, and introduce some elasticity. Motivated by the extreme control of genes generated by the controlled cloning method, coiled-coil block-copolymers were investigated with discrete protein domain spacing,

length and number. Moreover, it was hypothesized that the physical properties of the hydrogels could be manipulated by the coiled-coil domain lengths and frequencies.

7.2 Experimental Section

7.2.1 Gene and Protein Synthesis

Block-copolymer production followed the techniques for gene synthesis, protein expression, and purification that were discussed in detail previously in Chapter 5. For the creation of block-copolymer genes, oligos encoding ACID and BASE (IDT) were used in the controlled cloning process (Figure 7.2.1).

ACID:

(Gly Ala Gln Leu Glu Lys Glu Leu Gln
G CTA GCC ATA T**GC TCT TC**A GGT GCC CAA CTG GAG AAA GAA CTG CAA

Ala Leu Glu Lys Glu Leu Ala Gln Leu Glu Trp Glu Leu Gln Ala
GCA CTG GAG AAG GAA TTG GCG CAG CTG GAG TGG GAA TTG CAA GCA

Leu Glu Lys Glu Leu Ala Gln)
CTG GAG AAA GAA CTG GCT CAG GGT T**GA AGA G**GG ATC CAC TAG T

BASE:

(Gly Ala Gln Leu Lys Lys Lys Leu Gln
G CTA GCC ATA T**GC TCT TC**A GGT GCG CAA CTG AAG AAG AAA TTG CAG

Ala Leu Lys Lys Lys Leu Ala Gln Leu Lsy Trp Lys Leu Gln Ala
GCA CTG AAG AAG AAA TTG GCT CAG CTG AAA TGG AAA CTG CAG GCC

Leu Lys Lys Lys Leu Ala Gln)
TTG AAG AAA AAA CTG GCG CAA GGT T**GA AGA G**GG ATC CAC TAG T

Figure 7.2.1: DNA oligonucleotides encoding ACID and BASE. The *Sap* I enzyme recognition sequences are highlighted in blue, *Ear* I in green.

Genes encoding protein block-copolymer were created by inserting either the ACID or the BASE block with BQ_n or $K8_n$ in a controlled fashion using the controlled cloning procedure described previously.

7.2.2 Protein Solubility

The protein block-copolymer solubility was tested at 1-10 wt% in (1) PBS, (2) 50 mM Tris-HCl, 75 mM $CaCl_2$, 0.835 mM EDTA, pH 7.0 (3) 10 mM Tris-HCl, 50 mM NaCl, (4) 2 mM EDTA pH 7.3, and (5) MOPS gelation buffer (200 mM MOPS, 20 mM $CaCl_2$, pH 7.65). Samples were vortexed for 20 min at room temperature. In some cases, protein solutions were centrifuged in a 1.5 ml eppendorf tube both right-side up and inverted to assist in mixing. Furthermore, ACID-($K8_{15}$) was heated to 65°C to improve solubility.

7.2.3 Protein Block-Copolymer Characterization

Circular dichroism (CD) spectroscopy was conducted as described in Chapter 5, and the relative percents of helical and random structure were calculated from the spectra. Analytical ultracentrifugation (AUC) was used to characterize association state for the protein block-copolymer BASE-$K8_{30}$. The proteins were dissolved in phosphate buffer so the final optical densities of the proteins were OD_{220nm} was 0.3, 0.5, and 0.7. Sedimentation equilibrium experiments and analysis were conducted by Yoriel Marcano using the Keck Biophysics Facility at Northwestern University. Samples were centrifuged at 30,000 rpm for 10 h, followed by

37,590 rpm for 6 h and then 45,000 rpm for 3 h at 25°C. During centrifugation, absorbance at 280 nm and 220 nm was recorded for analysis.

7.2.4 Hydrogel Formation

Physically crosslinked hydrogels were formed by dissolving the protein block-copolymer at 15 wt% in ddH_2O and 2 mM EDTA pH 7.3. Samples were vortexed thoroughly, heated then shock frozen in liquid N_2, which enhanced solubility. Physical gelation was assessed by the ability to scoop up the gel and the inability to flow by gravity. Enzymatically crosslinked hydrogels were created with a final solution concentration of 8 wt% in (Base-$K8_{15}$)$_2$, 3 wt% BQ_6, 0.005 units/µl tTG in 1.25 mM EDTA, 75 mM MOPS, 75 mM $CaCl_2$, 5mM DTT. For enzymatically crosslinked hydrogels, the precursor solution without enzyme was allowed to physically gel for 24 h in a humid environment before the addition of enzyme.

7.2.5 Oscillating Rheology

Hydrogel bulk material properties were determined by oscillatory rheology as described in Chapter 6. A stainless steel cone and plate (25 mm diameter, 1° angle) device was used with 150 µl final sample volume. Approximately 112.5 µl 4 wt% (Base-$K8_{15}$)$_2$, 4 wt% BQ_6, in 0.75 mM EDTA, 75 mM MOPS, 75 mM $CaCl_2$, was placed on the thermostatted plate of the rheometer set at 37°C and allowed to physically gel for 24 h in a humid environment. The enzyme was then added at a final concentration of 4 units/ml tTG, and the final buffer composition was 1.25 mM EDTA, 75 mM MOPS, 75 mM $CaCl_2$, 5 mM DTT. Sample mixing was achieved by careful pipetting and ensuring no air bubble formation. A humid chamber was achieved by forming a

layer of wet kimwipes around the platform and placing a chamber cover on top. For frequency and strain sweep experiments, the cone and plate was lowered to the measuring height and held for 1 h with a temperature of 37°C. The measurements of the storage and loss modulus during frequency sweeps were taken in the oscillator mode at 1 % strain, and strain sweep experiments were performed with a strain ranging from 1% to 100% at an angular frequency of 10 1/s.

7.3 Results and Discussion

7.3.1 Coiled-Coil Protein Block Copolymer Synthesis

The controlled cloning method allowed for the creation of genes encoding protein block-copolymers of ACID and BASE with BQ_n and $K8_n$. The ACID DNA sequence, however, was challenging to synthesize; PCR and ligation reactions often resulted in base pair mutations. Regardless, the ACID gene was successfully combined with DNA of the random coil proteins and inserted into plasmids for expression (Figure 7.3.1).

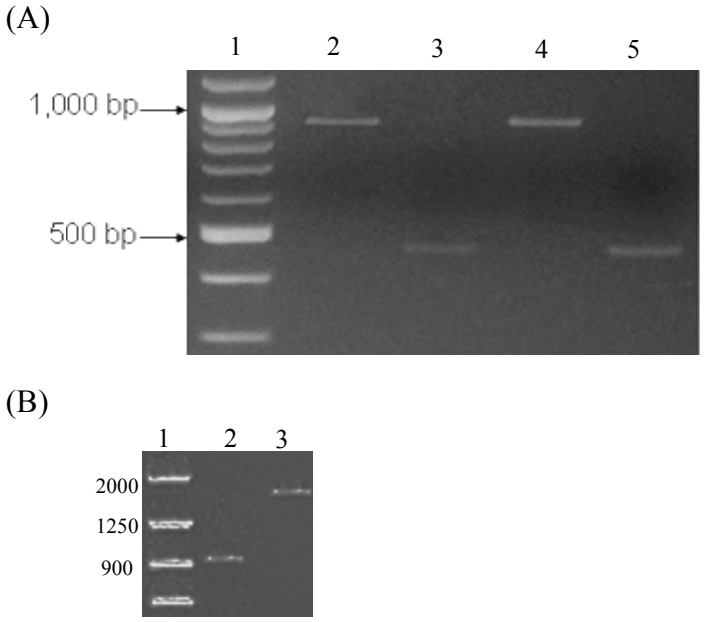

Figure 7.3.1: Agarose gel (1.5%) showing DNA genes digested from the expression plasmid by restriction enzymes *Bam*HI & *Nde*I. (A) Lane 1: DNA ladder, lane 2: $(ACID\text{-}K8_{15})_2$, lane 3: $ACID\text{-}K8_{15}$, lane 4: $(BASE\text{-}K8_{15})_2$, lane 5: $BASE\text{-}K8_{15}$ gene fragments. (B) Lane 1: DNA ladder, lane 2: $BASE\text{-}K8_{30}$, lane 3: $(BASE\text{-}K8_{30})_2$ digestion fragments

Protein expression and purification resulted in protein block-copolymers with the correct molecular weight as determined by PAGE gels and MALDI-TOF analysis (Figure 7.3.2, Table 7.3.1).

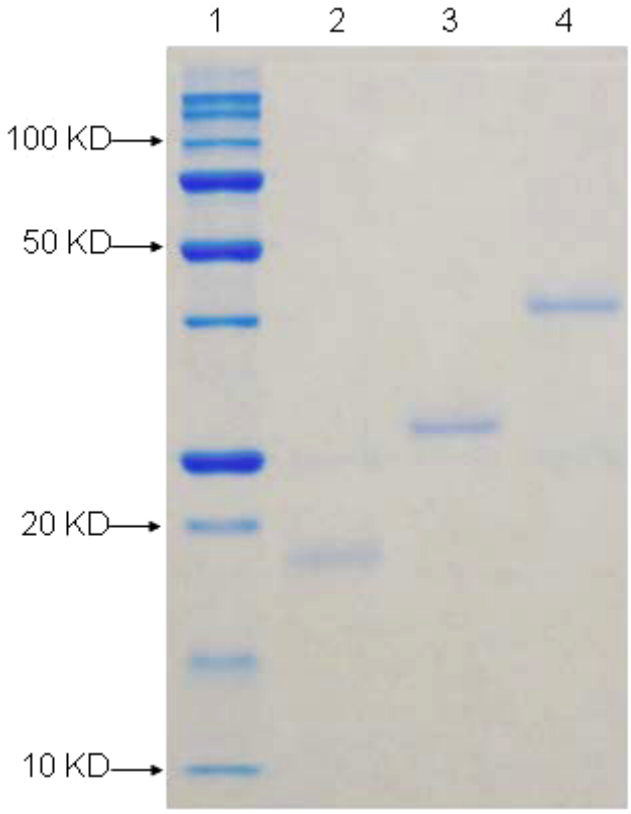

Figure 7.3.2: A representative SDS-PAGE gel of purified protein block-copolymers is shown. Lane 1: protein ladder, lane 2: BASE-$K8_{15}$, lane 3: (BASE-$K8_{15}$), lane 4: $(ACID\text{-}K8_{15})_2$

Table 7.3.1: Molecular Weight of Protein Block-Copolymers as Determined by MALDI-TOF Spectrometry

Protein	Repeats	Observed MW	Expected MW
$(ACID\text{-}K8_{15})_n$	n = 1, 2	15.9, na*	16.0, 29.0
$(ACID\text{-}BQ)_n$	n = 2	17.9	18.0
$(ACID\text{-}BQ_3)_m$	m = 3	49.0	49.1
$(K8_{30}\text{-}BASE)_n$	n = 1, 2	25.3, 47.9	25.3, 47.8
$(K8_{15}\text{-}BASE)_m$	m = 1, 2	16.1, 29.2	16.0, 29.0

* Sample molecular weight could not be determined by MALDI-TOF

7.3.2 Characterization of Secondary Structure

The expression of a protein block-copolymer with domains of distinct conformations carries some risk that the regions will interact with each other intramolecularly and potentially affect secondary structure. For this reason, secondary structure was evaluated by CD spectroscopy (Figure 7.3.3).

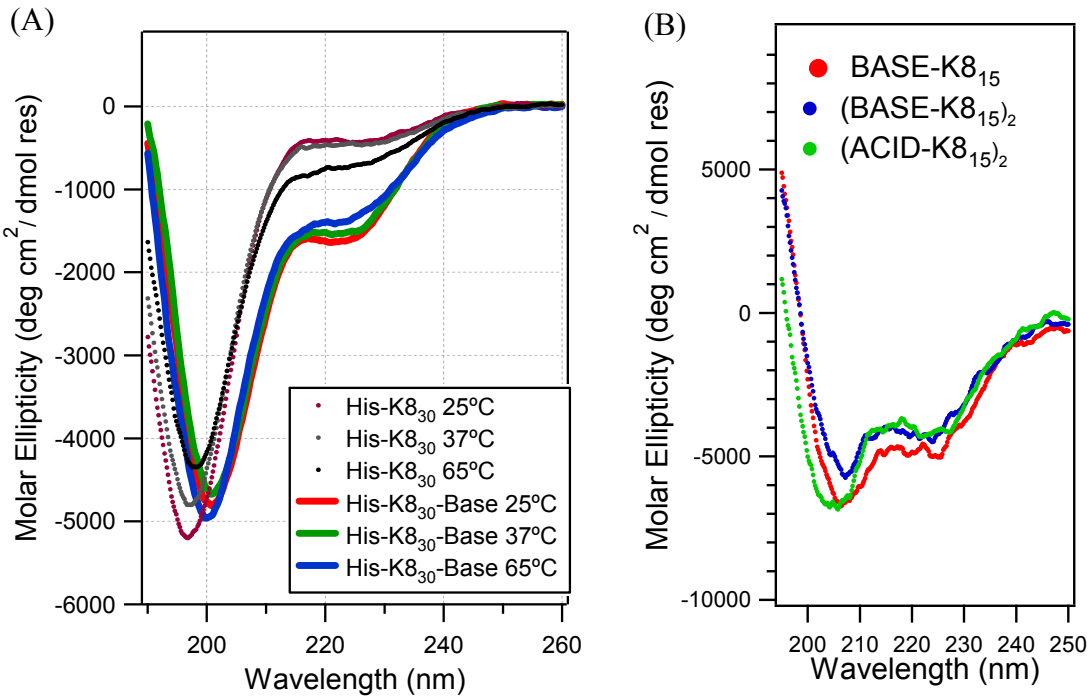

Figure 7.3.3: CD spectra of coiled-coil protein block-copolymers in H_2O. (A) BASE -K8$_{30}$ (B) ACID and BASE with K8$_{15}$ at 25°C.

The CD spectra indicated the protein polymers have α-helical conformation, as indicated by the minima at 222 nm. Furthermore, the random coil minima at 198 nm slightly shifted to near 200 nm for the protein block-copolymers containing only one coiled-coil domain, BASE-K8$_{30}$ (Figure 7.3.3A); the shift in the peak wavelength is likely due to the presence of the helical

domain, which has a secondary minimum at 208 nm. Furthermore, as temperature increased to 65°C the helicity slightly decreased suggesting an increased distribution in peptide bond rotation resulting from the unfolding of the helical domain. The CD spectra of block-copolymers that contain multiple coiled-coil blocks and less random coil domains have spectra that appear mostly helical (Figure 7.3.3 B and C). The relative percentages of each protein secondary structure were determined by the equations:

$$\% \text{ helix} = [\theta]_{222} / [\theta]_{max}$$

$$[\theta]_{max} = -39500\,[1-(2.57/n)] \quad (\text{deg cm}^2\ \text{dmol}^{-1})$$

were n = the number of residues in the protein and $[\theta]_{222}$ is the molar elipticity at 222nm. Table 7.3.2 displays both the predicted and calculated helical content of the protein block-copolymers.

Table 7.3.2: Percent Helicity of Protein Block-Copolymers

	Calculated Fraction Helical (%)	Expected Fraction Helical (%)
$(ACID\text{-}K8_{15})_2$	10.2	17.7
$(BASE\text{-}K8_{15})_2$	11.0	17.7
$BASE\text{-}K8_{15}$	11.7	16.4
$BASE\text{-}K8_{30}$	4.2	9.8

As indicated in Table 7.3.2, the protein block-copolymers have less than the predicted helical content, suggesting disruption or unfolding of the α-helix when expressed as a block-copolymer with an unstructured domain. The $BASE\text{-}K8_{30}$ protein block-copolymer had a very low helical content as observed by the CD spectra. It is interesting to note that as the expected helical

fraction increased from 9.8 to 16.4 the secondary structure, as exhibited in Figure 7.3.3 drastically increased where the spectrum in Figure 7.3.3B had a more pronounced α-helical conformation.

Coiled-coil association was investigated with AUC. Preliminary experiments suggested that BASE-$K8_{30}$ exhibited a dimeric association state, which was expected based on protein sequence. Future experiments will determine association of all protein block protein copolymers.

7.3.3 Solubility and Hydrogel Formation

Protein block-copolymers displayed limited solubility in solution possibly due to aggregation of the hydrophobic regions contained in the coiled-coil domain or electrostatic interactions with the random coil protein regions. The protein block-copolymers solubility in a variety of aqueous buffers is shown in Table 7.3.3.

Table 7.3.3: Solubility of Protein Block-Copolymers

	PBS Buffer	**50mM Tris Buffer**	**10 mM Tris Buffer**	**2mM EDTA Buffer**	**MOPS Buffer**	**H_2O**
ACID-$K8_{15}$	1 wt% not soluble	X*	X	1 wt% not soluble	1 wt% not soluble	1 wt% not soluble
(ACID-$K8_{15}$)$_2$	X	X	X	1 wt% not soluble	1 wt% not soluble	1 wt% not soluble
(ACID-BQ)$_2$	X	X	X	1 wt% not soluble	X	X
BASE-$K8_{30}$	X	X	X	10 wt% soluble	X	X
(BASE-$K8_{15}$)$_2$	1 wt% cloudy	1 wt% cloudy	1 wt% with basic pH clear	10 wt% soluble	5 wt% not soluble	10 wt% soluble

* X indicates conditions not tested

The block-copolymers that contained the ACID sequence were essentially not soluble in any condition tested and thus were not used for subsequent experiments. The lack of solubility of ACID is likely due to electrostatic interactions; ACID contains negative charges by the glutamic acid residues, when combined with cationic $K8_{15}$ proteins the attractive forces may cause precipitation in solution. Similarly, the BASE proteins contain an overall negative charge which may cause repulsive interactions with the $K8_n$ sequence. Buffers with increased salt content were testing to increase electrostatic shielding; however solubility remained the same (data not shown).

Hydrogels formed by self-assembly were investigated using (BASE-$K8_{15}$)$_2$ due to its enhanced solubility and two self-assembling domains. A self-sustaining hydrogel was rapidly formed by (BASE-$K8_{15}$)$_2$ at 15 wt% in H_2O (Figure 7.3.4).

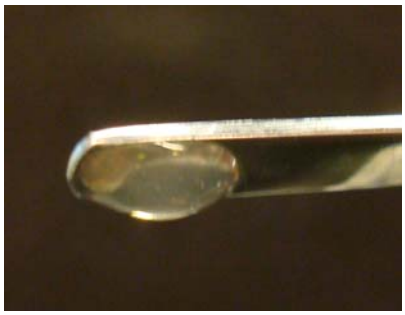

Figure 7.3.4: Photograph of self-assembled hydrogel formed by (BASE-$K8_{15}$)$_2$ at 15 wt% in H_2O.

The self-assembled hydrogel did not exhibit flow under gravity but had very weak mechanical properties. For this reason, a hybrid enzymatically crosslinked hydrogel was produced by the combination of (BASE-$K8_{15}$)$_2$, BQ_6, and tTG. After physical and enzymatic crosslinking, the

hydrogel appeared very similar to the materials created by the random coil, enzymatically crosslinked proteins.

7.3.4 Viscoelastic Properties by Rheometry

The combination of physically and enzymatically crosslinking hydrogels was hypothesized to enhance the material properties by increasing protein entanglement and adding elasticity to the hydrogel. For this reason, the linear viscoelastic behavior of the protein block-copolymer composed of $(K8_{15}\text{-BASE})_2$ and BQ_6 was characterized by an oscillatory frequency and strain sweep (Figure 7.3.5).

(A)

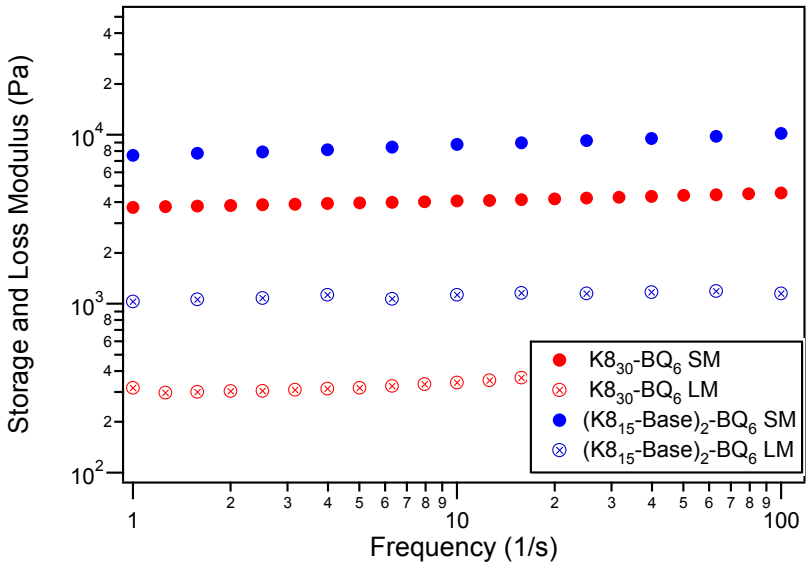

(B)

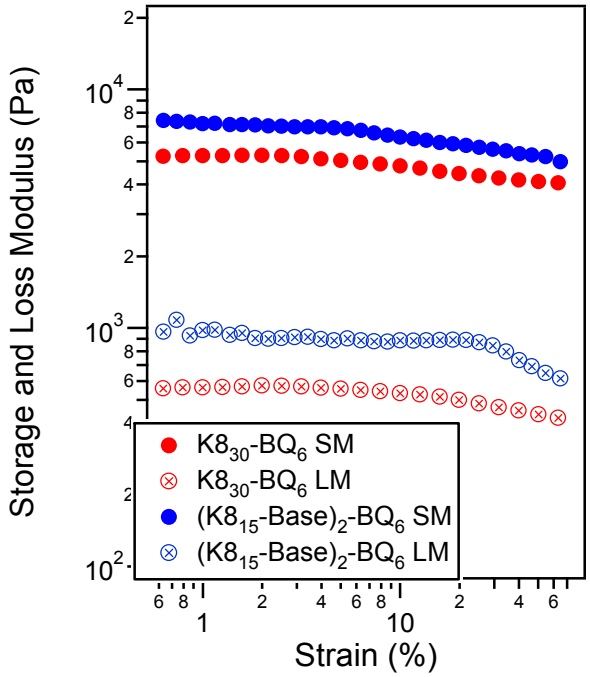

Figure 7.3.5: Oscillatory rheological properties of the protein block-copolymer $(K8_{15}\text{-BASE})_2/BQ_6$ in comparison to $K8_{30}/BQ_6$. Moduli as a function of a (A) frequency sweep and a (B) strain sweep. Storage modulus is indicated by the closed symbols and the loss modulus by the open symbols.

The addition of the coiled-coil block appears to enhance the moduli of the hydrogels. However, it is important to note that the molecular weight of the protein block-copolymer is greater than the random coil $K8_{30}$ protein. As shown previously, increased molecular weight of the hydrogel components results in a greater storage modulus. However, the hybrid hydrogels contained the same relative ratio of enzyme to crosslinking sites as the random coil protein polymer hydrogels. The AUC results and physical gelation at high concentrations suggest dimeric association of the protein block-copolymers, for this reason we hypothesize that the self-assembled physical crosslinking is contributing to the viscoelastic properties. It is important to note that the overall moduli at low strain increased with frequency, indicative of a robust material. The strain sweep shows a decrease storage modulus at ~5% strain, this is much less that the purely protein polymer based hydrogels, exhibiting a decrease at 10% strain (Chapter 6 Figure 6.3.7C). The decrease in material robustness may in part be due to the unraveling of the coiled-coil association at smaller strains. Increased material elasticity was not observed, as indicated by the decrease in storage modulus between the frequency sweep and strain sweep, regardless of the 10 min recovery time in between data collection. As hypothesized, the results clearly indicate an increase in material robustness by the inclusion of the self-assembling domain, however elasticity did not appear to be affected.

7.4 Conclusions and Future Directions

As a proof of concept, protein block-copolymers containing coiled-coil domains were created by genetic engineering and protein expression techniques. The controlled cloning method allowed for the creation of block-copolymers with selective, controlled frequency, and spacing of

the genes encoding the helical proteins. The protein block-copolymers maintained the expected secondary structures of the respective domains, however, exhibited slightly less helical secondary structure than the predicted values. This evidence supports the hypothesis that *de novo* protein block-copolymers can maintain the functionality of the different domains.

The coiled-coil forming proteins had differing solubilities when expressed as a block-copolymer, which limited further investigation of some of the proteins. The proteins that contain more than one BASE sequence, however, formed self-sustaining hydrogels by physical coiled-coil association. Furthermore, hybrid hydrogels of enzymatically crosslinked block-copolymers and random coil proteins formed viscoelastic hydrogels that displayed a higher modulus than proteins without the self-assembling region.

Further research should include altering the amino acid sequence of the block-copolymers containing the ACID domain to enhance solubility and allow for the investigation of the effects of association state and hydrogel material properties. Furthermore, the length of the coiled-coil containing block should be varied to determine its effects on the hydrogel properties. The ability to control hydrogel morphology and porosity should be investigated by SEM with a range of gel formulations. Finally, additional rheological experiments should investigate the ability of increased self-assembling blocks to enhance material elasticity.

Chapter 8

Conclusions and Recommendations

8.1 Summary

Biomaterials created from *de novo* protein polymers have important implications for material development with many potential applications. This thesis focused on creating recombinant proteins (1) for a biophysical study of patterned self-assembled molecules, which expand the range of biosynthetic materials for use in nanopatterning, and (2) as a foundation of protein polymer-based scaffolds for tissue engineering. Recombinant DNA technology has enabled the synthesis of genetically engineered protein polymers with precisely controlled sequence, molecular weight, and properties. Diverse motifs present in natural proteins were restructured at the molecular level into recombinant proteins, which created biosynthetic materials with properties that cannot be mimicked in conventional synthetic polymer systems. Furthermore, the material properties of these biosynthetic protein polymer-based materials can be modulated by altering sequence and length. For these reasons, materials based on recombinant proteins provide a unique and powerful approach to control macromolecular structure and function, which can be exploited for the field of biotechnology.

In the first section of this thesis in Chapters 3 and 4, monodisperse recombinant proteins were created as self-assembling nanomaterials. The self-assembly of ordered molecular patterns is an important method towards the development of new materials with structure and properties controlled at the nanoscale. Self-organization of monodisperse rod-shaped molecules and nanoparticles is an example of self-assembly that has been observed, for example, in concentrated solutions of virus particles and polymers with rigid backbones. This self-assembly is driven by excluded volume interactions between the particles, and the resulting ordering is directly controlled by the particle sizes and shapes. The phase diagrams of particle self-assembly have been extensively investigated using computer simulations. However, few studies have experimentally verified and exploited this phenomenon due to the lack of available methods for synthesis of nanoscale rod-shaped particles with controlled diameter and length. While several pioneering studies demonstrated synthesis of polymers with rigid elongated backbones, the resulting macromolecules had a distribution of length and, in some cases, concentration-dependent conformations. While there exists natural virus particles with monodisperse rod shapes, it is difficult to engineer their dimensions or to adjust their inter-particle interactions. The goals of Chapters 3 and 4 were to (i) develop a method for making monodisperse cylindrical macromolecules with controlled nanoscale sizes and (ii) to investigate experimentally order and phase transitions in solutions of these novel molecules.

To prepare molecules with defined length (L) and diameter (D) that could self-assemble into nanostructures having long-range order controlled by the exact molecular dimensions, a synthetic method was developed that combines molecular biology and synthetic chemistry. The protein molecules contained a backbone generated by bacterial expression and chemically

synthesized dendrons, with several generations and degrees of branching, were added as pendant groups. The resulting macromolecules self-assembled to form highly ordered liquid crystalline structures unique to molecules with absolutely defined shape and size. The observed long-range ordered self-assembly of these DPP materials was driven by excluded volume interactions between the rigid DPP cylinders. The phase behavior over a broad range of particle aspect ratios (L/D) and concentrations was experimentally investigated using high-resolution synchrotron X-ray diffraction and polarized optical microcopy. As a function of the increasing particle concentration, transitions from isotropic to nematic, to smectic and finally hexagonal columnar liquid crystal phases were observed. This experimental system was the first to validate the predicted smectic phase formation for rigid rods with L/D>4. In addition, a highly ordered lamellar smectic phase was observed and for the first time, the L/D=4 limit for the existence of nematic phase. Molecules with L/D<4 transitioned from isotropic directly to smectic phase, contradicting theories from computer simulations, thus, expanding the boundary for lamellar phase formation.

The second section of this thesis, discussed in Chapters 5-7, applied disordered recombinant protein polymers to the specific application as scaffolding for tissue engineering. Chapter 5 discussed the development of a new class of linear, cationic, random-coil protein polymers designed to act as scaffolds for multivalent display. Protein characterization determined that the proteins are random coil, soluble to high temperatures, and are non-toxic in μM concentrations. These polymers contain evenly spaced lysine residues that allowed for chemical or enzymatic conjugation of pendant functional groups. The inherent monodispersity of the protein polymers allowed for the precise determination of valency of attached functional

pendant groups. The amine-containing protein polymers were useful for integrating epitopes, to ultimately control cell material interaction. It was shown that the protein polymers could be chemically conjugated with a signaling peptide, RGD, an immune "shielding" polymer, PEG, and a small fluorophore to track proteins *in vitro* and *in vivo*. Moreover, enzymatic conjugation was used to covalently attach a peptide that contained both the glutamine recognition sequence for tTG and the RGD cell adhesion peptide. Furthermore, the incomplete derivitization allowed for both step-wise conjugation of pendant groups to create a polyvalent scaffold, and chemical crosslinking into a gel displaying these pendant groups.

The ability to create multivalent gels and use protein polymers as substrates for enzymatic recognition sites, inspired the development of tTG-crosslinked, protein polymer hydrogels presented in Chapter 6. To this end, a second class of protein polymers was developed that contained the glutamine substrate for tTG, where a highly porous, non-toxic protein polymer hydrogel was formed upon the addition of the transglutaminase enzyme. Rheological experiments indicated a rapid gelation, under 2 minutes, and the ability to modulate viscoelastic properties over 4-fold. In addition, hydrogel swelling and degradation were dependent on gel formulation. Hydrogels were initially applied to islet encapsulation for the treatment of type I diabetes. After 36 h, *in vitro* studies indicated encapsulated islets had some degree of apoptosis as determined by histology, potential due to islet damage during encapsulation. However, islets encapsulated in the hydrogel were functional *in vivo* at least to 8 weeks. In chemically-induced diabetic mice, hydrogels with islets were able to tightly control blood glucose levels. Onset of normal blood sugar, however, was slower than transplants of non-encapsulated islets. From these

studies, we concluded that the protein polymer hydrogels were a permissive platform for islet transplantation, but did not enhance allograft islet function.

We hypothesized that increasing hydrogel pore size may enhance islet survival. One method to achieve this was to create self-assembling block-copolymers. The cloning strategy utilized allowed for creation of protein block co-polymers containing self-assembling coil-coil domains (Chapter 7). Two coiled-coil domains that differ in association state were investigated; at neutral pH, one was predicted to form a dimer, while the other establishes equilibrium between monomer, dimer, and trimer. When combined, however, prior research suggested that a heterotetramer was formed.[78] These coiled-coil domains were cloned into the random coil polymers at different frequencies. Due to difficulties with solubility, only one protein block-copolymer was investigated for hydrogel formation. At 15 wt% a physical hydrogel was formed by coiled-coil dimeric association. Enzymatically crosslinked hydrogels with a combination of the self-assembled block-copolymers and disordered polymers displayed a 2-fold increase in elastic modulus. The ability to modulate hydrogel material properties and display multivalent epitopes suggests the potential to use enzymatically crosslinked protein polymers as tailor-made biomaterials.

8.2 Recommendations

The impact of protein polymer structure on function and self-assembly in solution has had limited experimental study. The first section of this thesis contributed to the study of self-assembly of protein polymers. The modular nature of this synthetic strategy can be used to expand the range of accessible DPP interactions and shapes through the variation of peptide

sequences, dendron functionality, and dendron architectures. In addition, this system can be used to determine the relationship between molecular shape and excluded volume interactions of monodisperse molecules. However, the materials presented herein lacked molecular orientation. An unrealized goal of this research was the production of protein block-copolymers that contain a terminal region with strong molecular assembly, such as β-sheet formation, that could orient materials for electromagnetic applications. In addition, biosynthetic polymers that form liquid crystal phases in aqueous solutions would be important for several biomaterial applications.

Protein polymers developed specifically for biomaterial applications was the second focus of this thesis. The full range of material properties based on formulation was not realized within the research presented. Subsequent experiments should focus on the control of morphology and viscoelastic properties by increasing enzyme, protein, and self-assembling domain concentrations. Furthermore, assays that calculated the number of free amines in the hydrogel would give an estimate of the degree of crosslinking and impact the observations of material properties herein.

Protein polymer hydrogels appeared to have limited degradation as suggested by the immune response still present after 8 weeks *in vivo*. Specifically, the hydrogels could be effectively remodeled and degraded by the inclusion of matrix metalloproteinases recognition sequences. The polymer precursor weight effects on hydrogel mesh size should be investigated to predict drug and protein delivery rates as well as dictate cell interaction and migration. In addition, bioactive epitopes should be incorporated into the hydrogel for controlled cellular behavior both *in vitro* and *in vivo*. An obstacle for protein polymers to be a viable *in vivo* biomaterial platform is the immune response elicited. The removal of endotoxins that may

accompany bacterially expressed proteins should be investigated to lower the immune response. Furthermore, hybrid hydrogels composed of protein polymers and PEG could be non-immunogenic due to the low immunogenicity and toxicity of PEG.

The multitude of functionality in natural proteins can be enhanced by non-natural protein polymer analogs. Protein polymer biomaterials can be designed to have controlled self-assembling and material properties. The primary obstacles for genetically engineered proteins as next-generation materials are both the improvement of mechanical properties as well as complete *in vivo* evaluation. The protein polymer materials presented herein, could provide a foundation to launch protein polymers-based materials to both clinical and biotech use in the future.

References

1. Collings, P. J., Hird, M., *Introduction to liquid crystals chemistry and physics*. Taylor and Francis: London, 1997.

2. Bolhuis, P.; Frenkel, D., Tracing the phase boundaries of hard spherocylinders. *Journal of Chemical Physics* **1997,** 106, (2), 666-687.

3. Frauenrath, H., Dendronized polymers - building a new bridge from molecules to nanoscopic objects. *Progress in Polymer Science* **2005,** 30, (3-4), 325-384.

4. Coyne, J. C.; Lin, J. S.; Barron, A. E., DNA sequencing and genotyping by free-solution capillary electrophoresis. In *Handbook of Capillary and Microchip Electrophoresis and Associated Microtechniques*, 3 ed.; Landers, J. P., Ed. CRC Press: New York, 2008; Vol. 1, p 1567.

5. Won, J. I.; Meagher, R. J.; Barron, A. E., Protein polymer drag-tags for DNA separations by end-labeled free-solution electrophoresis. *Electrophoresis* **2005,** 26, (11), 2138-2148.

6. Yu, S. J. M.; Conticello, V. P.; Zhang, G. H.; Kayser, C.; Fournier, M. J.; Mason, T. L.; Tirrell, D. A., Smectic ordering in solutions and films of a rod-like polymer owing to monodispersity of chain length. *Nature* **1997,** 389, (6647), 167-170.

7. Fahnestock, S. R.; Irwin, S. L., Synthetic spider dragline silk proteins and their production in Escherichia coli. *Applied Microbiology and Biotechnology* **1997,** 47, (1), 23-32.

8. Asakura, T.; Nitta, K.; Yang, M. Y.; Yao, J. M.; Nakazawa, Y.; Kaplan, D. L., Synthesis and characterization of chimeric silkworm silk. *Biomacromolecules* **2003,** 4, (3), 815-820.

9. Prince, J. T.; McGrath, K. P.; Digirolamo, C. M.; Kaplan, D. L., Construction, cloning, and expression of synthetic genes encoding spider dragline silk. *Biochemistry* **1995,** 34, (34), 10879-10885.

10. Yin, J.; Lin, J. H.; Li, T. Y.; Wang, D. I. C., Evaluation of different promoters and host strains for the highlevel expression of collagen-like polymer in Escherichia coli. *Journal of Biotechnology* **2003,** 100, (3), 181-191.

11. Urry, D. W.; Luan, C. H.; Parker, T. M.; Gowda, D. C.; Prasad, K. U.; Reid, M. C.; Safavy, A., Temperature of polypeptide inverse temperature transition depends on mean residue hydrophobicity. *Journal of the American Chemical Society* **1991,** 113, (11), 4346-4348.

12. Wright, E. R.; Conticello, V. P., Self-assembly of block copolymers derived from elastin-mimetic polypeptide sequences. *Advanced Drug Delivery Reviews* **2002,** 54, (8), 1057-1073.

13. Panitch, A.; Yamaoka, T.; Fournier, M. J.; Mason, T. L.; Tirrell, D. A., Design and biosynthesis of elastin-like artificial extracellular matrix proteins containing periodically spaced fibronectin CS5 domains. *Macromolecules* **1999,** 32, (5), 1701-1703.

14. Meyer, D. E.; Chilkoti, A., Genetically encoded synthesis of protein-based polymers with precisely specified molecular weight and sequence by recursive directional ligation: Examples from the elastin-like polypeptide system. *Biomacromolecules* **2002,** 3, (2), 357-367.

15. Nagapudi, K.; Brinkman, W. T.; Leisen, J.; Thomas, B. S.; Wright, E. R.; Haller, C.; Wu, X. Y.; Apkarian, R. P.; Conticello, V. P.; Chaikof, E. L., Protein-based thermoplastic elastomers. *Macromolecules* **2005,** 38, (2), 345-354.

16. Petka, W. A.; Harden, J. L.; McGrath, K. P.; Wirtz, D.; Tirrell, D. A., Reversible hydrogels from self-assembling artificial proteins. *Science* **1998,** 281, (5375), 389-392.

17. Wang, C.; Stewart, R. J.; Kopecek, J., Hybrid hydrogels assembled from synthetic polymers and coiled-coil protein domains. *Nature* **1999,** 397, (6718), 417-420.

18. McMillan, R. A.; Conticello, V. P., Synthesis and characterization of elastin-mimetic protein gels derived from a well-defined polypeptide precursor. *Macromolecules* **2000,** 33, (13), 4809-4821.

19. Krejchi, M. T.; Atkins, E. D. T.; Waddon, A. J.; Fournier, M. J.; Mason, T. L.; Tirrell, D. A., Chemical sequence control of beta-sheet assembly in macromolecular crystals of periodic polypeptides. *Science* **1994,** 265, (5177), 1427-1432.

20. Zhuravel, M. A.; Davis, N. E.; Nguyen, S. T.; Koltover, I., Dendronized protein polymers: Synthesis and self-assembly of monodisperse cylindrical macromolecules. *Journal of the American Chemical Society* **2004,** 126, (32), 9882-9883.

21. Liu, S.; Kiick, K. L., Architecture effects on the binding of cholera toxin by helical glycopolypeptides. *Macromolecules* **2008,** 41, (3), 764-772.

22. Kirshenbaum, K.; Carrico, I. S.; Tirrell, D. A., Biosynthesis of proteins incorporating a versatile set of phenylalanine analogues. *Chembiochem* **2002,** 3, (2-3), 235-237.

23. Kiick, K. L.; van Hest, J. C. M.; Tirrell, D. A., Expanding the scope of protein biosynthesis by altering the methionyl-tRNA synthetase activity of a bacterial expression host. *Angewandte Chemie-International Edition* **2000,** 39, (12), 2148-+.

24. Connor, R. E.; Tirrell, D. A., Non-canonical amino acids in protein polymer design. *Polymer Reviews* **2007,** 47, (1), 9-28.

25. Cantor, E. J.; Creel, H. S.; Deguchi, Y.; Dougherty, M. J.; Kothakota, S.; Krejchi, M. T.; Matsuki, K.; McGrath, K. P.; Parkhe, A. D.; Atkins, E. D. T.; Fournier, M. J.; Mason, T. L.; Tirrell, D. A., In-vivo synthesis and structural-analysis of alanylglycine-rich artificial proteins. In *Silk Polymers*, 1994; Vol. 544, pp 98-103.

26. Doel, M. T.; Eaton, M.; Cook, E. A.; Lewis, H.; Patel, T.; Carey, N. H., The expression in escherichia-coli of synthetic repeating polymeric genes-coding for poly(L-aspartyl-L-phenylalanine). *Nucleic Acids Research* **1980,** 8, (20), 4575-4592.

27. McGrath, K., Kaplan D., *Protein-Based Materials*. Birkhauser: Boston, 1997.

28. Urry, D. W., Physical chemistry of biological free energy transduction as demonstrated by elastic protein-based polymers. *Journal of Physical Chemistry B* **1997,** 101, (51), 11007-11028.

29. Welsh, E. R.; Tirrell, D. A., Engineering the extracellular matrix: A novel approach to polymeric biomaterials. I. Control of the physical properties of artificial protein matrices designed to support adhesion of vascular endothelial cells. *Biomacromolecules* **2000,** 1, (1), 23-30.

30. Meyer, D. E.; Kong, G. A.; Dewhirst, M. W.; Zalutsky, M. R.; Chilkoti, A., Targeting a genetically engineered elastin-like polypeptide to solid tumors by local hyperthermia. *Cancer Research* **2001,** 61, (4), 1548-1554.

31. Nicol, A.; Gowda, D. C.; Parker, T. M.; Urry, D. W., Elastomeric polytetrapeptide matrices - Hydrophobicity dependence of cell attachment from adhesive (GGIP)N to nonadhesive (GGAP)N even in serum. *Journal of Biomedical Materials Research* **1993,** 27, (6), 801-810.

32. Haider, M.; Megeed, Z.; Ghandehari, H., Genetically engineered polymers: status and prospects for controlled release. *Journal of Controlled Release* **2004,** 95, (1), 1-26.

33. Meyer, D. E.; Shin, B. C.; Kong, G. A.; Dewhirst, M. W.; Chilkoti, A., Drug targeting using thermally responsive polymers and local hyperthermia. *Journal of Controlled Release* **2001,** 74, (1-3), 213-224.

34. Liu, J. C.; Heilshorn, S. C.; Tirrell, D. A., Comparative cell response to artificial extracellular matrix proteins containing the RGD and CS5 cell-binding domains. *Biomacromolecules* **2004,** 5, (2), 497-504.

35. Nowatzki, P. J.; Tirrell, D. A., Physical properties of artificial extracellular matrix protein films prepared by isocyanate crosslinking. *Biomaterials* **2004,** 25, (7-8), 1261-1267.

36. Liu, C. Y.; Westerlund, U.; Svensson, M.; Moe, M. C.; Varghese, M.; Berg-Johnsen, J.; Apuzzo, M. L. J.; Tirrell, D. A.; Langmoen, I. A., Artificial niches for human adult neural stem cells: Possibility for autologous transplantation therapy. *Journal of Hematotherapy & Stem Cell Research* **2003,** 12, (6), 689-699.

37. Betre, H.; Liu, W.; Zalutsky, M. R.; Chilkoti, A.; Kraus, V. B.; Setton, L. A., A thermally responsive biopolymer for intra-articular drug delivery. *Journal of Controlled Release* **2006,** 115, (2), 175-182.

38. Valiaev, A.; Abu-Lail, N. I.; Lim, D. W.; Chilkoti, A.; Zauscher, S., Microcantilever sensing and actuation with end-grafted stimulus-responsive elastin-like polypeptides. *Langmuir* **2007,** 23, (1), 339-344.

39. Meyer, D. E.; Trabbic-Carlson, K.; Chilkoti, A., Protein purification by fusion with an environmentally responsive elastin-like polypeptide: Effect of polypeptide length on the purification of thioredoxin. *Biotechnology Progress* **2001,** 17, (4), 720-728.

40. Lim, D. W.; Nettles, D. L.; Setton, L. A.; Chilkoti, A., In situ cross-linkinig of elastin-like polypeptide block copolymers for tissue repair. *Biomacromolecules* **2008,** 9, (1), 222-230.

41. Beckwitt, R.; Arcidiacono, S., Sequence conservation in the C-terminal region of spider silk proteins (spidroin) from nephila-clavipes (tetragnathidae) and araneus-bicentenarius (Araneidae). *Journal of Biological Chemistry* **1994,** 269, (9), 6661-6663.

42. Hinman, M. B.; Lewis, R. V., Isolation of a clone encoding a 2nd dragline silk fibroin - Nephila-Clavipes dragline silk is a 2-protein fiber. *Journal of Biological Chemistry* **1992,** 267, (27), 19320-19324.

43. Kaplan, D. L.; Fossey, S.; Mello, C. M.; Arcidiacono, S.; Senecal, K.; Muller, W.; Stockwell, S.; Beckwitt, R.; Viney, C.; Kerkam, K., Biosynthesis and processing of silk proteins. *Materials Research Society Bulletin* **1992,** 10, 41-47.

44. Huang, J.; Foo, C. W. P.; Kaplan, D. L., Biosynthesis and applications of silk-like and collagen-like proteins. *Polymer Reviews* **2007,** 47, (1), 29-62.

45. Huemmerich, D.; Slotta, U.; Scheibel, T., Processing and modification of films made from recombinant spider silk proteins. *Applied Physics a-Materials Science & Processing* **2006,** 82, (2), 219-222.

46. Yang, J. J.; Barr, L. A.; Fahnestock, S. R.; Liu, Z. B., High yield recombinant silk-like protein production in transgenic plants through protein targeting. *Transgenic Research* **2005,** 14, (3), 313-324.

47. Rammensee, S.; Huemmerich, D.; Hermanson, K. D.; Scheibel, T.; Bausch, A. R., Rheological characterization of hydrogels formed by recombinantly produced spider silk. *Applied Physics a-Materials Science & Processing* **2006,** 82, (2), 261-264.

48. Sofia, S.; McCarthy, M. B.; Gronowicz, G.; Kaplan, D. L., Functionalized silk-based biomaterials for bone formation. *Journal of Biomedical Materials Research* **2001,** 54, (1), 139-148.

49. Karageorgiou, V.; Meinel, L.; Hofmann, S.; Malhotra, A.; Volloch, V.; Kaplan, D., Bone morphogenetic protein-2 decorated silk fibroin films induce osteogenic differentiation of human

bone marrow stromal cells. *Journal of Biomedical Materials Research Part A* **2004,** 71A, (3), 528-537.

50. Albarran, B.; To, R.; Stayton, P. S., A TAT-streptavidin fusion protein directs uptake of biotinylated cargo into mammalian cells. *Protein Engineering Design & Selection* **2005,** 18, (3), 147-152.

51. Asai, T.; Trinh, R.; Ng, P. P.; Penichet, M. L.; Wims, L. A.; Morrison, S. L., A human biotin acceptor domain allows site-specific conjugation of an enzyme to an antibody-avidin fusion protein for targeted drug delivery. *Biomolecular Engineering* **2005,** 21, (6), 145-155.

52. Icke, C.; Schlott, B.; Ohlenschlager, O.; Hartmann, M.; Guhrs, K. H.; Glusa, E., Fusion proteins with anticoagulant and fibrinolytic properties: Functional studies and structural considerations. *Molecular Pharmacology* **2002,** 62, (2), 203-209.

53. Park, E.; Starzyk, R. M.; McGrath, J. P.; Lee, T.; George, J.; Schutz, A. J.; Lynch, P.; Putney, S. D., Production and characterization of fusion proteins containing transferrin and nerve growth factor. *Journal of Drug Targeting* **1998,** 6, (1), 53-64.

54. Medintz, I. L.; Uyeda, H. T.; Goldman, E. R.; Mattoussi, H., Quantum dot bioconjugates for imaging, labelling and sensing. *Nature Materials* **2005,** 4, (6), 435-446.

55. Dubrovsky, T.; Tronin, A.; Dubrovskaya, S.; Guryev, O.; Nicolini, C., Langmuir films of Fc binding receptors engineered from protein A and protein G as a sublayer for immunoglobulin orientation. *Thin Solid Films* **1996,** 285, 698-702.

56. Slocik, J. M.; Naik, R. R.; Stone, M. O.; Wright, D. W., Viral templates for gold nanoparticle synthesis. *Journal of Materials Chemistry* **2005,** 15, (7), 749-753.

57. Zhou, C. Z.; Confalonieri, F.; Medina, N.; Zivanovic, Y.; Esnault, C.; Yang, T.; Jacquet, M.; Janin, J.; Duguet, M.; Perasso, R.; Li, Z. G., Fine organization of Bombyx mori fibroin heavy chain gene. *Nucleic Acids Research* **2000,** 28, (12), 2413-2419.

58. McGrath, K. P.; Tirrell, D. A.; Kawai, M.; Mason, T. L.; Fournier, M. J., Chemical and biosynthetic approaches to the production of novel polypeptide materials. *Biotechnology Progress* **1990,** 6, (3), 188-192.

59. Wang, Y.; Kiick, K. L., Monodisperse protein-based glycopolymers via a combined biosynthetic and chemical approach. *Journal of the American Chemical Society* **2005,** 127, (47), 16392-16393.

60. Halstenberg, S.; Panitch, A.; Rizzi, S.; Hall, H.; Hubbell, J. A., Biologically engineered protein-graft-poly(ethylene glycol) hydrogels: A cell adhesive and plasm in-degradable biosynthetic material for tissue repair. *Biomacromolecules* **2002,** 3, (4), 710-723.

61. Rizzi, S. C.; Hubbell, J. A., Recombinant protein-co-PEG networks as cell-adhesive and proteolytically degradable hydrogel matrixes. Part 1: Development and physicochernical characteristics. *Biomacromolecules* **2005,** 6, (3), 1226-1238.

62. Rizzi, S. C.; Ehrbar, M.; Halstenberg, S.; Raeber, G. P.; Schmoekel, H. G.; Hagenmuller, H.; Muller, R.; Weber, F. E.; Hubbell, J. A., Recombinant protein-co-PEG networks as cell-adhesive and proteolytically degradable hydrogel matrixes. Part II: Biofunctional characteristics. *Biomacromolecules* **2006,** 7, (11), 3019-3029.

63. Farmer, R. S.; Top, A.; Argust, L. M.; Liu, S.; Kiick, K. L., Evaluation of conformation and association behavior of multivalent alanine-rich polypeptides. *Pharmaceutical Research* **2008,** 25, (3), 700-708.

64. Polizzotti, B. D.; Maheshwari, R.; Vinkenborg, J.; Kiick, K. L., Effects of saccharide spacing and chain extension on toxin inhibition by glycopolypeptides of well-defined architecture. *Macromolecules* **2007,** 40, (20), 7103-7110.

65. Koltover, I.; Sahu, S.; Davis, N., Genetic engineering of the nanoscale structure in polyelectrolyte-lipid self-assembled systems. *Angewandte Chemie-International Edition* **2004,** 43, (31), 4034-4037.

66. Yu, S. J. M.; Soto, C. M.; Tirrell, D. A., Nanometer-scale smectic ordering of genetically engineered rodlike polymers: Synthesis and characterization of monodisperse derivatives of poly(gamma-benzyl alpha,L-glutamate). *Journal of the American Chemical Society* **2000,** 122, (28), 6552-6559.

67. Goeden-Wood, N. L.; Conticello, V. P.; Muller, S. J.; Keasling, J. D., Improved assembly of multimeric genes for the biosynthetic production of protein polymers. *Biomacromolecules* **2002,** 3, (4), 874-879.

68. Goeden-Wood, N. L.; Keasling, J. D.; Muller, S. J., Self-assembly of a designed protein polymer into beta-sheet fibrils and responsive gels. *Macromolecules* **2003,** 36, (8), 2932-2938.

69. Panitch, A.; Matsuki, K.; Cantor, E. J.; Cooper, S. J.; Atkins, E. D. T.; Fournier, M. J.; Mason, T. L.; Tirrell, D. A., Poly(L-alanylglycine): Multigram-scale biosynthesis, crystallization, and structural analysis of chain-folded lamellae. *Macromolecules* **1997,** 30, (1), 42-49.

70. McGrath, K. P.; Fournier, M. J.; Mason, T. L.; Tirrell, D. A., Genetically directed syntheses of new polymeric materials - Expression of artificial genes encoding proteins with repeating $(AlaGly)_3ProGluGly$ elements. *Journal of the American Chemical Society* **1992,** 114, (2), 727-733.

71. Creel, H. S.; Fournier, M. J.; Mason, T. L.; Tirrell, D. A., Genetically directed syntheses of new polymeric materials - efficient expression of a monodisperse copolypeptide containing 14 tandemly repeated $(AlaGly)_4ProGluGly$-elements. *Macromolecules* **1991,** 24, (5), 1213-1214.

72. Smeenk, J. M.; Otten, M. B. J.; Thies, J.; Tirrell, D. A.; Stunnenberg, H. G.; van Hest, J. C. M., Controlled assembly of macromolecular beta-sheet fibrils. *Angewandte Chemie-International Edition* **2005,** 44, (13), 1968-1971.

73. Tang, A.; Wang, C.; Stewart, R. J.; Kopecek, J., The coiled coils in the design of protein-based constructs: hybrid hydrogels and epitope displays. *Journal of Controlled Release* **2001,** 72, (1-3), 57-70.

74. Chao, H. M.; Bautista, D. L.; Litowski, J.; Irvin, R. T.; Hodges, R. S., Use of a heterodimeric coiled-coil system for biosensor application and affinity purification. *Journal of Chromatography B-Analytical Technologies in the Biomedical and Life Sciences* **1998,** 715, (1), 307-329.

75. Yu, B. Y., Coiled-coils: stability, specificity, and drug delivery potential. *Advanced Drug Delivery Reviews* **2002,** 54, (8), 1113-1129.

76. O'shea, E. K.; Rutkowski, R.; Kim, P. S., Mechanism of specificity in the Fos-Jun oncoprotein heterodimer. *Cell* **1992,** 68, (4), 699-708.

77. Harbury, P. B.; Zhang, T.; Kim, P. S.; Alber, T., A switch between 2-stranded, 3-stranded and 4-stranded coiled coils in GCN4 leucine-zipper mutants. *Science* **1993,** 262, (5138), 1401-1407.

78. Lumb, K. J.; Kim, P. S., Measurement of interhelical electrostatic interactions in the GCN4 leucine-zipper. *Science* **1995,** 268, (5209), 436-439.

79. Lau, S. Y. M.; Taneja, A. K.; Hodges, R. S., Synthesis of a model protein of defined secondary and quaternary structure - Effect of chain-length on the stabilization and formation of 2-stranded alpha-helical coiled-coils. *Journal of Biological Chemistry* **1984,** 259, (21), 3253-3261.

80. Wang, C.; Kopecek, J.; Stewart, R. J., Hybrid hydrogels cross-linked by genetically engineered coiled-coil block proteins. *Biomacromolecules* **2001,** 2, (3), 912-920.

81. Shen, W.; Lammertink, R. G. H.; Sakata, J. K.; Kornfield, J. A.; Tirrell, D. A., Assembly of an artificial protein hydrogel through leucine zipper aggregation and disulfide bond formation. *Macromolecules* **2005,** 38, (9), 3909-3916.

82. Megeed, Z.; Cappello, J.; Ghandehari, H., Genetically engineered silk-elastinlike protein polymers for controlled drug delivery. *Advanced Drug Delivery Reviews* **2002,** 54, (8), 1075-1091.

83. Dinerman, A. A.; Cappello, J.; Ghandehari, H.; Hoag, S. W., Swelling behavior of a genetically engineered silk-elastinlike protein polymer hydrogel. *Biomaterials* **2002,** 23, (21), 4203-4210.

84. Cappello, J.; Crissman, J. W.; Crissman, M.; Ferrari, F. A.; Textor, G.; Wallis, O.; Whitledge, J. R.; Zhou, X.; Burman, D.; Aukerman, L.; Stedronsky, E. R., In-situ self-assembling protein polymer gel systems for administration, delivery, and release of drugs. *Journal of Controlled Release* **1998,** 53, (1-3), 105-117.

85. Davis, N.; Koltover, I., unpublished data.

86. Wen, X.; Meyer, R. B.; Caspar, D. L. D., Observation of smectic-a ordering in a solution of rigid-rod-like particles. *Physical Review Letters* **1989,** 63, (25), 2760-2763.

87. Flory, P. J., Molecular theory of liquid-crystals. *Advances in Polymer Science* **1984,** 59, 1-36.

88. Xiao, X.; Wu, Y. G.; Sun, M. H.; Zhou, J. J.; Bo, Z. S.; Li, L.; Chan, C. M., Synthesis and self-assembly of amphiphilic dendronized conjugated polymers. *Journal of Polymer Science Part a-Polymer Chemistry* **2008,** 46, (2), 574-584.

89. Byerley, A. J.; Jennings, B. R.; Jerrard, H. G., Conformation parameter and gradient dependency of poly-gamma-benzyl-l-glutamate by viscometry. *Journal of Chemical Physics* **1968,** 48, (12), 5526-&.

90. Shenton, W.; Pum, D.; Sleytr, U. B.; Mann, S., Synthesis of cadmium sulphide superlattices using self-assembled bacterial S-layers. *Nature* **1997,** 389, (6651), 585-587.

91. Li, M.; Schnablegger, H.; Mann, S., Coupled synthesis and self-assembly of nanoparticles to give structures with controlled organization. *Nature* **1999,** 402, (6760), 393-395.

92. Bowden, N.; Terfort, A.; Carbeck, J.; Whitesides, G. M., Self-assembly of mesoscale objects into ordered two-dimensional arrays. *Science* **1997,** 276, (5310), 233-235.

93. Grzybowski, B. A.; Stone, H. A.; Whitesides, G. M., Dynamic self-assembly of magnetized, millimetre-sized objects rotating at a liquid-air interface. *Nature* **2000,** 405, (6790), 1033-1036.

94. Mathias, J. P.; Simanek, E. E.; Whitesides, G. M., Self-assembly through hydrogen-bonding - peripheral crowding - A new strategy for the preparation of stable supramolecular aggregates based on parallel, connected Ca(3).M(3) rosettes. *Journal of the American Chemical Society* **1994,** 116, (10), 4326-4340.

95. Duan, X. F.; Wang, J. F.; Lieber, C. M., Synthesis and optical properties of gallium arsenide nanowires. *Applied Physics Letters* **2000,** 76, (9), 1116-1118.

96. Norris, D. J.; Efros, A. L.; Rosen, M.; Bawendi, M. G., Size dependence of exciton fine structure in CdSe quantum dots. *Physical Review B* **1996,** 53, (24), 16347-16354.

97. Fowler, C. E.; Shenton, W.; Stubbs, G.; Mann, S., Tobacco mosaic virus liquid crystals as templates for the interior design of silica mesophases and nanoparticles. *Advanced Materials* **2001,** 13, (16), 1266-1269.

98. Lee, S. W.; Mao, C. B.; Flynn, C. E.; Belcher, A. M., Ordering of quantum dots using genetically engineered viruses. *Science* **2002,** 296, (5569), 892-895.

99. Chick, L. A.; Viney, C., Transitions to ordered phases in systems containing rodlike particles .1. a New continuum monte-carlo approach. *Molecular Crystals and Liquid Crystals* **1993,** 226, 25-40.

100. K. McGrath, D. K., *Protein-Based Materials*. Birkhauser: Boston, 1997.

101. Elliott, A.; Ambrose, E. J., Evidence of chain folding in polypeptides and proteins. *Disc. Faraday Soc* **1950,** 9, 246-251.

102. Atkins, P., *Physical Chemistry*. Oxford University Press: Oxford, 1978.

103. Onsager, L., The effects of shape on the interaction of colloidal particles. *Annals of the New York Academy of Sciences* **1949,** 51, (4), 627-659.

104. Holtzer, A., Application of old and new values of alpha-helix propensities to the helix-coil transition of poly(L-glutamic acid). *Journal of the American Chemical Society* **1994,** 116, (23), 10837-10838.

105. Nakajima, A.; Hayashi, T.; Ohmori, M., Phase equilibria of rodlike molecules in binary solvent systems. *Biopolymers* **1968,** 6, (7), 973-&.

106. Bohle, A. M.; Holyst, R.; Vilgis, T., Polydispersity and ordered phases in solutions of rodlike macromolecules. *Physical Review Letters* **1996,** 76, (8), 1396-1399.

107. Horton, J. C.; Donald, A. M.; Hill, A., Coexistence of 2 liquid-crystalline phases in poly(gamma-benzyl-alpha,L-glutamate) solutions. *Nature* **1990,** 346, (6279), 44-45.

108. McMaster, T. J.; Carr, H. J.; Miles, M. J.; Cairns, P.; Morris, V. J., Scanning tunneling microscopy of poly(gamma-benzyl L-glutamate). *Macromolecules* **1991,** 24, (6), 1428-1430.

109. Joshi, A. B.; Sawai, M.; Kearney, W. R.; Kirsch, L. E., Studies on the mechanism of aspartic acid cleavage and glutamine deamidation in the acidic degradation of glucagon. *Journal of Pharmaceutical Sciences* **2005,** 94, (9), 1912-1927.

110. Zhang, G., Fournier M., Mason, T., and Tirrell, D., Biological Synthesis of Monodisperse Derivatives of Poly(α, L-glutamic acid): Model Rodlike Polymers. *Macromolecules* **1992,** 25, 3601-3603.

111. Mawn, M. V.; Fournier, M. J.; Tirrell, D. A.; Mason, T. L., Depletion of free 30S ribosomal subunits in Escherichia coli by expression of RNA containing Shine-Dalgarno-like sequences. *Journal of Bacteriology* **2002,** 184, (2), 494-502.

112. Calogero, R. A., Pon, C. L., Canonaco, M. A., and Gualerzi, C. O., Selection of the mRNA translation initiation region by *Escherichia coli* ribosomes. *Proc. Natl. Acad. Sci. USA* **1988,** 85, 6427-6431.

113. Scherer, G. F., Walkinshaw, M. D., Arnott, S., Morre, D. J., The ribosome binding sites recognized by *E. coli* ribosomes have regions with signal character in both the leader and protein coding segments. *Nucleic Acids Res.* **1980,** 8, 3895-3907.

114. Shine, J., Dalgarno, L., Determinant of cistron specificity in bacterial ribosomes. *Nature* **1975,** 254, 34-38.

115. Pal, G.; Santamaria, F.; Kossiakoff, A. A.; Lu, W. Y., The first semi-synthetic serine protease made by native chemical ligation. *Protein Expression and Purification* **2003,** 29, (2), 185-192.

116. C. Cantor, P. S., *Biophysical chemistry part II: Techniques for the study of biological structure and function*. W. H. Freeman and Company: New York, 1980.

117. Bovey, F. A., NMR Observations of Polypeptide Confromations. *Macromolecular Reviews* **1974,** 9, 1-81.

118. Duke, R. W.; Dupre, D. B.; Hines, W. A.; Samulski, E. T., Poly(gamma-benzyl L-glutamate) helix-coil transition - Pre-transition phenomena in liquid-crystal phase. *Journal of the American Chemical Society* **1976,** 98, (11), 3094-3101.

119. Ugaz, V. M., Cinader, D. K., Burghardt, W. R., Origins of Region I Shear Thinning in Model Lyotropic Liquid Crystalline Polymers. *Macromolecules* **1997,** 30, 1527-1530.

120. Newkome, G. R.; Moorefield, C. N.; Vogtle, F., *Dendritic Molecules. Concepts, synthesis, perspectives*. VCH: Weinheim, 1996.

121. Helms, B.; Frechet, J. M. J., The dendrimer effect in homogeneous catalysis. *Advanced Synthesis & Catalysis* **2006,** 348, (10-11), 1125-1148.

122. Jain, N. K.; Asthana, A., Dendritic systems in drug delivery applications. *Expert Opinion on Drug Delivery* **2007,** 4, (5), 495-512.

123. Cheng, Y. Y.; Xu, Z. H.; Ma, M. L.; Xu, T. W., Dendrimers as drug carriers: Applications in different routes of drug administration. *Journal of Pharmaceutical Sciences* **2008,** 97, (1), 123-143.

124. Langereis, S.; Dirksen, A.; Hackeng, T. M.; van Genderen, M. H. P.; Meijer, E. W., Dendrimers and magnetic resonance imaging. *New Journal of Chemistry* **2007,** 31, (7), 1152-1160.

125. Grinstaff, M. W., Dendritic macromers for hydrogel formation: Tailored materials for ophthalmic, orthopedic, and biotech applications. *Journal of Polymer Science Part a-Polymer Chemistry* **2008,** 46, (2), 383-400.

126. Percec, V.; Ahn, C. H.; Ungar, G.; Yeardley, D. J. P.; Moller, M.; Sheiko, S. S., Controlling polymer shape through the self-assembly of dendritic side-groups. *Nature* **1998,** 391, (6663), 161-164.

127. Hudson, S. D.; Jung, H. T.; Percec, V.; Cho, W. D.; Johansson, G.; Ungar, G.; Balagurusamy, V. S. K., Direct visualization of individual cylindrical and spherical supramolecular dendrimers. *Science* **1997,** 278, (5337), 449-452.

128. Stocker, W.; Schurmann, B. L.; Rabe, J. P.; Forster, S.; Lindner, P.; Neubert, I.; Schluter, A. D., A dendritic nanocylinder: Shape control through implementation of steric strain. *Advanced Materials* **1998,** 10, (10), 793-797.

129. Stocker, W.; Karakaya, B.; Schurmann, B. L.; Rabe, J. P.; Schluter, A. D., Ordered dendritic nanorods with a poly(p-phenylene) backbone. *Journal of the American Chemical Society* **1998,** 120, (31), 7691-7695.

130. Yin, R.; Zhu, Y.; Tomalia, D. A.; Ibuki, H., Architectural copolymers: Rod-shaped, cylindrical dendrimers. *Journal of the American Chemical Society* **1998,** 120, (11), 2678-2679.

131. Wooley, K. L.; Hawker, C. J.; Frechet, J. M. J., Hyperbranched macromolecules via a novel double-stage convergent growth approach. *Journal of the American Chemical Society* **1991,** 113, (11), 4252-4261.

132. Schluter, A. D.; Rabe, J. P., Dendronized polymers: Synthesis, characterization, assembly at interfaces, and manipulation. *Angewandte Chemie-International Edition* **2000,** 39, (5), 864-883.

133. Hawker, C. J.; Frechet, J. M. J., Preparation of polymers with controlled molecular architecture - A new convergent approach to dendritic macromolecules. *Journal of the American Chemical Society* **1990,** 112, (21), 7638-7647.

134. Elliott, A.; Fraser, R. D. B.; Macrae, T. P., Xray diffraction patterns of poly-gamma-benzyl-glutamate. *Journal of Molecular Biology* **1965,** 11, (4), 821-&.

135. Herzfeld, J., Entropically driven order in crowded solutions: From liquid crystals to cell biology. *Accounts of Chemical Research* **1996,** 29, (1), 31-37.

136. Bertozzi, C. R.; Kiessling, L. L., Chemical glycobiology. *Science* **2001,** 291, (5512), 2357-2364.

137. Mammen, M.; Dahmann, G.; Whitesides, G. M., Effective Inhibitors of Hemagglutination by Influenza-Virus Synthesized from Polymers Having Active Ester Groups - Insight into Mechanism of Inhibition. *Journal of Medicinal Chemistry* **1995,** 38, (21), 4179-4190.

138. Mourez, M.; Kane, R. S.; Mogridge, J.; Metallo, S.; Deschatelets, P.; Sellman, B. R.; Whitesides, G. M.; Collier, R. J., Designing a polyvalent inhibitor of anthrax toxin. *Nature Biotechnology* **2001,** 19, (10), 958-961.

139. Duncan, R., The dawning era of polymer therapeutics. *Nature Reviews Drug Discovery* **2003,** 2, (5), 347-360.

140. Maeda, H.; Seymour, L. W.; Miyamoto, Y., Conjugates of Anticancer Agents and Polymers - Advantages of Macromolecular Therapeutics Invivo. *Bioconjugate Chemistry* **1992,** 3, (5), 351-362.

141. Allen, T. M., Ligand-targeted therapeutics in anticancer therapy. *Nature Reviews Cancer* **2002,** 2, (10), 750-763.

142. Cloninger, M. J., Biological applications of dendrimers. *Current Opinion in Chemical Biology* **2002,** 6, (6), 742-748.

143. Crespo, L.; Sanclimens, G.; Pons, M.; Giralt, E.; Royo, M.; Albericio, F., Peptide and amide bond-containing dendrimers. *Chemical Reviews* **2005,** 105, (5), 1663-1681.

144. Lee, C. C.; MacKay, J. A.; Frechet, J. M. J.; Szoka, F. C., Designing dendrimers for biological applications. *Nature Biotechnology* **2005,** 23, (12), 1517-1526.

145. van Baal, I.; Malda, H.; Synowsky, S. A.; van Dongen, J. L. J.; Hackeng, T. M.; Merkx, M.; Meijer, E. W., Multivalent peptide and protein dendrimers using native chemical ligation. *Angewandte Chemie-International Edition* **2005,** 44, (32), 5052-5057.

146. Crommelin, D. J. A.; Storm, G., Liposomes: From the bench to the bed. *Journal of Liposome Research* **2003,** 13, (1), 33-36.

147. Kiessling, L. L.; Gestwicki, J. E.; Strong, L. E., Synthetic multivalent ligands in the exploration of cell-surface interactions. *Current Opinion in Chemical Biology* **2000,** 4, (6), 696-703.

148. Haag, R.; Kratz, F., Polymer therapeutics: Concepts and applications. *Angewandte Chemie-International Edition* **2006,** 45, (8), 1198-1215.

149. Hersel, U.; Dahmen, C.; Kessler, H., RGD modified polymers: biomaterials for stimulated cell adhesion and beyond. *Biomaterials* **2003,** 24, (24), 4385-4415.

150. Kanai, M.; Mortell, K. H.; Kiessling, L. L., Varying the size of multivalent ligands: The dependence of concanavalin a binding on neoglycopolymer length. *Journal of the American Chemical Society* **1997,** 119, (41), 9931-9932.

151. Seymour, L. W.; Duncan, R.; Strohalm, J.; Kopecek, J., Effect of Molecular-Weight (Mbarw) of N-(2-Hydroxypropyl)Methacrylamide Copolymers on Body Distribution and Rate of Excretion after Subcutaneous, Intraperitoneal, and Intravenous Administration to Rats. *Journal of Biomedical Materials Research* **1987,** 21, (11), 1341-1358.

152. Godwin, A.; Hartenstein, M.; Muller, A. H. E.; Brocchini, S., Narrow molecular weight distribution precursors for polymer-drug conjugates. *Angewandte Chemie-International Edition* **2001,** 40, (3), 594-597.

153. Lorand, L.; Conrad, S. M., Transglutaminases. *Molecular and Cellular Biochemistry* **1984,** 58, (1-2), 9-35.

154. Sakiyama-Elbert, S. E.; Hubbell, J. A., Development of fibrin derivatives for controlled release of heparin-binding growth factors. *Journal of Controlled Release* **2000,** 65, (3), 389-402.

155. Schense, J. C.; Hubbell, J. A., Cross-linking exogenous bifunctional peptides into fibrin gels with factor XIIIa. *Bioconjugate Chemistry* **1999,** 10, (1), 75-81.

156. Schense, J. C.; Hubbell, J. A., Three-dimensional migration of neurites is mediated by adhesion site density and affinity. *Journal of Biological Chemistry* **2000,** 275, (10), 6813-6818.

157. Collier, J. H.; Messersmith, P. B., Enzymatic modification of self-assembled peptide structures with tissue transglutaminase. *Bioconjugate Chemistry* **2003,** 14, (4), 748-755.

158. Henaut, A., Danchin, A., Analysis and Predictions from Escherichia coli sequences in: Escherichia coli and Salmonella. In ed., N. F., Ed. ASM press: Washington, D.C., 1996; Vol. 2, pp 2047-2066.

159. Won, J. I.; Barron, A. E., A new cloning method for the preparation of long repetitive polypeptides without a sequence requirement. *Macromolecules* **2002,** 35, (22), 8281-8287.

160. Zuckermann, R. N.; Kerr, J. M.; Kent, S. B. H.; Moos, W. H., Efficient Method for the Preparation of Peptoids [Oligo(N-Substituted Glycines)] by Submonomer Solid-Phase Synthesis. *Journal of the American Chemical Society* **1992,** 114, (26), 10646-10647.

161. Won, J. I.; Meagher, R. J.; Barron, A. E., Characterization of glutamine deamidation in a long, repetitive protein polymer via bioconjugate capillary electrophoresis. *Biomacromolecules* **2004,** 5, (2), 618-627.

162. Trabbic-Carlson, K.; Setton, L. A.; Chilkoti, A., Swelling and mechanical behaviors of chemically cross-linked hydrogels of elastin-like polypeptides. *Biomacromolecules* **2003,** 4, (3), 572-580.

163. Farmer, R. S.; Argust, L. M.; Sharp, J. D.; Kiick, K. L., Conformational properties of helical protein polymers with varying densities of chemically reactive groups. *Macromolecules* **2006,** 39, (1), 162-170.

164. Creel, H. S.; Fournier, M. J.; Mason, T. L.; Tirrell, D. A., Genetically Directed Syntheses of New Polymeric Materials - Efficient Expression of a Monodisperse Copolypeptide Containing 14 Tandemly Repeated (Alagly)4proglugly-Elements. *Macromolecules* **1991,** 24, (5), 1213-1214.

165. Putnam, D.; Gentry, C. A.; Pack, D. W.; Langer, R., Polymer-based gene delivery with low cytotoxicity by a unique balance of side-chain termini. *Proceedings of the National Academy of Sciences of the United States of America* **2001,** 98, (3), 1200-+.

166. Wolfert, M. A.; Dash, P. R.; Nazarova, O.; Oupicky, D.; Seymour, L. W.; Smart, S.; Strohalm, J.; Ulbrich, K., Polyelectrolyte vectors for gene delivery: Influence of cationic polymer on biophysical properties of complexes formed with DNA. *Bioconjugate Chemistry* **1999,** 10, (6), 993-1004.

167. Staros, J. V.; Wright, R. W.; Swingle, D. M., Enhancement by N-Hydroxysulfosuccinimide of Water-Soluble Carbodiimide-Mediated Coupling Reactions. *Analytical Biochemistry* **1986,** 156, (1), 220-222.

168. Ruoslahti, E., RGD and other recognition sequences for integrins. *Annual Review of Cell and Developmental Biology* **1996,** 12, 697-715.

169. Simon, R. J., R.S. Kania, R.N. Zuckermann, V.D. Huebner, D.A. Jewell, S. Banville, S. Ng, L.; Wang, S. R., and et al., Peptoids: a modular approach to drug discovery. *Proc. Natl. Acad. Sci. U. S. A* **1992,** 89, (20), 9367-9371.

170. Zuckermann, R. N., J.M. Kerr, S.B.H. Kent, and W.H. Moos. , Efficient method for the preparation of peptoids [oligo(N-substituted glycines)] by submonomer solid-phase synthesis. *J. Am. Chem. Soc.* **1992,** 114, (26), 10646-10647.

171. Borman, S., Peptoids eyed for gene therapy applications. *Chem. Eng. News* **1998,** 76, (18), 56-57.

172. Miller, S. M., R.J. Simon, S. Ng, R.N. Zuckermann, J.M. Kerr, and W.H. Moos. , Comparison of the proteolytic susceptibilities of homologous L-amino acid, D-amino acid, and N-substituted glycine peptide and peptoid oligomers. *Drug Development Research* **1995,** 35, (1), 20-32.

173. Statz, A. R.; Meagher, R. J.; Barron, A. E.; Messersmith, P. B., New peptidomimetic polymers for antifouling surfaces. *Journal of the American Chemical Society* **2005,** 127, (22), 7972-7973.

174. Hu, B. H.; Messersmith, P. B., Rational design of transglutaminase substrate peptides for rapid enzymatic formation of hydrogels. *Journal of the American Chemical Society* **2003,** 125, (47), 14298-14299.

175. Karfeld, L. S.; Bull, S. R.; Davis, N. E.; Meade, T. J.; Barron, A. E., Use of a genetically engineered protein for the design of a multivalent MRI contrast agent. *Bioconjug Chem* **2007,** 18, (6), 1697-700.

176. Harris, J. M.; Chess, R. B., Effect of pegylation on pharmaceuticals. *Nature Reviews Drug Discovery* **2003,** 2, (3), 214-221.

177. Hahn, M. S.; Taite, L. J.; Moon, J. J.; Rowland, M. C.; Ruffino, K. A.; West, J. L., Photolithographic patterning of polyethylene glycol hydrogels. *Biomaterials* **2006,** 27, (12), 2519-2524.

178. Roman, G. T.; Carroll, S.; McDaniel, K.; Culbertson, C. T., Micellar electrokinetic chromatography of fluorescently labeled proteins on poly(dimethylsilokane)-based microchips. *Electrophoresis* **2006,** 27, (14), 2933-2939.

179. Griffin, M.; Casadio, R.; Bergamini, C. M., Transglutaminases: Nature's biological glues. *Biochemical Journal* **2002,** 368, 377-396.

180. Greenberg, C. S.; Birckbichler, P. J.; Rice, R. H., Transglutaminases - Multifunctional Cross-Linking Enzymes That Stabilize Tissues. *Faseb Journal* **1991,** 5, (15), 3071-3077.

181. Montaudo, G.; Montaudo, M. S.; Puglisi, C.; Samperi, F., Characterization of Polymers by Matrix-Assisted Laser-Desorption Ionization Time-of-Flight Mass-Spectrometry - Molecular-Weight Estimates in Samples of Varying Polydispersity. *Rapid Communications in Mass Spectrometry* **1995,** 9, (5), 453-460.

182. Lim, D. W.; Nettles, D. L.; Setton, L. A.; Chilkoti, A., Rapid cross-linking of elastin-like polypeptides with (hydroxymethyl)phosphines in aqueous solution. *Biomacromolecules* **2007,** 8, (5), 1463-1470.

183. Lutolf, M. P.; Hubbell, J. A., Synthetic biomaterials as instructive extracellular microenvironments for morphogenesis in tissue engineering. *Nature Biotechnology* **2005,** 23, (1), 47-55.

184. Van Tomme, S. R.; Storm, G.; Hennink, W. E., In situ gelling hydrogels for pharmaceutical and biomedical applications. *Int J Pharm* **2008,** 355, (1-2), 1-18.

185. Hubbell, J. A., In situ material transformations in tissue engineering. *Mrs Bulletin* **1996,** 21, (11), 33-35.

186. Ruel-Gariepy, E.; Leroux, J. C., In situ-forming hydrogels - review of temperature-sensitive systems. *European Journal of Pharmaceutics and Biopharmaceutics* **2004,** 58, (2), 409-426.

187. Gutowska, A.; Jeong, B.; Jasionowski, M., Injectable gels for tissue engineering. *Anatomical Record* **2001,** 263, (4), 342-349.

188. Chenite, A.; Chaput, C.; Wang, D.; Combes, C.; Buschmann, M. D.; Hoemann, C. D.; Leroux, J. C.; Atkinson, B. L.; Binette, F.; Selmani, A., Novel injectable neutral solutions of chitosan form biodegradable gels in situ. *Biomaterials* **2000,** 21, (21), 2155-2161.

189. Lee, K. Y.; Mooney, D. J., Hydrogels for Tissue Engineering. *Chemical Reviews* **2001,** 101, (7), 1869-1877.

190. Liu, L. S.; Thompson, A. Y.; Heidaran, M. A.; Poser, J. W.; Spiro, R. C., *Biomaterials* **1999,** 20, 1097.

191. Park, Y. D.; Tirelli, N.; Hubbell, J. A., Photopolymerized hyaluronic acid-based hydrogels and interpenetrating networks. *Biomaterials* **2003,** 24, (6), 893-900.

192. Park, Y.; Tirelli, N.; Hubbell, J., *Biomaterials* **2003,** 24, 893-900.

193. Matsuo, E. S.; Orkisz, M.; Sun, S. T.; Li, Y.; Tanka, T., *Macromolecules* **1994,** 27, 6791.

194. Carrick, L. M.; Aggeli, A.; Boden, N.; Fisher, J.; Ingham, E.; Waigh, T. A., Effect of ionic strength on the self-assembly, morphology and gelation of pH responsive beta-sheet tape-forming peptides. *Tetrahedron* **2007,** 63, (31), 7457-7467.

195. Stendahl, J. C.; Rao, M. S.; Guler, M. O.; Stupp, S. I., Intermolecular forces in the self-assembly of peptide amphiphile nanofibers. *Advanced Functional Materials* **2006,** 16, (4), 499-508.

196. Hartgerink, J. D.; Beniash, E.; Stupp, S. I., Peptide-amphiphile nanofibers: A versatile scaffold for the preparation of self-assembling materials. *Proceedings of the National Academy of Sciences of the United States of America* **2002,** 99, (8), 5133-5138.

197. Heskins, M.; Guillet, J. E., *J. Macromol. Sci. Chem. Ed.* **1968,** A2, 1441.

198. Burdick, J. A.; Frankel, D.; Dernell, W. S.; Anseth, K. S., An initial investigation of photocurable three-dimensional lactic acid based scaffolds in a critical-sized cranial defect. *Biomaterials* **2003,** 24, (9), 1613-1620.

199. Rydholm, A. E.; Bowman, C. N.; Anseth, K. S., Degradable thiol-acrylate photopolymers: polymerization and degradation behavior of an in situ forming biomaterial. *Biomaterials* **2005,** 26, (22), 4495-4506.

200. Bae, S. J.; Joo, M. K.; Jeong, Y.; Kim, S. W.; Lee, W. K.; Sohn, Y. S.; Jeong, B., Gelation behavior of poly(ethylene glycol) and polycaprolactone triblock and multiblock copolymer aqueous solutions. *Macromolecules* **2006,** 39, (14), 4873-4879.

201. Aeschlimann, D.; Paulsson, M., Transglutaminases - protein cross-linking enzymes in tissues and body-fluids. *Thrombosis and Haemostasis* **1994,** 71, (4), 402-415.

202. Sperinde, J. J.; Griffith, L. G., Synthesis and characterization of enzymatically-cross-linked poly(ethylene glycol) hydrogels. *Macromolecules* **1997,** 30, (18), 5255-5264.

203. Sanborn, T. J.; Messersmith, P. B.; Barron, A. E., In situ crosslinking of a biomimetic peptide-PEG hydrogel via thermally triggered activation of factor XIII. *Biomaterials* **2002,** 23, (13), 2703-2710.

204. Ehrbar, M.; Rizzi, S. C.; Hlushchuk, R.; Djonov, V.; Zisch, A. H.; Hubbell, J. A.; Weber, F. E.; Lutolf, M. P., Enzymatic formation of modular cell-instructive fibrin analogs for tissue engineering. *Biomaterials* **2007,** 28, (26), 3856-3866.

205. Ehrbar, M.; Rizzi, S. C.; Schoenmakers, R. G.; San Miguel, B.; Hubbell, J. A.; Weber, F. E.; Lutolf, M. P., Biomolecular hydrogels formed and degraded via site-specific enzymatic reactions. *Biomacromolecules* **2007,** 8, (10), 3000-3007.

206. McHale, M. K.; Setton, L. A.; Chilkoti, A., Synthesis and in vitro evaluation of enzymatically cross-linked elastin-like polypeptide gels for cartilaginous tissue repair. *Tissue Engineering* **2005,** 11, (11-12), 1768-1779.

207. Ryan, E. A.; Paty, B. W.; Senior, P. A.; Bigam, D.; Alfadhli, E.; Kneteman, N. M.; Lakey, J. R. T.; Shapir, A. M. J., Five-year follow-up after clinical islet transplantation. *Diabetes* **2005,** 54, (7), 2060-2069.

208. de Groot, M.; Schuurs, T. A.; van Schilfgaarde, R., Causes of limited survival of microencapsulated pancreatic islet grafts. *Journal of Surgical Research* **2004,** 121, (1), 141-150.

209. Bohman, S.; Waern, I.; Andersson, A.; King, A., Transient beneficial effects of exendin-4 treatment on the function of microencapsulated mouse pancreatic islets. *Cell Transplantation* **2007,** 16, (1), 15-22.

210. Blomeier, H.; Zhang, X. M.; Rives, C.; Brissova, M.; Hughes, E.; Baker, M.; Powers, A. C.; Kaufman, D. B.; Shea, L. D.; Lowe, W. L., Polymer scaffolds as synthetic microenvironments for extrahepatic islet transplantation. *Transplantation* **2006,** 82, (4), 452-459.

211. Weber, L. M.; Hayda, K. N.; Haskins, K.; Anseth, K. S., The effects of cell-matrix interactions on encapsulated beta-cell function within hydrogels functionalized with matrix-derived adhesive peptides. *Biomaterials* **2007,** 28, (19), 3004-3011.

212. Weber, L. M.; Cheung, C. Y.; Anseth, K. S., Multifunctional pancreatic islet encapsulation barriers achieved via multilayer PEG hydrogels. *Cell Transplantation* **2008,** 16, (10), 1049-1057.

213. Cheung, C. Y.; Anseth, K. S., Synthesis of immunoisolation barriers that provide localized immunosuppression for encapsulated pancreatic islets. *Bioconjugate Chemistry* **2006,** 17, (4), 1036-1042.

214. Anseth, K. S.; Bowman, C. N.; BrannonPeppas, L., Mechanical properties of hydrogels and their experimental determination. *Biomaterials* **1996,** 17, (17), 1647-1657.

215. Mason, T. G.; Weitz, D. A., Optical measurements of frequency-dependent linear viscoelastic moduli of complex fluids. *Physical Review Letters* **1995,** 74, (7), 1250-1253.

216. Levine, A. J.; Lubensky, T. C., One- and two-particle microrheology. *Physical Review Letters* **2000,** 85, (8), 1774-1777.

217. Xu, C. Y.; Breedveld, V.; Kopecek, J., Reversible hydrogels from self-assembling genetically engineered protein block copolymers. *Biomacromolecules* **2005,** 6, (3), 1739-1749.

218. Chen, X. J.; Zhang, X. M.; Larson, C.; Chen, F.; Kissler, H.; Kaufman, D. B., The epididymal fat pad as a transplant site for minimal islet mass. *Transplantation* **2007,** 84, (1), 122-125.

219. Sands, W.; Brubaker, K.; Messersmith, P., unpublished results.

220. Engler, A. J.; Sen, S.; Sweeney, H. L.; Discher, D. E., Matrix elasticity directs stem cell lineage specification. *Cell* **2006,** 126, (4), 677-689.

221. Magalhaes, P. O.; Lopes, A. M.; Mazzola, P. G.; Rangel-Yagui, C.; Penna, T. C. V.; Pessoa, A., Methods of endotoxin removal from biological preparations: a review. *Journal of Pharmacy and Pharmaceutical Sciences* **2007,** 10, (3), 388-404.

222. Farilla, L.; Bulotta, A.; Hirshberg, B.; Calzi, S. L.; Khoury, N.; Noushmehr, H.; Bertolotto, C.; Di Mario, U.; Harlan, D. M.; Perfetti, R., Glucagon-like peptide 1 inhibits cell apoptosis and improves glucose responsiveness of freshly isolated human islets. *Endocrinology* **2003,** 144, (12), 5149-5158.

223. Tourrel, C.; Bailbe, D.; Meile, M. J.; Kergoat, M.; Portha, B., Glucagon-like peptide-1 and exendin-4 stimulate beta-cell neogenesis in streptozotocin-treated newborn rats resulting in persistently improved glucose homeostasis at adult age. *Diabetes* **2001,** 50, (7), 1562-1570.

224. Newgard, C. B., Cellular engineering and gene-therapy strategies for insulin replacement in diabetes. *Diabetes* **1994,** 43, (3), 341-350.

225. Garcia-Ocana, A.; Takane, K. K.; Reddy, V. T.; Lopez-Talavera, J. C.; Vasavada, R. C.; Stewart, A. F., Adenovirus-mediated hepatocyte growth factor expression in mouse islets improves pancreatic islet transplant performance and reduces beta cell death. *Journal of Biological Chemistry* **2003,** 278, (1), 343-351.

226. Kaufman, D. B.; Gores, P. F.; Field, M. J.; Farney, A. C.; Gruber, S. A.; Stephanian, E.; Sutherland, D. E. R., Effect of 15-deoxyspergualin on immediate function and long-term survival of transplanted islets in murine recipients of a marginal islet mass. *Diabetes* **1994,** 43, (6), 778-783.

227. Pauling, L.; Corey, R. B., Compound helical configurations of polypeptide chains: structure of proteins of the [alpha]-keratin type. *Nature* **1953,** 171, (4341), 59-61.

228. Crick, F. H. C., Is [alpha]-keratin a coiled coil? *Nature* **1952,** 170, (4334), 882-883.

229. Hodges, R. S.; Sodek, J.; Smillie, L. B.; Jurasek, L., Tropomyosin - amino-acid sequence and coiled-coil structure. *Cold Spring Harbor Symposia on Quantitative Biology* **1973,** 37, 299-310.

230. Sodek, J.; Hodges, R. S.; Smillie, L. B.; Jurasek, L., Amino-acid sequence of rabbit skeletal Tropomyosin and its coiled coil structure. *Proceedings of the National Academy of Sciences of the United States of America* **1972,** 69, (12), 3800-3804.

231. Xu, C. Y.; Kopecek, J., Genetically engineered block copolymers: Influence of the length and structure of the coiled-coil blocks on hydrogel self-assembly. *Pharmaceutical Research* **2008,** 25, (3), 674-682.

232. Grayson, S. M.; Frechet, J. M. J., Convergent Dendrons and Dendrimers: from Synthesis to Applications. *Chemical Reviews* **2001,** 101, (12), 3819-3867.

233. Danishefsky, S.; Phillips, G.; Ciufolini, M., A fully synthetic route to the papulacandins. Stereospecific spiroacetalization of a C-1-arylated methylglycoside. *Carbohydrate Research* **1987,** 171, 317-27.

234. Barbera, J.; Iglesias, R.; Serrano, J. L.; Sierra, T.; de la Fuente, M. R.; Palacios, B.; Perez-Jubindo, M. A.; Vazquez, J. T., Switchable Columnar Metallomesogens. New Helical Self-assembling Systems. *Journal of the American Chemical Society* **1998,** 120, (12), 2908-2918.

235. Hawker, C. J.; Frechet, J. M. J., Preparation of polymers with controlled molecular architecture. A new convergent approach to dendritic macromolecules. *Journal of the American Chemical Society* **1990,** 112, (21), 7638-47.

236. Krishnamoorthy, K.; Ambade, A. V.; Mishra, S. P.; Kanungo, M.; Contractor, A. Q.; Kumar, A., Dendronized electrochromic polymer based on poly(3,4-ethylenedioxythiophene). *Polymer* **2002,** 43, (24), 6465-6470.

237. Gibtner, T.; Hampel, F.; Gisselbrecht, J.-P.; Hirsch, A., End-cap stabilized oligoynes: model compounds for the linear sp carbon allotrope carbyne. *Chemistry--A European Journal* **2002,** 8, (2), 408-432.

238. Andrus, M.; Meredith, E. Synthesis of resveratrol. 2001060774, 2001.

Appendices

Appendix A: Synthesis and Characterization of Dendrons and X-ray Diffraction Scans for Constructing the Phase Diagram

Preparation of dendritic side chains. The dendritic side chains were prepared using the convergent approach developed by Frechet.[232] The synthetic details are summarized in Scheme AB-1. The synthesis of **1**,[233] **3**,[233] **4**,[234] **5**,[235] **6,**[236] **7**,[237] **11**,[238] **12**,[235] **13**[237] were adapted from literature procedures.

Scheme A-1. Synthesis of the precursors to the dendritic side chains of DPPs.

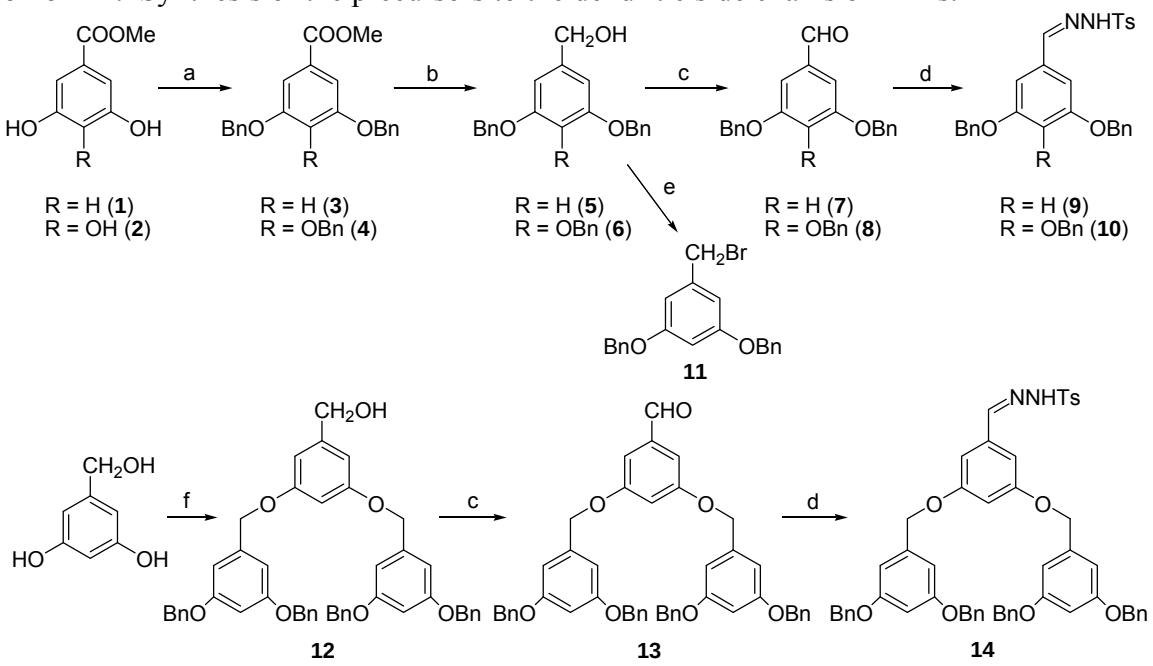

Reaction conditions: a) BnBr, K_2CO_3, acetone, reflux, 16 h. b) $LiAlH_4$, THF, 30 °C, 2-4 h. c) PDC, CH_2Cl_2, 1 h. d) NH_2NHTs, EtOH:Et_2O (1:1), reflux, 2-4 h. e) PBr_3, pyridine, CH_2Cl_2, 6-12 h. f) **11**, K_2CO_3, acetone, reflux, 16 h.

Synthesis of 3,4,5-tris(benzyloxy)benzaldehyde (8). Under N_2 atmosphere, a solution of 3,4,5-tris(benzyloxy)benzyl alcohol (15.50 g, 36.3 mmol) in dry and degassed dichloromethane (100 mL) was added to a 250 mL round bottom flask containing pyridinium chlorochromate (8.23 g, 1.05 equiv) and dichloromethane (50 mL) and the resulting dark solution was stirred for 1 h. The reaction mixture was then filtered through a celite/silica pad, washed with dilute NaOH (100 mL), 0.1 M HCl (100 mL), and saturated brine (3 x 100 mL). The organic layer was separated, dried over $MgSO_4$, and filtered. The solvent was removed to give the final product as an off-white solid (13.95 g, 90%) of sufficient purity for use in the next step. The analytical sample was purified by flash chromatography (dichloromethane, $R_f = 0.40$). Anal. Calcd. for $C_{28}H_{24}O_4$: C, 79.22; H, 5.70. Found: C, 79.25; H, 5.75. ^{1}H NMR ($CDCl_3$): δ 9.82 (1H), 7.46-7.32 (m, 12H), 7.31-7.25 (m, 3H), 7.20 (2H), 5.18 (6H). ^{13}C NMR ($CDCl_3$): δ 191.2 (*C*HO), 153.5, 144.0, 137.5, 136.6, 132.0, 128.9, 128.8, 128.5, 128.4, 128.3, 127.7, 109.1, 75.5 (*C*H_2), 71.5 (*C*H_2).

Synthesis of *N*-(3,5-bis(benzyloxy)benzylidene)-*N'*-tosyl hydrazone (9). In a 250 mL round-bottom flask equipped with a magnetic stirbar and a reflux condenser, a solution of 3,5-bis(benzyloxy)benzaldehyde (3.30 g, 10.4 mmol) and *p*-tosyl hydrazine (1.93 g, 10.4 mmol) in an EtOH/Et_2O mixture (50 mL, 1:1 v/v) was refluxed for 4 h. The precipitate was collected by filtration and dried in air to afford the final product as a colorless solid (4.83 g, 96%). Anal. Calcd. for $C_{28}H_{26}N_2O_4S$: C, 69.11; H, 5.39; N, 5.76. Found: C, 68.99; H, 5.46; N, 5.79. ^{1}H

NMR ($CDCl_3$): δ 8.14 (1H), 7.86-7.84 (m, 2H), 7.65 (1H), 7.50-7.20 (m, 10H), 6.81 (2H), 6.62 (1H), 5.02 (4H), 2.39 (3H), 1.73 (1H). ^{13}C NMR ($CDCl_3$): δ 160.2, 147.7, 144.5, 136.7, 135.4, 135.3, 129.9, 128.8, 128.3, 128.1, 127.7, 106.6, 104.7, 70.4 (CH_2), 21.8 (CH_3).

Synthesis of *N*-(3,4,5-tris(benzyloxy)benzylidene)-*N'*-tosyl hydrazone (10). In a 250 mL round-bottom flask equipped with a magnetic stirbar and a reflux condenser, a solution of 3,4,5-tris(benzyloxy)benzaldehyde (5.73 g, 13.5 mmol) and *p*-tosyl hydrazine (2.52 g, 13.5 mmol) in an EtOH/Et_2O mixture (100 mL, 1:1 v/v) was heated to reflux. White solid started to precipitate after 15 min. After refluxing for 2 h, the reaction mixture was allowed to cool down and filtered. The solid residue was dried in air to give the final product as a fluffy colorless solid (7.29 g, 91%). Anal. Calcd. for $C_{35}H_{32}N_2O_5S$: C, 70.92; H, 5.44; N, 4.73. Found: C, 71.07; H, 5.44; N, 4.75. ^1H NMR ($CDCl_3$): δ 7.98 (br, 1H), 7.83-7.81 (m, 2H), 7.59 (1H), 7.42-7.23 (m, 16H), 6.87 (2H), 5.08-5.06 (m, 6H), 2.40 (3H), 1.74 (br, 1H). ^{13}C NMR ($CDCl_3$): δ 153.2, 148.1, 144.5, 140.6, 137.7, 136.9, 135.4, 129.9, 128.9, 128.4, 128.2, 128.1, 128.1, 127.6, 107.1, 75.4 (CH_2), 71.4 (CH_2), 21.8 (CH_3).

Synthesis of *N*-[3,5-bis((3,5-bis(benzyloxy))benzyloxy)benzylidene]-*N'*-tosyl hydrazone (14). In a 250 mL round-bottom flask equipped with a magnetic stirbar and a reflux condenser, a solution of 3,5-bis(3,5-bis(benzyloxy)benzyloxy) benzaldehyde (2.39 g, 3.2 mmol) and *p*-tosyl hydrazine (0.60 g, 3.2 mmol) in an EtOH/Et_2O mixture (40 mL, 1:1 v/v) was refluxed for 12 h. The reaction mixture was cooled down to room temperature when a colorless precipitate appeared. This precipitate was collected by filtration and dried in air to afford the final product as a colorless solid (2.53 g, 86%). Anal. Calcd for $C_{56}H_{50}N_2O_8S$: C, 73.83; H, 5.53; N, 3.07. Found: C, 74.02; H, 5.50; N, 3.00. ^1H NMR ($CDCl_3$): δ 7.96 (1H), 7.87-7.85 (m, 2H), 7.62 (1H), 7.50-7.20 (m, 21H), 6.82 (2H), 6.70 (4H), 6.62 (3H), 5.06 (8H), 4.98 (4H), 2.39 (3H). ^{13}C NMR ($CDCl_3$): δ 160.4, 160.1, 147.6, 144.5, 139.2, 136.9, 135.4, 135.2, 129.9, 128.8, 128.2, 128.1, 127.8, 106.6, 106.5, 104.7, 101.8, 70.3 (CH_2), 70.2 (CH_2), 21.8 (CH_3).

Synthesis of 3,5-bis((3,5-bis(benzyloxy)benzyloxy))benzyl acetate (18). This synthesis is detailed in Scheme AB-2. In a 50 mL round-bottom flask equipped with a magnetic stirbar and a reflux condenser, a solution of G2-C=N-NHTs (147 mg, 0.16 mmol) in toluene (10 mL) was combined with aqueous NaOH (10 mL of 14 % w/w solution in water) and a catalytic amount of NEt_3BnCl. The resulting biphasic solution was refluxed with vigorous stirring for 2 h. The reaction was cooled down to room temperature. The bright orange organic phase was separated, washed with saturated brine (2 x 20 mL) and treated with excess glacial acetic acid. The resulting clear solution was washed with saturated solution of sodium bicarbonate (20 mL) and saturated brine (2 x 20 mL) and dried over $MgSO_4$. Evaporation of the solvent resulted in an oily liquid which was purified by flash chromatography (CH_2Cl_2, R_f = 0.40) to give the final product as colorless solid (24 mg, 19%). Anal. Calcd. for $C_{51}H_{46}O_8$: C, 77.84; H, 5.89. Found: C, 77.77 H, 5.89. ^1H NMR ($CDCl_3$): δ 7.45-7.33 (m, 20H), 6.70 (4H), 6.60 (4H), 6.57 (1H), 5.05 (10H), 4.98 (4H), 2.12 (3H). ^{13}C NMR ($CDCl_3$): δ 171.1, 160.4, 160.2, 139.3, 138.4, 136.9, 128.8, 128.2, 127.8, 107.3, 106.6, 101.9, 101.8, 70.3 (CH_2), 70.2 (CH_2), 21.2 (CH_3).

Scheme A-2. Synthesis of the diazo precursors to the dendritic side chains of DPPs.

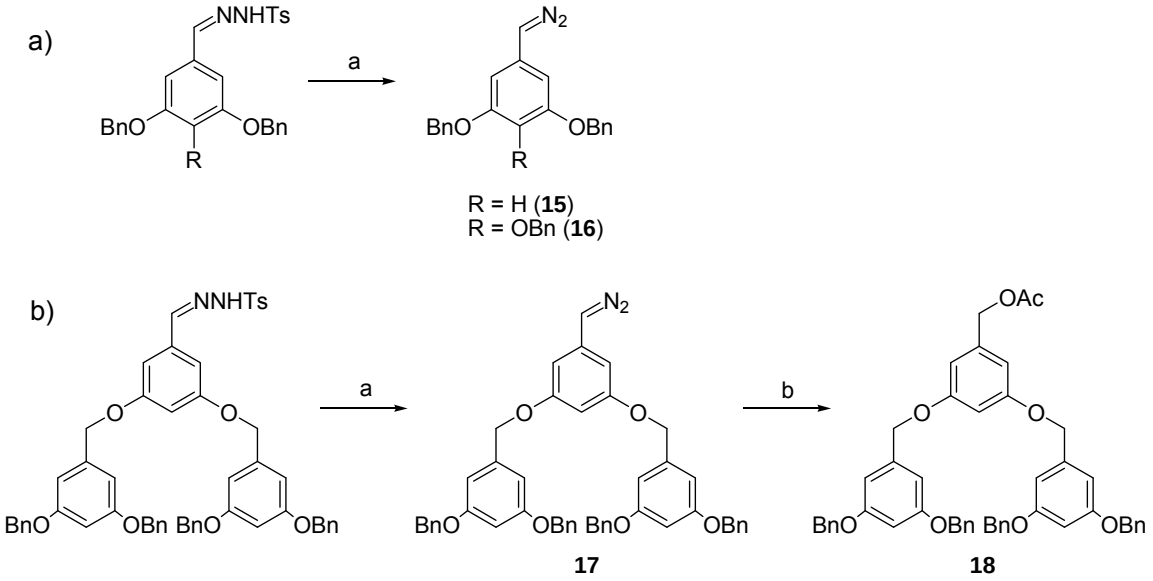

Reaction conditions: a) NaOH, Et_3BnNCl, C_6H_6 or toluene:H_2O (1:1), reflux, 2 h. b) HOAc, C_6H_6 or toluene, rt, 15 min.

Synthesis of dendronized protein polymers (DPPs). The procedure for dendronization of polypeptides is outlined in Schemes A-2 and A-3.

Active diazo compound were prepared by Bamford-Stevens reaction (Scheme A-2a). In a typical preparation, a diazo compound precursor (0.1-0.2 mmol, 5 equiv to the active acid functionality) was added to a 50 mL round-bottom flask equipped with a magnetic stirbar and a reflux condenser and suspended in benzene (10-20 mL) and an equal volume of NaOH solution (14% w/w). A small amount of the phase transfer catalyst NEt_3BnCl (20 mg) was added to the flask and the resulting slurry was heated to reflux while being vigorously stirred. The reflux was maintained for 1 h after all the solid starting materials has dissolved. For tri-substituted first-generation dendron precursors (T-based precursors), the preferred organic solvent was toluene and the reflux should not last more than 30 min after the solid starting materials completely dissolve. Prolonged heating in this case leads to considerable decomposition of the diazo compound and formation of **20**. The reaction mixture was cooled down and poured into a separatory funnel. The aqueous layer was separated and the organic fraction was washed repeatedly with water until the pH of the aqueous washes becomes neutral. The organic fraction was washed for two more times to ensure the complete removal of the base. The organic layer, bright orange for D_n- and magenta-red for T-based diazo compounds, was dried over Na_2SO_4 and filtered. The resulting solution may be stored overnight in fridge without any appreciable decomposition although we recommend using it immediately.

To test the reactivity of diazo dendrons, a small amount intermediate **17** was reacted with acetic acid (Scheme A-2b). The only identifiable reaction product was the desired ester **18**. While we never experienced any problems, certain diazo compounds are known to be explosive and we suggest reasonable caution when dealing with **15**-**17**.

The preparative procedure for the dendronized polypeptides (DPPs) is shown in Scheme A-3. In a typical reaction, the volume of the solution of the freshly prepared diazo compound was reduced to 20 mL (40 mL for T) before being added to a 100 mL round-bottom flask containing a solution of polypeptide (1 equiv) in DMSO (40 mL). The reaction mixture was capped with a septum, vented with a needle, protected from light using aluminum foil wraps, and allowed to stir for 5-7 days at ambient temperature upon which time the solvent was distilled off and the resulting yellow-orange sludge was dissolved in dichloromethane and precipitated in MTBE (methyl *tert*-butyl ether). The precipitated solids were dissolved in CH_2Cl_2 and purified using preparative GPC, eluting with CH_2Cl_2 (0.1% TFA, 6 mL/min, monitored at λ = 260 nm). Due to the large molecular weight difference between the DPPs and reaction byproducts, we were able to overload the GPC column and purify up to 200 mg of DPPs in a single separation (20 minutes). This was possible since the DPPs eluted in the void volume, cleanly separating from the impurities that can penetrate beads of the 500-Å column matrix. DPPs with D_0 and D_1 side-chains can be also be purified by prolonged Soxhlet extraction (3-4 days) with MTBE. The major identified impurities for D_1 and T were respectively dimers **19** and **20**. Purified polymers were precipitated into pentane and dried under vacuum for 16 h. The resulting solid was then crushed and dried in vacuum oven at 50 ºC for additional 16 h.

Scheme A-3. Dendronization of polypeptide cores.

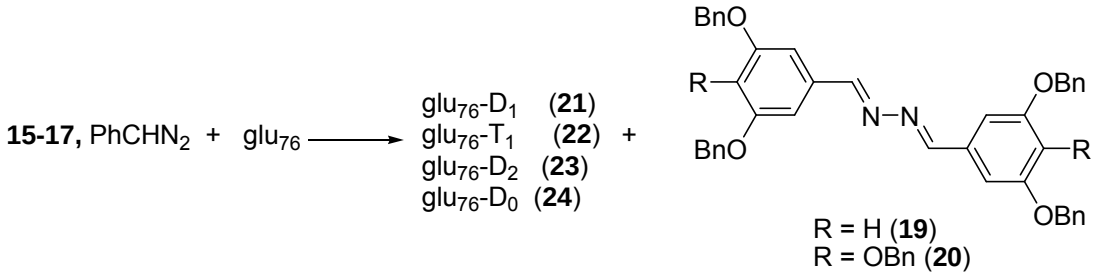

Reaction conditions: C_6H_6 (or toluene):DMSO (1:2), rt, 7 days.

***N*,*N*'-Bis-(3,5-bis(benzyloxy)benzylidene)hydrazone (19)**. An analytically pure sample was isolated by Soxhlet extraction of crude glu_{76}-D_1 with MTBE for 5 days. Anal. Calcd. for $C_{42}H_{36}N_2O_4$: C, 79.72; H, 5.73; N, 4.43. Found: C, 79.66; H, 5.72; N, 4.46. ^{1}H NMR ($CDCl_3$): δ 8.58 (2H), 7.47-7.33 (20H), 7.12 (4H), 6.75 (2H), 5.10 (4H). ^{13}C NMR ($CDCl_3$): δ 162.2 (*C*=N), 160.4, 136.8, 136.1, 128.8, 128.3, 127.8, 107.7, 105.7, 70.5. ESI-MS: calcd. for $C_{42}H_{36}N_2O_4$: 632.27, found: 633.3 [$(M+H)^+$].

***N*,*N'*-Bis-(3,4,5-tris(benzyloxy)benzylidene)hydrazone (20)**. An analytically pure sample was isolated by Soxhlet extraction of glu_{76}-T_1 with MTBE for 5 days. Anal. Calcd. for $C_{56}H_{48}N_2O_6$: C, 79.60; H, 5.73; N, 3.32;. Found: C, 79.20; H, 5.68, N, 3.19. ^{1}H NMR ($CDCl_3$): δ 8.51 (2H), 7.48-7.32 (24H), 7.30-7.22 (6H), 7.16 (4H), 5.17 (8H), 5.13 (4H). ^{13}C NMR ($CDCl_3$): δ 161.7 (*C*=N), 153.3, 141.3, 137.7, 137.0, 129.7, 128.8, 128.7, 128.4, 128.2, 128.1, 127.7, 108.1, 75.5, 71.5.

glu_{76}-D_1 (21). An off-white solid (271 mg, 80%). ^{1}H NMR ($CDCl_3$, 1% CF_3COOD) (Figure S5): δ 8.50-8.30 (br, 1H, NH), 7.40-7.00 (m, 10H, Ph), 6.60-6.20 (m, 3H, Ar), 5.10-4.60 (m, 6H, CH_2), 4.03 (br, 1H, α-glu), 2.80-2.10 (m, 4H, β,γ-glu).

glu_{76}-T (22). A yellow solid (197 mg, 67%). ^{1}H NMR ($CDCl_3$, 1% CF_3COOD) (Figure S6): δ 8.60-8.30 (br, 1H, NH), 7.45-6.90 (m, 15H, Ph), 6.43 (br, 2H, Ar), 5.20-4.60 (m, 8H, CH_2), 4.22 (br, 1H, α-glu), 2.90-2.10 (m, 4H, β,γ-glu).

glu_{76}-D_2 (23). A yellow solid (290 mg, 88%). ^{1}H NMR ($CDCl_3$, 1% CF_3COOD) (Figure S7): δ 7.50-7.00 (m, 20H, Ph), 6.70-6.20 (m, 9H, Ar), 5.10-4.40 (m, 14H, CH_2), 3.90 (br, 1H, α-glu), 2.60-1.80 (m, 4H, β,γ-glu).

glu_{76}-D_0 (24). A white solid (175 mg, 85%). ^{1}H NMR ($CDCl_3$, 1% CF_3COOD) (Figure S8): δ 8.29 (br, 1H, NH), 7.50-7.15 (m, 5H, Ph), 5.03 (br, 2H, CH_2), 3.96 (br, 1H, α-glu), 2.70-2.00 (m, 4H, β,γ-glu).

glu_{58}-D_1 (25). A yellow solid (197 mg, 65%). ^{1}H NMR ($CDCl_3$, 1% CF_3COOD) (Figure S9): δ 8.50-8.30 (br, 1H, NH), 7.40-7.00 (m, 10H, Ph), 5.10-4.60 (m, 6H, CH_2), 4.03 (br, 1H, α-glu), 2.80-2.10 (m, 4H, β,γ-glu).

glu_{94}-D_1 (26). A yellow solid (154 mg, 65%). ^{1}H NMR ($CDCl_3$, 1% CF_3COOD) (Figure S10): δ 8.50-8.20 (br, 1H, NH), 7.40-7.00 (m, 10, Ph), 6.50-6.30 (m, 3H, Ar), 5.10-4.60 (m, 6H, CH_2), 4.05 (br, 1H, α-glu), 2.70-2.10 (m, 4H, β,γ-glu).

Appendix B: Growth Curves of Cationic Proteins as Expressed in E. Coli

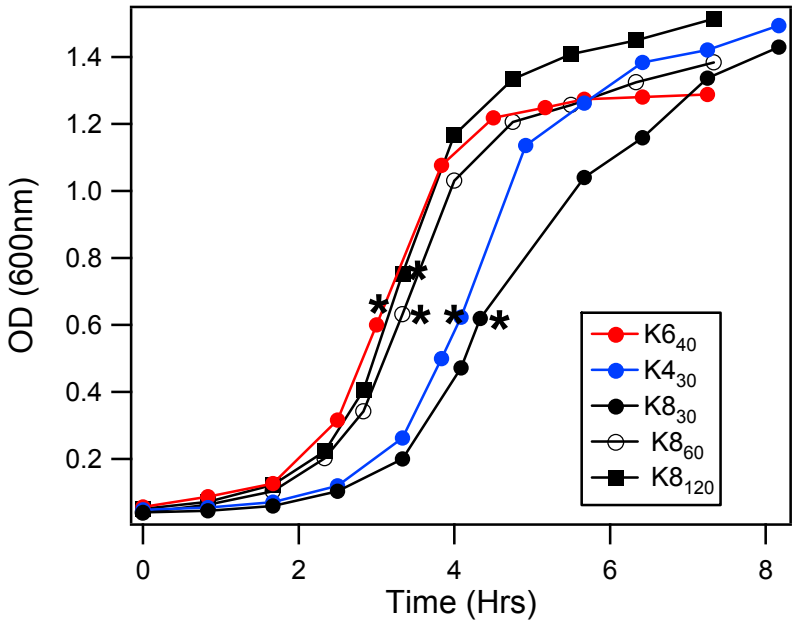

Figure AB-1: Optical density versus time as protein polymers are expressed in E. coli. Stars denote time of induction. As shown in the graph, as the cationic proteins are produced after induction, there is no decrease in optical density which would accompany cell death.

Appendix C: Solution Behavior of Cationic Proteins as Determined by Turbidity

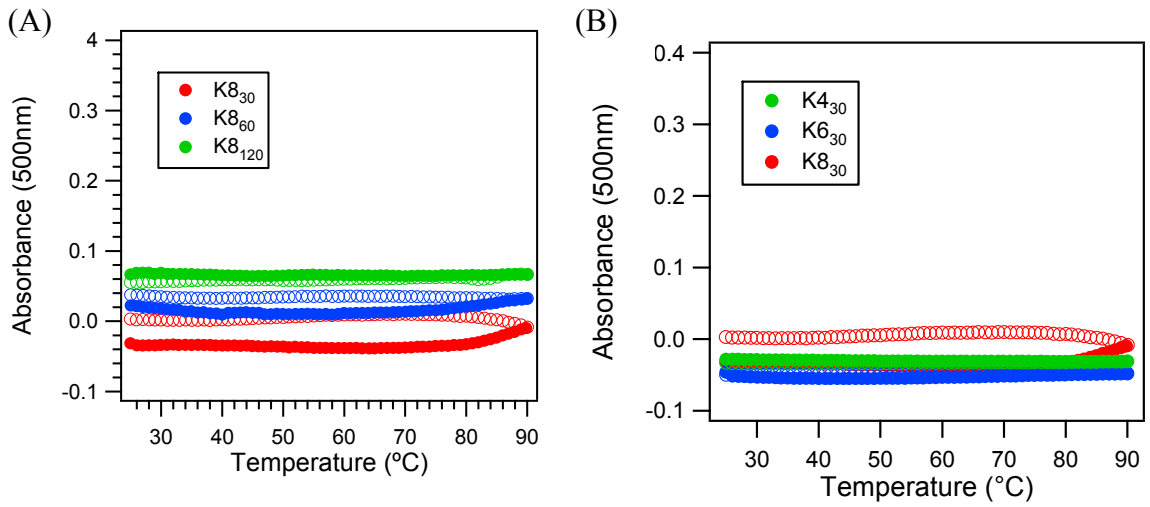

Figure AC-1: Solution turbidity as a function of protein polymer (A) length (B) and lysine spacing. All samples are 1 mg/ml in ddH_2O.